The Photophysical Properties of 2-Aminopurine and its Application as a Probe of DNA-Protein Interactions

Robert K. Neely

Degree of Doctor of Philosophy

The University of Edinburgh

2005

... they are ill discoverers that think there is no land when they can see nothing but sea.

Francis Bacon

Abstract

Steady-state and time-resolved fluorescence spectroscopies have been used to investigate the photophysical properties of the fluorescent DNA base analogue, 2-aminopurine (2AP). For the first time, the fluorescence decay of 2AP is shown to be biexponential. In aqueous solution, 2AP has lifetimes of 11.0ns and 13.5ns, which are shown to decrease in less polar solvents. These two lifetimes are attributed to the N7-H and N9-H tautomers of 2AP.

Crystals of 2AP have been grown and their structures have been determined by x-ray diffraction. Four singly hydrated 2AP molecules are seen in the crystal unit cell. The molecules within the crystal form an extensively hydrogen bonded network and also stack adjacent to one another, forming long chains of π-π interacting molecules. The interactions experienced by an individual 2AP molecule in this crystal are analogous to those that it might experience in the DNA duplex. Both the N7-H and N9-H tautomers are observed in the crystal structure. Steady-state fluorescence measurements indicate that, in the ground state, 2AP is present as both isolated, single molecules and as part of a π-stacked complex in the crystal. The red-shifted excitation and emission spectra of 'stacked-2AP' are consistent with the formation of excitons in the crystal. The time-resolved fluorescence response of both 'isolated' and 'stacked' 2AP in the crystalline state have been recorded and both are described by four discrete lifetimes. Both decays are dominated by a short ~100ps component, indicating highly efficient quenching of both the isolated excited-state 2AP and stacked, excitonically coupled molecules within the crystal.

The fluorescence responses of ten 2AP-labelled DNA duplexes have been recorded. The decays are fitted by four discrete components and all are dominated by a ~100ps component, which is consistent with efficient quenching of the 2AP by electron transfer from guanine. The fluorescence response of 2AP within the duplexes is sensitive to both the nature of the bases in its immediate vicinity and the extended nucleotide sequence.

2AP-labelled DNA has been used as a probe of base flipping by the M.HhaI methyltransferase enzyme. The DNA was labelled such that duplexes with the 2AP adjacent to, opposite and at the target site for base flipping have been studied. Duplexes with the 2AP outside the M.HhaI recognition sequence have also been investigated. When 2AP is the target base for flipping its fluorescence decay shows a significant response to enzyme binding. It is

shown that this change in photophysical behaviour can be used as a definitive indicator of the base flipping mechanism. A similar response is also shown for the M.TaqI base flipping enzyme. Placing the 2AP at positions adjacent to and opposite the target base for flipping demonstrate the amazing selectivity of HhaI for its target base and demonstrate the effectiveness of the enzyme's stabilisation of the DNA duplex during base flipping.

Declaration

I declare that the work presented in this thesis is my own unless otherwise stated by reference.

Signed.

Date. 1.7.05

Acknowledgements

I am indebted to many people for their help, collaboration and support in completing this work. Thanks to Anita Jones, my supervisor, for the huge amount of her time, effort and support she has offered to me throughout my PhD. Thanks also to David Dryden whose expertise and enthusiasm for molecular biology has been so important in helping me through this project.

An enormous amount of effort has been put into this work, and the research upon which this work was founded, by collaborators in The Institute of Molecular Biology in Vilnius, Lithuania and in The Institute for Organic Chemistry at Aachen, Germany. In particular, I must thank Saulius Klimašauskas and Dalia Daujotyte for their part in the substantial amount of research carried out using the M.HhaI methyltransferase enzyme. Thanks also to Elmar Weinhold and Thomas Lenz for their efforts with the work on the M.TaqI enzyme. Thanks also to T.J. Su, who helped me with the research with the EcoKI enzyme and several of the DNA duplexes used in this study.

Several people have made small but important contributions to this work, in particular Steven Magennis who has ensured the smooth running of the Ti:Sapphire laser and who has spent many an afternoon twiddling with harmonic generating crystals on my behalf.

I have had a fantastic time during the course of this study and this has been due in no small part to the friends who have come and gone over the past three years. Thanks particularly to Trish, Ian and Alistair but also to the numerous members of the Jones group past and present and to the Dryden group who have made the School a great place to be.

Finally, thanks to family and particularly my wife, Ailsa, for being patient, for the immense support you've given me and for being there whenever I've needed you.

List of Symbols Used

Ψ	The total molecular wavefunction
$\boldsymbol{\mu}$	The dipole moment operator
B	The Einstein B coefficient
ε_o	Permittivity of free space
h	Planck's Constnat
e	Charge on an electron
π	Pi
ρ	Energy density
Z	Nuclear charge
t	Time
S_0	Singlet ground state
S_1	First singlet excited state
T_1	First triplet (excited) state
v''	Denotes a vibrational level in the S_0 state
v'	Denotes a vibration level in the S_1 state
k_b	Boltzman's constant
m	Mass
T	Temperature
ω	Angular frequency
α	Amplitude (weighting factor)
τ	Fluorescence lifetime

ΔG^0	Standard thermodynamic free energy change
λ	Wavelength

Table of Contents

Chapter 1

Introduction

The DNA duplex will be forever associated with the famous structural model described by Crick and Watson[1], which was based on the x-ray data collected by Wilkins and Franklin. Though a remarkable scientific achievement, their description of the duplex as a static, double helical species merely marks the beginning of our understanding of the structure and function of this fascinating molecule. DNA is remarkably dynamic, with base pairs typically persisting for only milliseconds[2]. Such freedom of movement for individual DNA bases is crucial in allowing the duplex to interact with enzymes. Hence, the motions and conformational heterogeneity of the duplex play a key role in the operation and maintenance of cellular DNA[3]. This work is focussed on improving current understanding of how enzymes distort the DNA duplex in order to carry out simple maintenance operations that are crucial in all cellular organisms.

Fluorescence spectroscopy is ideally suited to the study of large and complex biomolecular systems because of the inherent selectivity and sensitivity of the technique. This work makes use of both steady-state and time-resolved fluorescence techniques to study the DNA-enzyme systems of interest.

In order to study these systems using fluorescence spectroscopy, a fluorescent probe must be introduced into the system. The probe that is both used and investigated in this thesis is 2-aminopurine (2AP). This molecule is a structural analogue of adenine (6-aminopurine) and can be inserted into the DNA duplex in place of one of the native DNA bases during the preparation of synthetic DNA. The fluorescence response of 2AP is supremely sensitive to its molecular environment and so it is potentially an ideal probe of the structure and function of DNA.

In order to fully utilise 2AP as a probe of the DNA duplex, there is a pressing need to understand how specific molecular interactions induce changes in its fluorescence response. Chapters 4 and 5 are an investigation into the fluorescence response of the 2AP base alone in the solution and

crystal phases, respectively. In these systems the response of 2AP to well characterised properties, such as the polarity of its local environment, are established.

Chapters 6, 7 and 8 of this work are used to investigate the application of 2AP as a probe of DNA structure. In Chapter 6, the time-resolved fluorescence response of 2AP in the DNA duplex is investigated. Chapters 7 and 8 describe the response of 2AP to a well-characterised distortion of the DNA duplex and will show how 2AP can be used to identify this structural perturbation in other DNA-enzyme interactions.

Chapter 2

Theory

The work presented in this thesis makes use of a range of theoretical principles. Central to this work is the study of the interaction of molecules with light using the technique of fluorescence spectroscopy and in particular, time resolved fluorescence spectroscopy. The purpose of this Chapter is to provide an account of the interaction of molecules with light and to explain how these interactions can be monitored.

2.1 Electronic Spectroscopy

The ability of a molecule to absorb and emit radiation is sensitively dependent on the electronic composition and nuclear framework of the molecule in question. Since both of these systems are, in principle, sensitive to the immediate environment of a given molecule, through monitoring the interaction of a molecule with light, an insight into its atomic scale behaviour can be gained[4].

2.1.1 Absorption

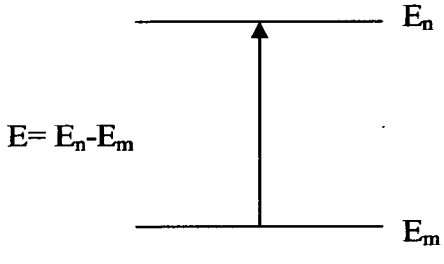

Figure 2.1- Absorption of radiation with energy, E, resulting in an electronic transition from the ground state, m, having a potential E_m, to an excited state, n with potential E_n.

The absorption of a photon of light, with energy E, by a molecule can promote an electron from the ground electronic state, m, to some vibrationally and electronically (vibronically) excited state, n.

Absorption of radiation occurs as the result of an interaction between the oscillating electrical component of the incident radiation and the electrons of the molecule. During absorption, the electric field imposes a force on the electrons such that they oscillate with an orientation, amplitude and frequency that are defined by the electric field component of the incident radiation. The charge separation effected by this oscillation is a vector quantity known as the transition dipole moment, μ_{mn}. This is related to the wavefunctions of the ground Ψ_m and excited Ψ_n states by the dipole moment operator μ.

$$\boldsymbol{\mu}_{mn} = \int \psi_m \mu \psi_n d\tau \qquad \textbf{Equation 2.1}$$

Where the term $d\tau$ describes the integral across all space (i.e. the volume element dxdydz). The square of transition dipole moment determines the probability of a given electronic transition occurring. Thus, in theory, if the transition dipole moment for a given transition is zero, then the probability of that transition taking place is zero and it is said to be forbidden. It is important then to understand the reasons that can lead to a transition becoming forbidden and this can be done by further resolving Equation 2.1.

The Born-Oppenheimer approximation states that the electronic and nuclear (vibrational) parts of the wavefunction are separable[5]. This is because the electrons are light and move quickly relative to the atomic nuclei. Furthermore, the electronic dipole moment operator, μ, operates on only the electronic spatial part of the wavefunction and so Equation 2.1 can be re-written as

$$\boldsymbol{\mu}_{mn} = \int \psi_{E,m} \boldsymbol{\mu} \psi_{E,n} d\tau \int \psi_{S,m} \psi_{S,n} d\tau \int \psi_{N.m} \psi_{N,n} d\tau \qquad \textbf{Equation 2.2}$$

where the sub-scripts E, S and N refer to the electronic, spin and nuclear parts of the transition dipole moment, respectively. Since μ_{mn} is the product of these three integrals it follows that if the result of any integral is zero then the transition will be forbidden. Equation 2.2 forms the basis for the selection rules for electronic transitions.

2.1.1.1 Selection Rules- Symmetry

The electronic transition moment is represented by the first term in Equation 2.2. An evaluation of whether or not this term is equal to zero for a given molecule can be made by assessing the symmetry properties of the molecular orbitals involved in the transition[6]. Since the dipole moment operator is a vector quantity, it can be resolved along the three Cartesian axes.

$$\int \psi_{E,m} \boldsymbol{\mu} \psi_{E,n} d\tau = \int \psi_{E,m} \mu_x \psi_{E,n} dx + \int \psi_{E,m} \mu_y \psi_{E,n} dy + \int \psi_{E,m} \mu_z \psi_{E,n} dz \qquad \textbf{Equation 2.3}$$

The symmetry of each of the spatial wavefunctions can be determined from the product of the electronic wavefunctions in the ground and excited states, with the electronic transition dipole moment operator along each axis. In order for the integral to be non-zero and, hence, the transition allowed, the symmetry of the transition must be totally symmetric. This follows from the fact that the transition dipole moment is a molecular property and, as such, must remain unaltered when a symmetry operation from the molecular point group is applied to it. For example, consider a molecule with point group C_{2v} symmetry. The character table shows that μ_x, μ_y and μ_z have symmetry of B_2, B_1 and A_2 respectively. For a transition from Ψ_m with say, A_1 symmetry to Ψ_n with B_1 symmetry, the integrals to consider for each of the Cartesian axes will be

$$\int \psi_{E,m} \mu_x \psi_{E,n} d\tau \rightarrow A_1 \times B_2 \times B_1 = A_2 \qquad \textbf{Equation 2.4}$$

$$\int \psi_{E,m} \mu_y \psi_{E,n} d\tau \rightarrow A_1 \times B_1 \times B_1 = A_1 \qquad \textbf{Equation 2.5}$$

$$\int \psi_{E,m} \mu_z \psi_{E,n} d\tau \rightarrow A_1 \times A_2 \times B_1 = B_2 \qquad \textbf{Equation 2.6}$$

It is evident that, for this molecule, only the transition along the y-axis is totally symmetric and, therefore, this transition is symmetry allowed. Hence, the symmetry selection rules state that electronic excitation of the molecule is allowed and is polarised along the the y-axis of this molecule.

2.1.1.2 Selection Rules- Spin

The electrons in a given electronic state can exist in either a spin-up or spin-down orientation. This orientation is described by the spin quantum number $\mathbf{m_s}$ for the electron, which takes values of either +½ or -½. Hence, the total spin quantum number for an electronic state is given by

$$\mathbf{S} = \sum_i \mathbf{m}_{s_i} \qquad \textbf{Equation 2.7}$$

The spin multiplicity of an electronic state is described by the total spin quantum number S of the state and is given by 2S+1. Consider a typical organic molecule with 2 electrons in its highest occupied molecular orbital. In the ground state the molecule will have spins of s_i and s_j, where these spins are opposing and $s_i \neq s_j$ and hence S=0. The multiplicity of this state is one and it is referred to as a singlet state. Upon excitation, the electrons will either remain opposing or can adopt parallel spins $s_i = s_j$ and hence S=1, where this state has a multiplicity of three and is referred to as a triplet state.

The transition dipole moment contains the overlap integral for the electronic spin wavefunctions, $\int \psi_{S,m} \psi_{S,n} d\tau$. The spin wavefunctions are designated as either α (spin up) or β (spin down).

Since these wavefunctions are orthogonal to each other the overlap integral is zero if the electronic spin is changed during the transition.

$$\int \alpha\alpha d\tau = \int \beta\beta d\tau = 1 \quad \textbf{Spin allowed} \qquad \textbf{Equation 2.8}$$

$$\int \alpha\beta d\tau = \int \beta\alpha d\tau = 0 \quad \textbf{Spin forbidden} \qquad \textbf{Equation 2.9}$$

Hence, only transitions between states of the same spin multiplicity are classically allowed.

2.1.1.3 Selection Rules- Nuclear Vibrations and the Franck-Condon Principle

Evaluation of the nuclear overlap integral, $\int \psi_{N,m}\psi_{N,n} d\tau$, from Equation 2.2 is achieved through examination of the vibrational wavefunctions for the ground and excited transition states. The Franck-Condon principle states that during an electronic transition the molecular nuclei do not move. Hence, when the transition is schematically represented for a diatomic molecule, as in Figure 2.2, it is shown as a vertical arrow. In both Figure 2.2 and Figure 2.3 the simple harmonic oscillator approximation is used to describe the vibrational structure of the molecules.

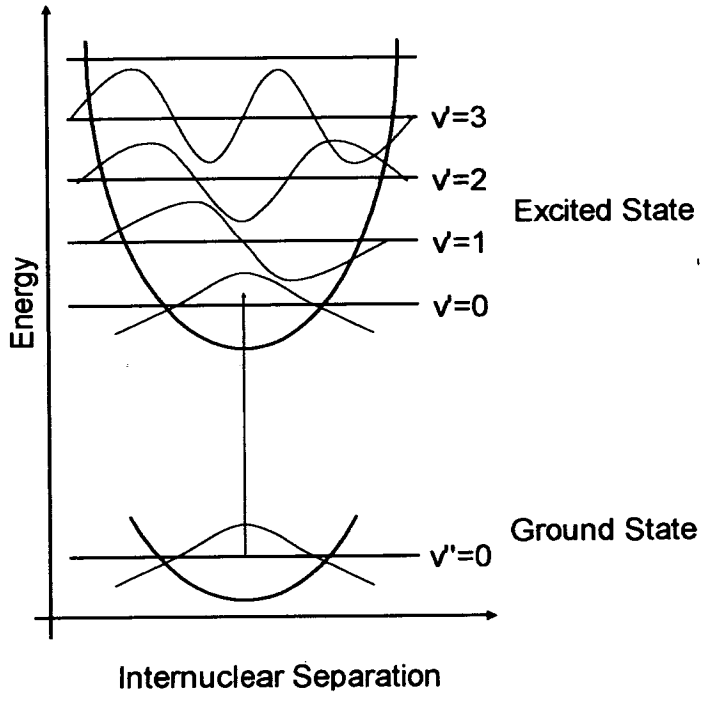

Figure 2.2- The vibronic transition for a diatomic molecule oscillating in a simple harmonic manner, where the internuclear separation is similar in both S_0 and S_1. Electronic states and vibrational levels with corresponding wavefunctions are shown.

The vibrational wavefunctions illustrate the probability associated with a given internuclear separation, since the square of the amplitude of the wavefunction is proportional to the probability of a given nuclear configuration existing. Figure 2.2 shows a molecule where the internuclear separation in the excited state is the same as that in the ground state. The most probable transition in this molecule is the v''=0 to v'=0 transition shown, which has the greatest overlap between the ground and excited state wavefunctions. Hence, in the absorption spectrum for this molecule we would expect to see one prominent band due to this 0-0 transition. The square of the nuclear (vibrational) overlap integral is termed the Franck-Condon factor.

Figure 2.3 shows a transition and predicted absorption spectrum for a diatomic molecule where the excited state has a greater internuclear separation than the ground state. This would occur where, for example, an electron is promoted from a bonding to a non- or anti-bonding orbital in the transition.

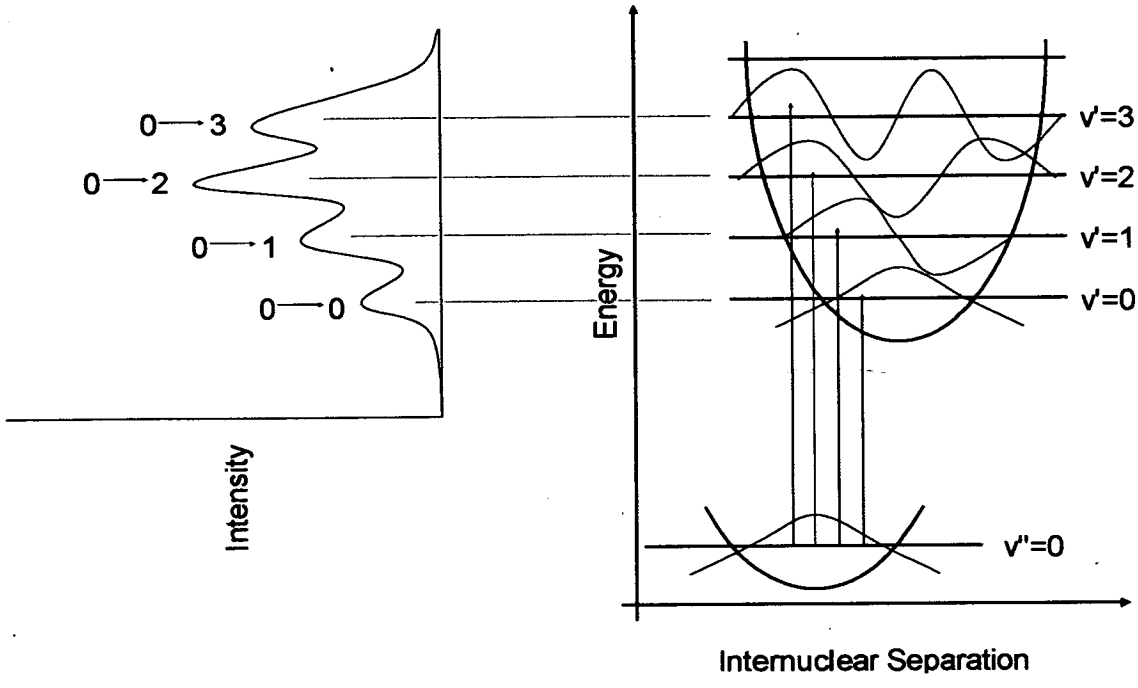

Figure 2.3- Vibronic transitions for a molecule with greater internuclear separation in the excited state than ground state. The possible form of the absorption spectrum is shown (left).

The absorption spectrum in Figure 2.3 illustrates the importance of the Frank-Condon factor in determining the overall shape of an absorption (or excitation) spectrum. Here, many v' levels are shown to have some overlap with v'' levels and so we see several bands in the absorption spectrum.

2.1.1.4 Forbidden Transitions

The selection rules are not absolute; in fact, they collapse if the assumptions upon which they are founded fail to hold. There are two important instances where the selection rules fail because of couplings between the different parts of the wavefunctions (Equation 2.2), which were, up to this point, assumed separable.

Transitions between electronic states of different spin multiplicities can be weakly allowed but require an inversion of the spin quantum number, $\mathbf{m_s}$, of an electron during the transition. Spin-orbit coupling provides a mechanism for this change in the electron spin state. It arises due to the orbital motion of the electron around the nucleus. This motion leads to an interaction between the magnetic component of the electron's inherent spin and the magnetic component of its angular momentum about the nucleus. This interaction leads to the breakdown of S as the appropriate quantum number and the singlet and triplet states become hybridised. Since the spin-orbit coupling is a magnetic interaction, its strength is proportional to Z^4, where Z is the atomic number of the atom. Hence, the presence of a heavy atom in the system undergoing a transition leads to a dramatic increase in the efficiency of the spin-orbit coupling.

Weak vibronic coupling occurs between the nuclear and the electronic spatial wavefunctions of a molecule during a transition. In these instances, the Born-Oppenheimer approximation, which allows independent consideration of these components of the transition moment, does not hold. This is the case because the motions of the nuclei and electrons affect each other, to a limited extent. Hence, transitions that are symmetry forbidden can be weakly allowed if nuclear vibrations distort the molecular symmetry sufficiently.

2.1.1.5 Absorption Measurements

The transition dipole moment is related to the Einstein B coefficient for absorption, B_{mn}, by

$$B_{mn} = \frac{3\pi^3}{4\pi\varepsilon_0 h^2}\left|\boldsymbol{\mu}_{mn}\right|^2 \qquad \textbf{Equation 2.10}$$

The Einstein B coefficient is related to the rate of change of the population N of the excited state n for absorption, as follows.

$$\frac{dN_n}{dt} = N_m B_{mn} \rho(\tilde{\nu}) \qquad \textbf{Equation 2.11}$$

where $\rho(\tilde{\nu})$ is the energy density of the incident radiation and $\tilde{\nu}$ denotes the wavenumber for the transition (normally taken as $\tilde{\nu}_{max}$ for a given absorption spectrum).

It is possible to relate the parameters defined above to experimentally observable quantities. The Beer-Lambert Law relates the absorbance of light, A, to sample concentration, c, the length of sample over which absorption occurs (path length), l and the molar absorption coefficient of the sample, ε.

$$A = \log \frac{I}{I_0} = \varepsilon(\tilde{\nu}) cl \qquad \textbf{Equation 2.12}$$

Where I_0 is the intensity of the incident radiation and I the intensity of light transmitted. Since the molar absorption coefficient and hence absorbance varies with wavenumber a more reliable method of determining the transition strength for absorption is to integrate ε over the whole absorption band. Thus, the integrated absorption coefficient A_i is defined as

$$A_i = \int_{\tilde{\nu}_1}^{\tilde{\nu}_2} \varepsilon(\tilde{\nu}) d\tilde{\nu} \qquad \textbf{Equation 2.13}$$

The integrated absorption coefficient is related to the transition dipole moment through a theoretical quantity known as the oscillator strength, *f*.

$$f_{mn} = \left[\frac{4\varepsilon_0 m_e c^2 \ln(10)}{N_A e^2} \right] A_i \equiv 4.319 \times 10^{-9} A_i \qquad \textbf{Equation 2.14}$$

The oscillator strength is used to express the strength of an electric dipole transition for a molecule as compared to that of a free electron oscillating in a simple harmonic manner in three dimensions[7]. It has a maximum value of one and values approaching this are often observed for

electric dipole allowed transitions. An oscillator strength of close to zero is expected for spin forbidden transitions. Oscillator strength is related to the transition dipole moment by

$$f_{mn} = \left[\frac{8\pi^2 m_e c}{3e^2 h}\right]\tilde{\nu}_{mn}\left|\boldsymbol{\mu}_{mn}\right|^2 \equiv 4.702\tilde{\nu}_{mn}\left|\boldsymbol{\mu}_{mn}\right|^2 \qquad \textbf{Equation 2.15}$$

2.1.2 De-excitation

A molecule in the excited state must inevitably return to the ground state via some de-excitation process. There are several possible mechanisms by which this can occur and these can be broadly divided into radiative and non-radiative decay processes[8]. It is possible to show these processes schematically using a Jablonski diagram as in Figure 2.4. Spectroscopic notation denotes the ground state of a molecule S_0 with subsequent singlet excited states being labelled S_1, S_2... (a triplet state is denoted by T_n). The absorption and radiative decay processes are depicted with straight vertical arrows, with the wavy arrows showing non-radiative processes. Horizontal lines represent the vibrational levels of the electronic states labelled in the diagram.

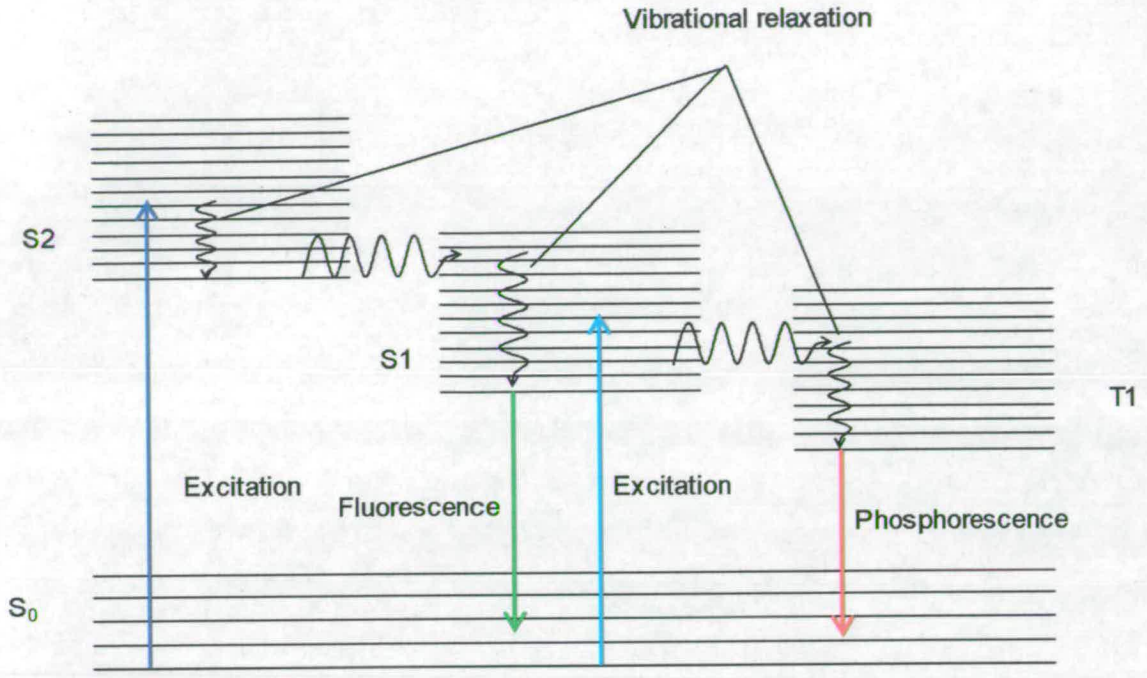

Figure 2.4- A Jablonski Diagram showing possible vibronic transitions for a molecule.

2.1.3 Radiative Decay

The radiative decay of a fluorophore is the energetic relaxation of the electronically excited molecule by the emission of a photon of radiation. This process is termed either fluorescence or phosphorescence, which are defined by the multiplicities of the states between which the transition occurs. Fluorescence is a radiative transition between electronic states of the same spin multiplicity, whereas phosphorescence occurs between states of different multiplicites. It is often possible to tell whether a substance is fluorescent or phosphorescent by eye because of the relative timescales of the two processes. Fluorescence occurs on a relatively short time scale (typically nanoseconds to picoseconds) and so does not persist (by eye) if the excitation source is removed. As a result of the forbidden nature of the transition between states of different multiplicities, phosphorescence occurs on a longer (millisecond to seconds) time scale. Phosphorescent compounds continue to emit light for some time after excitation of the molecule has ceased.

2.1.3.1 Fluorescence

Figure 2.4 shows that absorption of a photon by the fluorophore typically leads to the creation of a vibronically excited molecule in either S_1 or a higher electronically excited state. The non-radiative decay processes (wavy arrows) of vibrational relaxation, internal conversion (IC) and intersystem crossing (ISC) compete with those that lead to radiative decay. IC and ISC are the names given to isoenergetic transitions between different electronic states that are spin-allowed and spin-forbidden respectively. The mechanisms by which they occur are discussed in detail in subsequent sections of this Chapter. Vibrational relaxation is the transfer of vibrational energy from the excited molecule to its surroundings. In the condensed phases, due to the proximity of solvent (or coordinating) molecules to the fluorophore, vibrational relaxation is very efficient and is rapid (occurring on the picosecond timescale) in relation to fluorescence. This means that in these phases, for most organic molecules, fluorescence occurs only from levels that are thermally populated, according to the Boltzmann distribution (typically only the ground vibronic level of the S_1 state). This assumption is known as Kasha's rule. If Kasha's rule holds, then it follows that the emission spectrum for a given fluorophore in the condensed phases will be independent of the excitation wavelength. Figure 2.5 illustrates the absorption and emission processes for a molecule conforming to this rule.

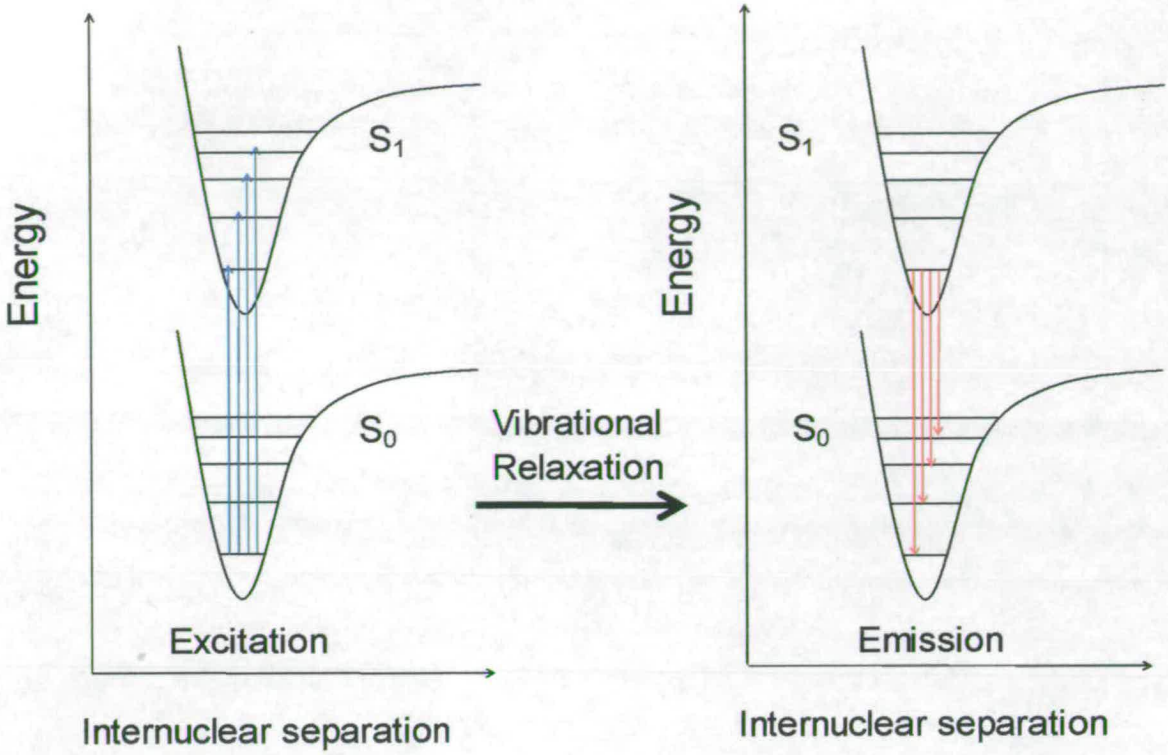

Figure 2.5- Schematic representation of transitions that occur during the excitation and emission events of a fluorophore

Figure 2.5 shows how fluorescence can be used to probe the vibrational structure of the ground and excited states of a fluorophore. The excitation process gives information on the excited state vibrational structure, whereas, emission can be used as a probe of the ground state vibrational structure. Steady-state spectroscopy can be used to study the dependence of emission intensity on excitation and emission wavelength. Emission spectra are obtained by monitoring fluorescence emission intensity as a function of the emission wavelength and relay information on the relative energies of the ground state vibrational levels. Excitation spectra show the variation in emission intensity as a function of excitation wavelength and contain information on the vibrational structure of the excited state.

2.1.3.2 Phosphorescence

Phosphorescence is a spin-forbidden radiative transition, usually from a triplet to a singlet state. The triplet state from which it originates is generally populated by ISC from the singlet manifold. The unpaired electrons in a triplet state are spatially well separated relative to those paired in the corresponding singlet state. Hence, the Coulombic repulsion between electrons in the triplet state is less than that in the corresponding singlet state. As a result, the triplet state is relatively low in energy compared to the singlet state and phosphorescence tends to occur at longer wavelengths than fluorescence. Since the transition from $T_n \rightarrow S_0$ is formally forbidden, the lifetime of the excited triplet state is long in comparison to those of the other excited state intermediates. The relatively long timescales required for phosphorescence mean that the triplet state is often depopulated by intermolecular (collisional) quenching processes before the radiative transition can occur.

2.1.3.3 Non-Radiative Decay

Internal conversion (IC) and intersystem crossing (ISC) are important intramolecular non-radiative decay processes. IC occurs between isoenergetic vibrational levels in electronic states of the same spin multiplicity whereas ISC is a spin forbidden transition between states with different multiplicities, Figure 2.6.

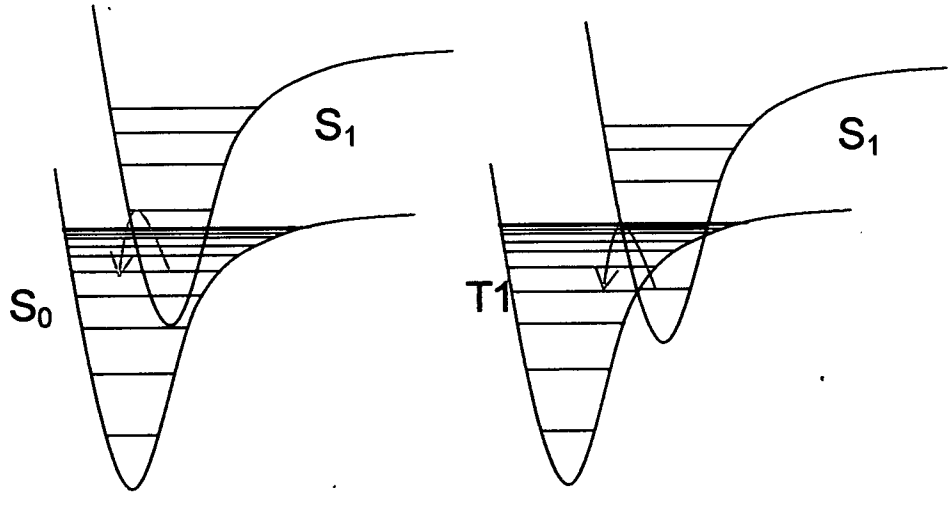

Figure 2.6- Schematic representation of internal conversion (red) and intersystem crossing (blue)

The probability of a non-radiative transition (IC or ISC) occurring depends on three factors. Firstly, the smaller the energetic separation of the two electronic states involved in the transition, the greater the transition probability. This is because the probability of the non-radiative transition depends on the vibrational overlap intergral between the two vibrational levels involved in the transition. It is generally the case that the overlap between a high and a low vibrational level will be small. Thus, IC, for example, between a low vibrational level of S_1 and a high level from S_0 is improbable. IC between electronic states higher than S_1 (e.g. $S_3 \rightarrow S_2$) is generally far more efficient than the $S_1 \rightarrow S_0$ IC transition. A greater density of vibronic states improves the probability of the transition. The probability of the non-radiative transition is also increased when the vibrational overlap integral (Franck-Condon factor) of the levels between which the transition is to occur is large. Since the vibrational wavefunctions have their maxima at the edges of the electronic potential energy surfaces (apart from in the vibrational ground state), the Franck-Condon factor is often maximised if the potential energy curves of the two electronic states overlap.

The spin-forbidden nature of ISC means that, as well as those factors discussed above, ISC relies on spin-orbit coupling in order to occur.

2.1.4 Excited Molecules in the Crystal Phase

The arrangement of molecules in a crystal is such that the interactions between them cannot be ignored in rationalising their photophysical behaviour[9]. Consider a the simple case of a dimer, where the molecules, A and B are oriented such that the ground state wavefunction of the dimer is given by

$$\psi_G = \psi_A \psi_B \qquad \textbf{Equation 2.16}$$

If radiation of the correct frequency is incident on the dimer then there is an equal probability that either one of the molecules A or B will be excited. The wavefunction for the excited state dimer is given by

$$\psi_{E_\pm} = \left(\frac{1}{\sqrt{2}}\right)(\psi_A^* \psi_B \pm \psi_A \psi_B^*) \qquad \textbf{Equation 2.17}$$

Equation 2.17 shows that the excited state of the dimer is split into two levels with wavefunctions, ψ_{E+} and ψ_{E-}, where the splitting between the levels is determined by the extent of the interaction between molecules A and B. The effect of this intermolecular coupling on the electronic transitions within a system is summarised in Figure 2.7.

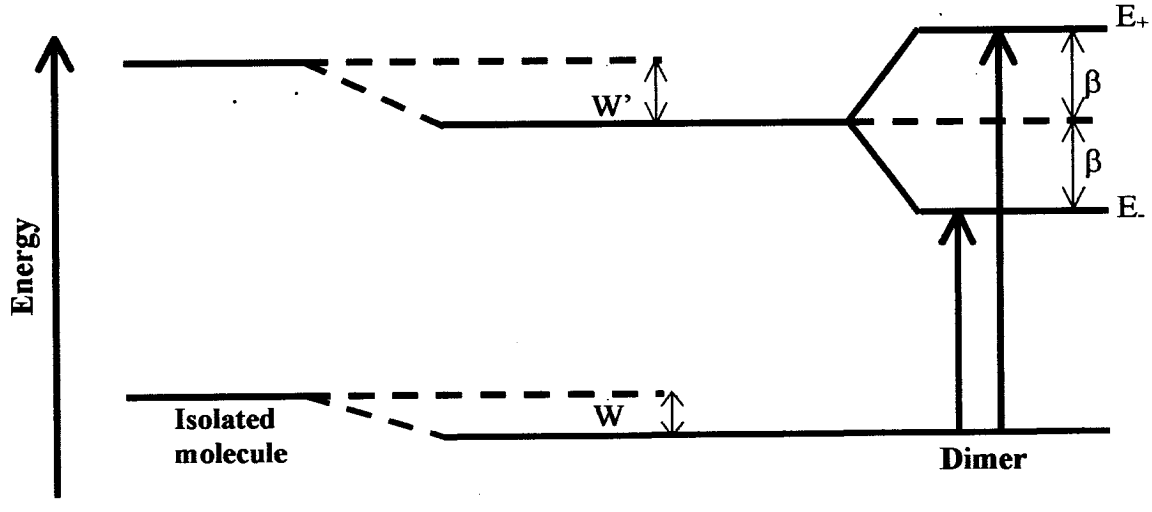

Figure 2.7- Schematic representation to show how the energetic levels of an isolated molecule are changed by dimerisation. W and W' represent the intermolecular coulombic interactions in the ground and excited states respectively and β represents the resonance interaction between the wavefunctions of the two molecules.

Figure 2.7 shows that the ground and excited-state energetic levels of an isolated molecule are both shifted in energy and the excited state is split into two distinct levels by the dimeric interaction. The shift in energy arises from the coulombic interaction, of magnitude W and W' in the ground and excited states respectively, formed between the molecules. β describes the resonance interaction resulting from the overlap of the molecular orbitals of the two molecules. Experimentally, the formation of a dimeric species can lead to shifts and splitting of both the excitation and emission spectra of a fluorophore, relative to the monomer.

The relative alignment of the transition dipole moments of molecules A and B is critical in determining whether the electronic transitions in a dimer system are allowed or forbidden. Figure 2.8 shows that there are three possible orientations of the two molecules to consider. In the first case, the transition dipole moments of molecules A and B lie parallel to each other. In this instance, only the high energy transition to E_+ is allowed. In the case where the molecules lie nose-to-tail to one another only the relatively low energy transition to E_- is allowed. Significantly, where there are two crystallographically inequivalent molecules in the dimer, the transitions to both E_+ and E_- are allowed. The splitting that this causes in the excitation and emission spectra of crystalline fluorophores is known as Davydov splitting.

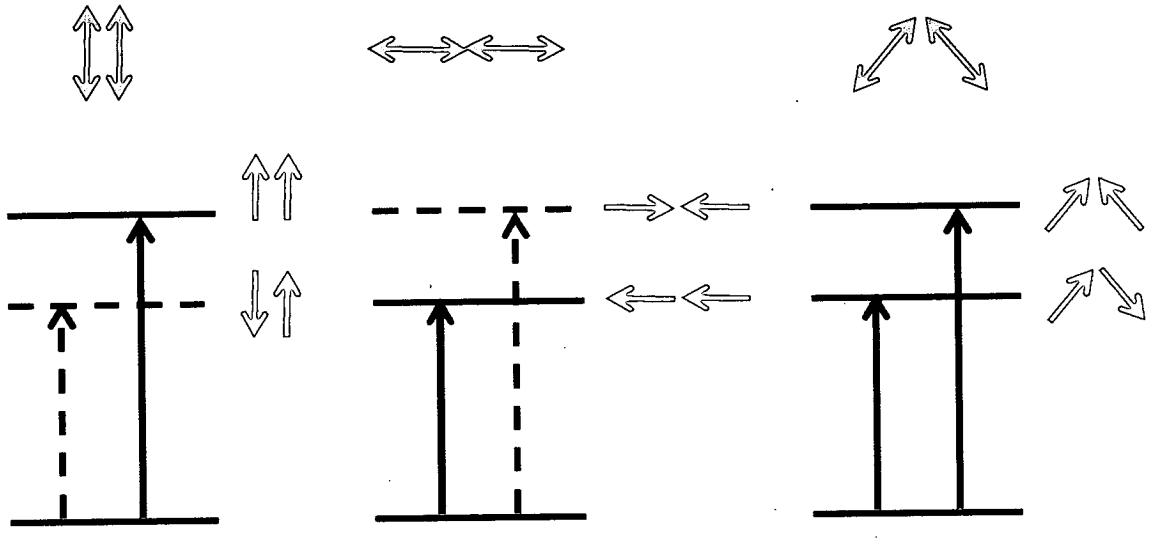

Figure 2.8- Schematic diagram showing the allowed (solid arrows) and forbidden (dashed arrows) transitions in a dimer. The molecular orientation of the two molecules in the dimer is described by the blue arrows. The red arrows indicate the relative orientations of the transition dipole moments in the dimer.

A crystal lattice can be considered as an infinite number of molecules interacting with one another in three-dimensional space. When a molecule in the crystal absorbs a quantum of excitation, this results in the production of an electron-hole pair, known as an exciton. The exciton is a neutral species and can be delocalised throughout the crystal. The arguments relating

to the electronic properties of the dimeric system are similarly applicable to the crystal lattice and Figure 2.7 might equally describe the interaction between two crystallographically inequivalent molecules as the formation of a dimeric, solution-phase species. There are three types of exciton, depending on the relative proximity of the electron to the hole within a crystal lattice. Frenkel excitons describe electron-hole pairs localised to the same molecular site. In a charge-transfer exciton, the electron occupies a molecule neighbouring the hole site. Finally, Wannier excitons are those where the electron, on average, occupies a molecule several molecules away from the hole.

2.1.5 Excited State Decay Kinetics

The overall rate of decay of an excited state population can be defined by considering the radiative (fluorescence and phosphorescence) and non-radiative (IC, ISC, quenching, etc) processes[8;10]. A population of excited state fluorophores, [M*], decays with a rate according to

$$-\frac{d[M^*]}{dt} = (k_R + k_{NR})[M^*] \qquad \textbf{Equation 2.18}$$

where k_R and k_{NR} are the rates of the radiative and non-radiative decay processes, respectively. Defining k_F as the sum of the rate constants for radiative and non-radiative decay processes ($k_F = k_R + k_{NR}$) and integrating Equation 2.18 gives an expression for the concentration of the excited state population as a function of time

$$[M^*](t) = [M^*]_0 e^{-(k_F t)} \qquad \textbf{Equation 2.19}$$

where and $[M^*]_0$ is the concentration of M* at t= 0.

The property observed during fluorescence experiments is the fluorescence intensity, I, which is directly related to the excited state population:

$$I(t) \propto k_R[M^*] \qquad \textbf{Equation 2.20}$$

substituting for [M*] from Equation 2.19 gives

$$I(t) = I_0 e^{\frac{-t}{\tau_f}} \qquad \textbf{Equation 2.21}$$

where I_0 is the intensity at the time of the excitation pulse ($\propto k_R[M^*]_0$) and $\tau = (1/k_F)$. τ is known as the fluorescence lifetime (the lifetime of the excited state population). Equation 2.21, relates the observable property of intensity to the fluorescence lifetime and allows its determination experimentally. One experimental method for obtaining τ is 'time-correlated single photon counting' (TCSPC) and this is discussed in greater detail in the subsequent sections of this thesis.

2.1.6 Time Correlated Single Photon Counting

Time-correlated single-photon counting (TCSPC) is the experimental technique used throughout this work in order to determine the fluorescence lifetime(s) of the fluorophores under investigation. TCSPC is used to record the time interval between excitation of a fluorophore with a short pulse of light and detection of the first photon of fluorescence from a sample. By repeating this experiment many times, a distribution of arrival times for individual photons at the detector is obtained. The distribution of these times allows determination of the fluorescence lifetime(s) of the sample. A generic experimental setup for TCSPC is shown in Figure 2.9.

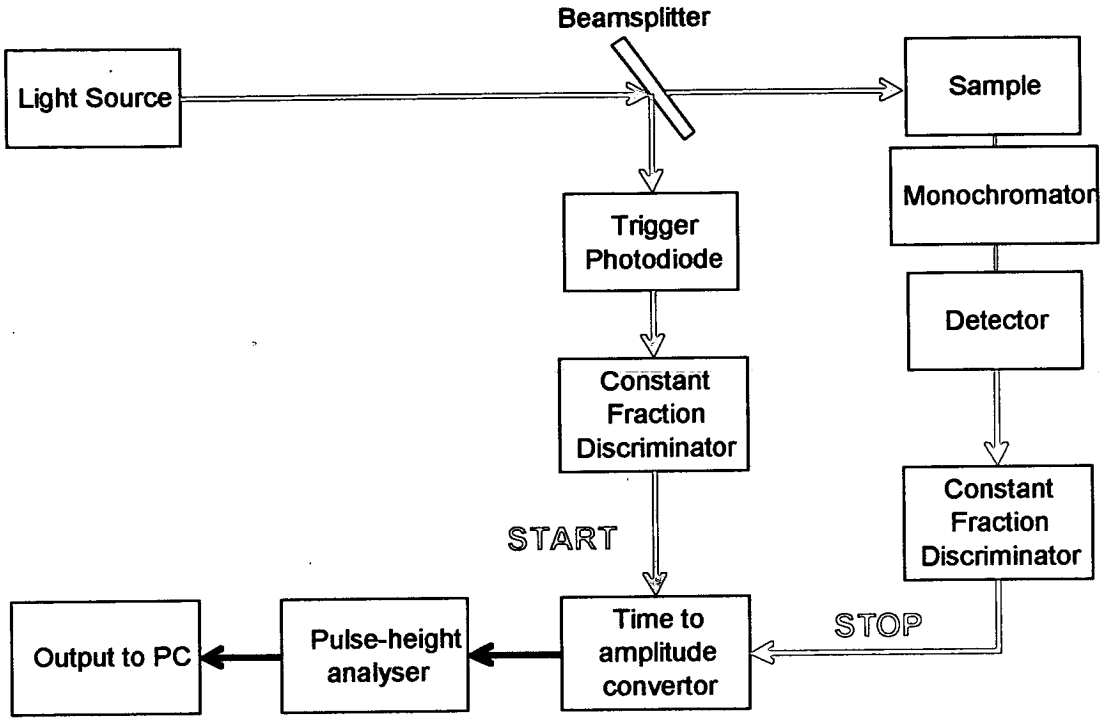

Figure 2.9- Schematic of components used to perform TCSPC measurements

A light source, such as a flashlamp or laser, is used to produce short (femtosecond-nanosecond in duration), pulses of light at a high repetition rate. With each optical pulse an electronic 'start' pulse is simultaneously generated. Often this is done by splitting off part of the optical excitation pulse and directing it towards a photodiode, as shown in Figure 2.9. The photodiode converts the optical pulse to the electrical 'start' pulse. This passes through an electronic device called the 'constant fraction discriminator' (CFD) and from there is relayed to the time-to-amplitude converter (TAC). The TAC, which can be considered analogous to a stopwatch, is effectively a capacitor that begins to charge at the arrival of the start pulse. The operation of the TAC and CFD are discussed in greater detail in the discussion that follows.

The remainder of the optical pulse is directed toward the sample. Excitation of the fluorophore leads to the emission of photons, some of which impact on the detector. The detector converts the energy from each photon into an electrical pulse. The first pulse released from the detector is used as the 'stop' pulse. It travels via the CFD to arrest the voltage ramp at the TAC. The TAC is then discharged and the resulting electrical pulse has a height that is directly related to the time

between start and stop pulses. The pulse-height analyser converts the analogue pulse from the TAC into a digital signal, which is registered as a single count on a histogram of fluorescence intensity (counts) against time. Collection of many thousands of these counts reveals an exponential decay curve that allows determination of the fluorescence lifetime(s) for the sample under investigation.

The timescale of the TCSPC experiment is such that both the generation of pulsed light and the detection of fluorescence are non-trivial. The discussion below outlines the techniques used throughout this work and the experimental implications of the approaches adopted.

2.1.6.1 Pulse Generation

The light source for this work used was a tuneable Ti:sapphire laser that produced pulses of light with a wavelength between 700nm and 1000nm, of approximately 200fs in width and with a repetition rate of 76MHz (one pulse approximately every 13ns). The Ti:sapphire laser uses passive modelocking in order to produce these pulses of light. As well as acting as the lasing medium, the Ti: sapphire crystal refracts light as a function of intensity. This effect is called the Kerr Lens effect and results in the dispersion of low powered light. Intense light is allowed to pass through the crystal with relatively little beam divergence. By placing an adjustable slit beyond the Ti: sapphire crystal the dispersed, low powered light can be clipped from the edges of the laser beam. This attenuation results in the amplification of the intense part of the beam only and leads to the generation of pulsed light. The Ti:sapphire crystal emits by stimulated emission over a range of wavelengths. The tunability of the laser is the result of a birefringent filter in the laser cavity. The filter rotates the plane of polarization of the beam as it passes through it. The alignment of the filter is set such that only light of the desired wavelength is rotated by 180°. A mirror is used to reflect the beam back through the birefringent filter, where only the light that has been rotated by 180° passes through the filter without attenuation. Hence light of the desired wavelength is amplified and output from the laser.

The light that is output from the Ti:sapphire laser is not useful for the present experiments for two reasons. The wavelength of the output is too long to excite most fluorophores directly since they are generally excited in the ultra-violet and visible regions of the spectrum. Furthermore, by

using the output directly from the Ti:sapphire laser, light pulses would arrive at the sample every 13ns. The consequence of this is that the fluorescence intensity is only allowed to decay for the 13ns period between any two successive pulses. Fluorescence from many fluorophores persists for much longer than this and this leads to an effect whereby the photons of fluorescence from the molecules excited by pulse *n* are still arriving at the detector as those resulting from pulse *n+1* begin to arrive. Hence, it becomes impossible to correlate any given 'START' pulse with the correct 'STOP' photon and the resulting 'decay curve' is meaningless.

The pulse repetition rate is reduced using a Coherent Model 9200 pulse picker. The pulse picker uses an acousto-optic Bragg cell in order to diffract the incoming laser beam. By applying a mechanical shear to the cell (in the form of an acoustic wave) a change in the refractive index of the cell is induced. This cell enables the path of the laser beam to be altered at a controlled frequency. The frequency of this distortion is typically set to deflect one pulse in sixteen in this manner. By deflecting this pulse toward the sample and blocking all other pulses an output from the pulse picker with a frequency of 4.75MHz (one pulse every 210ns) is obtained. The operation of the pulse picker significantly reduces the average power of the laser beam.

A harmonic generator is used in order to frequency double (or triple) the light from the Ti:sapphire laser. Frequency doubling is achieved by using a crystal which responds in a non-linear fashion to the electric field of the incident light. When light interacts with the crystal, an electronic polarization in the molecular structure of the crystal is induced (since the electrons oscillate relative to the atomic nuclei) and a dipole moment results. Expressed per unit volume, this dipole moment is termed the polarization, P, of the material. The polarization is typically linearly dependent on the applied electric field, E. The relationship between polarization and electric field in non-linear materials is given by Equation 2.22.

$$P = \varepsilon_0\left(\chi_1 E + \chi_2 E^2 + \chi_3 E^3 + \ldots\right) \qquad \textbf{Equation 2.22}$$

where ε_0 is the permittivity of light, χ_1 is the linear susceptibility and χ_2, χ_3... are the non-linear optical coefficients.

An electric field oscillating with angular frequency ω ($=2\pi\nu$) can be written

$$E = E_0 \sin \omega t$$ **Equation 2.23**

Substituting into Equation 2.22 gives

$$P = \varepsilon_0 \left(\chi_1 E_0 \sin \omega t + \chi_2 (E_0 \sin \omega t)^2 + \chi_3 (E_0 \sin \omega t)^3 + \ldots \right)$$ **Equation 2.24**

The second term of Equation 2.24, $\varepsilon_0 \chi_2 E_0^2 \sin^2 \omega t$, can be re-written as $\frac{1}{2}\varepsilon_0 \chi_2 E_0^2 (1-\cos 2\omega t)$. Hence, the polarization contains a term that is oscillating with a frequency that is twice that of the incident radiation. Since a dipole oscillating in this manner gives rise to an electromagnetic wave of the same frequency, some light with double the frequency of the incident light must be produced by the crystal. Since the incident light in this instance is laser radiation with a relatively high power density, the second harmonic irradiance is significant. The alignment of the non-linear crystal relative to the laser beam is such that phasematching is achieved between the fundamental and generated second harmonic light. This ensures that both fundamental and the second harmonic light travel at the same velocity through the crystal and hence prevents destructive interference.

2.1.6.2 Detectors

A photomultiplier is used to detect single fluorescent photons and convert their energy into electrical pulses. TCSPC experiments were carried out using a microchannel plate (MCP) photomultiplier tube. The MCP is a metal plate that is sandwiched between a photocathode and an anode. The channels in the plate are in the range of 6μm to 25μm in internal diameter. These channels act to amplify an electronic signal as shown in Figure 2.10.

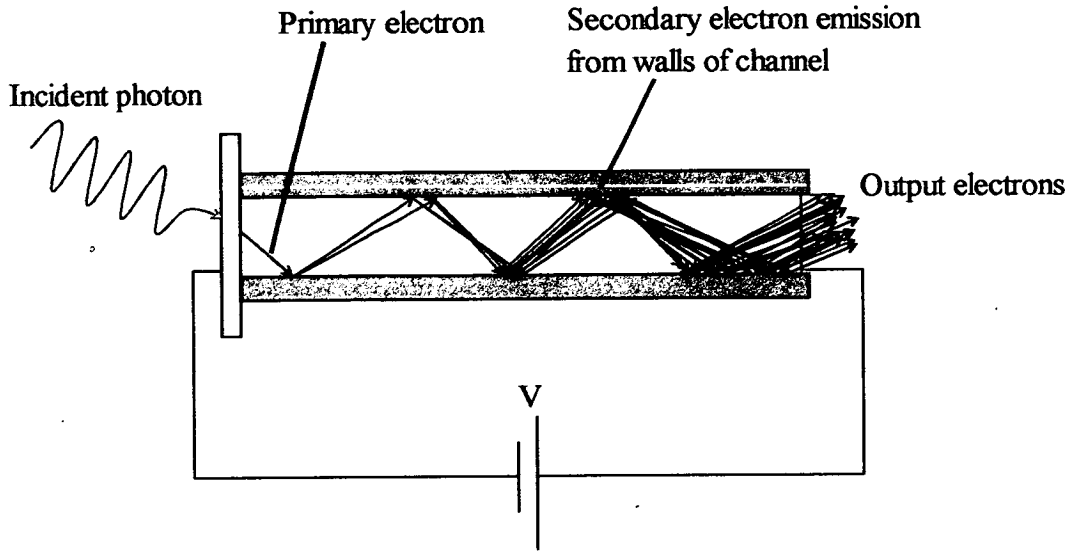

Figure 2.10- Schematic of the mechanism of action for a single channel of a MCP photomultiplier

Impact of a photon on the photocathode causes the emission of a photoelectron. The potential difference across the MCP causes the photoelectron to accelerate toward the anode. The photoelectron collides with the channel walls and causes the emission of several secondary electrons. These electrons collide with the channel walls a little further along and the repetition of this process leads to a logarithmic increase in the current of the channel. It is typical for the current to be amplified 10000 times during this process.

The most significant property of the photomultiplier when used in TCSPC is the transit time spread (TTS). This is the random variation in the time it takes for electrons to travel through the detector and is the property that limits the time resolution of the TCSPC experiment. TTS occurs because there are many possible routes through the PMT for any given electron. Figure 2.10 illustrates this phenomenon for the MCP where a single incident photon leads to an electrical signal that gives a distribution of possible arrival times for the photon. Narrowing the channels of the MCP leads to a decreased TTS.

Figure 2.11 shows a typical instrument response function (IRF). The IRF is recorded by scattering some of the incident light from a non-fluorescent sample into the detector. It shows the spectrometer's perception of the excitation pulse arriving at the sample. The full width at half

maximum intensity (FWHM) of the IRF is predominantly determined by the transit time spread for the MCP. However, it is also affected by the physical properties of the sample used, the wavelengths of the excitation and emission light and the settings used for the electronic components of the spectrometer, particularly the TAC. Figure 2.11 shows that the spectrometer detects the laser pulse, with a FWHM of ~200fs, as a pulse of 60ps FWHM followed by a low intensity 'afterpulse'. It is important to record the IRF because of the difference between the recorded width of the excitation pulse and the width of the pulse incident on the sample. This effect must be taken into account during the fitting procedure for fluorescence decay curves described in Section 2.1.6.5.

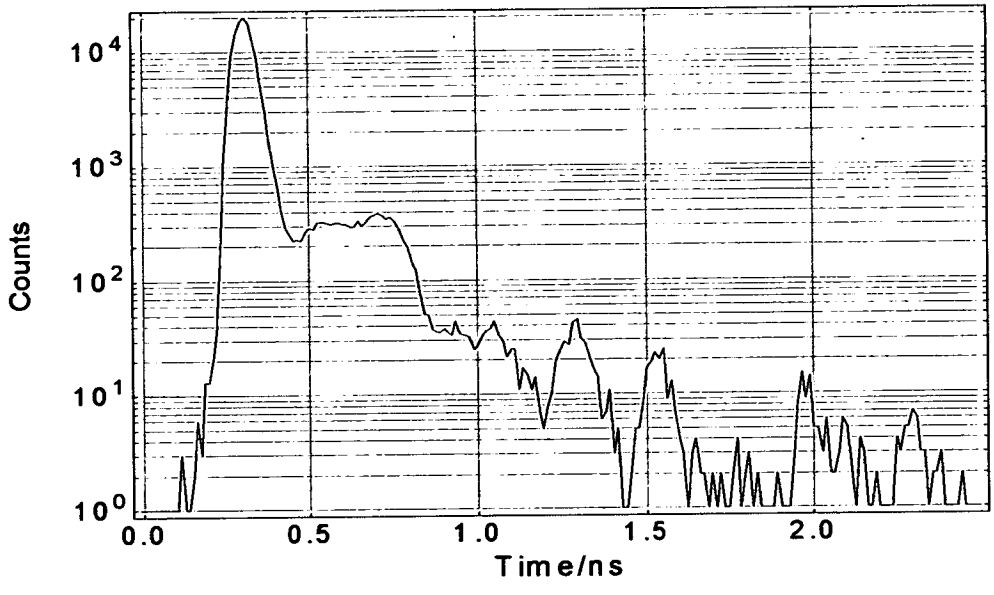

Figure 2.11- An instrument response function with FWHM of 60ps. Note that the y-axis is shown on a logarithmic scale

2.1.6.3 Electronics- The Constant Fraction Discriminator

The electronic pulses output from the PMT can vary in amplitude. This variation can affect the timing of the stop pulse for the TAC, as shown in Figure 2.12. If detection of an incoming pulse is set to a constant voltage level (threshold), then the determined time of arrival of any one pulse depends on the amplitude of that pulse. This mode of pulse detection is called leading edge

discrimination. The spread of arrival times with pulse amplitude results in a corresponding broadening of the instrument response function.

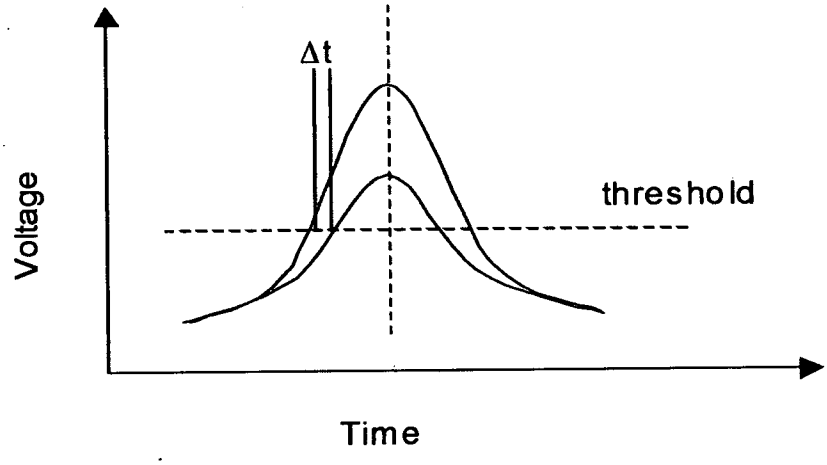

Figure 2.12- Leading edge discrimination

In order to avoid the broadening of experimental time resolution caused by leading edge discrimination, constant fraction discrimination is used, Figure 2.13.

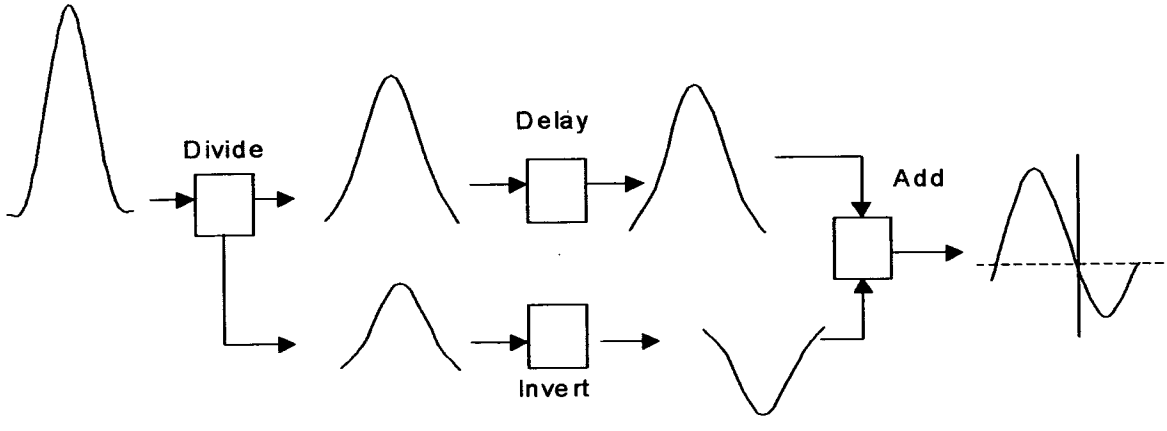

Figure 2.13- Constant fraction discrimination

In constant fraction discrimination, the incoming pulses from the photomultiplier are divided, by a predetermined fraction, into two pulses. One part of the pulse is delayed by about half its

width, whilst the other is inverted. The pulses are recombined giving a new profile whose potential crosses zero at a point that is independent of pulse amplitude. The TAC can be set to detect this zero crossing point and, hence, determine the time of arrival of a pulse independent of its amplitude.

2.1.6.4 Electronics- The Time to Amplitude Converter

The TAC is used to convert the time difference between start and stop pulses into an electrical signal. The mode of operation of the TAC is such that, when a stop pulse is detected, the timing capacitor is discharged and an output pulse is generated. This pulse is directly proportional in height to the time between start and stop pulses. Following discharge the TAC is reset, ready to receive another start pulse. These processes result in a period of 'dead time' in the operation of the TAC, during which, no incoming signals can be detected. In the system used in the current work, this dead time is less than 150ns in duration.

Pulse pile-up occurs as a result of more than one pulse arriving at the TAC, during a single TAC cycle. In this instance, only the first arriving photon will be detected. This leads to a bias of the TAC towards shorter lifetime emissions. Pulse pile-up is avoided by using a count rate that is significantly lower than one photon per excitation pulse. This condition ensures that the probability of a photon being detected is uniform over the range of the TAC and that the probability of a second photon arriving in the same excitation cycle is negligible. Hence, it is possible to obtain a true representation of the exponential decay curve of the species under investigation.

2.1.6.5 Data and Analysis

An example of the data obtained from a TCSPC experiment is shown in Figure 2.14.

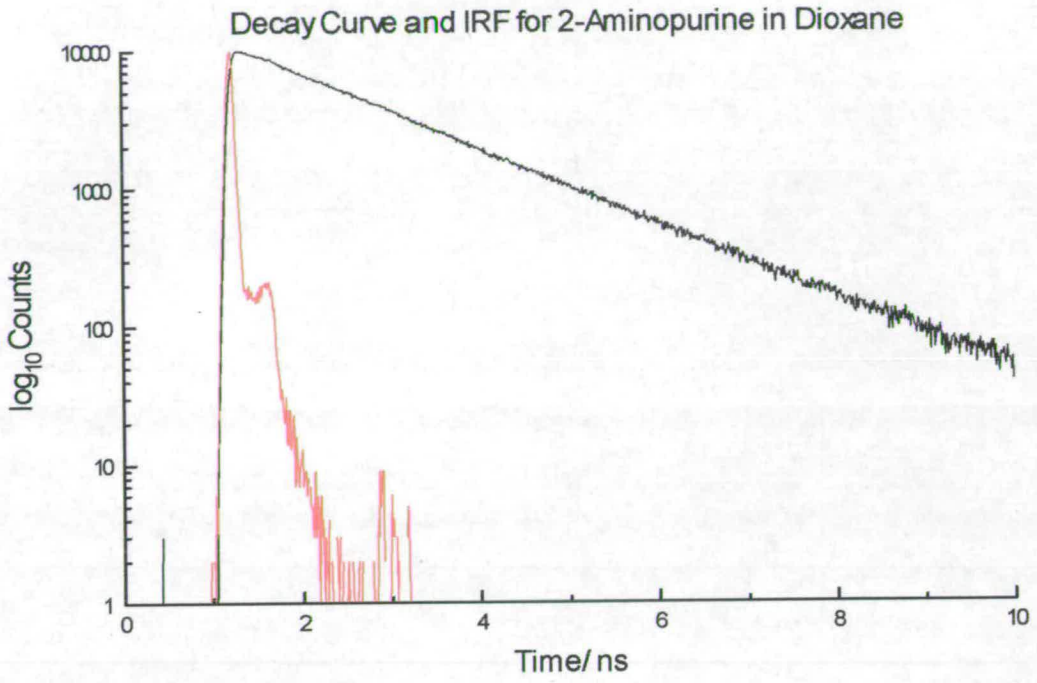

Figure 2.14- Example of data obtained from TCSPC experiment

Figure 2.14 shows a single exponential decay curve (black) for 2-aminopurine in dioxane. Also shown is the instrument response function (IRF) determined for this experiment (red). The number of counts per channel is plotted on a logarithmic scale in order to illustrate the distribution of the IRF more clearly.

A fluorescence decay can be fitted based on the kinetic principles discussed in Section 2.1.5. The decay curve is fitted iteratively according to

$$I(t) = A + \sum_i \alpha_i \exp^{(-t/\tau)}$$ **Equation 2.25**

where A is a constant to account for any background signal and α_i the amplitude for the i^{th} lifetime component for the sample, $\Sigma\alpha_i$ is normalised to unity.

A value for τ is determined by minimising the weighted sum of squares of residuals between the fitted function and the experimental data. This is referred to as least squares fitting and is done by minimising Equation 2.26.

$$\chi_a^2 = \sum_{i=n_1}^{n_2} \left\{ \frac{[I_0(t_i) - Y(t_i)]^2}{I(t_i)} \right\} \qquad \textbf{Equation 2.26}$$

where $I_0(t)$ is the background corrected intensity, Y(t) is the fitted function and I(t) is the uncorrected intensity. n_1 and n_2 are the first and last channels in the region of analysis respectively

The quality of any given fit is judged from the value of the reduced chi-squared function, χ^2

$$\chi^2 = \frac{\chi_a^2}{n_2 - n_1 + 1 - p} \qquad \textbf{Equation 2.27}$$

where p is the number of variable parameters in the fitting function. A χ^2 value of 1 indicates a perfect fit has been achieved. Values that deviate from this can be the results of either a poor fit or of 'imperfect' data. For the system used in this study a value for χ^2 of less than 1.2 typically describes a 'good fit'.

The goodness of fit of a decay curve can be illustrated by a plot of weighted residuals. The weighted residual values, r(t), between experimental and fitted points are determined using Equation 3.9.

$$r(t_i) = \frac{I_0(t_i) - Y(t_i)}{\sqrt{I(t_i)}}$$ **Equation 2.28**

Equation 2.25 fails to account for the instrument response function for the experiment when attempting to fit the decay curve. The finite width of the IRF, as compared with the incident pulse on the sample, means that the recorded fluorescence decay is distorted relative to the theoretical function that describes the decay curve for an infinitely narrow excitation pulse. This means that the experimentally observed decay curve, F(t), is actually the convolution of the theoretical decay curve, I(t), and the instrument response, E(t), such that

$$F(t) = E(t) \otimes I(t)$$ **Equation 2.29**

where ⊗ is the convolution operation.

The convolution integral, Equation 3.7, is evaluated by assuming that the IRF is comprised of an infinite number of infinitely narrow (delta) pulses. The amplitude of the delta pulses at any given time, t', is given by the function, E(t'). A delta pulse at time t' contributes E(t') I($t - t'$) to the observed fluorescence at any subsequent time, t. Hence, the intensity of the observed decay curve at time t, is given by the sum of the intensity contributions from all the delta pulses at times t' prior to t. The observed intensity F(t) can be expressed as an integral for the infinite sum of times from t to t':

$$F(t) = \int_0^t E(t')I(t - t')dt'$$ **Equation 2.30**

$$= E(t) \otimes I(t)$$

Convolution of the IRF with the theoretical decay curve allows the reconstruction of the experimentally recorded decay. Hence, by fitting the experimental decay with convolution of the IRF and the theoretical decay, the function describing the entire experimental decay curve, right from its rising edge can be determined. In practical terms, this allows the determination of fluorescence lifetimes with magnitudes significantly less than the width of the IRF. In the present system, it is possible to reliably determine lifetimes of down to approximately 20ps (where the IRF typically has a FWHM 50-60ps).

2.2 Biological Context

The purpose of this study is to understand the photophysical behaviour of 2AP and to use it as a probe of DNA structure and dynamics. In order to make an informed interpretation the data acquired, it is important to understand the biological systems under investigation. The following sections cover the principles of DNA and protein structure and will demonstrate the wider context of the investigations carried out in this thesis.

2.2.1 DNA Structure

Deoxyribonucleic acid (DNA) is a polymeric molecule whose linear (unbranched) structure is due to a repeating sugar-phosphate unit that forms the backbone of the molecule[11]. Attached to each of the deoxyribose sugars in the DNA backbone of is one of either the purine, adenine (A) and guanine (G), or pyrimidine, thymine (T) and cytosine (C) bases.

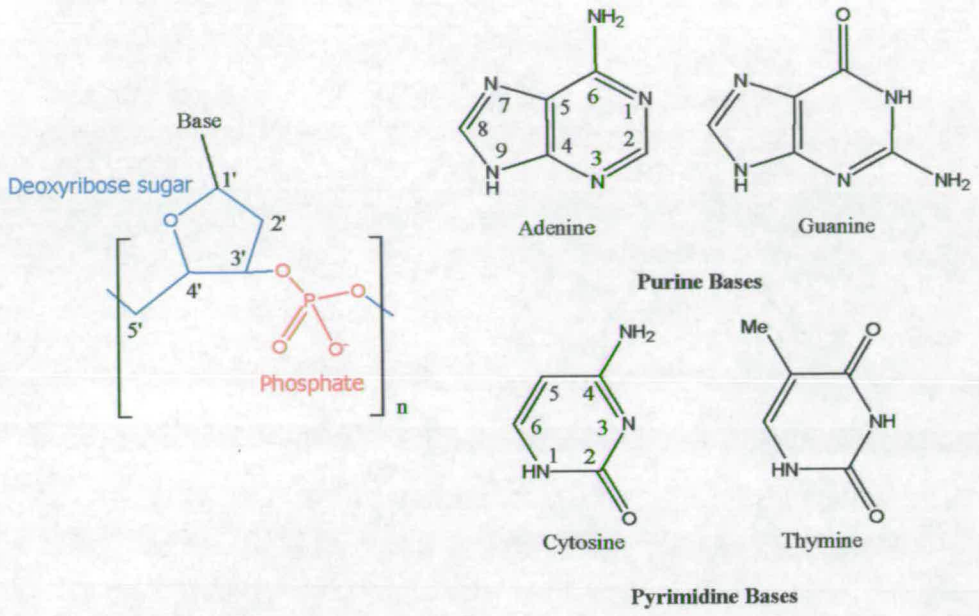

Figure 2.15- Structures and numbering schemes for the sugar-phosphate backbone and native bases of DNA

The structure and numbering schemes used to label a DNA strand are described in Figure 2.15. The deoxyribose sugar is labelled using primed numbers to distinguish it from the base numbering scheme. The sugar phosphate backbone is perpetuated through a 3'-5' phosphodiester bond. Purine bases are bound to the sugar C1' through a glycosidic bond at N9, whereas the pyrimidines are bound by N1. The subunit of DNA that contains just the base and deoxyribose sugar is referred to as a nucleoside. Nucleotides are nucleosides where the sugar is bound to one or more phosphate group(s), hence DNA is a polynucleotide.

The famous double helical structure derived from work by Wilkins[12], Franklin[13], Watson and Crick[1] is a result of two important features of the DNA structure. The hydrophobic nature of the bases relative to the DNA backbone means that by 'burying' the bases at the centre of the helix, a DNA duplex is stabilised in aqueous solution relative to two single DNA strands. Furthermore, the bases of the opposing DNA strands form stable hydrogen bonding interactions which maintain the fidelity of the double helical structure.

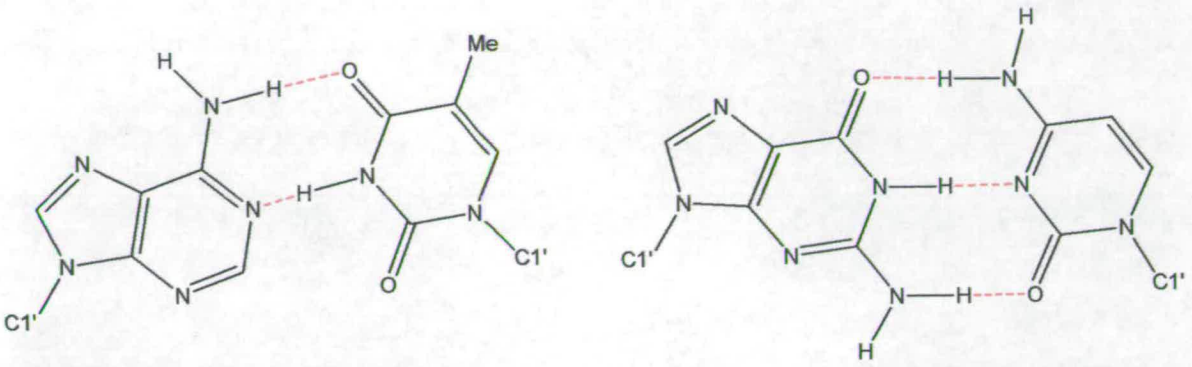

Figure 2.16- Watson-Crick base pairing with hydrogen bonds shown in red between adenine and thymine (left) and guanine and cytosine (right).

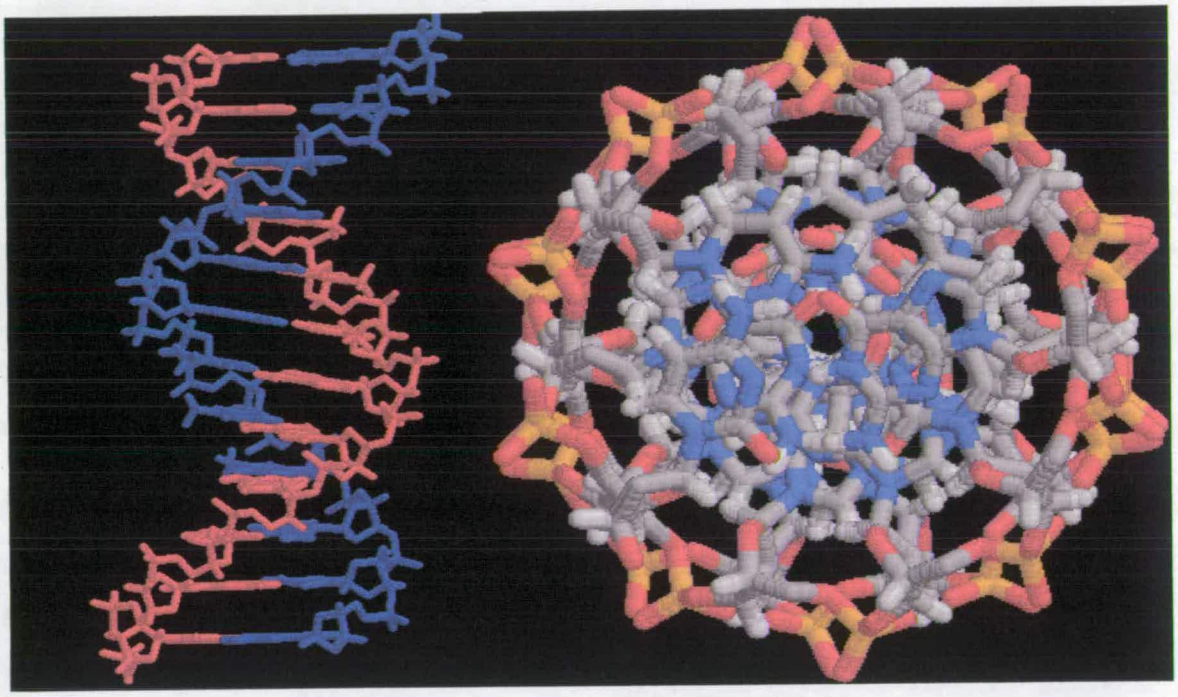

Figure 2.17- The double helical structure of DNA. Radial view showing the individual strands of the duplex (left) and axial view showing the bases packed into the centre of the helix (DNA structure taken from the protein data bank).

The two strands of the duplex are coiled about a central axis and the opposing strands run in opposite directions (3'→5' and 5'→3') to one another. In a 'normal' DNA duplex the bases pair up G-C and A-T in the manner shown in Figure 2.16. The bases lie almost perpendicular to the

alignment of the sugar-phosphate backbone and adjacent bases on a single strand are separated by approximately 3.4Å as shown in Figure 2.17.

The DNA helix completes one full turn every ten bases (34Å) and hence each successive base pair is rotated 36° relative to its neighbour. The helix is 20Å in diameter and can be of the order of centimetres in length, depending on the organism from which it originates[14].

2.2.2 Electron Transfer in DNA

The ability of DNA to transport charge over long distances through its π-stack is at present a somewhat controversial issue[15-19]. However, charge transport over relatively short distances (<20Å) has recently been established as an important process in the duplex[20]. In recent years 2AP has played a central role in the investigation of charge transfer in the DNA duplex, which will be discussed in greater detail in the chapters that follow. It is beyond the scope of this thesis to discuss electron transfer theory in detail. However, because the study of this process using 2AP accounts for much of the current literature on 2AP, it is important to give an overview of the principles of electron transfer in the context of the DNA duplex.

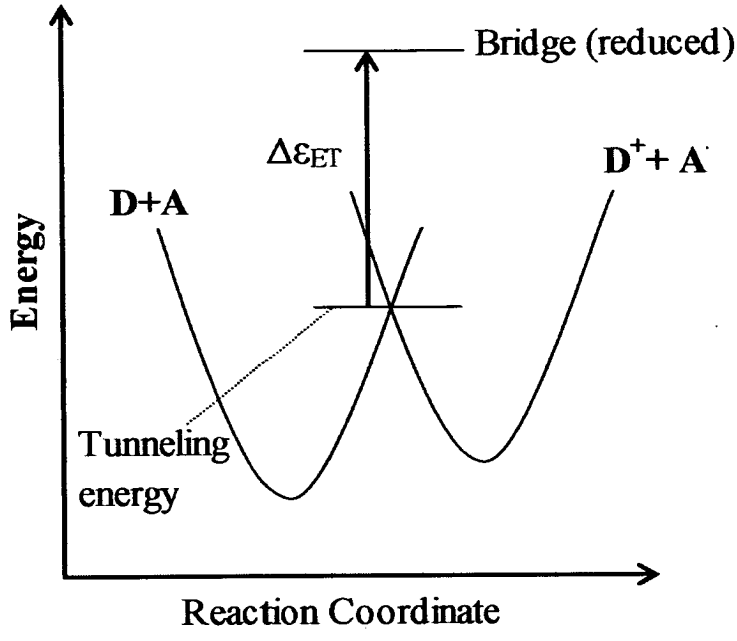

Figure 2.18- Schematic representation of the energetic levels involved in electron transfer between a donor (D) and acceptor (A) molecule , via a bridging molecule, which is reduced during the electron transfer process.

A schematic representation of the energetic steps required for electron transfer to occur in the DNA duplex is given in Figure 2.18[21]. Where the donor and acceptor bases are separated by one or more 'bridging' bases, the bridging base must be reduced for the electron transfer to occur efficiently.

The rate constant of electron transfer between donor (D) and acceptor (A) molecules along the duplex, k_{ET} is defined in Equation 2.31.

$$k_{ET} = \nu \kappa_E \kappa_N$$

Equation 2.31

Where ν defines the frequency of the nuclear motion along the transition state, κ_E is the probability of the reactants crossing the transition state to the products and κ_N is a nuclear reorganisation factor. κ_N is given by Equation 2.32.

$$\kappa_N = \exp(-(\Delta G^0 + \lambda)^2 / 4\lambda k_b T)$$

Equation 2.32

Where ΔG^0 is the thermodynamic free energy of the system and λ is a parameter to describe the extent of the nuclear motion required to reach the transition state. In the DNA duplex, where the interaction between the donor and acceptor molecules is weak, the rate of the reaction is determined by the rate of surface crossing at the transition state. Under these conditions the rate of electron transfer is described by Equation 2.33[21].

$$k_{ET}^0 = \sqrt{\frac{4\pi^3}{h^2 \lambda k_b T}} H_{AB}^2$$

Equation 2.33

Where H_{AB} describes a matrix element that defines the interaction between the reactants (D + A) and products (D^+ + A^-) at the transition state. For the case shown in Figure 2.18, where *n* bridging bases are involved in the transfer, H_{AB} is described by Equation 2.34[21].

$$H_{AB} = \frac{h_{Db} h_{bA}}{\Delta \varepsilon_{ET}} \left(\frac{h_b}{\Delta \varepsilon_{ET}} \right)^{n-1}$$

Equation 2.34

Where h_{Db} and h_{bA} describe the coupling between the donor and bridge and bridge and acceptor, respectively. For the case where there are more than one bridging base between the donor and acceptor molecules, the coupling between adjacent bridging base is described by h_b. $\Delta\varepsilon_{ET}$ is defined in Figure 2.18 and represents the energetic difference between the reduced state of the bridging base and the transition state between the donor and acceptor bases.

2.2.3 Protein Structure

Proteins are zwitterionic, linearly polymeric macromolecules that are composed of a series of amino acids linked through peptide bonds[11]. Figure 2.19 shows the structure of the L-amino acid subunits and how they combine to form a polypeptide.

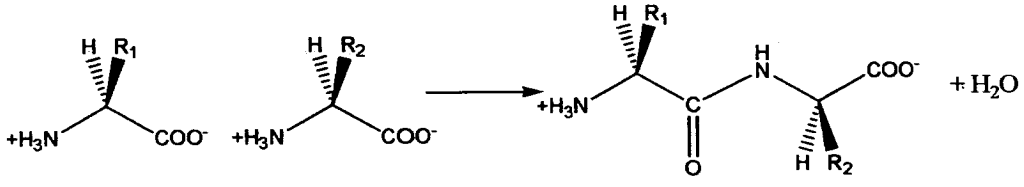

Figure 2.19- The formation of a peptide bond by two L-amino acids

There are twenty different L-amino acids found in proteins and all are based on the subunit shown in Figure 2.19. The possible structures for the 'R-group' side chain of each amino acid are shown in Figure 2.20.

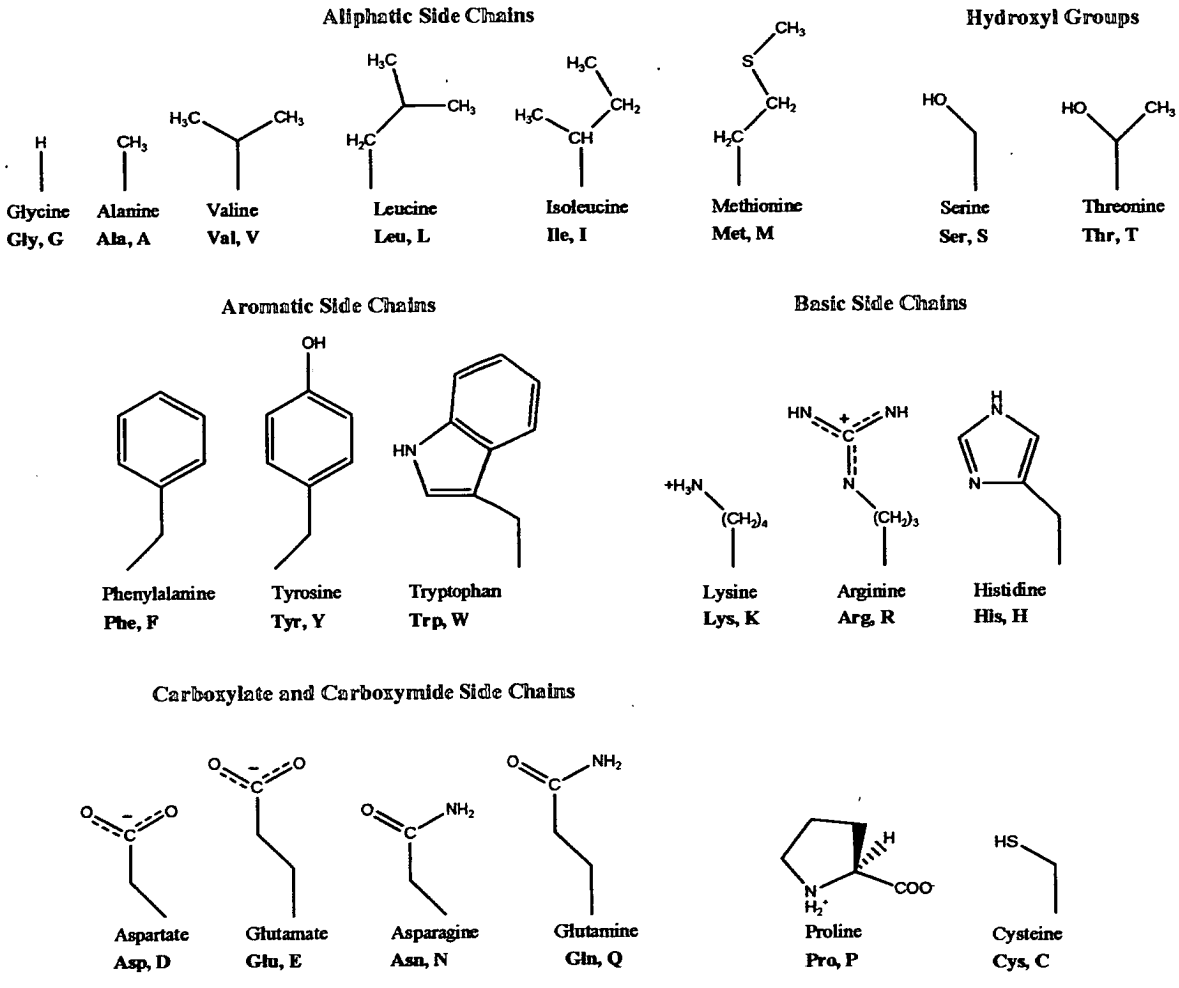

Figure 2.20- The 20 amino acid side chains that give proteins their structure and functional properties. Amino acid names, along with three and one letter abbreviations are given.

The subject of protein structure and function is vast and is not one that this thesis attempts to cover. It is important to note, however, that the atomic properties of the amino acid side chains provide the energetic driving forces that determine protein structure and function. For example, a protein that exists in an aqueous medium will have the aliphatic side chain amino acids buried at the centre of is three dimensional (ternary) structure, whereas the polar or charged groups are likely to be exposed to the solvent. Proteins are large, flexible macromolecules that are beautifully tailored to the tasks that they perform. The very specific interactions between the proteins investigated during this study and DNA are discussed in the relevant experimental chapters.

2.2.4 The Biological Function of DNA-Methyltransferases

The restriction (cutting) and modification of DNA is an important process in all living cells[22;23]. In prokaryotic organisms restriction-modification (R-M) systems play vital roles in both cell defence, gene expression and in the DNA repair mechanism. R-M systems are composed of endonuclease and methyltransferase (MTase) substituents that are responsible for restricting the replication of viral DNA and for labelling the cell's own (host) DNA, respectively.

Methyltransferases bind to the DNA within a cell and translocate it until they recognise a specific DNA sequence, typically of four to eight bases in length. Their function, upon finding this recognition sequence, is to transfer a methyl group from the cofactor, S-adenosyl-L-methionine (AdoMet) (see Figure 2.21), to either an adenine or cytosine base of the DNA duplex. In this way, a chemical distinction is made in the cell between host and invading viral DNA. The endonuclease part of the R-M system is able to take appropriate action based upon the degree of methylation of a given strand of DNA.

All of the methyltransferases rely on the presence of AdoMet in order to carry out methylation. AdoMet is the product of the addition of methionine and adenosine triphosphate and is ubiquitous in biological systems. It contains an electrophilic methyl group that catalyses methylation reactions in vivo. Figure 2.21 shows part of the 'activated methyl cycle', which shows how AdoMet and S-adenosine-L-homocysteine (AdoHcy) are related and are produced in vivo. Both of these compounds are utilised in the studies presented in this thesis.

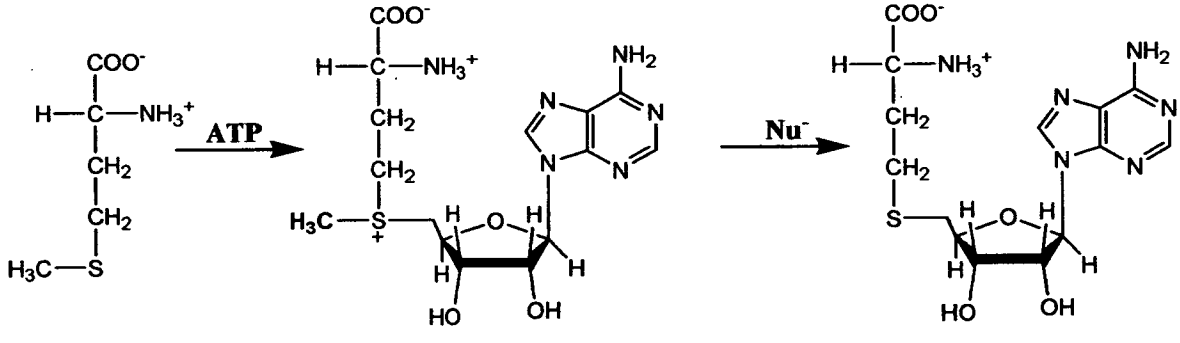

Methionine **AdoMet** **AdoHcy**

Figure 2.21- Conversion of methionine and ATP to AdoMet (activated methyl group shown in blue) and subsequent nucleophilic attack by Nu^- to give AdoHcy

The methyltransferases are subdivided into three classes based on their methylation target site. The three possible sites for methylation are the exocyclic amine group of adenine (methylated by the 'm^6A-MTases') and that of cytosine (methylated by the 'm^4C-MTases) and the carbon at the C5 position in cytosine (methylated by the 'm^5C-MTases'). The transformations performed by each class of methyltransferase are illustrated in Figure 2.22.

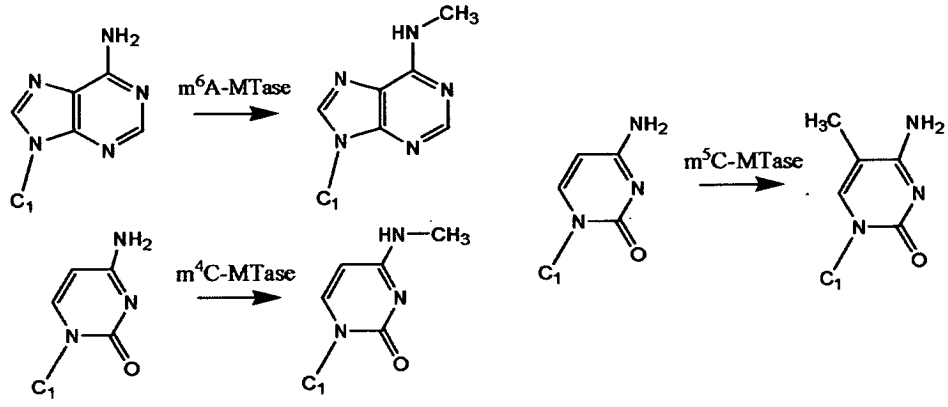

Figure 2.22- Transformations carried out by the methyltransferases. Note that 'C_1' denotes the C1 carbon atom in the deoxribose sugar of the DNA backbone.

The MTases used in this study and the mechanisms by which they perform their methylations are discussed in full in the experimental chapters that follow.

Chapter 3

Experimental

3.1 Introduction

Two main analytical techniques have been used in order to achieve the aims of this project. These were steady-state and time-resolved fluorescence spectroscopy. In this chapter a generic description of these methods is presented. Experimental details relevant to specific work are detailed in the appropriate chapter. A description of the materials used and the appropriate preparative schemes are also given.

3.2 Materials and Sample Preparation

2-aminopurine (>99%) was purchased from Aldrich and 2-aminopurine riboside (2APr) (>99%) from Sigma; both were used as received. Water was freshly distilled and ethanol, dimethylsulfoxide and 1,4-dioxane were of spectroscopic grade or equivalent and used as received from Aldrich. All solvents were checked for background fluorescence prior to use. 2AP and 2APr were used at a concentration of 10^{-5}M throughout this work unless otherwise stated. 2AP crystals were grown by slow evaporation from spectroscopic grade ethanol.

The 37-mer and 25-mer DNA oligodeoxynucleotides used with the MHhaI enzyme (named PT(GG), PC(AM), PG(GG)1, PG(GG)2 and PCGC in Chapter 6), M.HhaI and the T250G mutant of M.Hha1, cofactors s-adenosylmethionine (AdoMet) and s-adenosylhomocysteine (AdoHcy), buffer and DNA/protein crystals for this work were gratefully received from the Klimasauskas group at the Institute of Biotechnology, Vilnius, Lithuania. Oligonucleotide strands were originally obtained from Fermentas (Lithuania) and MWG Biotech (Germany). HhaI MTases (WT or T250G mutant) were overexpressed and purified as described by

Klimasauskas et al[24]. For the solution-phase experiments DNA oligodeoxynucleotides were annealed prior to use by heating the separate strands to 85°C in a water bath and allowing them to cool slowly overnight. A ten percent excess of the non-fluorescent oligodeoxynucleotide was used to ensure that none of the 2AP-labelled strand was left unbound in the final solution. Samples were prepared containing 1μM DNA, 3μM protein and 100μM cofactor. The buffer used was 10mM Tris-HCl, 0.5mM EDTA, 50mM NaCl to give a pH of 7.4. Crystals were grown using sitting-drop vapor diffusion at 19°C by mixing the solution containing the ternary complex M.HhaI-DNA-AdoHcy with an equal volume of well solution (50 mM sodium citrate pH 5.6, 1.2-2.0 ammonium sulfate, 0-15% glucose). The complexes formed rhombohedral crystals. The crystals were first washed with the well solution and then sucked from the wells into quartz capillary tubes of 1mm diameter (Hampton Research) using a micropipette. Once inside the capillaries, excess crystallisation liquor was removed from the area around individual crystals using fine paper wicks (Hampton Research). Care was taken to mount the crystals in such a way to prevent degradation whilst minimising background fluorescence from the crystallization solution. Figure 3.1 shows that in order to achieve this, only a small amount of the well solution was allowed to cover the crystal in the capillary.

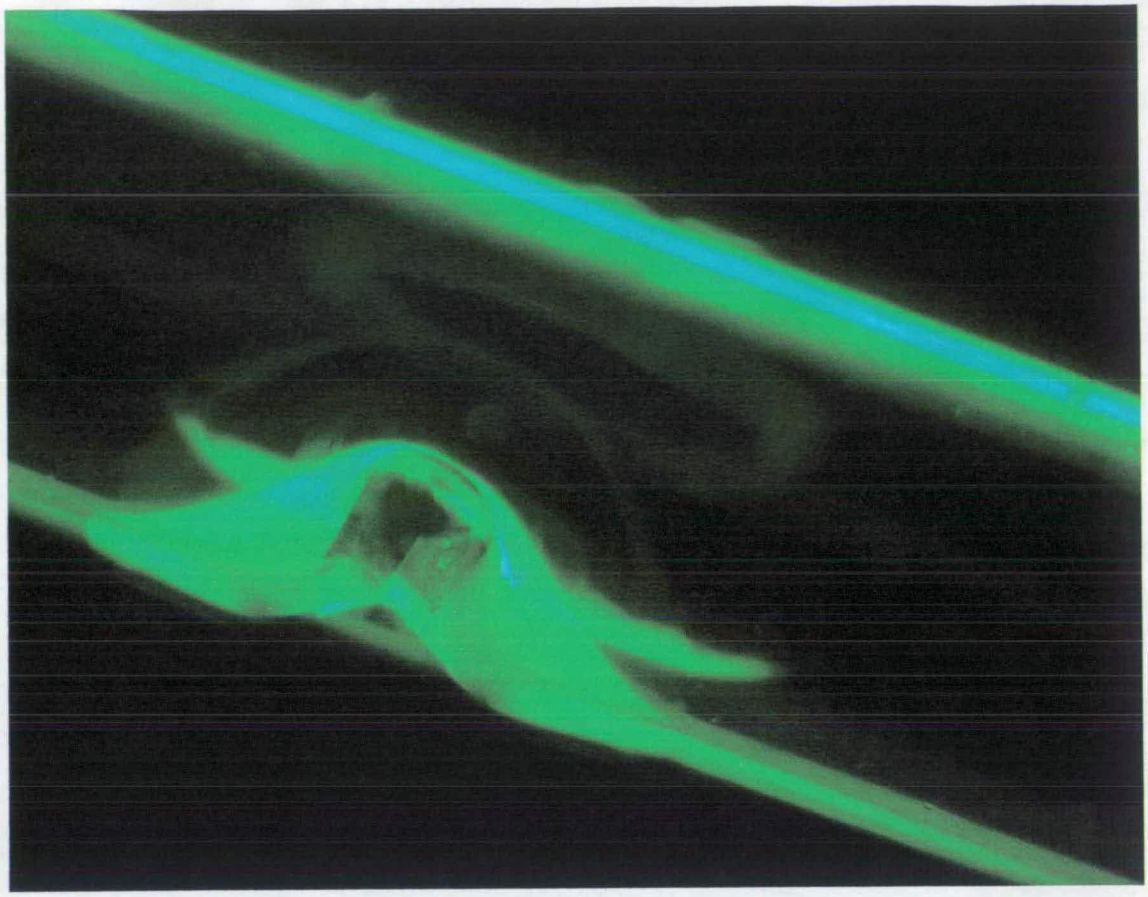

Figure 3.1- Microscopic image of a mounted DNA/ HhaI/ s-adenosylhomocysteine crystal. The image clearly shows the capillary tube (1mm diameter), the crystal and the small droplet of buffer solution that remains around the crystal.

Five other deoxyoligonucleotides were used during this study, described as duplexes PT(AC)1, PT(AC)2, PT(CC)1, PT(CC)2 and PT(TA) in Chapter 6. These were gratefully received from the Dryden laboratory at the University of Edinburgh and were synthesised using standard phosphoramidite chemistry[11] and purified by reverse phase HPLC. Annealing of duplexes was carried out by mixing a 1:2 ratio of the fluorescent: non-fluorescent oligodeoxynucleotide strands, followed by heating to 95°C and allowing the sample to cool slowly over several hours to room temperature. A 1μM concentration of DNA duplexes was used for TCSPC experiments.

The buffer used with these duplexes was 20mM Tris-HCl, 50mM NaCl, 0.1mM EDTA and 6mM $MgCl_2$ at pH 8.

3.3 Steady-State Fluorescence Measurements

Steady-state fluorescence measurements were made using a Jobin Yvon Spex Fluoromax Fluorimeter. Figure 3.2 is a schematic illustration of the components of the spectrometer.

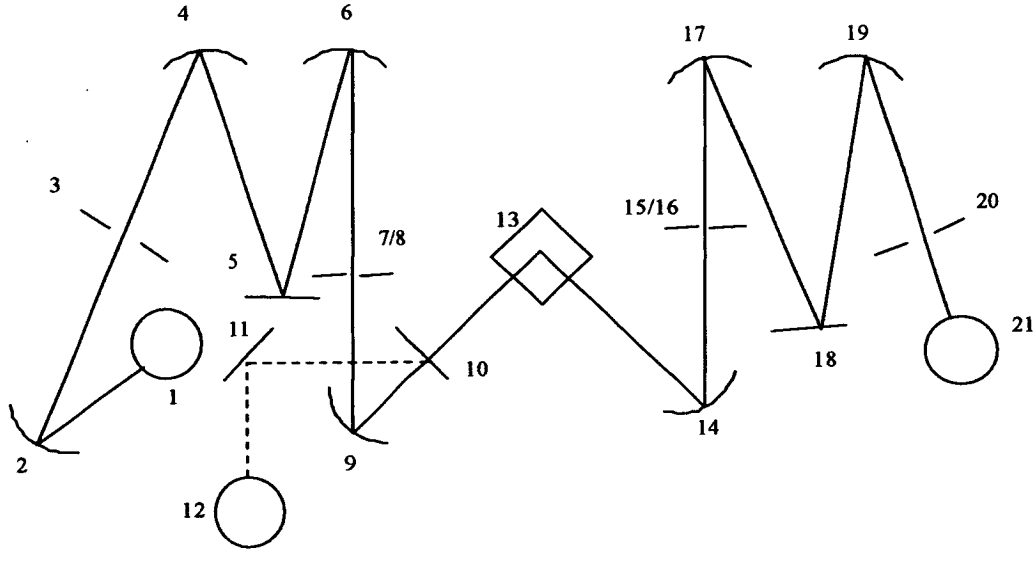

1. 150W Ozone-free xenon lamp
2. Collection mirror (excitation)
3. Entrance slit (excitation)
4. Collection mirror (excitation)
5. Grating
6. Focussing mirror (excitation)
7/8. Excitation slit/ shutter
9. Collection mirror (excitation)
10. Beam splitter
11. Deflection mirror (reference)
12. Photodiode reference detector
13. Sample position
14. Sample collection mirror
15/16. Emission shutter/ slit (emission)
17. Collection mirror (emission)
18. Grating
19. Focussing mirror (emission)
20. Exit slit
21. Photomultiplier tube

Figure 3.2- Schematic representation of the Fluoromax spectrometer

An ozone-free xenon lamp to supplies light over a wide spectral range from about 200nm up to around 700nm. Both excitation and emission monochromators employ modified Czerny-Turner mounted gratings allowing acquisition of both excitation and emission spectra. The excitation

grating has 1200 grooves/mm and is blazed at 330nm. The bandwidth of incident light is determined by the product of the excitation slit width and the system dispersion (4.25nm/mm for the 1200gr/mm grating). The gratings will effectively disperse light at wavelengths between 200nm and 900nm. Part of the incident light is split from the beam and used to obtain a reference signal. This is used to account for variations in the intensity of the xenon lamp as a function of wavelength. The sample was held in a 10mm path length quartz cuvette (Optiglass Ltd.), which is optically transparent between 170nm and 2700nm. Fluorescence from the sample is collected orthogonal to the incident light and dispersed by a monochromator allowing detection of emission at the required wavelength. Detection is by a red-sensitive photomultiplier tube, which enables detection of fluorescence as long as 850nm in wavelength. The spectrometer is coupled to a PC and controlled using Datamax software (Instruments SA Inc.). Parameters for individual experiments are set using this program.

Steady-state fluorescence measurements were also made on solid-phase systems (crystals with millimeter dimensions). Problems with sample mounting, scattered light and particularly emission intensity meant that the arrangement of the equipment described above became unsuitable for these particular measurements. Instead, the excitation light was transported from the sample chamber of the Fluoromax through a Glen Spectra fused silica fibre optic bundle to the sample. The optical fibre bundle produces a collimated beam of light of approximately 5mm in diameter. The excitation beam was directed toward the sample, which was resting on an optically transparent quartz cuvette as shown in Figure 3.3. Fluorescence was collected by a similar optical fibre and routed to the detection arm of the spectrometer. Emission was detected at an angle of approximately 45 degrees to the incident radiation, in order to minimise the amount of scattered light reaching the detection fibre.

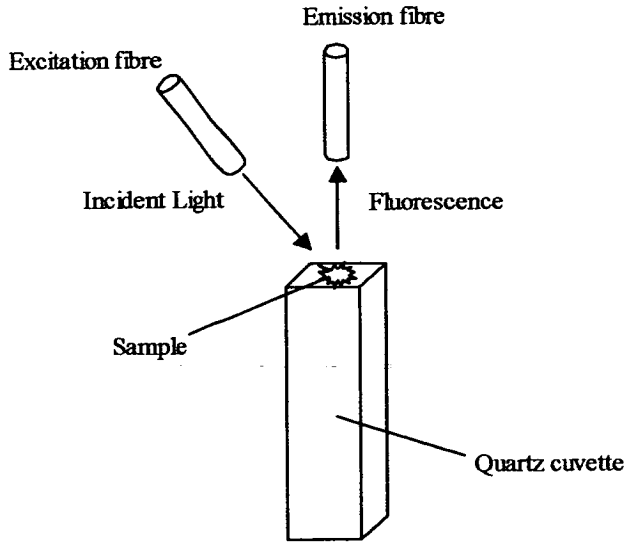

Figure 3.3- Experimental set-up for solid-phase, steady-state fluorescence measurements

3.4 Time-Resolved Fluorescence Measurements

Fluorescence lifetimes were determined using equipment housed in the COSMIC (Collaborative Optical Spectroscopy, Micromanipulation and Imaging Centre) facility at the University of Edinburgh. A schematic of the experimental equipment used to make these measurements is shown in Figure 3.4.

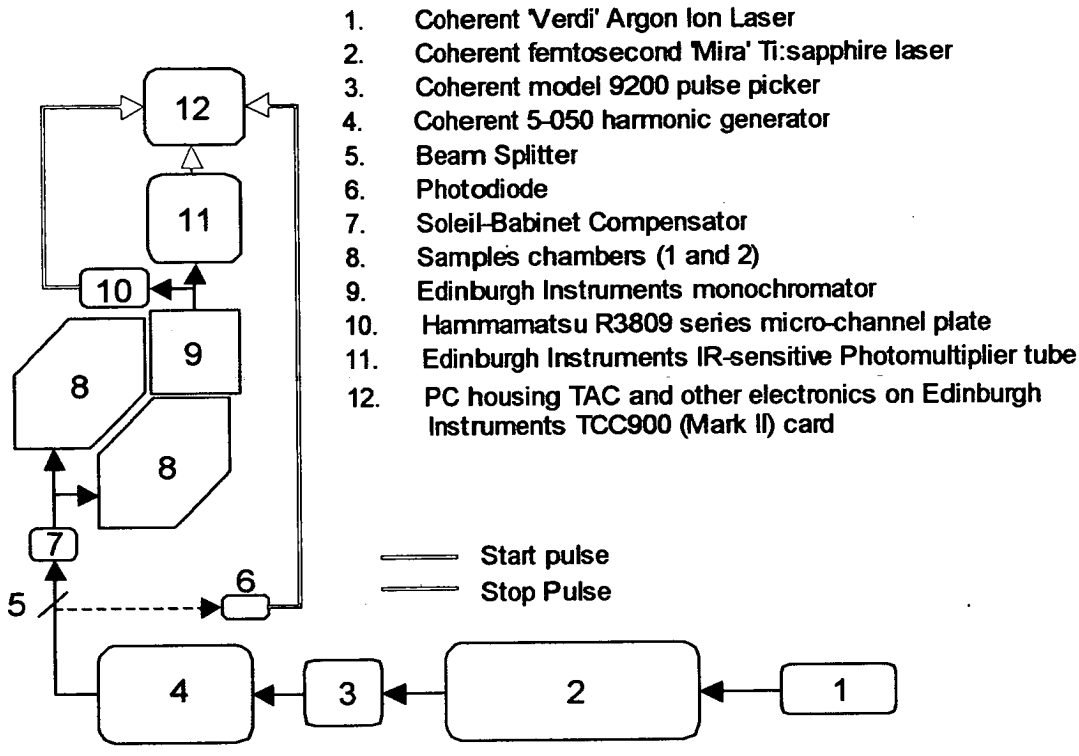

Figure 3.4 Schematic of equipment used for TCSPC in COSMIC

The excitation source for experiments was a tuneable, mode-locked Ti-Sapphire laser system. The Ti-sapphire laser is pumped by a Coherent Verdi V-10 continuous wave solid state laser. The Verdi operates using a Neodinium:Vanadate ($Nd:YVO_4$) lasing medium, which supplies light at 532nm at a power of 10W. The Coherent Mira 900-F Ti-Sapphire laser produces a pulsed fundamental beam that is tuneable over a wavelength range from approximately 700-1000nm. The passively modelocked pulses have a width of ~200fs and are produced at a repetition rate of 76MHz. This repetition rate is reduced to 4.75MHz using a pulse picker (Coherent 9200), giving a single pulse of light every 210ns. The light output from the pulse picker was either frequency doubled or tripled using a Coherent 5-050 harmonic generator. Average pulse power following frequency doubling/ tripling is typically a few milliwatts (doubled) or ~1mW for frequency tripled light. The operation of the Ti-sapphire laser, the pulse-picker and the harmonic generator are discussed in Chapter 2 of this thesis. Part of the output from the harmonic generator (~10%) is diverted to a fast photodiode. The photodiode converts the laser pulse to an electronic trigger (START) pulse. The amplitude of the START pulse (determined by the intensity of the incident light on the photodiode) was set to approximately -

700mV for all experiments. The discriminator for the START pulse was set to use constant fraction discrimination (CFD) with the level of the START threshold set at -300mV. This ensured that only pulses with a magnitude greater than 300mV trigger the time-to-amplitude converter (TAC). Both the CFD and TAC were located on the Edinburgh Instruments TCC900 photon counting card and controlled from the Edinburgh Instruments 'F900' software interface, whose operation and components are discussed further in Chapter 2. The TCC900 photon counting card allows decays with time resolution as high as 610fs per channel and has a dead time (the time it takes for the electronics to reset after recording an data point) of less than 150ns. This equates to a maximum count rate for the card of up to 6.6MHz.

The remainder of the excitation pulse is directed to one of the two spectrometer sample chambers via a Soleil-Babinet compensator, which allows control of the orientation of the plane of the polarised excitation pulse. The Soleil-Babinet compensator is a pair of quartz wedges that are aligned at 45 degrees to the incoming laser light. By varying the total thickness of the quartz that the beam passes through, the vertical or horizontal components of the incident beam can be optically retarded, this, allowing control of the plane of polarisation of the emerging light. The ability of the Soleil-Babinet compensator to rotate the plane of polarisation of light is dependent upon the wavelength of the light incident upon it. Hence, prior to performing an experiment a calibration factor must be set in the controlling software (Edinburgh Instruments F900) depending upon the wavelength of the incident light according to

$$\text{Calibration factor} = 41.62/\lambda$$

The excitation pulse is aligned vertically and, hence, for experiments where anisotropy measurements were not required, emission from the sample was detected at an angle of 54.4° (the 'magic angle') relative to this. The anisotropy of a fluorophore is determined by exciting it with vertically polarised light. Emission is detected perpendicular and parallel to the incident radiation and the anisotropy, r, of the sample is given by

$$r = \frac{I_{//} - I_{\perp}}{I_{//} + 2I_{\perp}} \qquad \text{Equation 3.1}$$

Where $I_{//}$ and $I_{\perp}$ are the intensities of emission parallel and perpendicular to the incident light respectively. By using a vertically polarised laser pulse to excite the sample for these experiments, a discrete population of the isotropically distributed fluorophores is preferentially excited; those with transition dipole moments aligned with the incident light. If, for example, vertically polarised emission is detected, then a fluorescence decay with a lifetime inversely related to the rate of rotational diffusion of the fluorophore will be observed. To avoid this complicating effect, the emission from a sample is collected at the magic angle (54.7 degrees), relative to the excitation pulse. The anisotropy at an angle, θ, relative to the incident light is given by

$$r = \frac{3(\cos^2\theta) - 1}{2} \qquad \text{Equation 3.2}$$

Setting $\theta = 54.7°$ gives $\cos^2\theta$ equal to 1/3 and, hence, r=0. Hence, observation of the emission at this angle omits any anisotropic effects from the recorded decay curve.

An aperture in the sample chamber is used to control the dispersion of the emission from the sample, prior to it reaching the monochromator. This aperture has a diameter of between 2mm and 37mm and is particularly important in controlling the width of the instrument response function (IRF) as it effectively controls the volume of sample from which fluorescence is detected. By narrowing the aperture, the area of photons that are incident on the detector is decreased, and thus the transit time spread through the microchannel plate is decreased. After the aperture, emission from the sample is focussed through a lens, through the emission polariser and is routed to the detector via two slits, one before and one after the monochromator. These slits were set to allow a 10nm bandpass unless otherwise indicated in the text.

Fluorescence emission was detected using either the Hammamtsu R3809-50 series microchannel plate (TCSPC) or the Edinburgh Instruments IR-sensitive photomultiplier tube (steady-state fluorescence). The microchannel plate has a transit time spread of 25ps and a dark count rate typically of 50Hz. Hence, the IRF for this detector was typically 60ps full width at half maximum intensity (FWHM). In a typical experiment a STOP count rate of approximately 20000Hz was used. The count rate was generally limited to this figure (the rate at which the MCP can function without incurring serious wear) but for highly quenched samples, including

2AP labelled DNA duplexes, the count rate was typically much lower (~1000Hz). Where necessary, the count rate was controlled using a pair neutral density filter wheels and the aperture in the sample chamber. Prior to each experiment, an IRF was collected, using scattered laser light from a dilute solution of Ludox (Aldrich). The IRF was collected at a low count rate, typically one tenth of that observed for emission from the sample. The IRF was collected using identical settings i.e. aperture diameter and slit widths to those used for decay collection. Neutral density filters were used to control the count rate for collection of the IRF. Fluorescence decay curves were collected to 10000 counts in the peak channel unless otherwise specified.

TCSPC measurements on solution phase systems were made in quartz cuvettes (Optiglass Ltd) with a 1cm path length. Excitation light was focussed into the cuvettes using a lens with a focal length of ~10cm. Excitation light that was not absorbed by the sample was directed into a beam stop in the sample chamber. Emission from the sample was collected at a right angle to the excitation beam, via an aperture with a variable diameter and a lens similar to that employed in the excitation beam path. An emission polariser was used and set at the magic angle relative to the excitation beam unless otherwise stated in the discussion that follows.

Solid phase samples were mounted in quartz capillaries. The capillaries were held vertically on a metal plate with a slit in it using crystallographer's putty, Figure 3.5

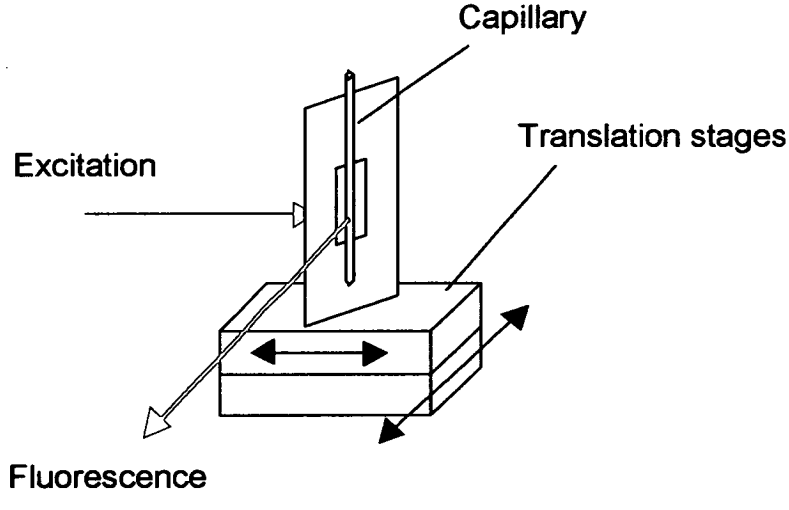

Figure 3.5- Schematic of the mounting stage for capillary tubes

The two orthogonal translation stages allow fine adjustment of the crystal's horizontal position. In the case of the crystals of 2AP, the capillaries were made 'in-house' from quartz tubing. DNA-protein crystals were mounted in thin-walled quartz capillaries of 1mm diameter (Hampton Research). Excitation beam height and direction was optimised using a scattering solution of Ludox (Aldrich) in distilled water. An instrument response function was also collected using this solution, which typically had a full width at half maximum height (FWHM) of 50ps. An appropriate long-pass filter (Schott) was used when making measurements on these solid-phase systems in order to prevent scattered light from the sample and capillary reaching the detector. Prior to making experimental measurements, this arrangement was tested for background fluorescence with an empty capillary. No significant emission was noted at the wavelengths used to detect 2AP emission.

Fluorescence decay curves were recorded using the Edinburgh Instruments 'F900' software. Individual decay curves were fitted using this programme. Global analysis of the data was carried out using Edinburgh instruments 'Level 2' software and Alango's 'FAST' software. Fits for both the global analysis and those for individual decay curves were carried out by initially attempting to fit the simplest (single exponential) model to the experimental data. By inspection of the residuals of the fit and the magnitude of the reduced χ^2 parameter, an assessment of the suitability of the fit was made. Extra terms were added to the theoretical decay as required. Fits were typically made from the rising edge of the decay curve, a few channels from the peak, to the end of the decay curve or a point where the photon counts for that channel was approximately 100, as appropriate. The background values used in fitting were estimated from the number of photons arriving before the rising edge of the IRF and were normally fixed during the fitting procedure.

Chapter 4

Spectroscopic Studies of 2-Aminopurine

4.1 Introduction

A grasp of the fundamental photophysical properties of any fluorophore is essential before measurements in more complex systems can be achieved reliably and interpreted accurately. This Chapter presents results from steady-state and time-resolved fluorescence studies together with UV-visible absorption measurements of the 2AP base and the 2AP ribonucleoside (Figure 4.1) in a range of solvents.

Stryer *et al* were the first group to report the steady-state fluorescence spectrum of 2-aminopurine (as the ribonucleoside)[25]. The spectrum has an excitation maximum at 303nm and an emission maximum at 370nm. Their study also illustrates the solvent dependence of the fluorescence emission of 9-ethyl-2-aminopurine (9E2AP), a more soluble analogue of 2AP. The emission shifts to the red with decreasing solvent polarity and the fluorescence quantum yield of 9E2AP decreases markedly with decreasing solvent polarity (0.68 in water to 0.013 in benzene). Over a range of pH, Stryer *et al* observe a red shift in the excitation spectrum of 2AP riboside at a pH of 2.5 ($\lambda_{ex\ max}$=310nm), attributed to a protonated form of the 2AP riboside. No emission is observed below pH 1, where the 2AP ring is thought to be protonated at all N-atoms.

Evans and co-workers have studied the steady-state fluorescence of the free 2AP base, Figure 4.1(a), noting similar properties to the earlier work by Stryer *et al*[26]. Evans *et al* reported a Lippert plot for 2AP, which shows how its Stokes shift is affected by solvent polarity. The Lippert plot was found to be linear for 2AP in a wide range of solvents, which suggests that the increase in Stokes shift for 2AP with increasing solvent polarity is due to general solvent effects. That is to say, the 2AP appears to undergo no specific (e.g. hydrogen bonding) interaction with

the solvents investigated. Dioxane and water, however, both give larger Stokes shifts than expected and this behaviour is attributed to their specific interactions with the 2AP molecules. In the case of water, the authors note that the excitation spectrum of 2AP is blue-shifted with respect to the other solvents. The emission spectrum in this case is shifted to the red, as expected, relative to 2AP in less polar solvents. The authors ascribe the blue shift in the excitation spectrum of 2AP in water to the ability of water to donate a proton to ground state 2AP. This assignment is somewhat contradictory to observations by Stryer *et al*, who note a red shift in the excitation spectrum of 2AP-riboside with decreasing solvent pH. Evans *et al* do not attribute the increased Stokes shift of 2AP in dioxane to any specific interaction.

Rachofsky, Osman and Ross studied both the steady-state and time-resolved fluorescence emission of 2AP as a function of solvent polarity[27]. For the five solvents investigated they observed similar steady-state trends to those previously reported by Stryer *et al* and Evans *et al*. The fluorescence lifetime of 2AP is noted as being monoexponential in four of the five solvents investigated (dioxane, DMF, ethanol and water) with 2AP in 2,2,2-tri-fluoroethanol exhibiting three lifetimes. The lifetime of 2AP is seen to increase with increasing solvent polarity, from around 2ns in dioxane to 11ns in water.

A more recent computational (complete active space self-consistent field (CASSCF)) study by Rachofsky *et al*[28] suggests a physical explanation for the increase in the quantum yield of 2AP with increasing solvent polarity. This study shows that the dipole moment of the $\pi\pi^*$ excited state is aligned closely to that of the ground state. However, the dipole moment of the $n\pi^*$ excited state lies in a significantly different orientation to that of the ground state molecule. In the ground state, solvent molecules in the immediate vicinity of the 2AP are oriented with the ground state dipole moment. Hence, these solvent molecules must reorient to a greater extent when the transition is to the $n\pi^*$ state as compared to the $\pi\pi^*$ state. As such, the $n\pi^*$ state will be destabilised relative to the $\pi\pi^*$ state upon excitation in polar solvents. Since the transition from the $n\pi^*$ to the ground state is forbidden, the destabilisation of this state leads to an increase in quantum yield, which is observed with increasing solvent polarity.

Dissolving free aminopurine base, adenine or 2AP, in a protic solvent allows the tautomerisation of molecules. Adenine is known to tautomerise by proton transfer between N7 and N9 (Figure 4.1). By analogy it seems reasonable to expect that 2AP could also adopt these tautomeric forms.

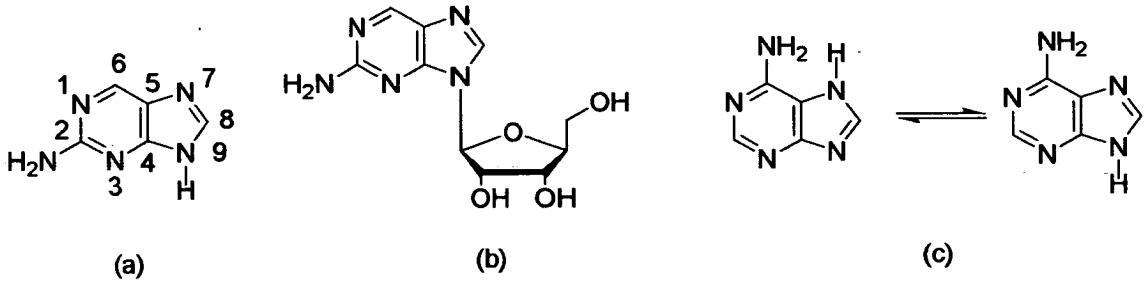

Figure 4.1- The structures of (a) 2AP (9-H tautomer), (b) 2AP riboside and (c) the 7H and 9H tautomers of adenine.

Tautomerisation in adenine has been studied in the solution phase by UV absorption and steady-state fluorescence spectroscopy (the 7H tautomer is fluorescent)[29], temperature jump measurements in conjunction with UV absorption[30] and most recently by ultrafast transient absorption spectroscopy[31]; in the gas phase by microwave spectroscopy[32], infrared and high resolution electronic spectroscopy[33]; and in computational studies[34;35]. The 9H tautomer of adenine is predominant in the gas phase, but the two tautomers coexist in polar solution at room temperature, because of the greater dipole moment of the 7H tautomer[30]. The fraction of the 7H isomer in solution has been reported as 6% in butanol[29] and 20% in aqueous solution[30]. For the parent molecule, purine, (i.e. 2AP without the amino group) the 7H and 9H tautomers have been found to exist in approximately equal proportions in aqueous solution at room temperature[36-39].

For 2AP, *ab initio* computational studies[40] have shown that, like adenine, only the 9H and 7H tautomers have low enough energy to be observed at room temperature. As for adenine, the 7H tautomer was predicted to have a significantly greater dipole moment than the 9H tautomer, 4.46D compared with 3.41D. Thus, the tautomeric equilibrium is expected to shift towards the 7H form in polar solution. In aqueous solution (using a bulk solvation model) the population of 7H tautomers was predicted to be 3%[40]. There is very little experimental evidence for tautomerism in 2AP. In a study of transition moments, Holmen *et al*[41] found that the linear dichroism (LD) spectrum of 2AP in stretched PVA films differed from that of related 9-

substituted molecules (which cannot tautomerise). They attributed this to the presence of a small amount of the 7H tautomer. In an early time-resolved fluorescence study, using flash lamp excitation, Santhosh and Mishra[42] found the fluorescence response function of 2AP in water to consist of a rise time of 2.1ns and a decay time of 24.6ns. They assigned the two lifetime components to the 9H and 7H tautomers. However, the validity of this work is questionable, since subsequent measurements with superior time resolution, including the work presented in this thesis, have found no evidence of a rise in the 2AP fluorescence response, nor a decay time as long as 25ns. Recently, an ultrafast transient absorption study of 2AP in aqueous solution reported the observation of a multi-exponential decay, implying heterogeneity of the chromophore in the excited state[43]. In addition to a picosecond solvent relaxation time, two nanosecond decay components were observed with lifetimes of ~3.5 ns and ~14 ns (these values have low precision because of the short (5ns) time window of the experiments). However, assignment of the two lifetimes to the 7H and 9H tautomers was ruled out because similar behaviour was observed for 9-substituted 2AP, in which tautomerism is prevented. Instead, the 3.5ns component was ascribed to a fluorescent state of the 9H tautomer and the 14ns component to a dark state of the same tautomer. This interpretation is inconsistent with results of time-resolved fluorescence measurements which find the fluorescence lifetime of 2AP in water to be ~12ns, as discussed below.

The fluorescence decay of 2AP in water is widely accepted to be monoexponential, with lifetime values of 11 to 12ns reported in the literature[41,27,8;44]. But, in previous studies, the fluorescence lifetime has generally been measured at only a single excitation wavelength and a single emission wavelength. In order to obtain a more complete picture of the photophysics of 2AP, and to explore the possibility of 9H-7H tautomerism, studies have been carried out to investigate the fluorescence decay as a function of both excitation and emission wavelengths in a range of solutions. Comparative measurements on 2AP riboside, in which the 7H tautomer is precluded, have also been undertaken.

4.2 Results

4.2.1 UV-Visible Absorption Spectra

Absorption spectra were recorded for 2AP in water and are shown in Figure 4.2.

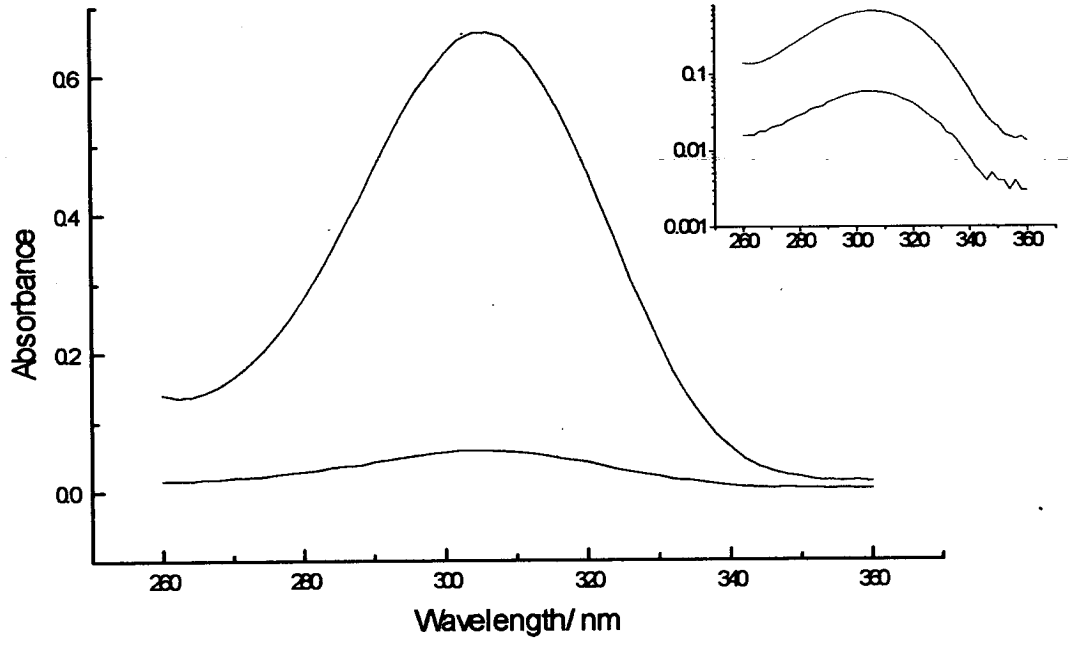

Figure 4.2- Absorption spectra for aqueous solutions of $1x10^{-4}$M 2AP (red) and $1x10^{-5}$M 2AP (black). Inset shows the same spectra on a logarithmic scale.

The recorded absorption spectra are in good agreement with previously reported spectra[25], showing a maximum absorption at 305nm and no apparent vibrational structure. The absorbance is linearly dependent on the 2AP concentration and the spectral profile appears to be independent of concentration. Hence, the molar extinction coefficient of the 2AP is not changed with increasing concentration, implying that there is no aggregation of the 2AP with increasing concentration, up to a concentration of 10^{-4}M. A solution with a maximum absorbance of ~0.1 at the excitation wavelength to be used is generally regarded as ideal for carrying out fluorescence studies. Hence, the work reported in the remainder of this Chapter was carried out using solutions with concentrations of $1x10^{-5}$M 2AP.

4.2.2 Steady-State Spectra

Steady-state spectra for 2-AP in water, 1,4-dioxane, ethanol and dimethylsulfoxide (DMSO) have been recorded. The spectra illustrate the effect of solvent polarity on the excitation and emission of 2AP, Figure 4.3.

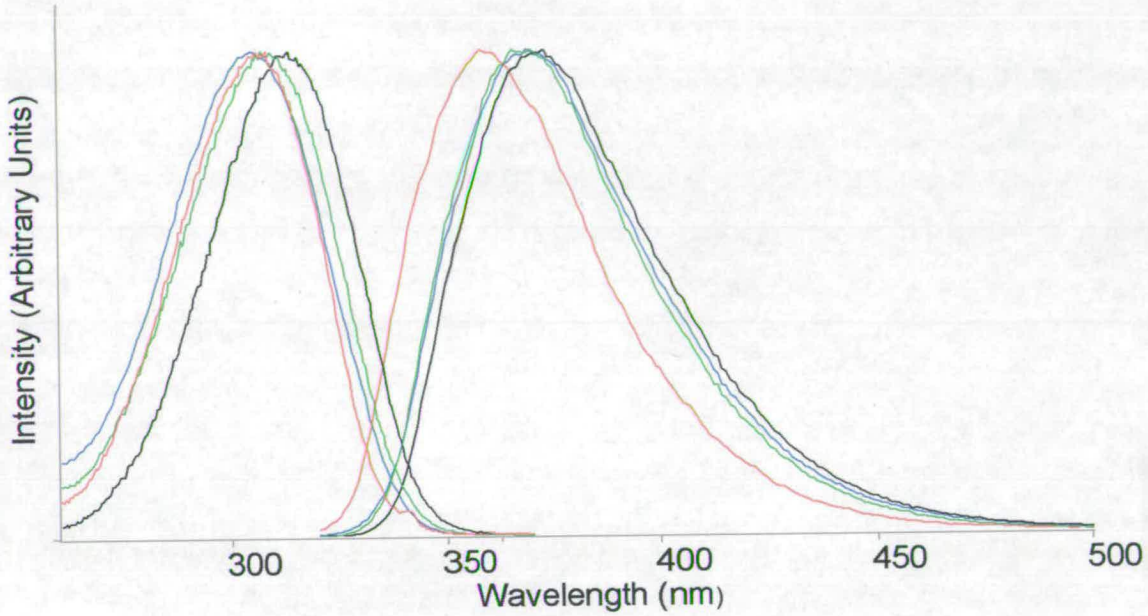

Figure 4.3-Excitation and emission spectra for 2-AP in water (blue trace), dioxane (red trace), ethanol (green trace) and DMSO (black trace). Excitation was at 310nm, emission at 380nm (370nm in the case of DMSO and water)

The steady-state spectra of 2-AP are relatively broad, with the emission spectrum particularly showing a long tail to the red edge of the spectrum. Neither excitation nor emission spectra show any vibrational structure at room temperature. There is some dependence of the peak of both excitation and emission spectra on solvent polarity. The dioxane emission spectrum is particularly blue-shifted relative to the other solvents. Table 4.1 summarises the shift in the spectral peak as a function of the orientation polarisability, f(ε,n), of the solvent, where f(ε,n) is given by

$$f(\varepsilon,n)=\frac{\varepsilon-1}{2\varepsilon+1}-\frac{n^2-1}{2n^2+1}$$ Equation 4.1

Where ε is the dielectric constant for the solvent and n its refractive index. The orientation polarisability describes the ability of a solvent to respond to the change in both the magnitude and direction of the permanent dipole of a solute molecule.

Solvent	f(ε, n)	Excitation max/ cm^{-1}	Emission max/ cm^{-1}	Stokes Shift/ cm^{-1}
Dioxane	0.0238	32573	27778	4796
DMSO	0.135	31949	26882	5067
Ethanol	0.289	32362	27100	5262
Water	0.32	32895	26882	6013

Table 4.1. Spectral peaks for excitation and emission spectra of 2AP in a range of solvents

The data from Table 4.1 is plotted in a Lippert plot in Figure 4.4.

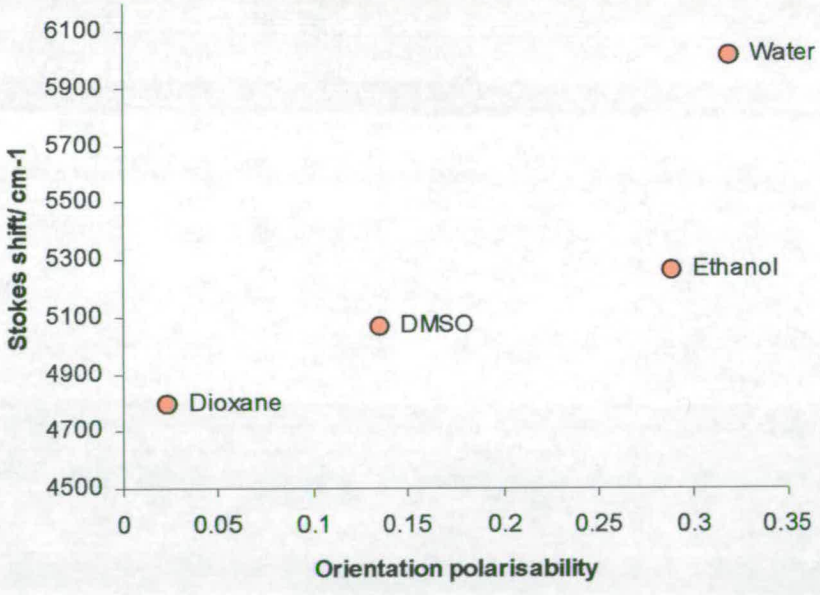

Figure 4.4- Lippert plot for 2AP in four different solvents

The changes in the steady-state excitation and emission spectral maxima of 2AP show that the Stokes shift for 2AP increases with increasing solvent polarity. This is in good agreement with previous work[25-27] and Figure 4.4 shows that Stokes shift is approximately linearly dependent upon the orientation polarisability. The Lippert equation states that

$$\bar{\nu}_E - \bar{\nu}_F = \frac{2}{hc}\left[\frac{\varepsilon - 1}{2\varepsilon + 1} - \frac{n^2 - 1}{2n^2 + 1}\right]\frac{(\mu_E - \mu_G)^2}{a^3} + k \qquad \text{Equation 4.2}$$

Where $\bar{\nu}_E$ and $\bar{\nu}_F$ are the maxima of the excitation and emission spectra in wavenumbers, respectively, h is Planck's constant, c is the speed of light, μ_G and μ_E are the permanent dipole moments of the ground and excited states, respectively, a is the radius of the spherical volume that the fluorophore occupies and k is a constant.

By inspection of Equation 4.2, it is evident that the linear dependence of the Stokes shift on f(ε,n), in Figure 4.4, indicates that the dipole moments of the ground and excited states are not perturbed by the solvent. Hence, it is possible to argue that no specific, electronic interactions (e.g. hydrogen bonding) take place between the 2AP and these four solvents.

Figure 4.5 shows that the excitation and emission spectra of 2AP in aqueous solution exhibit a small wavelength dependence. Comparison of the spectra in Figure 4.5 to those of the 2AP riboside (2APr), shown in Figure 4.6 illustrates that the shift is present. The shift is to the red with increasing emission wavelength in the excitation spectrum. Similarly, for the emission spectrum, the shift is to the red with increasing excitation wavelength.

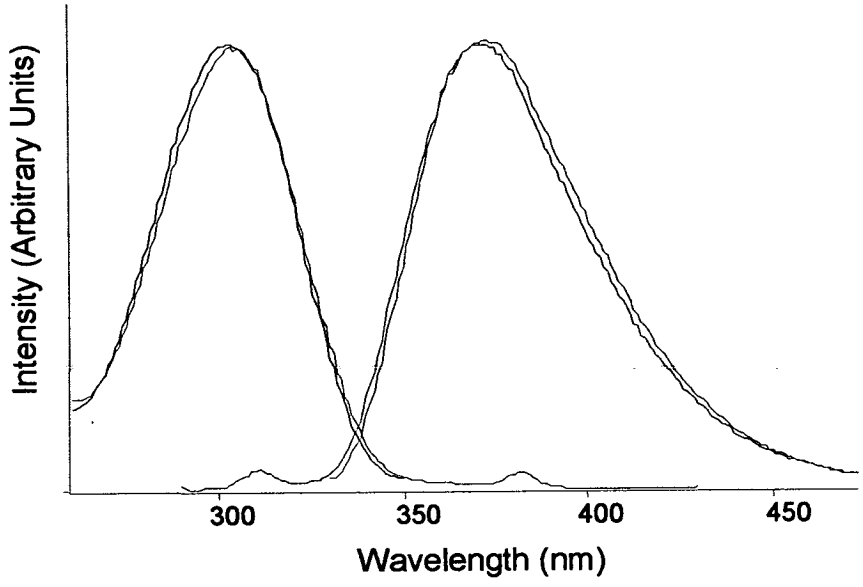

Figure 4.5- Excitation and emission spectra for 2-AP in water. Excitation spectra are at emission wavelengths of 360nm (black) and 440nm (blue). Emission spectra are at excitation wavelengths of 280nm (red) and 320nm (green).

The wavelength dependence of both the excitation and emission spectra is indicative of the presence of more than one molecular species in the solution. This shift is apparent for 2AP in all of the solvents investigated.

The steady-state spectra of 2-aminopurine riboside in water are shown in Figure 4.6. This shows that neither the excitation nor emission spectra of 2APr show any wavelength dependence. Hence, replacement of the N9H proton with the bulky ribose group appears to prevent the formation of two distinct chromophores in the solution.

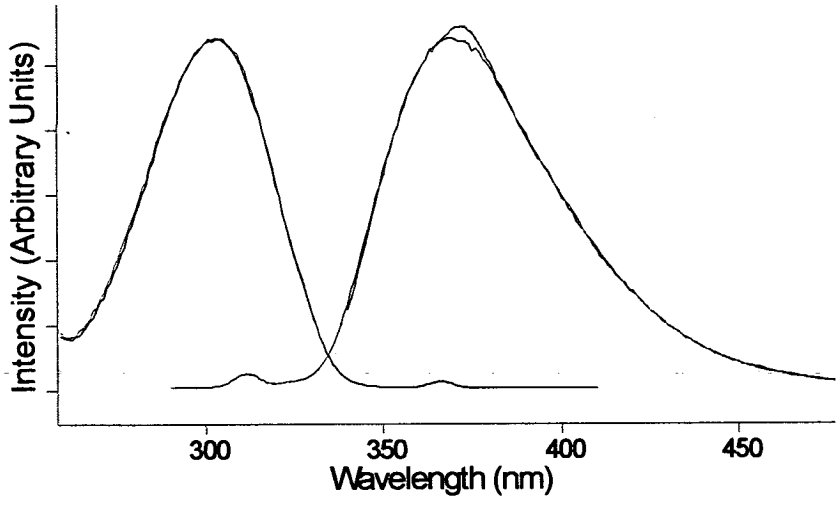

Figure 4.6- Excitation and emission spectra for 2APr. Excitation spectra at emission wavelengths of 350nm (green) and 420nm (black). Emission spectra at excitation wavelengths of 280nm (blue) and 330nm (red). Note that the red spectrum shows a Raman peak at ~370nm that distorts the peak of the spectrum slightly.

The evidence from these steady-state fluorescence measurements is consistent with the presence of N9H to N7H tautomerisation in 2AP in the solution phase. However, the spectral shifts upon which this argument is based are slight and no quantitative information is available on the extent of the tautomerisation of the 2AP molecules in each solvent. Time-resolved fluorescence experiments were carried out in order to investigate this system further.

4.2.3 Time Correlated Single Photon Counting

TCSPC was used to measure the fluorescence lifetimes of 2AP in the solvents discussed above. The fluorescence decay of 2AP in aqueous solution was measured at emission wavelengths of 370, 390 and 420 (or 410) nm, and at three excitation wavelengths, 280, 300 and 320nm. Each decay curve could be well fitted by a single exponential function and the lifetimes obtained are shown in Table 4.2.

Excitation Wavelength/ nm	Emission Wavelength/ nm	τ/ ns	χ^2
280	370	11.8	1.11
	390	12.0	1.12
	420	12.1	1.06
300	370	11.9	1.09
	390	12.1	1.05
	420	12.1	1.15
320	370	12.2	1.20
	390	12.3	1.12
	410	12.3	1.13

Table 4.2. Fluorescence lifetimes and reduced chi-square values for 2AP fluorescence decays measured in water, as a function of excitation wavelength and emission wavelength.

It can be seen that there is a significant variation in the lifetime with emission and excitation wavelength, ranging from 11.8ns (excitation at 280nm, emission at 370nm) to 12.3 ns (excitation at 320nm, emission at 390/410nm). On the basis of measurements of a standard fluorophore with a known single exponential decay, a statistical variation of <1% in the fluorescence lifetime would be expected. This wavelength-dependence suggests that there may be more than one emitting species present. Global analysis of the nine decays confirmed that they could not be adequately described by a single fluorescence lifetime, as shown by the χ^2 values in Table 4.3. However, global analysis in terms of two common lifetimes yielded excellent fits, as shown in Table 4.4. Thus, there appear to be two emitting species, with lifetimes of 11.0 and 13.5 ns, contributing to the fluorescence of 2AP in aqueous solution.

τ(global) = 12.1ns **χ^2(global) = 1.39**

Excitation Wavelength/ nm	Emission Wavelength/ nm	χ^2
280	370	2.34
	390	1.52
	420	1.20
300	370	1.23
	390	1.05
	420	1.08
320	370	1.20
	390	1.48
	410	1.62

Table 4.3. For 2AP in water, results of global fitting of all decay curves to a monoexponential function with common lifetime. The global fluorescence lifetime, global chi-square and individual chi-square values for each decay are given.

		τ_1(global)/ns	τ_2(global)/ns	χ^2(global)
		11.0	**13.5**	**1.06**
Excitation Wavelength/ nm	Emission Wavelength/ nm	A_1	A_2	χ^2
280	370	0.70	0.30	1.03
	390	0.65	0.35	1.04
	420	0.53	0.47	1.06
300	370	0.65	0.35	1.05
	390	0.59	0.41	1.02
	420	0.57	0.43	1.06
320	370	0.52	0.48	1.07
	390	0.50	0.50	1.04
	410	0.49	0.51	1.04

Table 4.4. For 2AP in water, results of global fitting of all decay curves to a biexponential function with common lifetimes. The global fluorescence lifetimes and global chi-square are given, followed by the A factors and chi-square values for each decay.

The presence of two emitting species is also clearly apparent in ethanol. As for aqueous solutions, fluorescence decays were measured at three emission wavelengths and three excitation wavelengths. Individual fitting of each decay curve to a single exponential function yielded poor χ^2 values of about 1.5, and significant variation in lifetime with excitation and emission wavelength, ranging from 6.1ns (at 280nm excitation, 370nm emission) to 6.5ns (at 320nm, 410nm). As shown in Table 4.5 and Table 4.6, global analysis confirmed that the decays could not be described by a single lifetime, but are well fitted by a biexponential decay with common lifetimes. The two emitting species have lifetimes of 5.8 and 7.5ns.

τ(global) = 6.4ns **χ^2(global) = 1.47**

Excitation Wavelength/ nm	Emission Wavelength/ nm	χ^2
280	370	1.84
	390	1.56
	420	1.36
300	370	1.56
	390	1.25
	420	1.24
320	370	1.20
	390	1.67
	410	1.52

Table 4.5. For 2AP in ethanol, results of global fitting of all decay curves to a monoexponential function with common lifetime. The global fluorescence lifetime, global chi-square and individual chi-square values for each decay are given.

		τ_1(global)= 5.8ns	τ_2(global)= 7.5ns	χ^2(global)=1.09
Excitation Wavelength/ nm	Emission Wavelength/ nm	A_1	A_2	χ^2
280	370	0.87	0.13	1.08
	390	0.83	0.17	1.09
	420	0.80	0.20	1.04
300	370	0.84	0.16	1.09
	390	0.79	0.21	1.07
	420	0.79	0.21	1.08
320	370	0.72	0.28	1.02
	390	0.66	0.34	1.01
	410	0.65	0.35	1.07

Table 4.6. For 2AP in ethanol, results of global fitting of all decay curves to a biexponential function with common lifetimes. The global fluorescence lifetimes and global chi-square are given, followed by the A factors and chi-square values for each decay.

Decay curves for 2AP in the aprotic solvents DMSO and 1,4-dioxane are also described by a bi-exponential model as shown in Table 4.7. Global analysis of the data shown in Table 4.7, with a single exponential fit, gave lifetimes of 4.85ns and 1.73ns and global chi-squared values of 1.947 and 4.919 for 2AP in DMSO and dioxane, respectively.

	DMSO	**τ_1(global)= 4.7ns**	**τ_2(global)= 7.5ns**	**χ^2(global)= 1.129**
Excitation Wavelength/ nm	Emission Wavelength/ nm	A_1	A_2	χ^2
280	370	0.94	0.06	0.952
	390	0.93	0.07	1.101
	420	0.93	0.07	1.110
300	370	0.97	0.03	1.168
	390	0.96	0.04	1.109
	420	0.95	0.05	1.093
	1,4-Dioxane	**τ_1(global)= 1.6ns**	**τ_2(global)= 3.9ns**	**χ^2(global)= 1.084**
320	370	0.99	0.01	1.071
	390	0.97	0.03	1.071
	420	0.97	0.03	1.109

Table 4.7- For 2AP in DMSO (top) and 1,4-dioxane (bottom). Results of global fitting of all decay curves to a biexponential function with common lifetimes (for each solvent). The global fluorescence lifetimes and global chi-square are given, followed by the A factors and chi-square values for each decay.

To determine whether the two emitting species could be identified with the two tautomeric forms of 2AP, comparative measurements were made on 2AP riboside. As shown in Figure 4.1, the presence of the ribose substituent at N9 in 2APr prevents formation of the 7H tautomer.

The fluorescence decays of 2APr were measured in aqueous and ethanolic solutions at emission wavelengths of 370, 390 and 410 nm and excitation wavelengths of 300 and 320nm (aqueous solution only).

	2APr in Water	**$\tau 1$= 10.6ns**	**χ^2(global)=1.167**
	Excitation Wavelength/ nm	Emission Wavelength/ nm	χ^2
Water	300	370	1.038
	300	390	1.091
	300	410	1.157
	320	370	1.285
	320	390	1.227
	320	410	1.227
	2APr in Ethanol	**$\tau 1$= 5.8ns**	**χ^2(global)=1.037**
Ethanol	300	370	1.144
	300	390	1.063
	300	410	1.050

Table 4.8- For 2AP riboside in water (top) and ethanol (bottom). Results of global fitting of all decay curves to a single exponential function with common lifetimes (for each solvent). The global fluorescence lifetimes and global chi-square are given, followed by the A factors and chi-square values for each decay.

In each solvent, global analysis showed that the fluorescence decays of 2APr across the entire excitation/emission space could be fitted by a single common fluorescence lifetime, with chi-square values typically being <1.2, indicating the presence of a single emitting species. The data recorded for the aqueous solution of 2APr at an excitation wavelength of 320nm shows higher chi-square values than the other samples. This data was recorded during a period when the TCSPC experiment was being established and the decay curves were showing some oscillatory interference. This problem was resolved by using a different region of the TAC for these experiments. Addition of a second component to the decay curves exhibiting this interference showed no improvement in the value of the chi-square parameter. The fluorescence lifetime of 2APr was found to be 10.6 ns in water and 5.8 ns in ethanol.

4.3 Discussion

Current understanding of the photophysics of 2AP in aqueous solution holds that its fluorescence decay is single exponential with a lifetime of around 11.5ns [41,27,8,44]. The results of this work show that, for an individual decay curve measured at a particular excitation and emission wavelength, this is indeed the case. However, measurement over a range of excitation and emission wavelengths reveals biexponential decay kinetics for 2AP in all of the solutions investigated, indicating the presence of two emitting species. Comparison with 2APr, which demonstrably behaves as a single emitting species in both water and ethanol, leads to the conclusion that the two species observed for 2AP are the 9H and 7H tautomers. In water, the 2APr lifetime of 10.6ns is very similar to the 11ns decay component of 2AP; therefore, the latter is assigned to the 9H tautomer and the 13.5ns lifetime to the 7H tautomer. Similarly, in ethanol, the 5.8ns lifetime is assigned to the 9H tautomer (*cf* 5.8ns 2APr lifetime) and the 7.4ns lifetime to the 7H tautomer. Following this trend, in DMSO and dioxane the longer of the two lifetimes is ascribed to the 7H tautomer, with the 9H tautomer having a relatively short lifetime. The marked decrease in the fluorescence lifetimes with decreasing solvent polarity is consistent with the previously reported lifetimes of 6ns and 1.5ns for 2AP in ethanol and dioxane respectively [12].

The fractional contribution of the ith lifetime component to the total integrated (steady state) emission intensity, at a particular excitation and emission wavelength, is given by

$$\frac{A_i \tau_i}{\sum_i A_i \tau_i} \qquad \textbf{Equation 4.1}$$

Thus, measurement of the fluorescence decay of 2AP in water at a series of wavelengths across the emission envelope allowed the emission spectra of the two tautomers to be constructed, as shown in Figure 4.7.

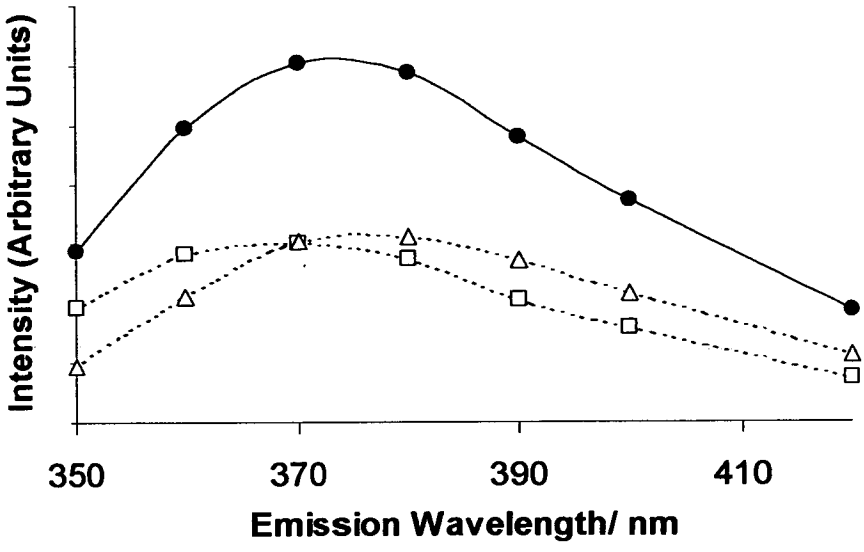

Figure 4.7. The emission spectra (at an excitation wavelength of 320nm) of the 9H tautomer (squares) and the 7H tautomer (triangles) of 2-AP in aqueous solution, derived from time-resolved fluorescence data. The total emission spectrum is shown by the solid line.

The spectra overlap closely; the maxima are separated by about 7 nm (~500 cm^{-1}), with the spectrum of the 7H tautomer lying at longer wavelength. The excitation wavelength dependence of the A factors in Tables 3 and 5 also suggests that the excitation spectrum of the 7H tautomer is red-shifted relative to the 9H. These observations are in agreement with the results of ab initio calculations by Broo[45] that predict both tautomers to be fluorescent (having lowest excited states of $\pi\pi^*$ character) and the emission maximum (for a vertical transition from the relaxed excited state) of the 7H tautomer to be about 1000 cm^{-1} below that of the 9H tautomer. The existence of the two tautomers is apparent in the steady state emission of 2AP as shown in Figure 4.5. Excitation on the red edge of the excitation spectrum gives an emission spectrum significantly red-shifted from that obtained with blue-edge excitation.

If the radiative lifetimes of the two tautomers can be assumed to be similar, then the A factors indicate the fraction of the emitting population constituted by each tautomer. This appears to be a reasonable assumption, since the fluorescence lifetimes of the two tautomers are similar and their oscillator strengths are predicted to be similar[45], 0.37 for 9H and 0.25 for 7H. Examination

of the A factors in Tables 4.4, 4.6 and 4.7 indicates that the proportion of the 7H tautomer is substantial in both of the protic solvents, about 40% in water and about 20% in ethanol. These values are somewhat greater than those reported for adenine, 20% in water[30] and 6% in butanol[29], although the 40% value in water is similar to the observation of equal proportions of 7H and 9H tautomers for purine[37-39] in aqueous solution. The proportion of 7H tautomer in both of the aprotic solvents, DMSO and dioxane, is low, around 3-5%. The observation of a decreasing fraction of the 7H tautomer with decreasing solvent polarity is consistent with the prediction of a larger dipole moment for this tautomer[40]. However, the magnitude of the 7H tautomer population is much greater than the 3% predicted for 2AP in water in the same ab intio study. The calculations may significantly underestimate the effect of polar solvation in shifting the equilibrium towards the 7H tautomer, since they neglect specific solvent-solute interactions. Specific interactions between the solvent and 2AP play an important role in mediating the 9H-7H tautomerisation and may contribute to the low proportion of the 7H tautomer in both the aprotic DMSO and dioxane solutions.

It is important to recognise that in these experiments the excited state tautomer population is being observed and to consider how this relates to the ground state population. Ab initio calculations by Broo[45] predict the 7H tautomer to be much closer in energy to the 9H tautomer in the excited state than in the ground state, for both 2AP and adenine in the gas phase. If the solvent effect on the relative excited state energies of the two tautomers were of the same magnitude as in the ground state, this would result in the two tautomers lying very close in energy, giving comparable proportions in the equilibrated excited state population. This might account for our observation of a relatively high proportion of 7H tautomer in the protic solvents. However, we see no sign, in the fluorescence response functions, of any rise components (negative A factors) that would indicate a shift in the tautomer equilibrium following excitation. If the re-equilibration on excitation occurs faster than the time resolution of our measurements, i.e. on the picosecond timescale or less, we may be observing the fluorescence decay of the fully equilibrated excited state tautomer population. However, we see a definite dependence of the A factors (proportions of 7H and 9H tautomers in the emitting population) on excitation wavelength, indicating that memory of the ground state population is retained in the emitting population. It seems more likely, therefore, that the response of the tautomer equilibrium to excitation is slow compared with the lifetime of the excited state, and the excited state population that we observe reflects the composition of the ground state population.

4.4 Conclusion

Steady state fluorescence and fluorescence lifetime measurements have shown that 2AP exists as both the 9H and the 7H tautomer in four different solvents at room temperature. In the polar, protic solvents, there is a substantial proportion of the 7H isomer in the emitting population: about 40% in water and about 20% in ethanol. In aprotic solvents only 3-5% of the emitting population is in the 7H tautomeric form. The two tautomers have closely overlapping fluorescence spectra but can be distinguished by their fluorescence lifetimes. The tautomeric composition of the emitting population depends on excitation wavelength and no evidence of a change in the tautomeric equilibrium in response to excitation is observed. Therefore, it is concluded that the observed excited state tautomer population arises directly from that in the ground state.

The observation of tautomerism in 2AP is further evidence of the similarity of this molecule to adenine and affirms its suitability as a fluorescent analogue of the nucleic base. It also offers the opportunity of applying sensitive fluorescence methods to the study of the tautomerisation process.

Chapter 5

Studies on 2AP in the Crystal Phase

5.1 Introduction

With a view to producing a model system of 2AP in a π-stacked (as in the DNA duplex) but conformationally well-defined environment, crystals of the 2AP base were grown by slow evaporation from ethanol. The crystal structure of the 2AP was determined by x-ray diffraction (XRD) and steady-state and time-resolved fluorescence measurements were made on the crystals.

When the 2AP base is bound in the DNA duplex the relatively simple fluorescence response of the free, solution phase base becomes much more complex and is described by the sum of four exponential terms[46-49]. As can be seen in the subsequent Chapters of this thesis, the assigned lifetimes typically have values of <100ps, ~0.5ns, ~2ns and ~10ns. It is widely accepted that the longest and shortest of these lifetimes can be ascribed to DNA molecules adopting physically well-defined conformations. The 10ns component is close to the lifetime of the 2AP base or 2AP riboside in aqueous solution, as were described in the previous Chapter (in DNA 2AP is bound to the phosphate backbone at N9, so no tautomerisation is possible). Hence, it is attributed to 'unstacked' 2AP in the DNA duplex, i.e. 2AP that is experiencing an extrahelical, solution-like environment. Recent studies have shown that the component of <100ps is due to efficiently quenched 2AP that is well stacked in the duplex. One of the mechanisms responsible for the rapid quenching in this instance has been shown to be electron transfer from nearby guanine bases to excited state 2AP[20;50]. The two intermediate lifetimes of ~0.5ns and ~2ns are similar in magnitude to those noted for the 2AP base, in the previous Chapter, in apolar solvents such as dioxane and DMSO and may represent 2AP molecules in intrahelical, similarly apolar environments where efficient relaxation of the excited state is energetically unfavourable[51]. In

general, interpretation of the fluorescence response of 2AP in these relatively complex systems is somewhat limited by the current lack of understanding of the processes affecting it.

To date, there have been no structural or spectroscopic studies made on 2AP in the crystalline phase. However, the crystal structures of three C6-substituted 2AP derivatives have recently been characterised using X-ray diffraction (XRD)[52] and Harnden *et al* have reported the structure of 9-[4-acetoxy-3-(acetoxymethyl)-butyl]-2-aminopurine[53]. There are several theoretical studies that have reported ground state structures, calculated *ab initio* for 2AP[28;40;45;54;55]. The crystal structure of adenine was first determined (as adenine hydrochloride) in an early paper by Broomhead[56].

In a study of the polarised reflectance spectra of single crystalline adenine, Chen and Clark found evidence of exciton coupling between adenine molecules, manifested as Davydov splitting[57]. A recent study by Rist *et al* showed the possibility of excitonic coupling occurring between adjacent 2AP bases and, to a lesser extent, between 2AP and neighbouring canonical bases in the DNA duplex[58]. Two distinct peaks are observed in the excitation and emission spectra of 2AP with peaks at 320nm and 370nm and at 370nm and 440nm in the excitation and emission spectra respectively. Although, the authors observe no Davydov splitting, this study certainly indicates the formation of a ground-state complex between 2AP and other nearby aromatic molecules, probably through a π-π interaction. The interaction between adjacent 2AP bases in DNA has also been used a mechanism for studying the conformational dynamics of DNA by circular dichroism (CD) spectroscopy[59]. In the same way that the canonical bases show a distinct signal for excitonic coupling between adjacent bases, 2AP in a dinucleotide stack gives a CD signal consistent with the formation of a dimeric 2AP complex. Further evidence of the formation of ground state complexes by 2AP in the DNA duplex comes from work by Jean and Hall, who made a computational study of the photophysical properties of 2AP in DNA dinucleotides and trinucleotides[60;61]. Although the main focus of these studies is the electronic composition of the DNA duplex (which will be discussed in subsequent Chapters of this thesis), the trimer calculations predict the formation of ground-state complexes between 2AP and adjacent DNA nucleobases. Importantly, these complexes are expected to show red-shifted transitions relative to the isolated 2AP base.

Crystals of 2AP.H_2O have been grown and their x-ray crystal structure has been determined. Structural, steady-state and time-resolved fluorescence studies indicate that the 2AP crystal represents a good model system for 2AP in a DNA duplex-like environment. A ground-state interaction in the crystal that leads to a red-shift in the 2AP spectra is observed. The time-resolved 2AP fluorescence response is complex even in this apparently uniform system.

5.2 Experimental Details

TCSPC measurements were made on the 2AP crystals mounted in quartz capillary tubes (Hampton Research). Before measuring the fluorescence response of the crystals, the path of the laser was optimised using a dilute scattering solution of Ludox (Aldrich). This enabled alignment of the laser such that the width of the instrument response function and amount of light reflected within the sample chamber were minimised whilst maximising the count rate from the sample. The capillaries were vertically mounted in the sample chamber, with a single 2AP crystal attached (electrostatically) to one side of the capillary. Allowing the crystals to fall to the bottom of the capillary tube was found to lead to a large amount of light scattering from the bottom edge of the capillary. The height of the crystal was set to align with the laser beam. The lateral positioning of the crystal was estimated from the path of the laser and by placing the crystal in the path of the incident beam and orthogonal to the emission-side focussing lens, as shown in Figure 5.1. The focussing lens on the excitation side of the sample was removed so that the laser beam was relatively defocused and incident on a large area of the crystal. The position of the crystal was optimised for the maximum count rate using the translation stages upon which, it was mounted (sample mounting for crystalline samples is described in the Experimental Chapter). Fluorescence decay curves were recorded on the 20ns timescale using 4096 channels and were collected to 10000 counts in the peak channel.

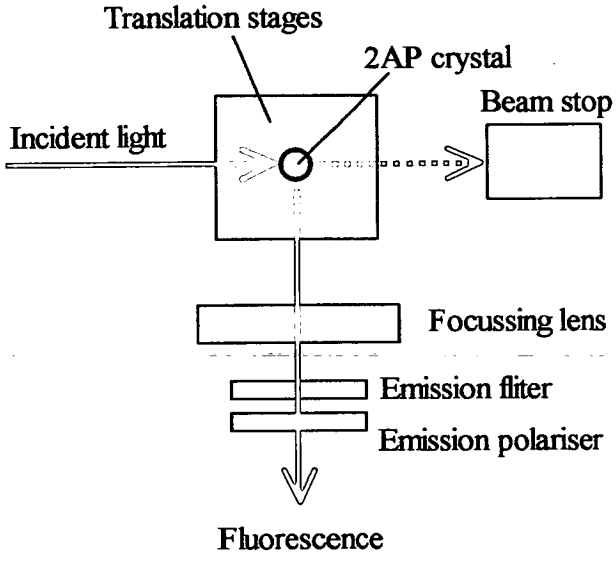

Figure 5.1- Experimental set-up within the Edinburgh Instruments spectrometer sample chamber for TCSPC experiments on crystalline 2AP.

Crystal data for 2AP.2H$_2$O. $C_5H_7N_5O$, M = 153.14, monoclinic, space group $P2_1/c$. Cell dimensions: a = 3.6295(8), b = 17.587(4), c = 10.597(2) Å, β = 98.477(4)°, V = 669.0(2) Å^3. X-ray diffraction data were collected at 150 K on a Bruker Smart APEX diffractometer equipped with an Oxford Cryosystems low-temperature device. An absorption correction was applied using the multiscan procedure SADABS[62]. The structure was solved by direct methods (SIR92)[63], and refined by full-matrix least-squares against F^2 (CRYSTALS)[64]. All non-hydrogen atoms were refined with anisotropic displacement parameters, while H-atoms were located in difference Fourier syntheses. Although the primary site of protonation in the purine is N9, a weak difference synthesis peak next to N7 was interpreted as hydrogen-atom disorder, and weak peaks in the region of the water of crystallization appeared to confirm this. The part-weight hydrogen atoms attached to N7 and N9 were refined subject to the restraint that equivalent distances and angles involving the hydrogen atoms were similar. Explicit geometry restraints were applied to the water of crystallization. The occupancies of the two disorder components refined to 0.87(5) and 0.13(3). The final conventional R factor [based on F and 1133/1598 data with $F > 4\sigma(F)$] was 0.0507, and the final difference map extremes were + 0.22 and -0.23 eÅ^3.

5.3.1 Crystal Structure

The asymmetric unit of the 2AP crystal consists of one molecule of monohydrated 2AP, the structure of which is shown in Figure 5.2(a). The 2AP molecule is planar apart from the protons of the amine group which lie slightly out of the plane of the rest of the molecule. There is a hydrogen bond of 1.974 Å between the water (H11) and N7 of 2AP. Electron density peaks in the Fourier difference map indicate the presence of some disorder in the crystal structure. A hydrogen atom (H7) is bound to N7, with an occupancy of 0.13(3), thus, approximately 13% of the 2AP molecules in the crystal exist as the 7H tautomer. This figure is consistent with our findings from fluorescence lifetime measurements on 2AP in solution, which showed approximately 20% of the 7H tautomer to be present in ethanolic solution[65]. In conjunction with the 7H tautomer, the water molecule adopts a different orientation, with its protons in sites H13 and H14, as shown in Figure 5.2(a), and the oxygen hydrogen bonded to H7 of 2AP.

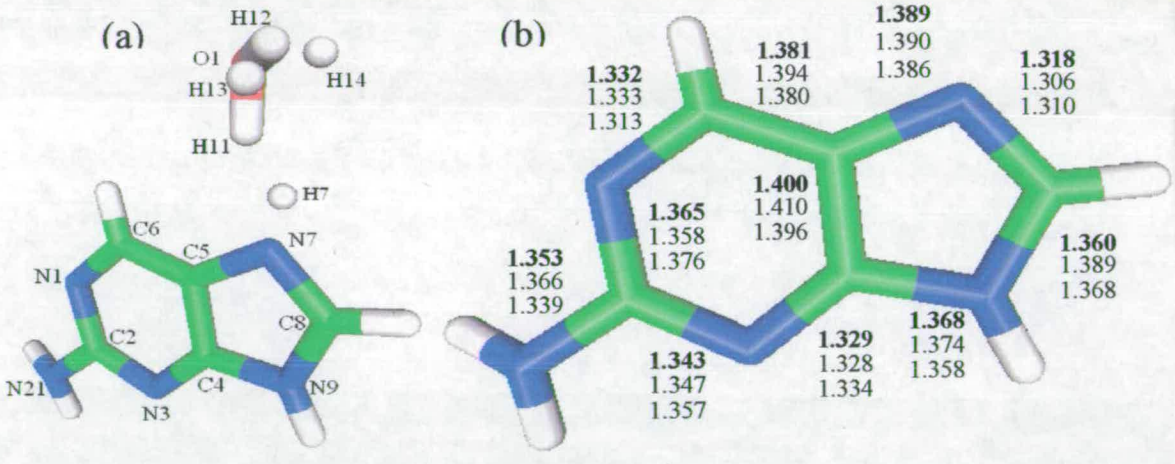

Figure 5.2. (a) The asymmetric unit and numbering scheme for 2AP.H_2O in the crystal structure. (b) The bond lengths (Å) determined in the present work (top, bold); those calculated for the 9-H tautomer of 2AP[40] (middle); those for the x-ray structure of 2-amino-6-chloropurine[53] (bottom).

The bond lengths and bond angles derived from the crystal structure are shown in Table 5.1. Selected bond lengths are shown in Figure 1(b) together with those calculated for the 9H 2AP tautomer[40] and those measured by x-ray crystallography for 2-amino-6-chloropurine[53]. In general, there is good agreement between the two x-ray structures. Comparison with the structure calculations of Broo[40] for 2AP shows that the measured N9-C8 bond length is distinctly shorter than that predicted for the 9H tautomer. This is consistent with the presence in the crystal of 13% of the 7H tautomer which has a substantially shorter N9-C8 bond (1.319Å)[40].

Bond Lengths (Å)		Bond Angles (deg)	
N1-C2	1.365	N1-C2-N3	126.54
N1-C6	1.332	N1-C2-C10	116.11
C2-N3	1.343	N10-C2-N3	117.34
C2-N21	1.353	C2-N3-C4	112.42
N3-C4	1.329	N3-C4-C5	126.52
C4-N9	1.368	C4-C5-C6	115.85
C4-C5	1.400	C5-C6-N1	120.33
N9-C8	1.360	C6-N1-C2	118.33
N9-H9	0.871	N3-C4-N9	127.82
C8-N7	1.318	C4-C5-N7	110.04
C8-H8	0.974	C5-N7-C8	103.93
N7-C5	1.389	N7-C8-N9	113.91
C5-C6	1.381	N8-N9-C4	106.45
C6-H6	0.955		
N21-H211	0.890		
N21-H212	0.883		

Table 5.1- Bond lengths and bond angles of 2AP.

Figure 5.3shows the unit cell which contains four monohydrated 2AP molecules. An extensive hydrogen bonding network is apparent. As shown in Figure 5.4(a), adjacent 2AP molecules hydrogen bond through an N9H to N1 interaction, and each 2AP molecule is hydrogen bonded to 3 neighbouring water molecules via N7 and the two amine protons. The hydrogen bonds formed in the crystal are all of moderate strength with those involving ring atoms being around 0.2Å shorter than those of the amine group.

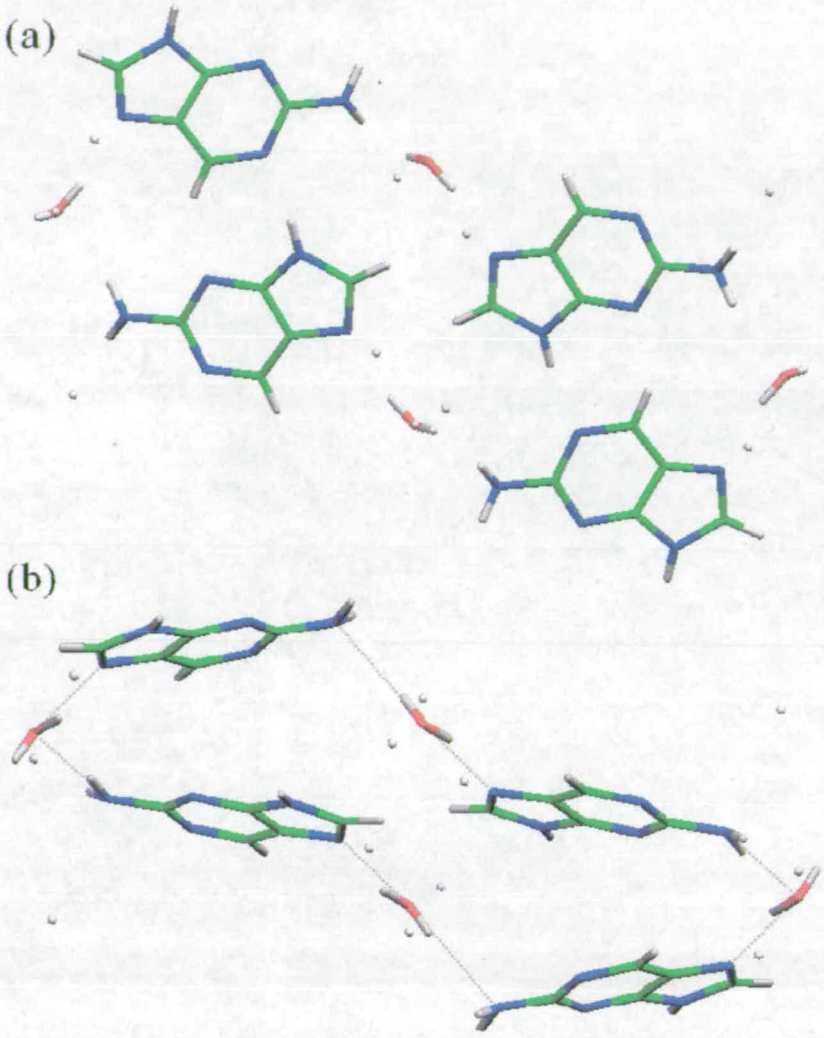

Figure 5.3. (a).The unit cell of the 2AP.H_2O crystal viewed along the crystallographic a-axis. (b) Illustration of the packing of molecules in the unit cell (rotated about b-axis, relative to (a)).

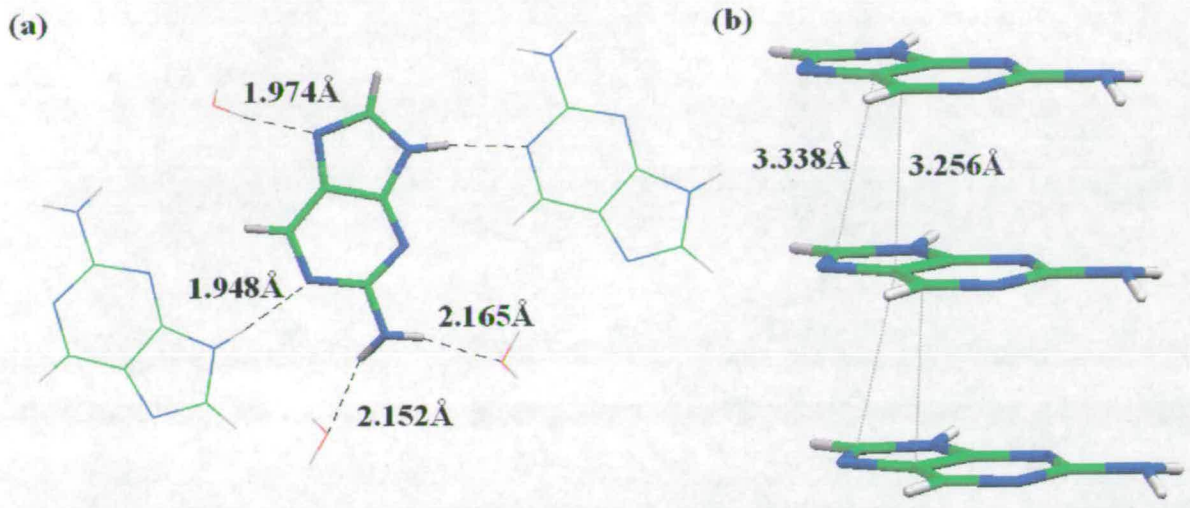

Figure 5.4- Intermolecular interactions in the 2AP crystal. (a) Hydrogen bonds (bond distances are given for H-acceptor separation) (b) π-stacking interactions.

The hydrogen bonding interactions of 2AP in the crystal mimic those that the molecule experiences in the DNA duplex, where 2AP base pairs with adenine, thymine or cytosine via hydrogen bonding at one of the amino protons and at N1. Ordered solvation shells of water are formed in both the minor and major grooves of the DNA duplex[66]. Given this water-rich environment and the ability of 2AP to form hydrogen bonds, water molecules are likely to be hydrogen-bonded to the free amino proton and N7 of 2AP in the DNA duplex as in they are in the crystal.

Extended columns of π-stacked 2AP molecules are present in the crystal, as illustrated in Figure 5.4(b) The closest contacts between adjacent molecules in these stacks are between C5 and C6 (3.256Å) and between C8 and C5 (3.338Å). Thus, molecules in the stack are staggered, with the imidazole and pyrimidine rings of adjacent molecules overlapping. The centre of the imidazole ring lies above the C8 atom of the molecule below it when looking perpendicular to the plane of the 2AP molecules. In many ways, the interaction between 2AP molecules in these stacks mimics base-stacking interactions in the DNA duplex. Hassan and Calladine have reviewed the structures of some 60 DNA duplexes[67] and show that the rise between adjacent base steps is essentially sequence independent and has a magnitude of 3.4Å. Adjacent DNA bases are also offset relative to one another, as the 2AP molecules in the crystal are, though Hassan and

Calladine show that this 'slide' parameter varies in a sequence specific manner. The 2AP crystal does not mimic the rotational displacements of the DNA bases.

Although the XRD data confirms the presence of both the 7H and 9H tautomers of 2AP, it is important to note that no insight into the mechanism by which this disorder arises is derived from the crystallographic data. Since the heterogeneity within the crystal is likely to influence the fluorescence response of the 2AP it is important to consider the form of this disorder. Consider the case where the entire crystal is composed of molecules in a dynamic equilibrium, where the heterogeneity (proton transfer) is facilitated by the intermolecular interactions between the 2AP molecules and between 2AP and water. In this situation the quoted occupancies represent the probability of a given tautomer being formed. Figure 5.3 shows that, in the crystal unit cell, there is no plausible mechanism by which the 7H tautomer can be formed. The only proton in the proximity of the N7 atom is H11, of the water molecule. It seems highly unlikely that this proton would tunnel to bond with N7. Indeed, protonation of N7 by the water molecule is inconsistent with the with the x-ray structure, which shows that the water molecule is in its native form (occupying the alternative H13/ H14 conformation) when the 7H tautomer is also present. Hence, it must be concluded that the heterogeneity in the 2AP crystal is introduced during the crystal growth. The excellent agreement between the A-factor of the 7H 2AP tautomer in ethanolic solution, described earlier in this thesis (~0.2), and the occupancies derived from the XRD data supports this hypothesis.

5.3.2 Steady-State Fluorescence Spectra

Single-crystal 2AP shows two distinct emission bands, each with its own excitation spectrum, indicating the presence of two ground state species with quite different electronic structures. As shown in Figure 5.5, excitation of the crystal at 300nm or less gives an emission spectrum that resembles that of 2AP in aqueous solution, with a peak at around 370nm. Excitation at longer wavelength results in red-shifted emission peaking at around 420nm. Overlap between the two spectra prevents a quantitative measure of their relative intensities, but the longer wavelength emission is estimated to be about five times more intense than the short wavelength band. The excitation spectra of the two emission bands are shown in Figure 5.6.

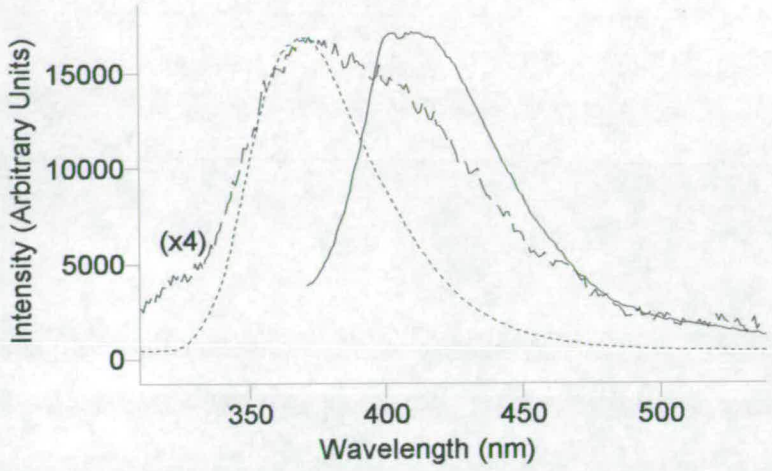

Figure 5.5- Emission spectra of 2AP crystal at excitation wavelengths of 280nm (dashed line, with intensity multiplied by a factor of four) and 360nm (solid line, contains a Raman band at 402nm). Also shown is the emission spectrum for 2AP in water at an excitation wavelength of 300nm, for comparison (dotted line).

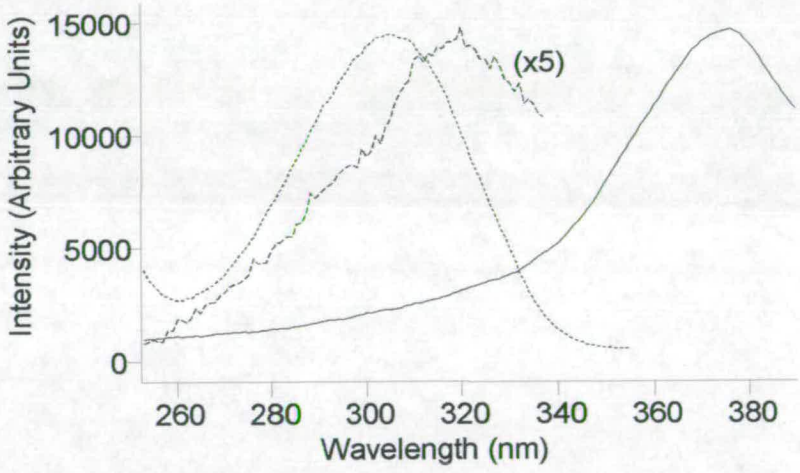

Figure 5.6- Excitation spectra of 2AP crystal at emission wavelengths of 360 nm (dashed line) and 440nm (solid line). Also shown is the excitation spectrum for 2AP in water at an emission wavelength of 370nm, for comparison (dotted line).

The long wavelength excitation and emission spectra are very similar to those reported by Rist et al[58] for a 2AP-labelled DNA duplex containing pairs of adjacent 2AP bases. Using an excitation

wavelength of 343nm, Rist et al report an emission spectrum for their 2AP labelled DNA duplex with a peak at approximately 370nm and a significant shoulder at ~430nm. Hence, the interaction between the adjacent 2AP bases gives rise to a dimer-like species with lower excitation energy than free 2AP. This suggests that in the crystal the major influence on the excitation energy of 2AP is the interaction between adjacent molecules in the π stack. The predominant long-wavelength emission of the 2AP crystal can thus be attributed to dimer- or trimer-like species resulting from ground-state interaction between neighbouring molecules in the π stack. Hereafter, this long-wavelength emitting species will be referred to as "stacked 2AP".

The short-wavelength excitation and emission spectra are characteristic of 2AP molecules unperturbed by intermolecular interactions. In the crystal, such 2AP molecules may be found at defect sites where the local lattice structure is disturbed. All molecular crystals contain defects, and their form ranges from point defects, where, for example, a vacancy in the crystal lattice leads to a localised disruption of the crystal structure, to more delocalised features such as grain boundaries and dislocations, which affect the crystal lattice structure over many molecules. In the present case, an obvious source of lattice imperfections is the presence of a small fraction of the 7H tautomer. The 7H tautomer differs in both its dipole moment (magnitude and direction, Figure 5.7) and hydrogen bonding sites from the 9H tautomer and its presence will cause local disruption of intermolecular interactions. The short wavelength emission may arise from the 7H tautomer itself or from 9H molecules in the disrupted lattice. 2AP molecules at surface sites may also show emission characteristic of the free molecule. The short-wavelength emitting species will be referred to as "isolated 2AP".

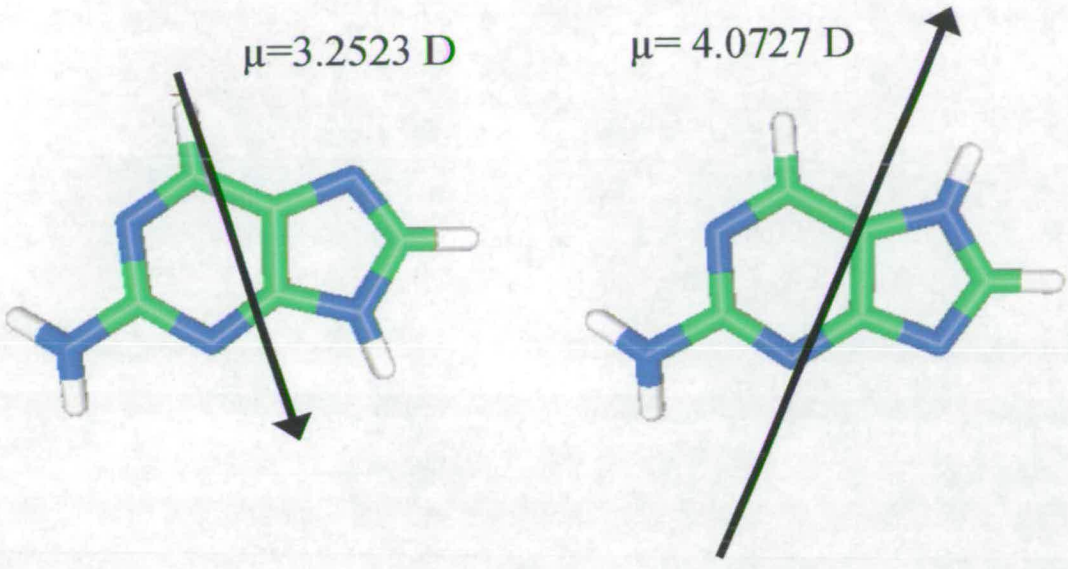

Figure 5.7- Calculated ground-state dipole moments for the 9H (left) and 7H (right) tautomers of 2AP. Calculations were carried out using Gaussian98[68] and the B3LYP/6-311+g(d,p) basis set.

The spectral perturbation induced by intermolecular interaction in a crystal has two contributions: (i) the difference in the interaction energy (e.g. dipole-dipole, dipole-induced dipole, dispersion) with its neighbours of the molecule in its ground state and in its excited state; (ii) the resonance interaction energy or exciton coupling. The first causes a mean shift of the excitation energy (relative to the free molecule) and the second causes splitting of the molecular excited state into a number of exciton states, some of which may be forbidden, or only weakly allowed. These perturbations are described diagrammatically in Figure 2.7, in the Theory Chapter of this thesis. The presence of four crystallographically inequivalent 2AP molecules in the unit cell should give rise to four exciton states for each free molecule state. Emission will occur from only the lowest exciton state (in accordance with Kasha's rule), but energetically higher (allowed) states should be apparent in the excitation spectrum. The excitation spectrum of stacked 2AP (Figure 5.6) shows no obvious sign of splitting. The band maximum at ~370nm corresponds to direct excitation into the emitting state (the Stokes shift is comparable to that between the excitation and emission maxima of the isolated molecule). However, there is a weak short wavelength tail on the excitation spectrum that extends to about 270nm, overlapping with

the isolated 2AP spectrum. Comparison of the crystal emission spectrum excited at 280nm with that of 2AP in solution (Figure 5.5) confirms that excitation in this short wavelength region results in a significant intensity of red-shifted, stacked AP emission. This may be indicative of excitation via higher energy crystal states, but could also be due to excitonic energy transfer , i.e. the reabsorption of fluorescence from isolated 2AP by stacked 2AP.

5.3.3 Time-Resolved Fluorescence

Fluorescence decay curves of the isolated 2AP and stacked 2AP crystal species were recorded at excitation wavelengths of 300nm and 400nm, respectively, and over a range of emission wavelengths across the two emission bands.

Global lifetimes: τ_1=0.04ns, τ_2=0.30ns, τ_3=1.18ns, τ_4=4.85ns
Global χ^2=1.07

Emission wavelength / nm	A_1	A_2	A_3	A_4	Local χ^2
350	0.73	0.22	0.05	0.00	1.13
360	0.76	0.17	0.06	0.01	1.04
370	0.75	0.18	0.06	0.01	1.09
390	0.72	0.21	0.07	0.01	1.06
410	0.72	0.21	0.07	0.01	1.08

Table 5.2- Decay parameters of the isolated 2AP fluorescence from the single crystal. Fluorescence was excited at 300nm and decays obtained at the 5 emission wavelengths shown were fitted globally to 4 common lifetimes.

Isolated 2AP showed a multiexponential decay that could be fitted globally by 4 common lifetimes across the emission envelope. The lifetimes and A-factors are given in Table 5.2. Fits made using only three lifetimes give significantly poorer results with χ^2 values typically of 1.7-1.8. The observation of a multiexponential decay indicates that the emitting isolated 2AP molecules exist in a heterogeneous environment, with the different decay components representing populations of 2AP molecules subject to different intermolecular interactions in the crystal lattice.

Although four decay components were required to satisfactorily fit the decay data, the amplitudes of the two components with the longest lifetimes, 1.18 and 4.85ns, are very small; together these represent less than 10% of the emitting isolated 2AP molecules. The dominant emitting species, >70% of the population, has a very short lifetime of 40ps. A second species with a lifetime of 300ps constitutes a significant fraction (>10%) of the emitting molecules.

As will be demonstrated in the next Chapter of this thesis, the fluorescence spectrum typical of 2AP in DNA is very similar to that of isolated 2AP in the crystal and the characteristic 4-component decay of 2AP in DNA also resembles that observed here.

Excitation at 400nm leads to an excited state population that consists of the stacked 2AP molecules that undergo excitonic coupling with their neighbours. The resulting emission is best fitted with four lifetimes and the derived parameters are shown in Table 5.3.

Global lifetimes: τ_1=0.12ns, τ_2=0.56ns, τ_3=1.56ns, τ_4=6.13ns
Global χ^2=1.09

Emission wavelength / nm	A_1	A_2	A_3	A_4	Local χ^2
430	0.60	0.29	0.10	0.01	1.12
460	0.56	0.28	0.14	0.02	1.07
490	0.41	0.36	0.21	0.03	1.07
520	0.39	0.34	0.24	0.03	1.08

Table 5.3- Parameters derived from global fits of 2AP crystal fluorescence response with laser excitation at 400nm.

The dominant species in the fluorescence response of stacked 2AP has a lifetime of 0.12ns and its A-factor falls off rapidly with increasing emission wavelength; from 60% at 430nm to only 39% of the emitting 2AP molecules at 520nm. Approximately 30% of the emitting population has a lifetime of 0.56ns. At 430nm, only 10% of the excited state species are accounted for by a 1.56ns decay but this rises to 24% of the excited state population at an emission wavelength of 520nm. A very small proportion of the excited 2AP molecules have a lifetime of 6.13ns. Note, however, that because of their relatively long fluorescence lifetime, these molecules contribute a

similar intensity to the steady-state emission spectrum (16%) at 430nm as the 60% of 2AP molecules with a. 0.12ns lifetime. Overall, lower excitation energy stacked 2AP species emit at longer wavelengths and over a longer time period than the isolated 2AP molecules.

It is significant that the fluorescence responses of both the isolated and stacked 2AP species are described by complex, multiexponential decays. Clearly, several mechanisms of deactivation of the excited state of 2AP within this crystal are available to both species, regardless of the number of 2AP molecules in the excited state complex and, hence, the relative energetic levels of the excited state. This is indicative of the complex, interactive environment in which each excited-state species is located.

In the case of isolated 2AP, one obvious mechanism of de-excitation is via energy transfer to the energetically low lying excited state of the stacked 2AP species. This is likely to be the efficient and predominant mechanism for de-excitation of isolated 2AP described by τ_1. The remaining fraction of the isolated 2AP population is likely to be accounted for by molecules that occupy sites in the crystal where the crystal lattice is disrupted. De-excitation through energy transfer is likely to be hindered or precluded in these minor conformational populations.

For the isolated 2AP, there is essentially no variation in the A-factors of the four decay components with emission wavelength. Hence, the emission spectra of all the isolated 2AP species are similar. This infers that the ground and excited states of the isolated 2AP species represented by τ_1-τ_4 are similar. Hence, subtle changes in the environment of the 2AP must lead to gross changes in its fluorescence lifetime. The efficiency of energy transfer, mediated through π-π interactions will be extremely sensitive to the configuration of the donor-acceptor system. Hence, energy transfer provides a mechanism for heterogeneity within the 2AP fluorescence response that is entirely consistent with both the steady-state and time-resolved measurements that have been made.

The results of Rist et al[58] show that perturbation of a 2AP molecule by stacking with one neighbour (i.e. a dimeric interaction) is sufficient to produce a red-shifted emission spectrum very similar to that observed for stacked 2AP in the crystal. The interaction of 2AP with a second neighbour in the crystal lattice (a trimeric interaction) appears to have little additional

effect on the spectrum. It is reasonable, therefore, to expect the emission from stacked 2AP to result from these dimeric and trimeric 2AP complexes.

The lifetimes of these stacked species are substantially longer than those of the short-wavelength emitting isolated 2AP molecules. In common with all molecular crystals, a major non-radiative decay channel will be excitonic energy transfer. Rapid exciton migration through the crystal lattice occurs, until a defect with lower excitation energy (a trap) is encountered, resulting in irreversible energy transfer. Examination of the dependence of the A factors on emission wavelength (Table 5.3) suggests that the longer-lived species have lower excitation energies than the short-lived species, which is consistent with energy transfer being an important decay mechanism.

The heterogeneous decay of the long wavelength emission can be interpreted in terms of the stacked geometry of the 2AP complexes. The de-excitation of a stack of *n* interacting 2AP molecules through energy transfer will depend on the orientation of the stack with respect to the two molecules in the crystal lattice at either one of its ends. Different degrees of overlap with these neighbouring 2AP molecules and/or stacks will lead to different rates of de-excitation for individual stacks.

5.3.4 2AP in DNA

The fluorescence response of 2AP labelled DNA is discussed in detail in the next Chapter of this thesis. The work presented in this Chapter presents something of a paradox with regard to current understanding of the photophysical behaviour of 2AP in the DNA duplex. That is, the very short decay component of 2AP in DNA is attributed to a stacked conformation of the duplex, where the 2AP undergoes a strong π-π interaction with either one or both neighbouring bases. However, this species emits in the short wavelength region and does not correspond to the long-wavelength-emitting stacked 2AP observed in the crystal. In computational studies of 2AP-nucleobase dimers and trimers, Jean and Hall[60;69] have found that π-stacking interaction leads to formation of two or more excited states with charge-transfer character energetically below a localised 2AP-like state. These low-lying states are predicted to have small oscillator strengths. For example, in a G-2AP-G trimer, the S_1 state is predicted to lie some 3500 cm^{-1} below that of

isolated 2AP and to have about one tenth the oscillator strength[69]. In the absence of experimental evidence for weak transitions to the red of the normal, localised 2AP transition in 2AP-labelled DNA, the predicted low-lying charge transfer states have been assumed to be dark states. Prompted by the observation of a low energy emissive state for π-stacked 2AP and the observation of similar emission by Rist et al[58] for oligonucleotides containing multiple 2AP bases, an oligonucleotide duplex labelled with a single 2AP base has been studied, to see if excitation at wavelengths longer than those normally used to excite 2AP in DNA (typically 300-320nm) would reveal red-shifted emission. The results are shown in Figure 5.8.

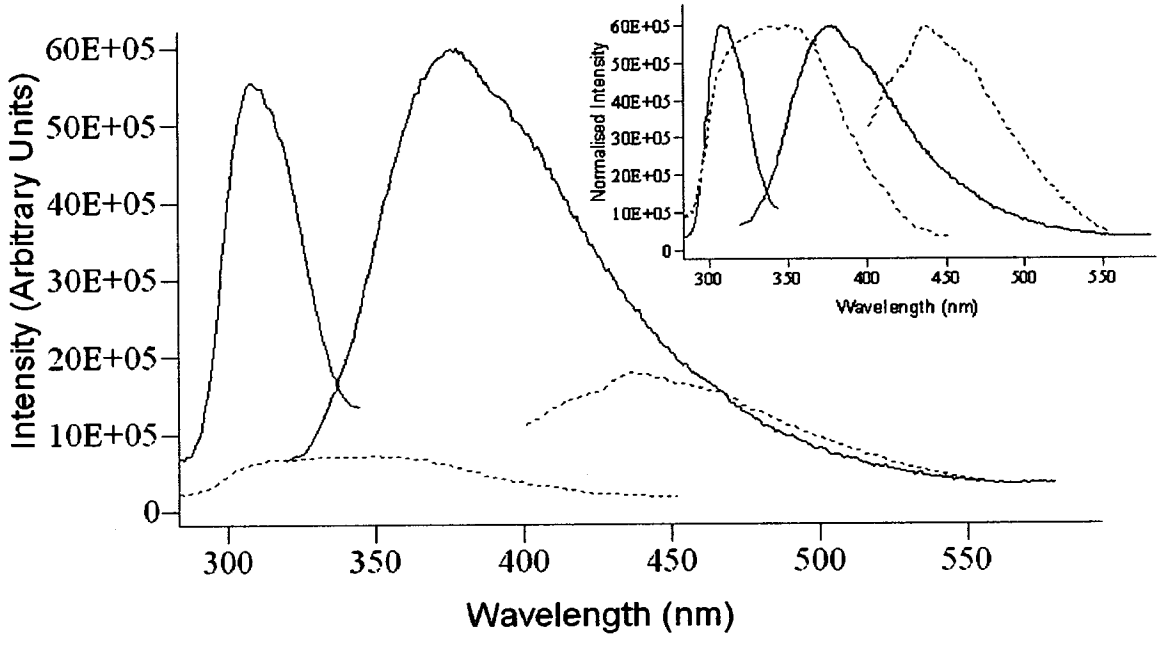

Figure 5.8- Excitation (blue) and emission (red) spectra for the 2AP labelled PG(GG)1 duplex (sequence described in Figure 6.3). Excitation spectra are taken at emission wavelengths of 360nm (solid line) and 480nm (dashed line). Emission spectra are for excitation at 300nm (solid line) and 380nm (dashed line). Inset shows spectra normalised to the maximum intensity of the 300nm emission spectrum.

The 2AP in this duplex (labelled PG(GG)1) is opposite to and flanked by guanine bases, its full sequence is described in Chapter 6, Figure 6.3. Excitation at 300nm produces the familiar 2AP emission spectrum, similar to that presented for aqueous 2AP in the previous Chapter. However,

excitation at 380nm does indeed give rise to longer wavelength emission, causing a shift in the emission maximum to 450nm. The long wavelength emission band is substantially weaker than the short wavelength band. The excitation maximum for this band is around 350nm. These preliminary results suggest the existence of a stacked conformation in which 2AP interacts with its guanine neighbours to form a heterotrimer-like species, analogous to the long-wavelength emitting π-stacked 2AP found in the crystal. The implication is that the short-lived, short-wavelength emission of 2AP in DNA is not due to a conformational state with a fully stacked ground-state structure, but to a locally excited state of the 2AP molecule, which is efficiently quenched by interbase electron transfer before it reaches a fully overlapped trimer-like structure.

Recently, Su *et al*[70] reported unusual red-shifted 2AP fluorescence emission and excitation spectra from a complex of 2AP-labelled DNA with the EcoKI methyltransferase (M.EcoKI). The long-wavelength emitting species is formed on base-flipping of 2AP into the enzyme active site and corresponds to a specific three-dimensional arrangement of the protein, the cofactor (S-adenosyl methionine) and DNA around the 2AP itself. Examination of mutant enzymes showed that the red-shifted emission depended on the location of an aromatic amino acid residue (Phe269) in the active site. The spectra reported by Su *et al* are very similar to those we observe for stacked 2AP. It seems likely, therefore, that the red-shifted emission arises from 2AP stacked with aromatic groups (possibly Phe269 and S-adenosyl methionine) in the M.EcoKI active site. There is evidence for such π-stacking in the co-crystal structure of a related methyltransferase, M.TaqI[71], which features in Chapter 8 of this work.

5.4 Conclusions

The work presented in this Chapter has demonstrated that the photophysical properties of 2AP are, to a great extent, determined by the π-stacking interactions that the molecule experiences. The structure and fluorescence response of 2AP in the DNA duplex is mimicked by the crystalline 2AP.

The crystal structure of 2AP shows π-stacking and hydrogen-bonding interactions analogous to those found in duplex DNA. Interaction between neighbouring 2AP molecules in the π-stacks results in fluorescence excitation and emission spectra that are substantially red-shifted relative

to those of locally excited 2AP. In addition to the long-wavelength-emitting stacked 2AP molecules in the bulk of the crystal lattice, there exist, at defect sites, 2AP molecules which are essentially unperturbed by intermolecular interactions. The latter, isolated 2AP molecules have the short-wavelength excitation and emission spectra characteristic of locally excited 2AP, as observed for free 2AP in solution. The short-wavelength 2AP emission may be associated with the presence of a small fraction (~15%) of the 7H tautomer in the crystal lattice; it may originate from the 7H tautomer itself or from 9H molecules in the vicinity of a 7H tautomer, where the local lattice structure is disrupted.

Although the very short decay component of 2AP in DNA is commonly attributed to a stacked conformation, it does not display the spectral characteristics of strong ground-state interbase interaction, seen for stacked 2AP in the crystal. The short-wavelength fluorescence typical of 2AP-labelled DNA resembles that of isolated 2AP in the crystal. The multiexponential decay of the isolated 2AP fluorescence reflects the heterogeneous structure of defect sites in the crystal. The predominant decay component has a very short lifetime of ~40ps, indicating that rapid non-radiative decay can occur by processes other than electron transfer from guanine. A range of static intermolecular interactions in the crystal gives rise to similar non-exponential decay behaviour to that shown by 2AP in DNA, demonstrating that such behaviour does not necessarily involve conformational fluctuations.

Low lying excited states have been predicted to exist in stacked 2AP-nucleobase dimers and trimers, but have been assumed to be dark states. However, evidence of a long-wavelength-emitting stacked conformational state of 2AP in DNA has been presented. In this conformational state, the electronic structure of 2AP is significantly perturbed by interaction with its neighbouring bases, whereas, in the short-wavelength emitting conformations the electronic structure of isolated 2AP is essentially retained.

The present observations taken together with two recent reports from other groups[58;70] suggest that red-shifted fluorescence from 2AP may be a widespread phenomenon, observable when 2AP intimately π-stacks with other aromatic species. However, where this emission coexists with intense, short-wavelength 2AP emission, as in the DNA helix, it may only be apparent at excitation wavelengths longer than those normally used to excite 2AP.

Chapter 6

2AP as a Probe of the DNA Duplex

6.1 Introduction

The studies presented in Chapters 4 and 5 of the thesis have given a good indication of the sensitivity of the fluorescence response of 2AP to its immediate environment. The studies on 2AP in the crystal and in aqueous solution demonstrate the principle that lies at the heart of the use of 2AP as a probe of the DNA duplex. In the constrained π-stacked environment of the 2AP crystal, the fluorescence lifetime of the vast majority of 2AP molecules is significantly shorter than that of a 2AP molecule in aqueous solution. Similarly, 2AP fluorescence for 2AP stacked within the DNA duplex is highly quenched, but is enhanced if the duplex structure is perturbed in some way. Such perturbations in duplex structure are frequently caused by protein binding and as a result 2-AP emission intensity has been used for monitoring DNA polymerase reactions[72], helicase activity[73] and the action of DNA repair enzymes[47;74-76] and methyltransferases[77-79]. However, a change in fluorescence intensity can result from many different processes and does not necessarily infer a defined structural distortion of the DNA duplex. The measurement of fluorescence lifetimes provides a means of obtaining quantitative information that describes the number of 2AP molecules in distinct environments within the DNA duplex. By understanding how environment affects the fluorescence lifetime of 2AP an understanding of the behaviour of the ensemble of DNA molecules can be acquired in terms of the DNA base dynamics.

The first polynucleotides to be synthesised containing 2AP comprised alternating 2AP/ RNA bases and were produced and studied by Stryer et al[25]. When stacked in the polynucleotide duplexes, 2AP fluorescence is quenched 100-fold relative to the free base and a red shift in the excitation spectrum is observed ($\lambda_{ex\ max}$=315nm compared to 303nm in aqueous solution). Melting of the duplex causes a blue shift in the excitation spectrum. No significant change in the

emission spectrum of the polynucleotide relative to the free base was observed. Later work by Evans and co-workers[26] also notes a blue shift in the excitation spectrum upon melting of a 2AP-labelled DNA decamer. They state that the shift in excitation maximum occurs 5°C or more below the duplex melting temperature and attribute it to exposure of the 2AP to hydrogen bonding water molecules.

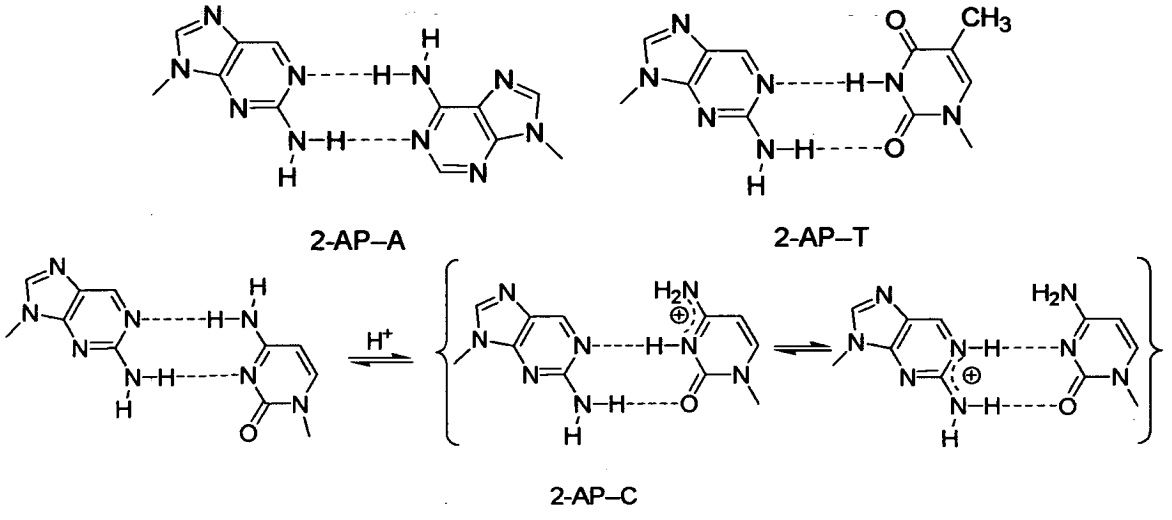

Figure 6.1- Proposed base pair structures for 2AP and three nucleic acid bases for which it is known to form stable hydrogen bonding interactions. Hydrogen bonding between 2AP and cytosine takes the form of either the wobble base-pair (left) or the protonated base-pair (right).

The efficient fluorescence quenching observed for 2AP in a polynucleotide duplex compared to the free 2AP base has been explained by quenching mechanisms that are dependent on base stacking, inter-strand hydrogen bonding or both. A study of 2AP-containing heptamers by Eritja et al[80] shows that it is possible to monitor the cooperativity of hydrogen bonding between 2AP and an opposing base, for short DNA duplexes, using UV absorption measurements as measure of the duplex melting temperature. This and subsequent studies study show that the strength of the base pairs is as follows; 2AP-T > 2AP-A ~ 2AP-C > 2AP-G [81;82]. Proposed structures for the 2AP-X (where X= T, A, C) are illustrated in Figure 6.1. The 2AP-G base pair shows no change in cooperativity with temperature; the two opposing bases in this case do not hydrogen bond and so no structure for this interaction is shown in Figure 6.1. Melting temperatures for these base

pairs show that 2AP-X pairs dissociate at temperatures 2-3°C less than the 'natural' base pairs in the heptamer studied[80].

Early studies by Sowers et al[83] proposed that the protonated 2AP-cytosine base pair shown in Figure 6.1 was the predominant form of bonding between these bases. More recent research, however, favours the wobble base pair, Figure 6.1, between the two bases. Both conformations are thought to be present at physiological pH in the ratio of 25:1 (wobble: protonated structures)[84]. NMR studies have shown that the 2AP-T base pair has a lifetime significantly shorter than the A-T base pair lifetime in a DNA decamer[2;83]. The lifetimes of base pairs are of the order of milliseconds but vary significantly depending upon the sequence context and distance from the end of the duplex of the pair in question.

Nordlund et al[46] studied the time-resolved fluorescence of a 2AP labelled DNA decamer that contained the recognition sequence for the *Eco*RI protein. The 2AP was incorporated into the helix such that it was base-paired with either another 2AP molecule or adenine. Time-correlated single photon counting (TCSPC) showed that the fluorescence decay could be described by the sum of no fewer than four exponential terms. The recorded lifetimes were τ_1= 100ps, τ_2= 0.64ns, τ_3= 3.0ns and τ_4= 8.2ns, these components have A-factors of 0.46, 0.32, 0.13 and 0.09 (at 25°C) respectively. Decay curves were recorded as a function of temperature through the melting point of the duplex (33°C). The fluorescence lifetimes varied considerably as a function of temperature. In the case of τ_{1-3} their magnitude increased from low temperatures (T= 4.3°C) to a maximum value at around 25°C when the duplex began to melt. After melting these lifetimes remained constant. The magnitude of τ_4 was seen to decrease constantly with increasing temperature. The A-factor for each component remained reasonably constant over the range of temperatures investigated. On the basis of these measurements, Nordlund et al attributed τ_4 to an unstacked 2AP base that experiences a solution-like environment, whereas τ_{1-3} were ascribed to heterogeneously π-stacked 2AP molecules, each experiencing a different microenvironment. τ_1, τ_2 and τ_3 were thought to increase with heating, since the duplex becomes increasingly mobile and accessible to solvent molecules. Upon duplex melting these lifetimes decreased due to increased collisional quenching and a change in stacking interactions associated with the dissociation of the duplex. After melting, in the single stranded oligos τ_{1-3} represented a more dynamic system that remains relatively unperturbed by increasing the temperature. Quoted χ^2

values for fits to these decays are generally poor- ranging from 1.34 to 4.69 and so these results must be viewed with some caution. Indeed, values of χ^2 as high as 4.69 clearly indicate that the fitted response is a poor representation of the experimental data. Nordlund et al also noted that the 2AP-labelled DNA has a bi-exponential anisotropy decay with rotational correlation times of 150ps and 900ps (25°C). These were attributed to internal motion of the 2AP base and overall rotation of the DNA decamer respectively. Correlation times for both rotations decrease with increasing temperature.

A later study by Guest *et al*[49] gives a systematic assessment of the fluorescence properties of 2AP in the DNA helix as a function of its complementary base and system temperature. The outcomes of their study are in line with the observations made by Nordlund et al[46]. 2AP lifetimes of <80ps and >6ns are attributed to π-stacked and solvent-exposed 2AP respectively. For 2AP paired with T or G the study showed that the amplitude of the shortest lifetime component (τ_1) did not vary with temperature (between 4°C and 40°C). However, when the complementary base was either A or C, the amplitude of τ_1 was seen to decrease with increasing temperature. This phenomenon is explained by the relative strengths of the base pairs. The 2AP-T bond is too strong to be perturbed by this increase in temperature. In the case of opposing 2AP-G bases there was no apparent cooperativity between the bases and so the amplitudes of the π-stacked and solvent-exposed 2AP components were unaffected by an increase in temperature. The weak 2AP-C and 2AP-A hydrogen bonds, however, were perturbed by the temperature increase investigated and this, the authors argue, gave rise to the decrease in the amplitude of τ_1.

There are few theoretical studies on the electronic properties of 2AP in an environment that approaches the complexity of the DNA helix. Recent works by Jean and Hall[69;85] examine the response of the electronic properties of 2AP to its immediate environment. Their calculations on stacked dimeric and trimeric nucleic acid bases show that the distribution of electronic density in these systems varies greatly depending on the bases present and their orientations relative to one another. These studies predict the formation of ground state complexes between 2AP and the DNA bases. Charge transfer is highlighted by Jean and Hall as an important process in the DNA duplex. These calculations support the argument given by Nordlund et al[46] that the multi-exponential decay of 2AP in DNA could be due to subtly different stacking conformations of 2AP in the helix.

The ability of 2AP to probe base π-stacking and excision, evident from the studies by Nordlund *et al*[46] and Guest *et al*[49], has been used to probe DNA-protein interactions in several systems. Examples include work by Goodman et al, Millar et al and Joyce et al on the proofreading and repair mechanism of the Klenow fragment of DNA polymerase I [48;72;86], work by Rao et al on the DNA recombination protein RecA [87] and work by Stivers, Ross et al on abasic site repair by uracil DNA glycosylase [47;75;88].

A novel use of the ability of 2AP to report the extent of stacking within a DNA duplex was described by Tashiro and Sugiyama who have developed a 'nanothermometer' based on a 2AP labelled DNA molecule[89]. The thermometer is a DNA decamer, which shows a reversible transition between the Z-DNA and B-DNA forms over the temperature range of 2°C -32°C. By positioning the 2AP base so that it is 'unstacked' in Z-DNA, but not in the B-form, the thermometer shows a fluorescence intensity which is directly related to the proportion of Z-DNA in the solution and hence the solution temperature.

The ability of adjacent bases in the DNA duplex to interact with each other, leading to energy transfer is illustrated by Nordlund *et al*[90;91]. The group show UV-absorption data and steady-state fluorescence measurements that provide firm evidence of energy transfer to 2AP from neighbouring DNA bases. Energy transfer efficiency is of the order of a few percent and is seen to decrease with increasing duplex temperature until the duplex melts. In single stranded DNA, energy transfer occurs with low efficiency but this increases with increasing temperature. Later studies by the same group show that π-stacked adenine bases transfer energy to 2AP an order of magnitude more efficiently than the other bases and that there is no preferred direction for the transfer along the helix. Linn *et al* showed that inter-strand energy transfer in 16-mer DNA duplexes can be almost as efficient as intra-strand transfer, depending on the sequence context of the 2AP[92]. The presence of adenine and a well-stacked 2AP base were shown to be important in maintaining efficient energy transfer.

Recent work by Johnson et al[59] and Rist et al[58] has identified the formation of excitonic interactions in the DNA duplex. This work was discussed in the previous Chapter in the context

of the interaction between 2AP molecules in the pure 2AP crystal. The π-π interactions between 2AP and the bases adjacent to it in the duplex are vitally important in understanding the complex fluorescence response of 2AP.

A recent study by Hall and Williams compares NMR and TCSPC data to the simulated dynamical motions of 2AP within an RNA hairpin [51]. Reported fluorescence decays are of poor quality and relatively low resolution (32ps/channel) but largely show results consistent with previous studies. Simulations illustrate the dynamic nature of the RNA system but fail to further current understanding of the isotropic fluorescence decay of 2AP. The group report anisotropy decays for 2AP with rotational correlation times of ~300ps and 1.7ns. The short correlation time is ascribed to a combination of the rapid motions of the 2AP base and depolarisation of the emission dipole through mixing of the excited state of 2AP with adjacent bases. Hall and Williams argue that the 1.7ns decay is too fast to be accounted for by global tumbling of the RNA hairpin. This is therefore ascribed to a combination of this tumbling and other supermolecular motions such as twisting and bending.

Electron transfer in DNA has recently been established as one of the mechanisms contributing to the non-radiative decay of excited 2AP in DNA. Kelley and Barton showed that electron transfer from guanine to excited-state 2AP occurs in the DNA helix [20]. The driving force for electron transfer (ET) is the relatively low oxidation potential of guanine, estimated as E^0= 1.3V vs NHE (normal hydrogen electrode), as compared to the other bases [93]. (Oxidation potentials for the other DNA bases are A: E^0=1.4V vs NHE, C: E^0=1.7V vs NHE, T: E^0=1.8V vs NHE). Kelley and Barton calculated the reduction potential of excited-state 2AP (2AP*) to be +1.5V versus NHE implying that electron transfer from guanine and perhaps adenine is feasible. Their study shows that the intensity of 2AP fluorescence is strongly dependent on the proximity of the 2AP to a guanine base. Electron transfer occurs both intra- and interstrand, though the kinetics of the transfer varies in each instance. Intrastrand electron transfer was shown to occur on a timescale faster than 100ps. Transfer efficiency depends on several factors including the G-2AP distance, the bases mediating the transfer and the extent of π-stacking in the duplex. Interstrand ET is less efficient and thought to be slower than intrastand transfer. However, its efficiency decreases less with distance than for intrastrand ET. Interstrand ET depends sensitively on the extent of the

base stacking, and, hence, the proximity of the 2AP acceptor base to the opposite strand of the duplex.

The Barton group followed their initial study with a methodical investigation into the effect of changing the driving force for ET, the effect of changing the base adjacent (3') to 2AP and the distance dependence of ET rates[94]. Using transient absorption and fluorescence upconversion measurements the study showed that ET to an adjacent (3') guanine base occurs with a lifetime (1/rate of electron transfer) of 10ps (analogous lifetimes for the other native bases are reported as 120ps for thymine, 260ps for adenine and 300ps for cytosine). The authors argue that these decay rates for 2AP, with different bases adjacent to and 3'- of it, are indicative of both oxidative (G, A) and reductive (A, T) charge transfer by 2AP. The authors present this hypothesis based on the observed trend in charge transfer kinetics, where the reported rate of charge transfer decreases as the 3' base to 2AP is changed from G>T>A>C. Since this trend cannot be explained by either the driving force for either oxidative (G>C>A>T) or reductive (T>A>C>G) charge transfer a combination of the two processes is used to explain the experimentally observed decay kinetics. Despite this neat extrapolation, data from these experiments is of low precision and assigned lifetimes must be viewed with caution. Barton el al[94] also investigate the variation in charge transfer rate with various 'bridging' bases. The bridging base(s) are those between the 2AP and the 'driving force' for the ET, guanine. Adenine is found to be the most efficient base for mediating ET, whereas the pyrimidine bases (T, C) effectively prevent it from occurring. Electron transfer remains measurable over a distance of three adenine bases (~14Å) between 2AP and G.

Larsen *et al*[95] use a fluorescence streak camera to measure the decay kinetics of 2AP in a DNA hairpin on a similar timescale (with picosecond resolution) to Wan *et al*[94]. Their data show that the 2AP decay is fitted by the sum of four exponentials on the 2ns timescale of their experiments. Recorded lifetimes are of 10-20ps, 50-100ps, 400-600ps and >8ns. The group show that whether 2AP is near to or far from a guanine base in the helix a short lifetime component (of 10-20ps) is seen in the decay curve. In the case where 2AP is adjacent to and to the 3' side of a guanine base this component dominates the decay, accounting for the rapid decay of 90% of the excited state population. In agreement with previous interpretations by Nordlund et al [46] and Wan et al [96] the authors propose that 2AP experiences a range of different stable conformations in the DNA duplex. In each conformation 2AP has a different efficacy for ET and gives rise to a

slower or faster decay time depending on the probability of ET occurring in that conformation. Fluorescence emission spectra for each of the four decay components in this study are essentially identical suggesting that the immediate environment of 2AP is similar for each of the conformations it adopts.

A recent publication by Jean and Hall[97] describes how structural heterogeneity combined with an efficient quenching mechanism, such as electron transfer from guanine, can lead to a multi-exponential fluorescence decay of 2AP in an oligodeoxynucleotide trimer. The authors describe a conformationally stacked, energetic 'sink' in the duplex, accessible to the excited 2AP molecule, where de-excitation of 2AP* is particularly efficient. 2AP molecules sample this sink as they move from 'unstacked' to 'stacked' conformations. The authors argue that the existence of short-lived (picoseconds- nanoseconds), unstacked conformations for the 2AP would give the requisite non-exponential fluorescence response. The use of dynamics to explain the heterogeneity of the 2AP fluorescence decay is valid but the work presented in the previous Chapter of this thesis shows that a multiexponential decay for 2AP is seen in a static system. Hence, the observation of a multiexponential decay does not imply a system that is dynamic on the timescale of the TCSPC experiment. This model is discussed in more detail in the rationalisation of the results presented later in this Chapter.

Subsequent studies by Barton and O'Neill add further weight to the case for charge transfer as a mechanism for quenching of 2AP fluorescence in DNA [98-100]. Both steady-state and ultrafast time-resolved fluorescence measurements are used in this work. Electron transfer from guanine is shown to be most efficient in the 3' to 5' direction and the efficient mediation of ET by adenine is also confirmed. Direct evidence for ET from guanine to 2AP has been delivered in a recent paper by O'Neill, Dohno and Barton [50]. The group use cyclopropylguanine (^{CP}G) to trap the intermediate oxidised guanine radical before the redistribution of charge (back electron transfer) along the helix can occur. Figure 6.2 shows the mechanism for the 'hole trapping'.

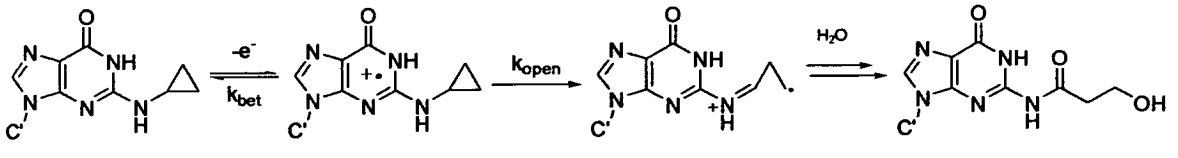

Figure 6.2- Hole trapping by cyclopropyl guanine

The study shows that the concentration of ^{CP}G in the sample falls as sample exposure time to 325nm irradiation increases. Interestingly, the photodecomposition of ^{CP}G occurs only in the case when there is more than one intervening base pair between the 2AP and ^{CP}G bases. In this instance, the group attribute the lack of ^{CP}G oxidation to back electron transfer (BET) from ^{CP}G to 2AP on a significantly shorter timescale than that of the ring opening process (Figure 4). Hence, the lifetime of the charge separated intermediate in the ET process is related to the distance between the donor and acceptor bases.

During the course of the present investigation the fluorescence response of ten different 2AP labelled DNA duplexes have been recorded, each at a single excitation and three different emission wavelengths. These duplexes were specifically designed in order to investigate the interactions with the enzymes introduced in subsequent Chapters and so do not allow a complete systematic investigation of the 2AP fluorescence response as a function of its DNA sequence context. However, the data collected from these duplexes form an important body of information and some interesting conclusions can be drawn with regards to the photophysical behaviour of 2AP in the DNA duplex. The complete DNA sequences for these duplexes are shown in Figure 6.3.

PT(AC)1	5'-CACGGGCCTAPCGATATCGTGCGTACGAGC-3' 3'-GTGCCCGGATTGCTATAGCACGCATGCTCG-5'
PT(AC)2	5'-CACGGGCCTAPCGATATCGTGCGTACGAGC-3' 3'-GTGCCCGGATTGCTATAGCMCGCATGCTCG-5'
PT(CC)1	5'-CPCGGGCCTAACGATATCGTGCGTACGAGC-3' 3'-GTGCCCGGATTGCTATAGCACGCATGCTCG-5'
PT(CC)2	5'-CACGGGCCTAACGATATCGTGCGTACGAGC-3' 3'-GTGCCCGGATTGCTATAGCPCGCATGCTCG-5'
PT(TA)	5'-CACGGGCCTPACGATATCGTGCGTACGAGC-3' 3'-GTGCCCGGATTGCTATAGCACGCATGCTCG-5'
PT(GG)	5'-GACAGTATCAGGCGCCTCCCCACAA _-3' 3'-_ TGTCATAGTCCGMGGPGGGGTGTTG-5'
PC(GC)	5'-GACTGGTACAGTATCAGPCGCTGACCCACAACATCCG _-3' 3'-_ TGACCATGTCATAGTCCGMGACTGGGTGTTGTAGGCT-5'
PC(MC)	5'-ACTGGTACAGTATCAGGCGCTGACCCACAACATCTG-3' 3'-TGACCATGTCATAGTCCPMGACTGGGTGTTGTAGAC-5'
PG(GG)1	5'-GACTGGTACAGTATCAGGPGCTGACCCACAACATCCG _-3' 3'-_ TGACCATGTCATAGTCCGMGACTGGGTGTTGTAGGCT-5'
PG(GG)2	5'-GACAGTATCAGGCGCCGCCCCACAA _-3' 3'-_ TGTCATAGTCCGMGGPGGGGTGTTG-5'

Figure 6.3- DNA duplex sequences and nomenclature; P is used to denote 2AP and M to denote a methylated cytosine or adenine base. Duplexes are named PX(Y1Y2), where X denotes the base paired to 2AP, and Y1, Y2 are the bases immediately 5' and 3' of 2AP respectively.

The top five duplexes in Figure 6.3 (PT(AC)1, PT(AC)2, PT(CC)1, PT(CC)2 and PT(TA)) are based on the same sequence of 30 DNA bases and, for all but PT(AC)2, vary only in the position of the adenine base that has been substituted for 2AP. PT(AC)2 is identical to PT(AC)1 but has a methylated adenine ('M') on its lower strand, as illustrated. The PT(GG) and PG(GG)2 duplexes are identical, apart from, as their names indicate, the base opposite the 2AP. The PC(GC), PC(MC) and PG(GG)1 are similar to one another but the ends of the PC(GC) and PG(GG)1 duplexes have single overhanging (unpaired) bases.

6.2 Experimental

Crystals of the DNA-protein-cofactor complex were grown using in small wells of liquor, using the vapour diffusion method by the Klimasauskas group at the Institute of Biotechnology in Vilnius, Lithuania. The solution containing the DNA-M.HhaI-cofactor ternary complex was diluted in an equal volume of the aqueous crystallisation solution containing 50 mM sodium citrate at pH 5.6, 1.2-2.0mM ammonium sulfate and 0-15% glucose. The crystals tended to grow on the floor of the wells. In order to mount them in the quartz capillaries used for the fluorescence experiments, the crystals were first dislodged from the well floor. This was done using an improvised tool made of a glass Pasteur pipette, in the end of which a short hair was mounted with some sealing wax. The hair (actually from a pet rat as human hair tends to be too fine for this purpose) allowed the fragile crystals to be gently pushed from the base of the wells. Once mobile, the crystals were sucked into a quartz capillary of 1mm diameter (Hampton Research) using the following method. The capillary was attached, using sealing wax, to a 20μL pipette, via a pipette tip. A small amount of the well solution (i.e. the salt-solution, free of the ternary complex) was sucked into the capillary. The tip of the capillary was then placed into the crystal-containing solution, in close proximity to one, or a number of crystals. The solution was sucked into the capillary in one, swift motion such that the crystals were carried along with the well solution into the capillary. As much of the well solution as possible was removed from the proximity of the crystals as possible using thin paper wicks (Hampton Research). A small droplet of this well solution was left intact around a suitable crystal to prevent it from becoming dehydrated. Finally, a small amount of the well solution was sucked into the capillary, the capillary was detached from the pipette tip and the two ends of the capillary were sealed using sealing wax.

Fluorescence decay curves were collected at an excitation wavelength of 317nm, at three different emission wavelengths (370nm, 390nm and 410nm). For the crystalline duplexes, fluorescence decay curves were collected to 10000 counts in the peak channel on a timescale of 50ns and with a resolution of 12.2ps per channel. For the solution phase DNA duplexes, data was collected on two timescales (50ns with resolution of 24.41ps/ channel and 20ns with resolution of 4.883ps/ channel) for each DNA duplex.

Fits of the data from solution phase systems were made globally (at all wavelengths) but on the 20ns and 50ns timescales separately, since the programme (Edinburgh Instruments' 'Level 2' software) used to fit the decay curves did not allow the simultaneous fitting of data collected with different time resolution. To make full use of both the high time resolution of the data recorded on the 20ns timescale (4.9ps/channel) and the long period of the 50ns timescale the data from each of these timescales were fitted 'globally' using a manual iteration, as described below.

Initially, global fits for the 20ns timescale were calculated. The shortest lifetime component from this fit was then fixed in the global analysis of the decays collected on the 50ns timescale. The longest lifetime determined for this fit was then fixed in the second round of analysis of the data for the 20ns timescale data. Complete data for these samples are presented in the Appendix of this thesis.

6.3 Results

6.3.1 2AP-labelled DNA duplexes in the crystal phase

The steady-state emission spectra and time-resolved fluorescence responses for 2AP in two crystalline DNA duplexes were recorded. Crystals of protein-bound DNA, where the 2AP base is located several base-pairs from the protein binding site, allow the effective study of 2AP in a static DNA duplex. Two different DNA duplexes, PT(GG) and PG(GG)2, were examined using this method. The crystal structures of the ternary complexes in which these duplexes are bound are shown in Figure 6.4 and illustrate how the 2AP in each duplex is relatively unperturbed by the protein.

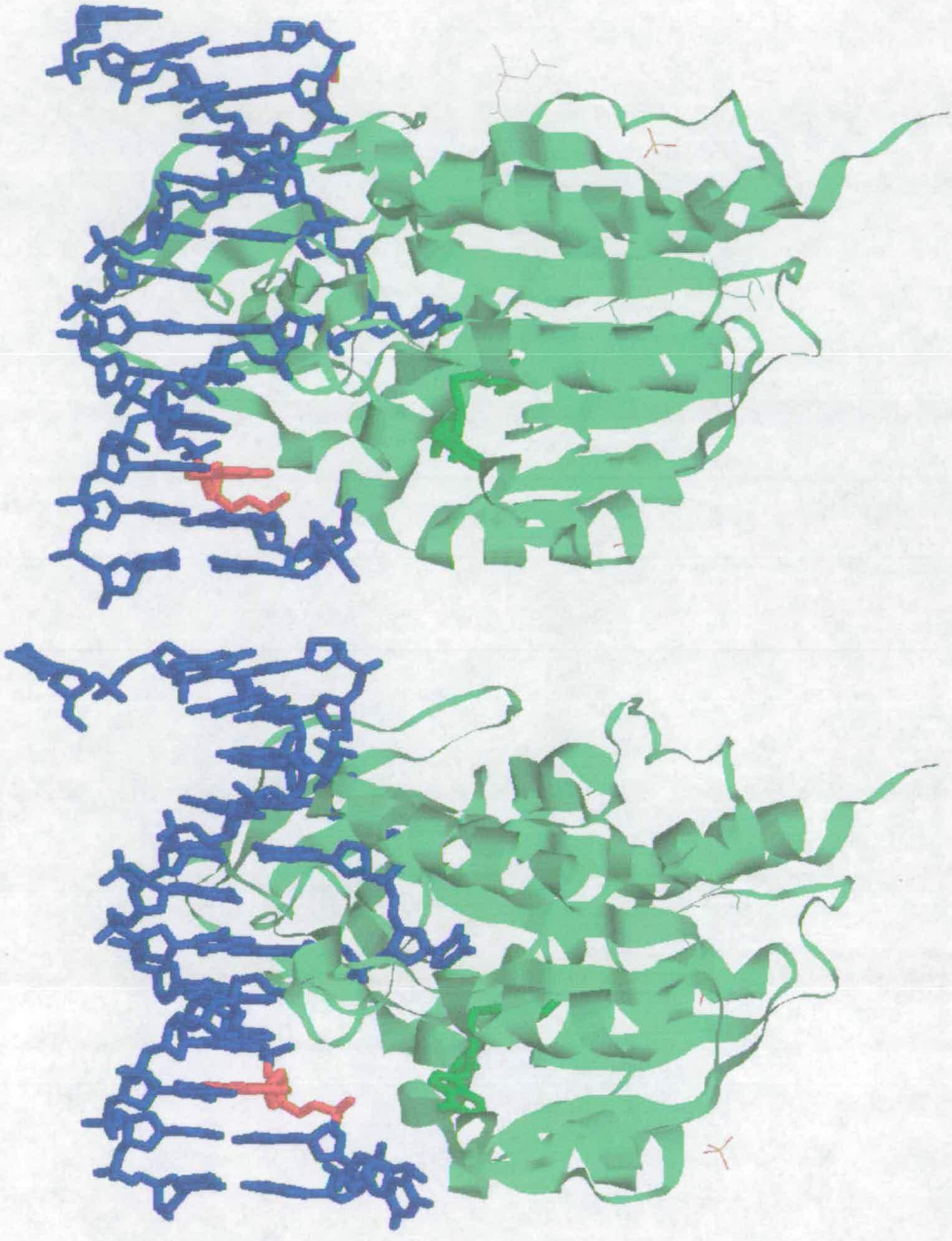

Figure 6.4- The crystal structures of the PG(GG)2 (top) and PT(GG) duplexes (blue) in ternary complexes with HhaI (green ribbons) and the AdoHcy cofactor (green sticks). The 2AP base is shown in red.

Figure 6.5 and Figure 6.6 illustrate the local environment of the 2AP probe in the PG(GG)2 and PT(GG) duplexes respectively.

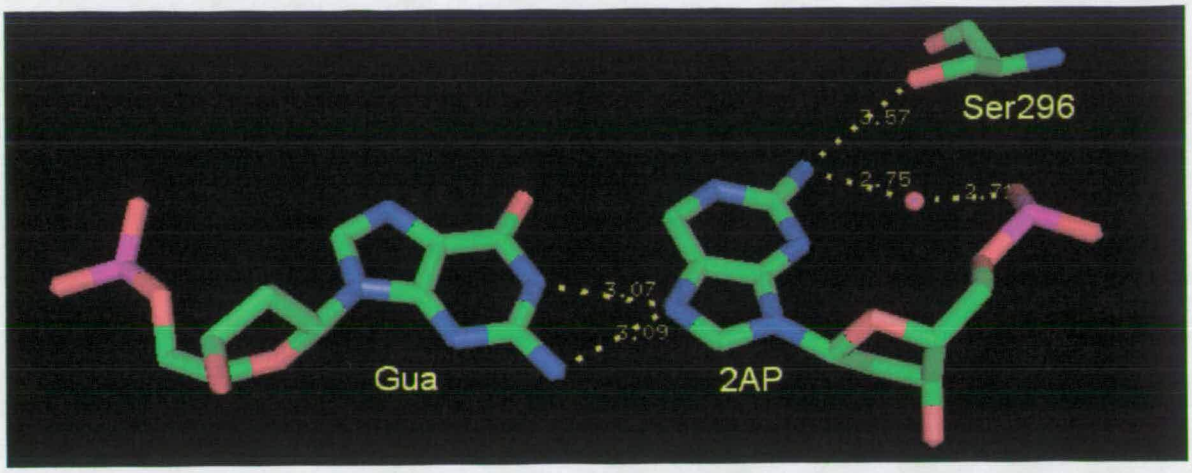

Figure 6.5- The immediate environment of 2AP in the crystalline PG(GG)2 duplex. Note that the lone oxygen atom (red) in the image denotes the presence of a water molecule. Distances shown are for donor-acceptor interactions between hydrogen bonding atoms.

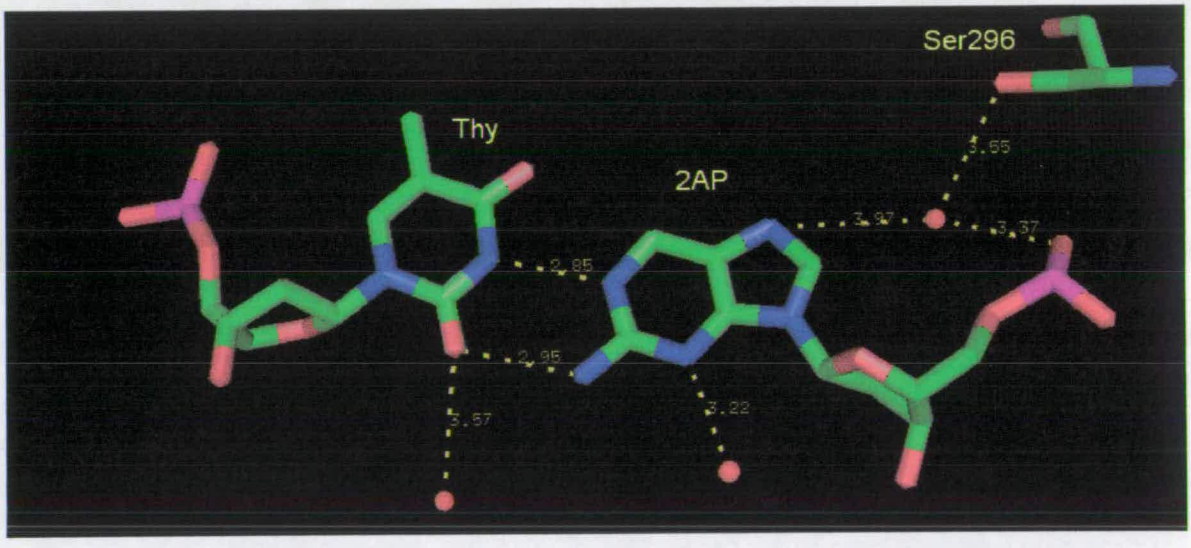

Figure 6.6- The immediate environment of 2AP in the crystalline PT(GG) duplex. Water molecules are shown as lone oxygen atoms (red). Distances shown are for donor-acceptor interactions between hydrogen bonding atoms.

Figure 6.4 shows the position of the 2AP probe in relation to the position of the HhaI enzyme and the contacts it makes with the DNA duplex. In both the PG(GG)2 and PT(GG) duplexes, the

2AP is intrahelical and its immediate environment is relatively unperturbed by the enzyme. Figure 6.5 shows the atomic environment of 2AP in the PG(GG)2 duplex. Remarkably, the 2AP adopts a *syn* conformation in the duplex, forming a Hoogsteen-type base pair[101] with the guanine opposite it. This conformation is adopted as the result of a simple rotation of the 2AP about the N9-C1' bond between the 2AP and sugar. The driving force for this conformational change is perhaps a combination of the formation of the hydrogen bonds between the guanine amine group, guanine N1-H and 2AP N7, and the formation of a similar bond between the 2AP amine and the water molecule that is positioned between the 2AP amine group and the phosphate group of the DNA backbone. The hydroxyl sidechain of serine 296 is a relatively long way away from the 2AP, at least, in terms of its hydrogen bonding interaction, and is unlikely to be important in stabilising the syn conformation of the base relative to its other intermolecular interactions. Figure 6.6 illustrates the stable Watson-Crick base pair formed between 2AP and thymine in the DNA duplex. A single water molecule is seen to form a hydrogen bond with N3 of the 2AP.

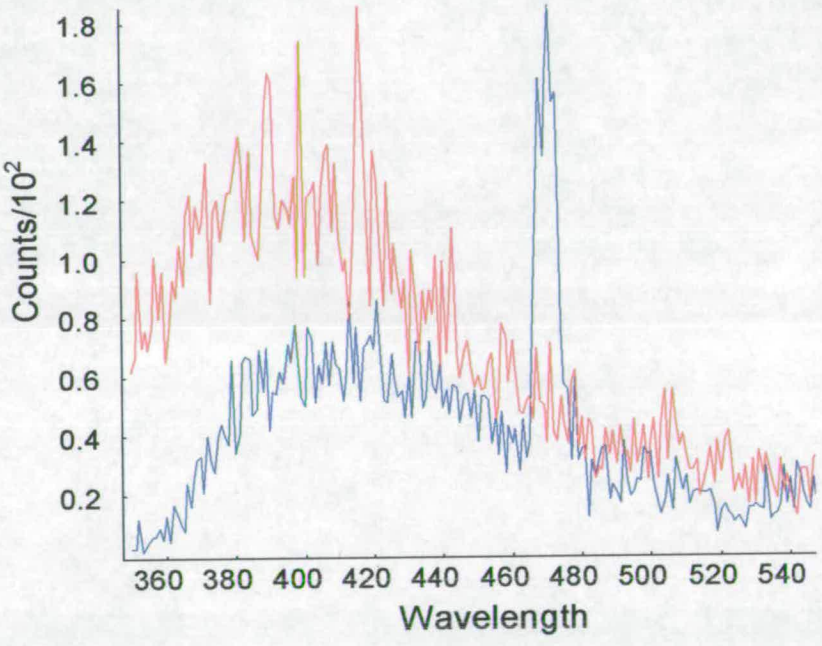

Figure 6.7- The steady-state emission spectra of PT(GG) (red) and PG(GG)2 (blue) with laser excitation at 320nm. Note that the spectra are particularly noisy as a result of the limited emission from a single crystal of micrometer dimensions. The large, sharp peak in the spectrum of PG(GG)2 is due to scattered (second harmonic) laser light.

The steady-state emission spectra of single crystals of the PG(GG)2 and PT(GG) duplexes were recorded at an excitation wavelength of 320nm, prior to the fluorescence lifetime measurements and are shown in Figure 6.7.

Although the spectra of the crystalline DNA duplexes in Figure 6.7 are of poor quality a red shift in the PG(GG)2 duplex as compared to the PT(GG) duplex is discernible. Determining the point at which these spectra peak is somewhat subjective but the spectrum for PT(GG) peaks at approximately 395-405nm, whereas the peak of the PG(GG)2 duplex is at about 405-415nm.

Fits of the time-resolved data were made globally, at three emission wavelengths, for each DNA duplex. Fits made with three components show non-random deviations in their residuals and have reduced χ^2 values of greater than 1.3. Reduced χ^2 values for the reported four component fits are consistently less than 1.1. Figure 6.8 illustrates the results of using these two fits for the PG(GG)2 duplex.

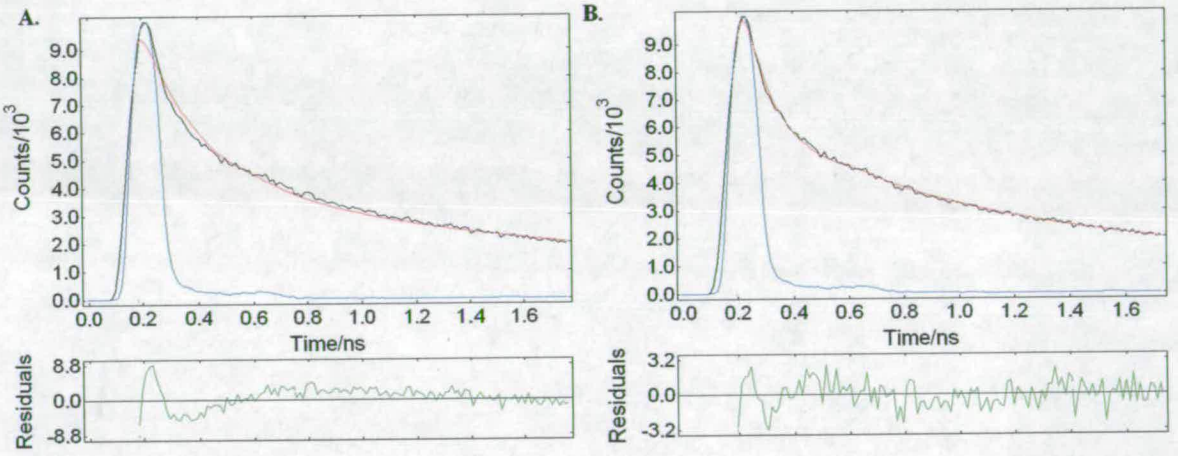

Figure 6.8- A. Reconvolution fit of experimental data with three components. B. Reconvolution fit of experimental data with four components. Data shown is the first 2ns of the fluorescence decay curve (black), the IRF (blue) and fit (red) for the PG(GG)2 duplex emission at 390nm on 50ns timescale. Residuals (green) are also shown. χ^2 is 1.539 for three component fit compared to 1.171 for 4 component fit.

Table 6.1 and Table 6.2 show the globally fitted parameters for the emission from the crystalline PT(GG) and PG(GG)2 duplexes.

Global Lifetimes: τ_1=0.07ns, τ_2=0.53ns, τ_3=2.07ns, τ_4=7.36ns
Global χ^2=1.052

Emission Wavelength/ nm	A1	A2	A3	A4	Local χ^2
370	0.62	0.21	0.14	0.03	1.038
390	0.64	0.19	0.14	0.03	1.073
410	0.66	0.16	0.15	0.03	1.045

Table 6.1- Parameters derived from global fit of the fluorescence response of the crystalline PG(GG)2 duplex.

Global Lifetimes: τ_1=0.09ns, τ_2=0.67ns, τ_3=2.26ns, τ_4=7.31ns
Global χ^2=1.044

Emission Wavelength/ nm	A1	A2	A3	A4	Local χ^2
370	0.59	0.19	0.18	0.05	1.056
390	0.61	0.20	0.15	0.04	1.023
410	0.64	0.20	0.12	0.05	1.053

Table 6.2- Parameters derived from the global fit of the fluorescence response of the crystalline PT(GG) duplex.

The time-resolved fluorescence data, shown in Table 6.1 and Table 6.2, illustrate that the 2AP fluorescence response is described by parameters of a similar magnitude in both systems. The relative standard deviation in the quoted lifetimes is <5%. This was estimated by calculating the relative standard deviation for the (solution-phase DNA) fits on the 20ns and 50ns timescales, then averaging these errors values over ten different systems. The fluorescence decay of both the PT and PG paired duplexes is dominated by a short component of <100ps. Less than 5% of the

2AP molecules in each duplex have fluorescence lifetimes, of around 7.3ns, approaching that of the 2AP ribonucleoside in aqueous solution. There is no significant dependence of the A-factors on the emission wavelength.

6.3.2 2AP labelled DNA duplexes in the solution phase

Tables 6.3 to 6.12 show the results obtained for the ten solution phase duplexes described in Figure 6.3. Note that where values for global and local χ^2 are not given, the presented parameters are derived from separate global fits of decays on the 20ns and 50ns timescales. Full details of these fits are given in the Appendix of this thesis.

Global Lifetimes: τ1=0.12ns, τ2=0.39ns, τ3=2.71ns, τ4=10.81ns

Emission Wavelength/ nm	A1	A2	A3	A4
370	0.88	0.08	0.02	0.02
390	0.84	0.10	0.03	0.02
410	0.81	0.12	0.04	0.03

Table 6.3- Results derived from the global fit of the fluorescence response of the PT(AC)1 duplex.

Global Lifetimes: τ1=0.10ns, τ2=0.25ns, τ3=2.63ns, τ4=11.50ns
Global χ2=1.102

Emission Wavelength/ nm	A1	A2	A3	A4	Local χ^2
370	0.79	0.15	0.02	0.04	1.097
390	0.68	0.24	0.03	0.05	1.092
410	0.63	0.26	0.06	0.06	1.116

Table 6.4- Results derived from global analysis of the PT(AC)2 duplex. Parameters shown are for the fluorescence responses recorded on the 50ns using 4096 channels

Global Lifetimes: τ1=0.05ns, τ2=0.38ns, τ3=2.59ns, τ4=8.51ns

Emission Wavelength/ nm	A1	A2	A3	A4
370	0.75	0.14	0.07	0.05
390	0.75	0.13	0.07	0.05
410	0.69	0.17	0.08	0.06

Table 6.5- Results derived from the global fit of the fluorescence response of the PT(CC)1 duplex.

Global Lifetimes: τ1=0.03ns, τ2=0.45ns, τ3=2.61ns, τ4=10.78ns

Emission Wavelength/ nm	A1	A2	A3	A4
370	0.96	0.02	0.01	0.01
390	0.92	0.04	0.02	0.02
410	0.85	0.08	0.05	0.02

Table 6.6 - Results derived from the global fit of the fluorescence response of the PT(CC)2 duplex.

Global Lifetimes: τ1=0.12ns, τ2=0.58ns, τ3=2.44ns, τ4=8.14ns

Emission Wavelength/ nm	A1	A2	A3	A4
370	0.49	0.34	0.12	0.05
390	0.45	0.36	0.13	0.06
410	0.41	0.37	0.14	0.07

Table 6.7- Results derived from the global fit of the fluorescence response of the PT(TA) duplex.

Global Lifetimes: τ1=0.04ns, τ2=0.44ns, τ3=2.71ns, τ4=10.69ns

Emission Wavelength/ nm	A1	A2	A3	A4
370	0.72	0.10	0.08	0.10
390	0.64	0.15	0.10	0.11
410	0.62	0.19	0.11	0.08

Table 6.8- Results derived from the global fit of the fluorescence response of the PT(GG) duplex.

Global Lifetimes: τ1=0.04ns, τ2=0.45ns, τ3=2.63ns, τ4=10.33ns

Emission Wavelength/ nm	A1	A2	A3	A4
370	0.89	0.06	0.03	0.02
390	0.83	0.09	0.05	0.02
410	0.77	0.14	0.07	0.02

Table 6.9- Results derived from the global fit of the fluorescence response of the PC(GC) duplex.

Global Lifetimes: τ1=0.05ns, τ2=0.50ns, τ3=2.98ns, τ4=9.81ns

Emission Wavelength/ nm	A1	A2	A3	A4
370	0.69	0.12	0.09	0.10
390	0.64	0.16	0.11	0.10
410	0.59	0.21	0.12	0.09

Table 6.10- Results derived from the global fit of the fluorescence response of the PC(MC) duplex.

Global Lifetimes: τ1=0.08ns, τ2=0.58ns, τ3=2.94ns, τ4=9.60ns

Emission Wavelength/ nm	A1	A2	A3	A4
370	0.60	0.18	0.13	0.09
390	0.53	0.26	0.14	0.06
410	0.51	0.30	0.14	0.05

Table 6.11- Results derived from the global fit of the fluorescence response of the PG(GG)1 duplex.

Global Lifetimes: τ1=0.04ns, τ2=0.50ns, τ3=2.95ns, τ4=11.01ns

Emission Wavelength/ nm	A1	A2	A3	A4
370	0.78	0.08	0.08	0.07
390	0.70	0.13	0.10	0.08
410	0.65	0.19	0.11	0.06

Table 6.12- Results derived from the global fit of the fluorescence response of the PG(GG)2 duplex.

Table 6.13 gives a summary of the results contained in Tables 6.4 to 6.22. The lifetimes shown were calculated from the mean of the lifetimes determined on the two timescales for each duplex. Similarly, the reported A-factors are for emission at 390nm and are the mean of the values given in both timescales.

DNA Duplex	A-Factor				Lifetimes/ ns			
	A1	A2	A3	A4	τ1	τ2	τ3	τ4
PT(AC)1	0.84	0.10	0.03	0.02	0.12	0.39	2.71	10.81
PT(AC)2	0.68	0.24	0.03	0.05	0.10	0.25	2.63	11.50
PT(CC)1	0.75	0.13	0.07	0.05	0.05	0.38	2.59	8.51
PT(CC)2	0.92	0.04	0.02	0.02	0.03	0.45	2.61	10.78
PT(TA)	0.45	0.36	0.13	0.06	0.12	0.58	2.44	8.14
PT(GG)	0.64	0.15	0.10	0.11	0.04	0.44	2.71	10.70
PC(GC)	0.83	0.09	0.05	0.02	0.04	0.45	2.63	10.33
PC(MC)	0.64	0.16	0.11	0.10	0.05	0.50	2.98	9.81
PG(GG)1	0.53	0.26	0.14	0.06	0.08	0.58	2.94	9.60
PG(GG)2	0.70	0.13	0.10	0.08	0.04	0.50	2.95	11.01

Table 6.13- Results derived from global analysis of fluorescence decay curves for 2AP labelled DNA duplexes in buffered aqueous solution. Reported A-factors are for 2AP emission at 390nm.

The fluorescence response will be assumed to be a good a reporter of the distribution of the 2AP ground state population. This infers that the distribution of the ground state population does not change upon excitation and is reasonable since there is no rise component seen in the fluorescence response of 2AP in DNA.

Four discrete fluorescence lifetimes are fitted to the decay curves of all the duplexes. The decays are dominated by an efficiently quenched species, with a lifetime of approximately 100ps. In all but one of the duplexes this component accounts for at least 50% of the excited state 2AP molecules and it is always the most abundant emitting species in the free duplex. The A-factors decrease with increasing fluorescence lifetime.

6.4 Discussion

6.4.1 Steady-State Spectra

Figure 6.7 shows the steady-state fluorescence spectra for the crystalline DNA duplexes, PG(GG)2 and PT(GG). With laser excitation at 320nm, the emission spectrum of the PG(GG)2 duplex is significantly red-shifted compared to that of PT(GG). This suggests that the *syn* conformation of 2AP in the PG(GG)2 duplex results in a stronger π-π interaction than the *anti* conformation it adopts in the PT(GG) duplex. Figure 6.9 and Figure 6.10 show the structures of 2AP and its flanking bases in the PG(GG)2 and PT(GG) DNA duplexes, respectively. Figure 6.11 shows the guanine base 5' of the 2AP, along with the 2AP bases from the PG(GG)2 and PT(GG) duplexes superimposed on one another, to illustrate the different stacking interactions between the guanine and 2AP in each duplex.

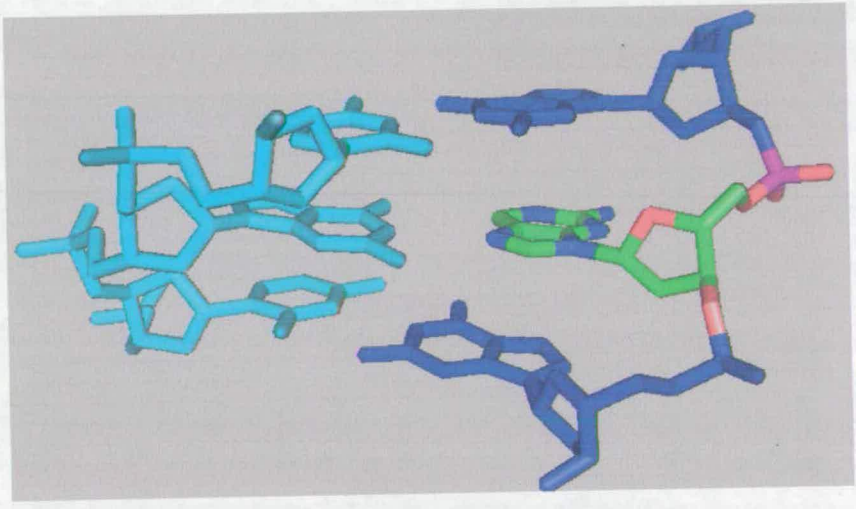

Figure 6.9- Stacking interactions between 2AP and the two adjacent guanine bases in the PG(GG)2 duplex. For the 2AP containing oligonucleotide strand (right), the bases are shown 5' to 3' going from the top to bottom of the Figure.

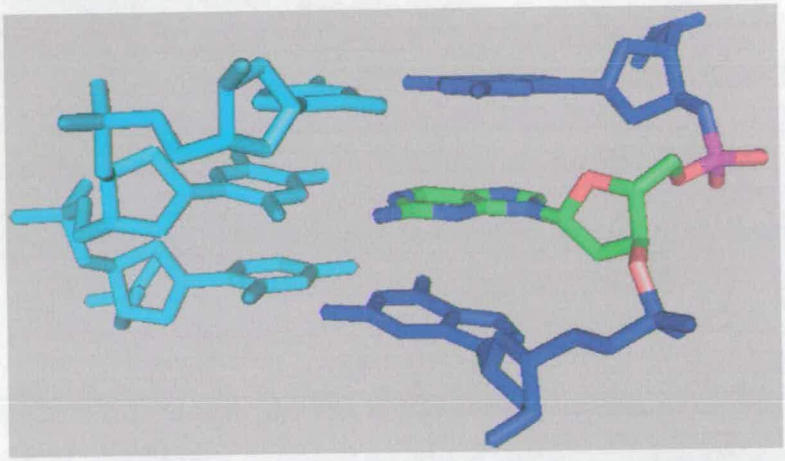

Figure 6.10- Stacking interactions between 2AP and the two adjacent guanine bases in the PT(GG) duplex. For the 2AP containing oligonucleotide strand (right), the bases are shown 5' to 3' going from the top to bottom of the Figure.

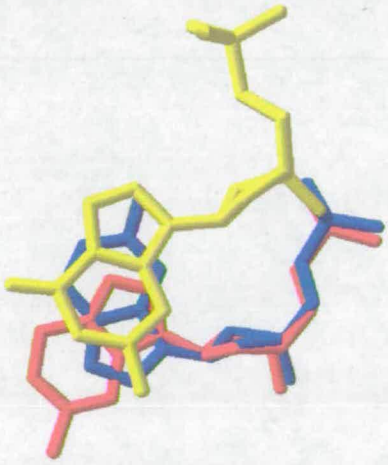

Figure 6.11- Stacking geometry of PT(GG) and PG(GG)2 duplexes. Superimposed 2AP bases for the PT(GG) (red) and PG(GG)2 (blue) duplexes. Also shown is the guanine base (yellow) that is 5' of the 2AP in both duplexes.

It is clear from Figure 6.9, 6.10 and Figure 6.11 that the overlap between the π-electronic orbitals of 2AP and the guanine 5' of the 2AP is significantly different, depending on the conformation, *syn* (PG(GG)2) or *anti* (PT(GG)) of the 2AP. Figure 6.11 shows a view down the DNA duplex, which confirms that the orbital overlap between guanine (yellow) and 2AP is greater in the *syn* conformation (blue), where it is aligned antiparallel to the 5' guanine, as compared to *anti* (red), conformation. The work carried out in the previous Chapter of this thesis

and the study by Rist et al[58] show that a π-stacking interaction between 2AP and a neighbouring base leads to the formation of a ground-state complex between the molecules. The emission from this heterodimer-like species is red-shifted, relative to the emission of the isolated 2AP base. The red-shifted emission of the PG(GG)2 duplex (Figure 6.7), which has a large π-overlap with the 5' guanine as compared to the PT(GG) duplex, is entirely consistent with these observations. It is interesting to consider that in the preceding solution-phase studies, the nature of the π-stacking interaction (i.e. the relative conformations of the bases) that led to heterodimer or heterotrimer formation could not be described. In the present work, the crystal structure of these two duplexes provides the first structural evidence that by increasing the π-overlap (i.e. 'stacking') between 2AP and an adjacent base, the probability of heterodimer formation is increased.

6.4.2 Time-Resolved Fluorescence Response

In both the crystalline and the solution phase DNA duplexes, the fluorescence response of 2AP is described by four exponential terms. The published literature in this field focuses on the dynamic nature of the DNA duplex as the cause of this heterogeneity in the fluorescence response of 2AP. Studies on the pure 2AP crystal clearly indicate that in a static system, a heterogeneous fluorescence response from 2AP is possible. Presently, it is unclear to what extent, at room temperature, the dynamics of the DNA duplex are restricted in the DNA-protein crystals. Hence, although the dynamic nature of the DNA duplex supplies the means to a complex fluorescence response, it is not necessarily the mechanism by which this is achieved.

6.4.2.1 Crystalline DNA duplexes

In a similar manner to the 2AP crystal, the crystalline 2AP labelled duplexes show a complex, multi-component decay despite the relatively constrained environment conferred on them by the crystal phase. In the 2AP crystal, the heterogeneity in the decay of isolated 2AP was attributed to the different degrees of π-overlap between the isolated 2AP molecules and those flanking them. The probable mechanism for de-excitation of isolated 2AP in the 2AP crystal is through rapid energy transfer to neighbouring, stacked 2AP complexes.

The DNA duplex is structurally similar to the 2AP crystal and so it is likely that the mechanism(s) of non-radiative decay in both systems will be similar. Hence, the π-π interactions of the 2AP will be crucial in determining its photophysical behaviour. Since the 2AP has a significant amount of rotational freedom about the sugar–phosphate backbone, the π-π interactions it forms with flanking bases are of varying strengths as a result of the varying degrees of overlap between the bases. This heterogeneity in the duplex is mediated by the base dynamics and is an attractive explanation for the complexity inherent in the fluorescence response of 2AP in DNA. Although evidence of energy transfer from the canonical DNA bases to 2AP exists[90;91], the excited state of 2AP is too low in energy for the reverse process to occur. The excitation energy of the canonical bases could be decreased if they were to form ground state complexes in the context of the duplex. Indeed, there is evidence for the existence of π-stacked, excitonic complexes[102] within the DNA duplex. However, the absorption spectrum of these complexes is not significantly red-shifted relative to that of the individual bases and, hence, energy transfer from 2AP to neighbouring base complexes is not a plausible non-radiative decay route.

Electron transfer from guanine to excited 2AP is a good candidate for an efficient non-radiative decay route for excited state 2AP in the DNA duplex, which depends on the conformation of the π-stacking interactions in the duplex. O'Neill *et al* have demonstrated that electron transfer occurs in the duplex with experiments that show guanine is readily oxidised in the presence of excited-state 2AP (2AP*) in the DNA duplex[50]. The Barton group have contributed much of the literature to this field and non-radiative decay through electron transfer from guanine to 2AP* is now established as an efficient non-radiative decay route for 2AP* in the context of the DNA duplex[20;94;96;98-100;103;104]. Jean and Hall have recently proposed a model where electron transfer is the only mechanism for de-excitation of 2AP in the DNA duplex[97]. Figure 6.12 schematically illustrates the key components to this model.

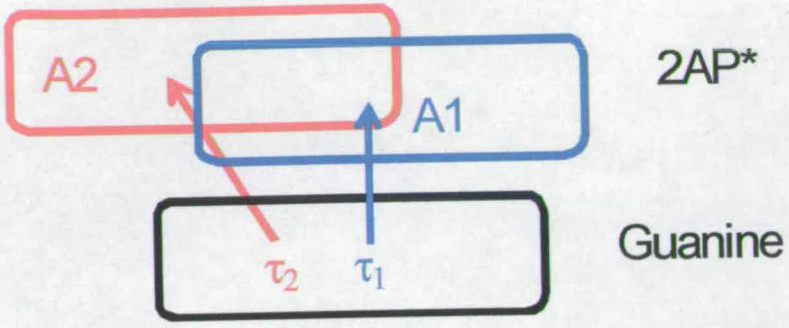

Figure 6.12- Schematic representation of adjacent 2AP and guanine bases in the DNA duplex. 2AP adopts conformations 1 and 2, whose relative populations are described by A1 and A2, respectively. Excited state 2AP is non-radiatively quenched by electron transfer from guanine, on a timescale, τ_1 or τ_2, that is determined predominantly by the relative orientations of the two bases.

Jean and Hall[97] argue that 2AP* can only accept an electron from guanine in a stacked (as opposed to 'unstacked') conformation of the duplex. If the only non-radiative decay channel available to the 2AP* is via charge transfer to guanine, the heterogeneity in the 2AP fluorescence response is due to the overlap between these bases and, hence, the conformational disorder of the DNA duplex. Consider Figure 6.12, for the case where the dynamical motion of the 2AP* is fast compared to the rates of de-excitation through charge transfer given by $1/\tau_1$ and $1/\tau_2$. During its lifetime, the 2AP* samples both of the conformations, 1 and 2, described in Figure 6.12, each of which has a different non-radiative rate of decay via charge transfer. Jean and Hall argue that the fluorescence response resulting from this dynamic system would be described by a single exponential decay, with a lifetime that is defined by the equilibrium between the populations of the two conformations, A1 and A2. The other extreme of this model is the case where the conformation of the DNA duplex is static on the timescale of the TCSPC experiment. In this case, Figure 6.12 would describe a bi-exponential decay curve. In reality, there is a continuum of conformations accessible to the bases between those two shown in Figure 6.12. Hence, for a real duplex, which was static on the timescale of these experiments, the fluorescence response would be non-exponential and discrete lifetimes fitted to such a fluorescence response would represent 'average' conformations adopted by the system across the conformational continuum. Jean and Hall[97] argue that in their experimental studies, they see a combination of these two extreme cases for the dynamical behaviour of the DNA duplex. Their

proposed model for the duplex is a system where the short decay components of 2AP are for 'substantially stacked' 2AP molecules, which undergo rapid de-excitation by electron transfer, whereas the longer decay components are due to unstacked 2AP molecules, which reorient to stacked 2AP, within the excited-state lifetime, and subsequently decay non-radiatively on the timescale of picoseconds to nanoseconds.

The results presented for the crystalline DNA duplexes in Table 6.1 and Table 6.2 show that the fluorescence decay of 2AP in the duplex is multiexponential in the crystalline DNA duplex. This result is in good agreement with Jean and Hall's 'static' model of the DNA duplex and is consistent with the argument that 2AP* undergoes intrinsically different rates of electron transfer with guanine, depending on the relative orientations of the bases within the duplex. Each of the four discrete lifetimes fitted to this data almost certainly represents one or more distributions of DNA conformers. It is certainly not possible to rule out some contribution to the recorded response from the DNA duplex dynamics. This is particularly true in the light of recently published results by Barton and O'Neill[103]. This report investigates the efficiency of electron transfer between G and 2AP using steady-state fluorescence measurements on 2AP labelled DNA, in rigid glasses at 77K. In these truly static duplexes, the 2AP labelled DNA is shown to have a quantum yield equal to that of the free 2AP base (in an identical matrix at 77K) when the 2AP is not adjacent to a guanine base in the duplex. Hence, electron transfer appears to be 'switched off' in a static duplex. When the 2AP is adjacent to guanine in the duplex its quantum yield is approximately half that of the free 2AP base. This suggests that there is indeed a favourable conformation for the G to 2AP electron transfer and that this process does occur efficiently between adjacent bases in a static system.

Comparison of the decays for the crystalline duplexes with their corresponding solution phase systems provides evidence for the relatively static nature of the DNA duplex in the crystalline phase. The shortest component of the decay of the crystalline DNA duplexes is approximately twice as long as that component for the corresponding solution phase duplex; in the DNA-enzyme-cofactor ternary complex. These values are 30ps and 60ps for the solution-phase PG(GG)2 and PT(GG) duplexes, respectively (Chapter 7, Table 7.16) and 70ps and 90ps for these duplexes in the crystal, as shown in Table 6.1 and Table 6.2. Barton et al[20;94;96;99] have shown that 2AP undergoes non-radiative decay via electron transfer to guanine on this sub-100ps timescale and that the probability of electron transfer in duplexes containing 2AP adjacent

to a 3'-guanine base is sensitively dependent on temperature[100]. Hence, it is thought that base dynamics play an important role in mediating electron transfer. The increase in the <100ps lifetime of the PG(GG)2 and PT(GG) duplexes with the transition from the solution phase to crystalline phase indicates that the DNA duplex is less dynamic in nature in the crystal, than in solution.

The crystal structures of both the PG(GG)2 and PT(GG) duplexes show that the majority of the 2AP bases in these duplexes are stacked within the DNA helix. Correspondingly, in both duplexes, approximately 60% of the 2AP molecules have very short lifetimes, represented by a decay component of <100ps and 95% of the emitting species have lifetimes of less than 2.5ns; considerably shorter than the ~10.6ns lifetime of free 2AP riboside in water.

The crystal structures of the PG(GG)2 and PT(GG) provide further insight into the photophysical behaviour of 2AP in the DNA duplex. These structures show that 2AP occupies two, quite distinct conformations within each duplex; *syn* for the PG(GG)2 duplex and *anti* for the PT(GG) duplex. Figure 6.11 shows that this has the effect of decreasing the π-overlap between 2AP and the 5'-guanine in the PT(GG) duplex, relative to that in the PG(GG)2 duplex. The result of this conformational change is an apparent decrease in the lifetimes of the three shortest lived components of the PG(GG)2 response, as compared to the PT(GG) fluorescence response. These changes in lifetime are large, compared to their expected relative standard deviations of <5% (calculated as described in the Results section of this Chapter). Hence, this is good evidence that the three shortest components of the fitted decay are sensitive to the intrahelical conformation of 2AP. It follows that these components are the result of emission from 2AP molecules that interact closely with the bases around them in the duplex and can be termed 'stacked'. The fluorescence responses of both the PT(GG) and PG(GG)2 duplexes have a small fraction (<5%) of a long decay component, of 7.3ns, which approaches the lifetime of the free 2AP base. The similarity of the lifetime of this component in each duplex is striking, indicating that the lifetime of this component is independent of the 2AP base stacking interactions. Hence, this long-lived component results from unstacked 2AP, which is not quenched by charge transfer in the DNA duplex.

6.4.3 Solution Phase DNA Duplexes

It is useful to consider the summary of the general trends that appear in all of the DNA duplexes investigated, presented in Table 6.14, which shows the mean values for the data described by Table 6.13.

	A1	A2	A3	A4	τ1	τ2	τ3	τ4
Mean	0.70	0.17	0.08	0.06	0.07	0.45	2.72	10.1

Table 6.14- Mean values of A-factors and lifetimes derived from the ten solution phase DNA duplexes.

The mean values calculated in Table 6.14 show that the A-factors of the 2AP labelled duplexes increase with a decreasing 2AP lifetime. The major component of the decay curve accounts for approximately 70% of the 2AP molecules in the duplex and has a short lifetime of less than 100ps. Together, the 2AP molecules giving rise to A2/τ2 and A3/τ3 account for around a quarter of the 2AP molecules. A small fraction (~5%) of the 2AP population has a lifetime of approximately 10ns and can be considered extrahelical.

A further general trend can be seen in the Tables from Table 6.3 to Table 6.12 inclusive. Consistently, the magnitude of the A-factor representing the shortest-lived 2AP* species, A1, falls with increasing emission wavelength and the 2AP* population, A2, with the next longest lifetime (~0.5ns) shows an increase in magnitude with increasing emission wavelength. Hence, these two species have distinctly different emission spectra, with the 2AP population described by A1 emitting at short wavelengths relative to that described by A2. This is good evidence that the 2AP species with 100ps and ~0.5ns lifetimes represent two distinct conformations of the DNA duplex. Thus, the fluorescence response of 2AP labelled DNA is not, as proposed by Rachofsky et al[27;47], simply the result of emission from a duplex where the 2AP occupies a continuum of orientations, which give rise to a continuous distribution of fluorescence lifetimes. Rather, this evidence indicates that there are discrete, conformational potential energy wells accessible to the bases as they move within the duplex. Furthermore, because the emission spectra of the 2AP species with ~100ps and ~0.5ns lifetimes are distinct, the distinct duplex conformations giving rise to these species must be 'static' for the lifetime of the excited state

2AP. It is crucial to indicate that the use of 'static' here implies that the bases cannot hop from one energetic well to another on the nanosecond timescale described by the lifetime of excited-state 2AP. However, this does not rule out the possibility of relatively small amplitude motions of the duplex on the timescale of our experiments. This important observation is not consistent with the dynamic description of the DNA duplex, given by Jean and Hall[97]. Their model describes a duplex where the intrahelical 2AP (as distinct from 'extrahelical' 2AP, which has a lifetime of ~10ns) is free to move to an orientation where electron transfer is favourable during the lifetime of the excited state. In this case, all intrahelical 2AP would exhibit the same, averaged, emission spectrum. The wavelength dependence of the other A-factors is slight. A3 shows some tendency to increase with increasing emission wavelength. The A-factor for the longest-lived species is small and has no clear trend with emission wavelength.

In general terms, it is possible to describe three distinct orientations for 2AP within the duplex and to assign approximate fluorescence lifetimes to them. The first is an intrahelical conformation, where electron transfer is favourable and the lifetime of 2AP is correspondingly short. The lifetime of 2AP within this potential well is described by the probability of de-excitation of 2AP* by electron transfer to guanine. Studies on the lifetime of this species, as a function of temperature, by O'Neill and Barton[99] and the increase in its lifetime with crystallisation, show that dynamics, on the timescale of tens or hundreds of picoseconds, play a crucial role in defining the lifetime of this species. The crystal structures for the PT(GG) and PG(GG)2 duplexes show that both the *syn*- and *anti*- isomers of the 2AP, within the duplex can adopt this orientation.

The second DNA conformation is one where the 2AP is intrahelical, but in an orientation where electron transfer to guanine is unfavourable. It is important to point out that this does not necessarily preclude electron transfer as a mode of non-radiative decay for this species. However, in Chapter 4 of this thesis, it was shown that lifetimes of this magnitude are observed for 2AP in an apolar environment; the dominant component of the 2AP fluorescence decay in dioxane has a lifetime of 1.6ns. It seems reasonable that 2AP stacked within the apolar DNA duplex, which is not in a favourable orientation for electron transfer, will have a radiative lifetime of the same order of magnitude as that seen for free 2AP in dioxane, i.e. ~1ns. It is unclear whether the two discrete lifetimes, of ~0.5ns and ~2ns, fitted to the fluorescence

response of 2AP labelled DNA represent a broad distribution of states or are distinct conformations of the duplex.

The third orientation adopted by 2AP in the duplex is to be extrahelical, with a lifetime that approximates that of free 2AP in aqueous solution. The lines between intra- and extra- helical are rather poorly defined but broadly speaking, extrahelical implies the 2AP is free from the π-stacking interactions of the DNA duplex.

Consider the general model, given for the DNA duplex above. The conformation of the DNA duplex at any given instant is defined in the simplest case, in terms of three potential energy wells. The breadth and depth of these wells, and the height of the barriers between them, are then defined by the specific interactions between bases at any given point in the duplex. Thus, by considering the specific interactions between 2AP and the bases about it, some understanding of the factors that influence the duplex conformational dynamics can be achieved.

Duplex	Nearest 3' guanine/ bases	Nearest 5' guanine/ bases	Nearest guanine (opposite strand)/ bases
PT(AC)1	2	5	1
PT(AC)2	2	5	1
PT(CC)1	2	NA	1
PT(CC)2	2	2	1
PT(TA)	3	4	2
PT(GG)	1	1	3
PC(GC)	2	1	1
PC(MC)	2	2	1
PG(GG)1	1	1	0
PG(GG)2	1	1	0

Table 6.15- The proximity of 2AP to guanine, expressed in numbers of bases, for each DNA duplex investigated. A value of '1' indicates an adjacent guanine base and '0' guanine that is directly opposite 2AP.

The Barton group have clearly established that electron transfer from guanine to 2AP* results in the efficient non-radiative decay of 2AP*. Given this, Table 6.15 shows the proximity of 2AP to guanine in each of the duplexes investigated.

The studies of the Barton group highlight some key areas for consideration in understanding how the presence of guanine might affect the shortest lifetime component of the 2AP decay. Intrastrand electron transfer is more efficient than interstrand transfer, though both occur[99]. The electron transfer efficiency (from guanine to 2AP*) is greater in the 3'-5' direction and is less dependent on distance than the 5'-3' electron transfer. In this instance, it is more intuitive to consider hole transfer from 2AP* to guanine, which is more efficient in the 5'-3' direction. Electron transfer is possible between guanine and 2AP* over distance of up to ~14Å. The transfer is most efficient when the bridging bases, between G and 2AP*, are adenines. Pyrimidine bases attenuate the transfer efficiency significantly.

Consider intrastrand electron transfer for the three DNA duplexes, PT(GG), PG(GG)1 and PG(GG)2, where the 2AP is flanked on either side by guanine bases. Table 6.13 shows that the PT(GG) and PG(GG)2 duplexes both have short-lived, 'electron transfer components', with lifetimes of 40ps. Furthermore, both duplexes have large A-factors for these components, of approximately 65-70%. This behaviour is consistent with the predictions made the Barton group. In the case of the PG(GG)1 duplex, however, it's shortest lifetime is twice that of the PT(GG) and PG(GG)2 duplexes and this component accounts for the decay of only 53% of the excited state species. An important feature of this duplex is that the guanine base 3' of the 2AP is paired with a methylated cytosine. Hence, not only is the duplex structure disrupted by the 2AP-G mismatch, but the base pair adjacent to this is disrupted. This localised disruption of the duplex stacking interactions has a profound effect on the efficiency of electron transfer to 2AP*. Such sensitivity of electron transfer to base stacking interactions is an observation that is in line with those made by O'Neill and Barton[98].

Particularly long lifetimes for the electron-transfer decay component are apparent for the PT(AC)1, PT(AC)2 and PT(TA) duplexes, as shown in Table 6.13. Table 6.14 shows that of all the duplexes investigated the PT(TA) duplex has the greatest distance between the 2AP and guanine. In this case there should be little or no rapid electron transfer between 2AP* and guanine and the low A factor (0.45) and relatively long lifetime of this species (120ps) support

this. Both the PT(AC)1 and PT(AC)2 duplexes have relatively long-lived electron transfer components, of 120ps and 100ps, respectively, which are indicative of the absence of an intrastrand guanine base adjacent to the 2AP. Table 6.14, shows that both of these duplexes, however, have their closest guanine base on the opposite strand, paired to the cytosine adjacent to and 3' of the 2AP. The 120ps and 100ps lifetimes of the of the short-lived species in these duplexes are in contrast to the 50ps and 30ps lifetimes of the similar species in the PT(CC)1 and PT(CC)2 duplexes. In all four of these duplexes, the closest intrastrand, 3' guanine base is 2 base pairs from the 2AP and the bridging base between 2AP and G is a cytosine. Since the bridging cytosine hinders the intrastrand electron transfer, interstrand electron transfer will be relatively favourable. The striking difference between the lifetimes of the electron transfer components in the PT(AC) duplexes, as compared to the PT(CC) duplexes indicates that this interstrand transfer process is extremely sensitive to the conformation of the DNA duplex in the region where the transfer takes place.

An interesting anomaly arises from the data collected, which is for the PT(AC)1 and PT(AC)2 duplexes. These are essentially identical; the only difference between them is an adenine base, some nine base pairs away and on the opposite strand to the 2AP, which is methylated in PT(AC)2 and unmethylated in PT(AC)1, as shown in Figure 6.3. Despite this, their fluorescence responses are notably different (Table 6.13 shows that the parameters fitted to the fluorescence responses of PT(AC)1 and PT(AC)2 are not all similar). The methylation of the exocyclic amine group of this adenine base will certainly affect its ability to base pair. This result suggests that the 2AP fluorescence response is sensitive to changes in the duplex, which are a number of bases away. Such behaviour is certainly consistent with the theory that the fluorescence response of 2AP is sensitive to the base stacking within the duplex. By disrupting the duplex at a single base, its global structure is distorted. Such 'long-range' disruption of the helix is not surprising given the need for enzymes to easily locate or recognise such structural alterations to the duplex.

There is some significant variation in the lifetimes of the extrahelical 2AP species in the duplexes tested, shown in Table 6.13. Of particular note are the two duplexes, PT(CC)1 and PT(CC)2, which have lifetimes for extrahelical 2AP of 8.51ns and 10.78ns, respectively. The 2AP in the PT(CC)1 duplex lies adjacent to the cytosine base at the end of the deoxyoligonucleotide strand. The relatively short lifetime for this species is consistent with duplex melting experiments by Guest el al[49], who show that an increase in the dynamical

disorder of the DNA duplex, such as might be expected at the either end of the duplex as compared to the centre, results in a decrease in the lifetime of the extrahelical 2AP species.

6.5 Conclusions

The fluorescence response of 2AP in DNA is characterised by four discrete components of ~100ps, ~0.5ns, 2-3ns and >7ns. These discrete lifetime values represent distinct populations of 2AP species, described by the conformations of the DNA duplex. These populations can be stacked within the DNA duplex, in an orientation favourable for hole transfer to guanine, in which case their lifetime is ~100ps, or they can be extrahelical 2AP species with lifetimes of greater than 7ns. There is at least one further distinct conformational distribution of 2AP species, represented by the two intermediate lifetime components of the fluorescence response. The fluorescence response of the free DNA duplexes is dominated by the short ~100ps component, which typically accounts for 70% of the 2AP species in the duplex. A small fraction (~5%) of the 2AP molecules experience an extrahelical environment as a result of the conformational dynamics of the duplex.

The fluorescence response of crystalline DNA closely resembles that of the analogous solution-phase duplex. The crystal structures confirm the stacked orientation of the 2AP in the majority of the duplexes in the sample. Where 2AP is mismatched with a guanine base, the crystal structure shows that the 2AP adopts the *syn-* isomeric form, as opposed to the normal *anti-* form. The result of this isomerisation is to increase the stacking interactions between the 2AP and its 5'-guanine. This sees a reduction in the lifetime of the three shortest components of the 2AP fluorescence response.

The results presented show that 2AP within the DNA duplex can occupy one of three distinct orientations during the lifetime of the 2AP excited state. These are described by the 'stacked', 'intermediate' and 'extrahelical' components of the fluorescence response. Some small amplitude motions must occur on this timescale and, in the case of the stacked component of the 2AP decay, these play an important role in precisely defining the magnitude of its lifetime. The

2AP molecules in extrahelical orientations remain extrahelical during the lifetime of the excited state.

Non-radiative decay of excited-state 2AP via electron transfer from guanine plays an important role in influencing the lifetime of stacked 2AP in the DNA duplex. For the duplexes investigated, there has been shown to be some correlation between the proximity and orientation of the nearest guanine base to 2AP and the lifetime of the stacked component of the 2AP fluorescence response. There is no clear evidence that electron transfer from guanine is important in influencing the lifetime of the intermediate component of the 2AP response.

Chapter 7

2-Aminopurine as a probe of DNA-Protein Interactions; the HhaI methyltransferase enzyme

7.1 Introduction

In this Chapter, the interaction between 2AP labelled DNA and a DNA methyltransferase enzyme has been used to study the effect of a defined conformational change of the DNA duplex on the time-resolved fluorescence response of 2AP.

The enzyme used in this investigation was the HhaI methyltransferase, which is part of the restriction/ modification (R-M) system of the Haemophilus haemolyticus bacterium. The Roman numeral 'I' simply denotes that this is system 'I' (i.e. the first isolated R-M enzyme) from this particular bacterial organism. Commonly, the prefix 'M.' is used to denote 'methyltransferase' as opposed to the endonuclease component of an R-M system.

M.HhaI belongs to the class of m^5C-MTases, described in Chapter 2 of this thesis. It binds to the four base sequence, 5'-GCGC-3', and it methylates the cytosine residue towards the 5' end of this sequence. M.HhaI is one of the smallest (327 amino acids) and most studied of the m^5C-MTases. Kumar *et al*[105] made the first observations of the crystal structure for M.HhaI complexed to the S-adenosyl-L-methionine (AdoMet) cofactor. The structure was subsequently refined by Cheng *et al*[106]. The enzyme is shown to have two domains (large and small) connected by a hinged region. The three regions combine to give the enzyme a tertiary structure that contains a cleft suitable for the accommodation of a DNA duplex. The AdoMet binding domain is located at the centre of the cleft, on the face of the large domain. Figure 7.1 shows the ternary DNA/M.HhaI/AdoHcy complex, first crystallised by Kilmasauskas et al[107].

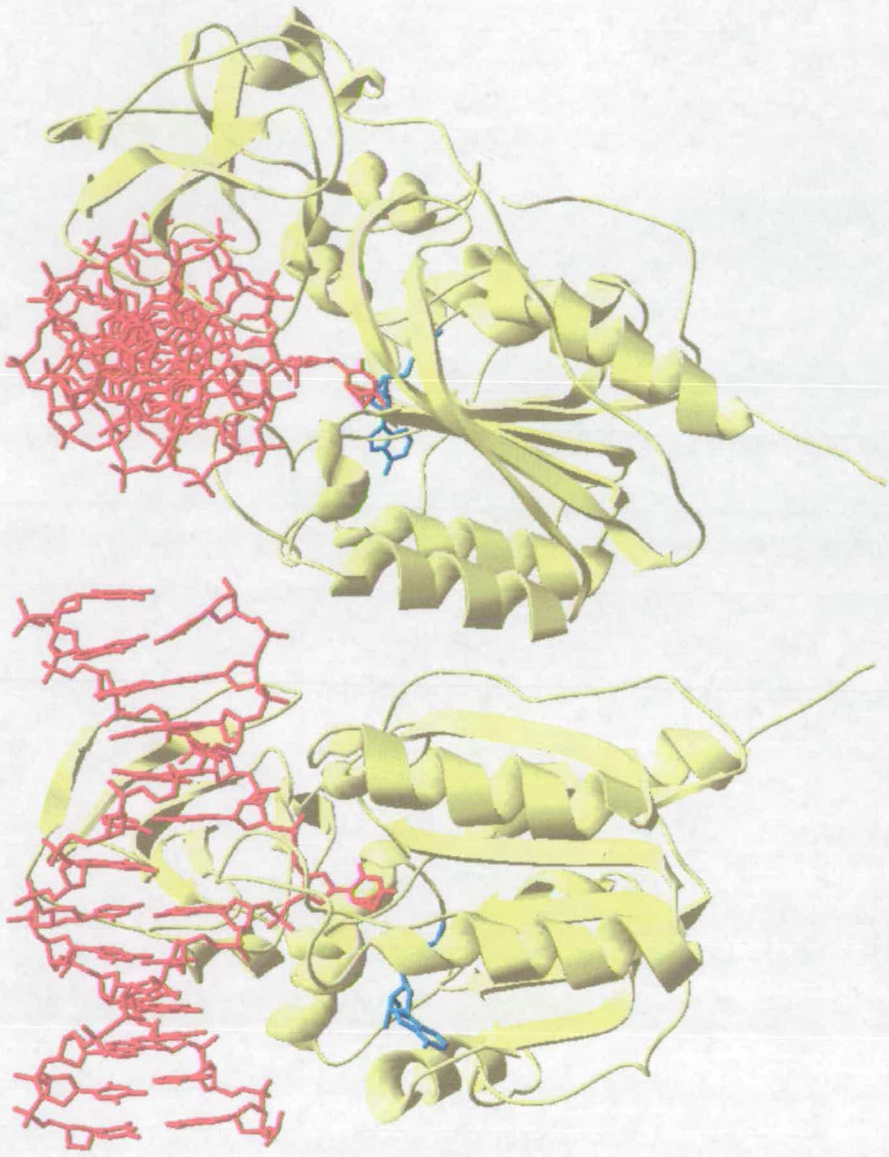

Figure 7.1- Images taken from the crystal structure of the ternary DNA/ M.HhaI/ AdoHcy complex, reported by Klimasauskas et al[107]. Images show the DNA (red), MHhaI (yellow) and AdoHcy (blue). The cytosine base flipped into the M.HhaI active site is both fluorinated and methylated at the C5 position. The crystal structure resolution of 2.8Å cannot distinguish these groups, hence, the bonds shown at the flipped cytosine C5 are merely used to indicate a large amount of electron density in this region.

The crystal structure obtained indicates that methylation of the target cytosine has taken place during the crystallisation period and confirms the cleft in M.HhaI as the DNA binding domain.

Remarkably, the target cytosine in this ternary complex is rotated, perpendicular to the long axis of the DNA duplex, by 180° out of the helix and into the protein active site. This was the first direct observation of 'base-flipping' by an enzyme. Figure 7.2 shows the structural distortion of the DNA helix caused by the base flipping by M.HhaI.

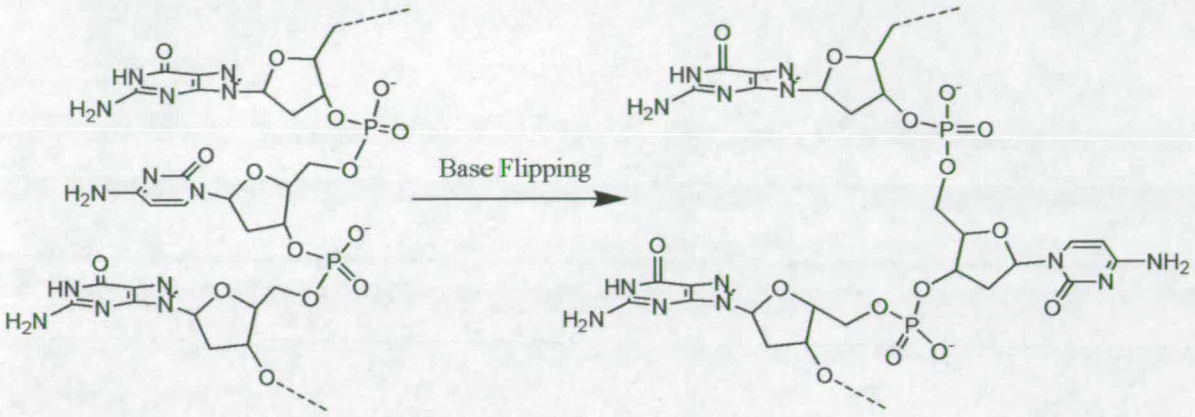

Figure 7.2-The structural distortion conferred on the DNA helix during base flipping (structure taken from Klimasauskas et al[107]).

Evidence for base flipping by only three HhaI[107], TaqI[71] and HaeIII[108] methyltransferases has been produced by solving their crystal structures. The crystallisation of enzyme-DNA is time consuming, problematic and may even be impossible with some enzyme-DNA combinations. Furthermore, the crystal structure of any compound provides only a snapshot of the system and reveals little about its dynamic or kinetic behaviour. Here, the fluorescence response of 2AP labelled DNA-enzyme complex, in the crystalline phase, is used to establish the photophysical response of 2AP to base flipping. The results of this study are then applied to the same DNA-enzyme complexes in the solution phase, in order to probe base flipping in this dynamic environment.

Base flipping occurs through rotation of the phosphodiester bonds of the DNA backbone. The P-P bond distance is significantly larger in the flipped structure than in the stacked duplex. Klimasauskas *et al* argued that this distortion allows the base to be rotated through the minor groove of the DNA and into the enzyme active site[107].

The structure in Figure 7.3 shows the species captured in the crystal structure. Several amino acids in the active site of M.HhaI stabilise the interaction between the flipped cytosine and the enzyme. Hydrogen bonds are formed with the carboxyl group of glutamine-119, the main chain carbonyl linked to phenylalanine-79 and the non-terminal nitrogen of arginine-165.

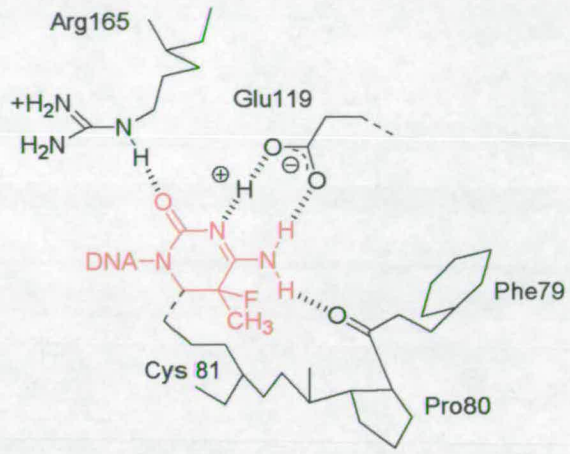

Figure 7.3- The flipped out cytosine base, shown in red, in the M.HhaI active site; residues immediately interacting with chemically trapped flipped out cytosine base are pictured (from Klimasauskas et al[107]).

Significantly, Figure 7.3 shows that a covalently bound reaction intermediate is formed during the methylation process. Here, the sulphur atom of cysteine 81 forms a covalent bond with C6 and the two atoms are only 1.8Å apart. Klimasauskas *et al* noted that the trapped intermediate formed is consistent with the mechanism for cytosine C5 methylation originally proposed by Wu and Santi[109], illustrated in Figure 7.4.

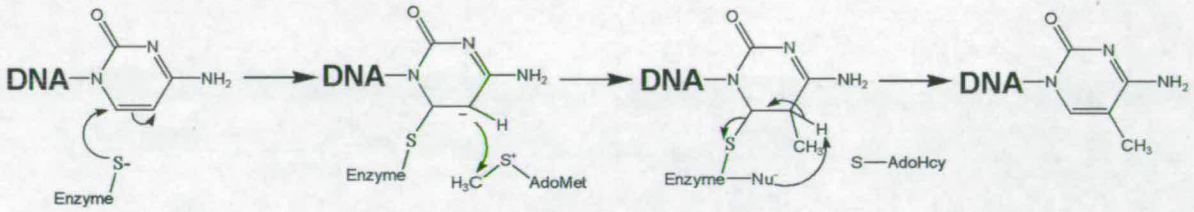

Figure 7.4- Mechanism of cytosine C5 methylation

The structural study by Klimasauskas *et al*[107], which led to the first structural evidence of base flipping, is in excellent agreement with the mechanism of methylation proposed in Figure 7.4. This study employed a DNA 13-mer where the cytosine base that was the target for base flipping and methylation was fluorinated at the C5 position. This fluorination was crucial in preventing the dissociation of the enzyme from the DNA by blocking the third step in the reaction scheme shown in Figure 7.4. Furthermore, it was found that AdoHcy (S-Adenosyl-homocysteine, which is described in the Theory Chapter) is present in the crystal structure despite AdoMet being used in the reaction mixture, since the methylation step, step two, of the reaction mechanism shown in Figure 7.4 is allowed to take place in the complex.

Subsequent studies confirmed that the mechanism of methylation is initiated by nucleophilic attack by the sulfhydryl group of cysteine 81 on the cytosine C6 [110]. It is thought that the electron withdrawing interactions conferred on the cytosine by HhaI, which act on the exocyclic amine group, N3 and carboxyl groups of cytosine, play an important role in facilitating this step of the methylation. Furthermore, protonation of N3 is thought to be concerted with the sulfhydryl attack and is essential in stabilising the intermediate species created by this step[111]. Transfer of the methyl group from AdoMet to C5 is followed by dissociation from the enzyme, which is effected by β-elimination across the C5-C6 bond[112].

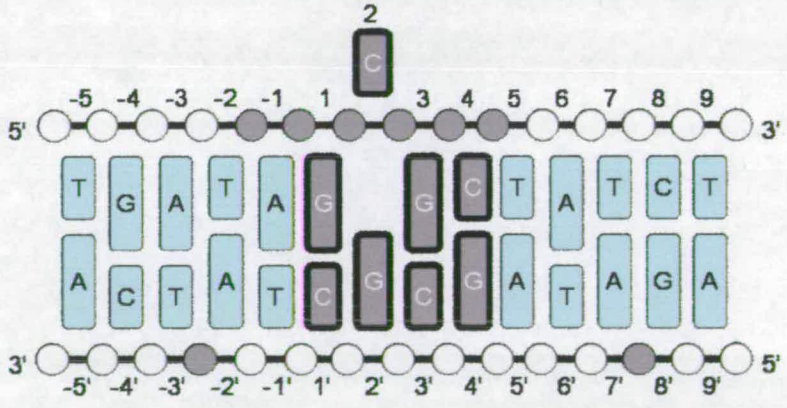

Figure 7.5- DNA sequence and points of contact on the duplex during methylation by HhaI. Phosphate groups are shown as circles with grey shading denoting groups that are in contact with the enzyme. Emboldened boxes represent bases in the HhaI recognition sequence.

M.HhaI binds the DNA duplex over a region spanning several base pairs. Figure 7.5 shows schematically the points of contact between the DNA duplex and HhaI.

The crystal structure determined by Klimasauskas *et al* reveals that the HhaI binds to the 'orphan base' (i.e. the base opposite the target for base flipping- G2' in Figure 7.5) to stabilise the duplex during base flipping[107]. Two residues from opposite sides of the DNA binding cleft of HhaI, glutamine 237 and serine 87, move to occupy the site vacated by the target cytosine during base flipping, as shown in Figure 7.6.

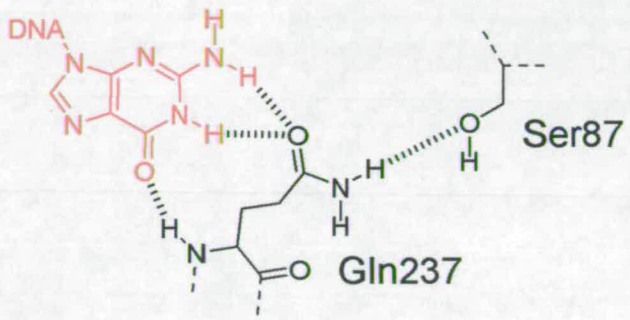

Figure 7.6- Binding of the orphan G2' base by HhaI

The glutamine and serine residues come from opposite sides of the HhaI DNA binding loop so that the enzyme encircles the flipped base. Glutamine 237 is extricated from the small domain of HhaI and forms Watson-Crick-type hydrogen bonds to G2', whilst stabilising the DNA stack through hydrophobic interactions with G1 and G3. Serine 87 lies in the large domain of free HhaI and forms a single hydrogen bond to glutamine 237 in order to stabilise its position in the DNA binding complex.

Klimasauskas and Roberts showed, using electrophoretic mobility shift analysis, that base flipping by HhaI occurs independently of the nature of the target base[113]. They found that the stability of the HhaI-DNA complex increased as the strength of the base pair at the target site for base flipping decreased. This solution phase study was corroborated by later work by O'Gara *et al* who solved the crystal structures for the G-A, G-U and G-'abasic site' pairings at the target site for base flipping by M.HhaI[114]. Of particular interest is the flipping of the abasic deoxyribose sugar by HhaI, which implies that the mechanism of base flipping is effected by

interactions between the DNA sugar-phosphate backbone and HhaI and does not require the presence of a target base in the DNA duplex. This study also shows that flipped adenine is accommodated in the enzyme active site and forms several hydrogen bonding interactions with residues in close proximity to it.

The dynamics of the base flipping mechanism were investigated by Klimasauskas *et al* using ^{19}F NMR spectroscopy[115]. Two cytosine bases in the duplex were labelled with the ^{19}F probe atoms; one at the target site for base flipping and one three nucleotides 5' of the target base (a location that does not contact the enzyme). The study shows at least four distinct signals in the ^{19}F NMR spectra of the labelled duplex. These are attributed to the free DNA duplex, a binary DNA-HhaI complex incorporating a stacked target base, a DNA-HhaI complex with an extrahelical target base and the ternary DNA-HhaI-AdoHcy complex where the base is flipped and locked in the enzyme active site, Scheme 6.1.

$$\text{HhaI+DNA} \leftrightarrow \text{HhaI-DNA}_{\text{stacked}} \leftrightarrow \text{HhaI-DNA}_{\text{flipped}} \leftrightarrow \text{HhaI-AdoHcy-DNA}_{\text{locked}}$$

Scheme 7.1- Suggested binding and conformational equilibria between HhaI, DNA and the AdoHcy cofactor analogue

In the binary complex it is thought that the target cytosine exists in equilibrium between the flipped and unflipped conformations. The ^{19}F-NMR signal from the flipped base in the binary complex is distinct from that in the ternary complex. Hence, in the DNA-HhaI complex, the target base is thought to occupy an ensemble of extrahelical positions that are simply stabilised by enzyme binding. Addition of AdoHcy to the system apparently 'locks' the target base into a well defined, extrahelical conformation in the enzyme active site. A recent study by Vilkaitis *et al* showed, by using a radiolabelled cofactor, that a stable binary complex between AdoMet and HhaI is formed in the absence of DNA. Hence, AdoMet is likely to associate with HhaI at any given step in reaction Scheme 6.1[116].

Holz *et al* used steady-state fluorescence spectroscopy of 2-aminopurine as a probe of the base flipping mechanism for the HhaI and TaqI methyltransferases[24]. Replacement of the target cytosine base with 2AP gives a fluorescent duplex that shows a 54-fold increase in fluorescence intensity upon enzyme binding. The authors use this distinctive fluorescence signature to

indicate that base flipping may be the mechanism of action for the M.TaqI enzyme. This study also shows that that the addition of AdoHcy leads to a shift in the emission spectrum of the 2AP labelled DNA, relative to the binary complex. This is interpreted as being consistent with previous ^{19}F-NMR experiments[115] that demonstrate the 'locking' of the extrahelical conformation of the target base upon ternary complex formation.

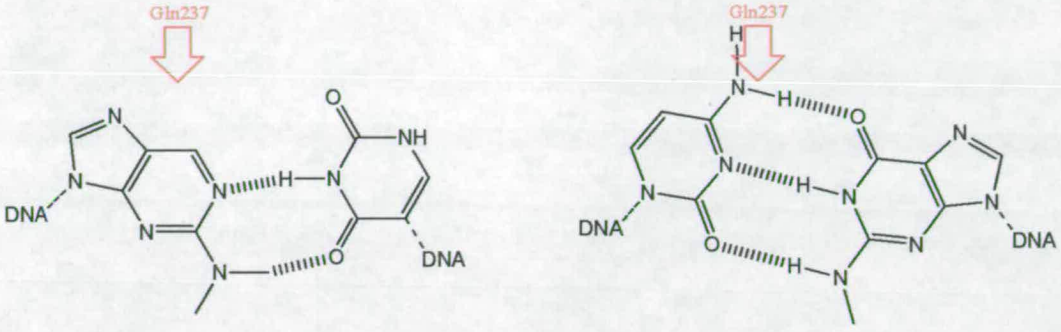

Figure 7.7- Schematic representation of the steric interactions between the 2AP-T base pair and Gln237 (right) and the G-C base pair and Gln237 (left)

A recent study by Daujotyte et al[117] clarifies the mechanism by which base flipping is initiated by HhaI and lends further support to the mechanism of action proposed by Klimasauskas et al[115], shown in Scheme 7.1. The study employed 2AP as the target base for flipping, with the character of the 'orphan' base (i.e. that opposite the 2AP) being varied. Consistent with an earlier study by Klimasauskas and Roberts[118], the extent of DNA binding by HhaI was found to correlate inversely with the predicted strength of the base pair at the target site. The use of 2AP as the target base shows that base flipping decreases in line with the association constant of the DNA-HhaI complex. The study showed an interesting exception to this rule in the 2AP-T base pair. Here, the extent of base flipping (described by the 2AP steady-state fluorescence intensity) is much lower than might be expected for the measured association constant. Molecular modelling was used to show that base excision from the helix is initiated, in part, because of a steric interaction between the Gln237 residue (which bonds to the orphan base during flipping as shown in Figure 7.6) and an exocyclic amine group on the target base which lies in the major groove of the DNA helix, as shown in Figure 7.7.

In the case of the 2AP-T base pair, 2AP possesses no exocyclic group protruding into the major groove and so there is no steric driving force for base excision. Since the 2AP-T base pair bonds through a Watson-Crick type interaction it is relatively stable compared to the other 2AP-'native DNA base' base pairs. This study shows that a combination of the stable 2AP-T base pair and the lack of a suitable driving force for the excision of 2AP are sufficient to significantly inhibit base flipping.

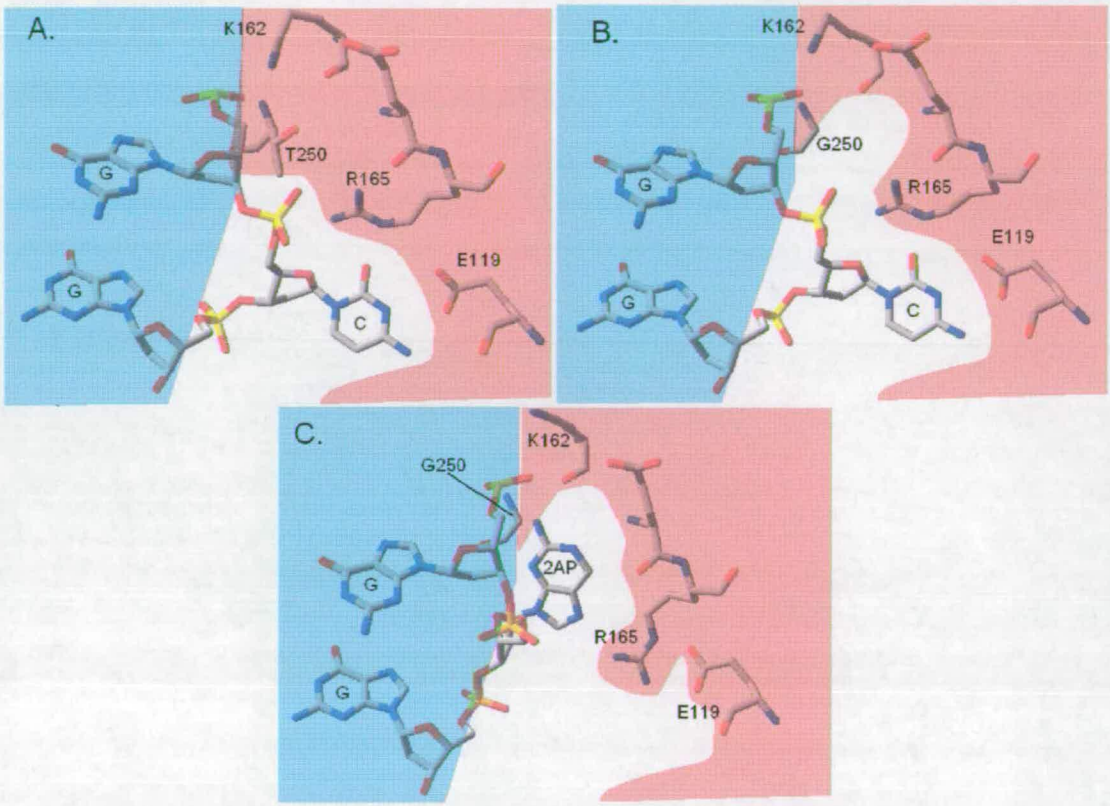

Figure 7.8- Structures of the M.HhaI in the region around residue 250. Blue regions indicate the DNA duplex and red-shaded regions are used to highlight the enzyme amino acid residues; A. wild-type enzyme with flipped cytosine base in the enzyme active site; B. T250G mutant with flipped cytosine showing the void created by the T250G mutation; C. T250G mutant with flipped 2AP base occupying the void, where the R165 residue has been displaced into the region defined as the enzyme 'active site' for the wild-type HhaI[119].

Vilkaitis *et al*[119] have studied the effect of mutating HhaI at threonine 250 on the binding affinity and flipping kinetics of the enzyme, where 2AP is substituted as the target base. Crystal

structures of the ternary DNA-HhaI-AdoHcy complex show that the Thr250 residue is not in direct contact with the flipped cytosine base but that it does play a role in binding the enzyme to the DNA backbone, as shown in Figure 7.8.

In terms of the fluorescence response, of the mutants investigated by Vilkaitis *et al*, the most interesting results are seen for the T250G mutant (i.e. the mutation of threonine 250 to a glycine residue). Figure 7.8 (A and B) shows the crystal structure of the wild type and T250G mutant enzymes with cytosine flipped into the active site. Although the structure is similar in both instances the role of T250 is clearly shown to be in stabilising the interaction between the DNA backbone and HhaI. Removal of the threonine side-chain by mutation to glycine results in the creation of a small void between the protein and DNA. Vilkaitis *et al* use stopped-flow measurements of 2AP fluorescence intensity to show that the overall rate of base flipping, in the case of both the wild-type and T250G mutant enzymes, is described by the sum of two exponential terms. These are attributed to the initial flipping of the base into the active site, followed by a relaxation of the probe molecule into an alternative, stable environment. Steady-state fluorescence measurements using 2AP show a significantly red-shifted emission for the T250G mutant, suggesting that, in solution, the flipped probe occupies a position in the mutant enzyme that is distinct from that which it takes up in the wild-type enzyme. The red-shifted emission and relative resistance to acrylamide quenching by the flipped 2AP in the T250G mutant suggests that the environment of the 2AP in the mutant enzyme is more polar and less solvent accessible than that of the wild-type HhaI. The crystal structure for the flipped 2AP in the T250G mutant (Figure 7.8, C), which has only recently become available[120], shows that the 2AP fills the void created by the mutation, thus occupying a site close to the negatively charged phosphate groups of the DNA backbone. O'Gara *et al* showed that adenine is accommodated in the active site of wild-type M.HhaI, occupied by cytosine in Figure 7.8A. By analogy, it seems likely that 2AP is also accommodated in the active site of the wild-type enzyme. Hence, in the mutant, a reasonable rationalisation of the two-step kinetics of base flipping is that the 2AP flips initially into the 'normal' active site of HhaI and subsequently relaxes into the position described by Figure 7.8.

In the present work, 2AP was used as a probe of base flipping by M.HhaI. 2AP has previously been used as a fluorescence reporter for this and many other DNA-protein systems because of its ability to respond to structural distortions of the DNA duplex. Systems investigated include

DNA polymerase reactions[121], helicase activity[73], and the action of DNA repair enzymes[47;74-76] as well as the methyltransferases[24;77-79]. All of these studies have used the fluorescence intensity of 2AP to report structural changes induced by enzyme action on the DNA duplex. However, studies by Gowher and Jeltsch[122] and Reddy and Rao[123] on methyltransferase enzymes with 2AP placed at the target site for methylation show no change in fluorescence intensity with protein binding. Furthermore, both studies show that when 2AP is in close proximity to, but not at, the target site for base flipping a fluorescence enhancement is observed. Clearly the steady-state fluorescence intensity only relates information about some distortion of the DNA duplex and cannot be used as a diagnostic tool for a particular mode-of-action by an enzyme, such as base flipping.

The preceding chapters of this thesis have shown that the time-resolved fluorescence response of 2AP can be used as a sensitive probe of its immediate environment. Furthermore, some key features of the fluorescence response of 2AP have been linked to defined orientations of the 2AP within the DNA duplex. It has been shown that 2AP stacked within the DNA duplex has a short ~100ps lifetime. When the 2AP is extrahelical, it has a lifetime close to 10ns. In the work that follows, the time-resolved fluorescence response of 2AP is used to characterise the extent of base flipping by M.HhaI. Furthermore, comparison of the fluorescence responses from crystalline and solution phase DNA-HhaI complexes, allows features of the fluorescence response of 2AP to be unambiguously ascribed to defined structural distortions of the DNA duplex.

Time-resolved fluorescence decays were collected for a group of five different 2AP-labelled DNA duplexes in DNA-enzyme and DNA-enzyme-cofactor complexes. 2AP was substituted at (AP_{target}), opposite (AP_{opp}) and adjacent (AP_{adj}) to the target site for base flipping by HhaI. Two further duplexes were also prepared as reference samples, where 2AP was outside of the HhaI recognition sequence and paired with either a guanine (GP_{out}), giving a mismatched (non-bonded) base pair, or thymine (TP_{out}), forming a Watson-Crick type base pair. All duplexes were investigated in ternary DNA-HhaI-cofactor crystal-phase complexes as well as in solution. Figure 7.9 shows the sequences of the bases at the centre of the DNA duplexes that were investigated. It is important to note that the recognition sequence for HhaI is 'palindromic' so that HhaI will methylate the 5'-most cytosine residue on either one of the DNA strands. In order

to direct base flipping to the desired strand a methylated cytosine base is used in the strand opposite that containing the 'target' for base flipping.

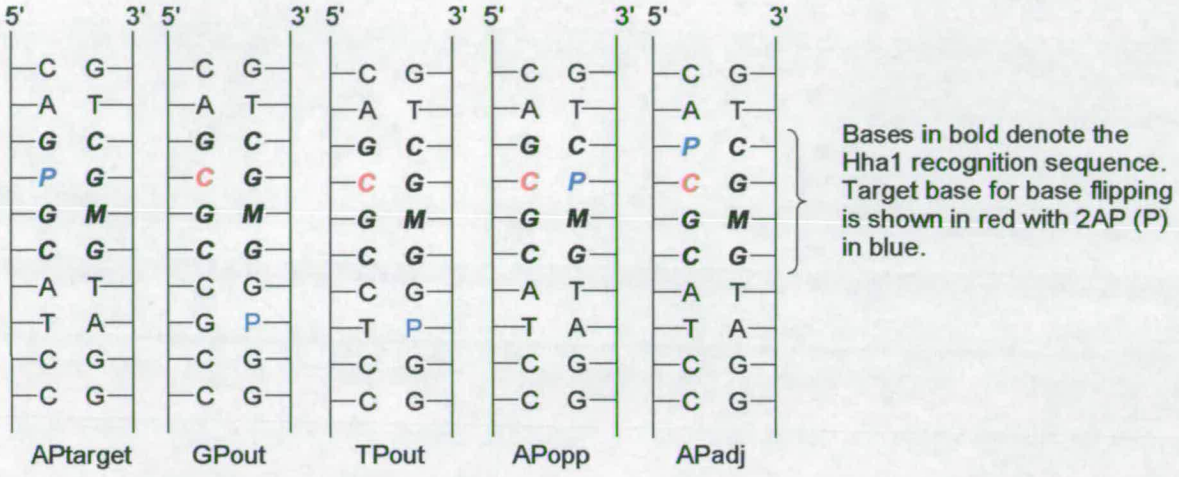

Figure 7.9- DNA duplex sequences for the ten bases at the centre of the five oligonucleotides investigated. The AP_{target}, AP_{opp} and AP_{adj} duplexes are 37mers, whereas the GP_{out} and TP_{out} duplexes are 25 bases in length. Note that M represents a methylated cytosine base (used to direct enzyme binding to the opposite strand of the duplex)

The sequences of the dodecamer duplexes used in the ternary crystals are slightly different to those used in the solution phase measurements. However, the immediate environment of the 2AP is the same as those duplexes used for solution phase measurements in all but the AP_{adj} duplex. For this duplex, the base 5' of the 2AP is adenine, whereas it is guanine in the solution phase experiments. The duplexes used here are five of those investigated in the Chapter 6, however, nomenclature here has been changed to emphasise the 2AP position with respect to the recognition sequence and target for base flipping by HhaI. The same nomenclature is used in the discussion of both solution and crystal phase duplexes. Binary and ternary complexes involoving the wild-type and T250G mutant of HhaI will be referred to as wt-XX and m-XX, where XX is the bound DNA duplex (e.g wt-AP_{target}). The cofactors AdoMet and AdoHcy will be denoted by a superscript M or H, respectively. Hence the ternary AP_{target}/ wild-type HhaI/ AdoMet complex will be written as ^{M}wt-AP_{target}.

In the solution phase, both binary (HhaI-duplex) and ternary complexes were studied. The cofactor, AdoMet was used in the case of the experiments carried out with the AP_{target} duplex. In order to prevent methylation of the target cytosine base (and subsequent dissociation of the enzyme from the DNA) AdoHcy was used as the cofactor in all other experiments.

7.2 Experimental Details

M.HhaI methyltransferase was overexpressed and purified by the Klimasauskas group at the Institute of Biochemistry, Lithuania[115]. 2AP-labelled oligonucleotides were obtained from Fermentas (Lithuania) and MWG Biotech (Germany). For the solution-phase experiments DNA oligodeoxynucleotides were annealed prior to use by heating the separate strands to 85°C in a water bath and allowing them to cool slowly overnight. A ten percent excess of the non-fluorescent oligodeoxynucleotide was used to ensure that none of the AP-labelled strand was left unbound in the final solution. In order to ensure complete binding of the DNA by M.HhaI, samples were prepared containing 1μM DNA, 3μM M.HhaI and 100μM cofactor. (K_d for the ternary DNA-HhaI-AdoHcy complex is 4.2pM[119]). The buffer used was 10mM Tris-HCl, 0.5mM EDTA, 50mM NaCl, pH of 7.4. The cofactor S-adenosyl methionine (AdoMet) was used in experiments on the AP_{target} duplex, whereas the cofactor analogue S-adenosyl homocysteine (AdoHcy) was used with all other duplexes in order to prevent methylation of the target cytosine base and subsequent dissociation of the enzyme from the duplex.

Crystals were grown using sitting-drop vapour diffusion at 19°C. The enzyme (wild type for APout crystal and T250G mutant for AP_{target} crystal) was mixed with the oligonucleotide and AdoHcy at a 1:1.2:1.5 molar ratio and a final protein concentration of 7mg/ml. This sample was mixed with an equal volume of well solution (50 mM sodium citrate pH 5.6, 1.2-2.0mM ammonium sulfate, 0-15% glucose). Rhombohedral crystals were obtained and were soaked for several seconds in a cryobuffer containing 25% glycerol and flash-frozen at 90K in a gaseous nitrogen stream.

Crystals were mounted, as described in Chapter 6, in quartz capillaries of 1mm diameter (Hampton Research).

Fluorescence decay curves were collected at an excitation wavelength of 317nm, at three different emission wavelengths (370nm, 390nm and 410nm) and, for the solution phase DNA duplexes, on two timescales (50ns with resolution of 24.41ps/ channel and 20ns with resolution of 4.883ps/ channel) for each system. Fits of the data were made as described in Chapter 6. Tables of decay parameters for all of the individual measurements made on these systems are shown in the Appendix of this thesis.

7.3 Results and Discussion

It has been shown, in the previous chapter of this thesis, that a four component fit is required to suitably model the fluorescence response of 2AP when it is in a predominantly intrahelical environment. This is the case for the GP_{out}, TP_{out}, AP_{adj} and AP_{opp} duplexes in all of the systems presented below. Hence, no three component fits for systems containing these duplexes are shown. However, justification, in the form of an '(n-1)-component' fit, is always given for the case where 2AP is extrahelical and an 'n-component' fit is used.

7.3.1 Crystal Phase Studies

The effect of base flipping on the fluorescence response of 2AP can be clearly established using comparative studies on crystals of known structure, with the 2AP flipped out of the duplex and stacked within it. Crystals of the ^{M}wt-AP_{target}, ^{H}wt-GP_{out} and ^{H}wt-TP_{out} complexes were examined in order to achieve this. Data were also collected from crystal-phase samples of the ^{H}wt-AP_{opp} and ^{H}wt-AP_{adj} complexes and from the ^{M}m-AP_{target} and ^{H}m-AP_{target} complexes. The crystal structures for the ^{H}wt-GP_{out} and ^{M}m-AP_{target} complexes are shown in Figure 7.10.

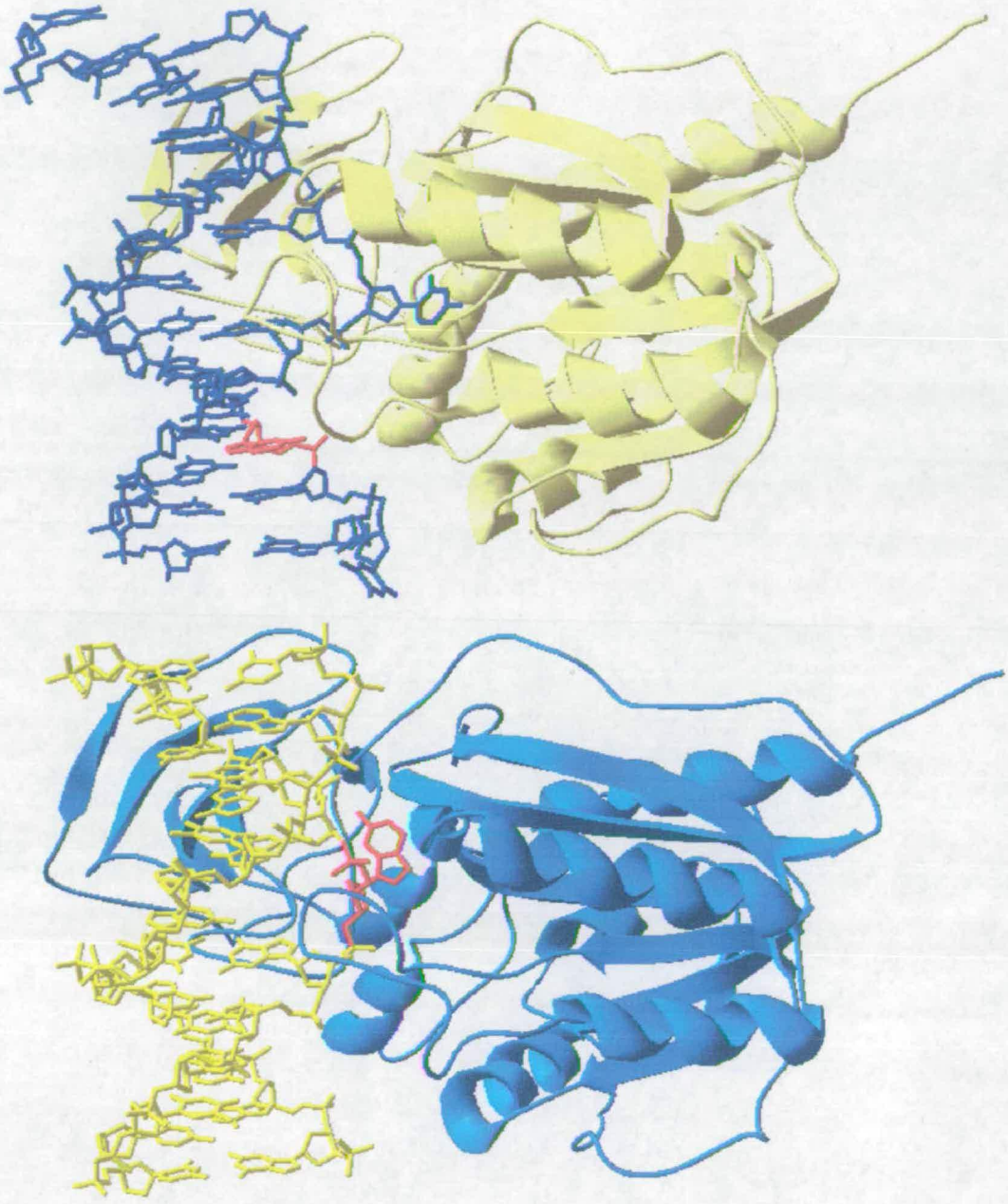

Figure 7.10- Crystal structures for the ^{H}wt-GP$_{out}$ (top) and ^{M}m-AP$_{target}$ (bottom) complexes. In both structures 2AP is the base shown in red.

The crystal structures and important intermolecular interactions for each DNA-enzyme-cofactor complex are discussed in detail alongside the relevant fluorescence data, in the sections of this Chapter that follow. The crystal structures in Figure 7.10 show that the DNA duplex is held in a

cleft between the two domains of the enzyme. The major domain is shown in the figure to the right of the DNA duplex and the minor domain extends behind the duplex. A looped region of the enzyme embraces the flipped base and fills the vacant region of the duplex which results from base flipping.

7.3.1.1 Steady-state emission spectra from single crystals

Figure 7.11 shows the emission spectra taken from single crystals of the ^{M}wt-AP$_{target}$, ^{H}wt-AP$_{opp}$ and ^{H}wt-AP$_{adj}$ complexes.

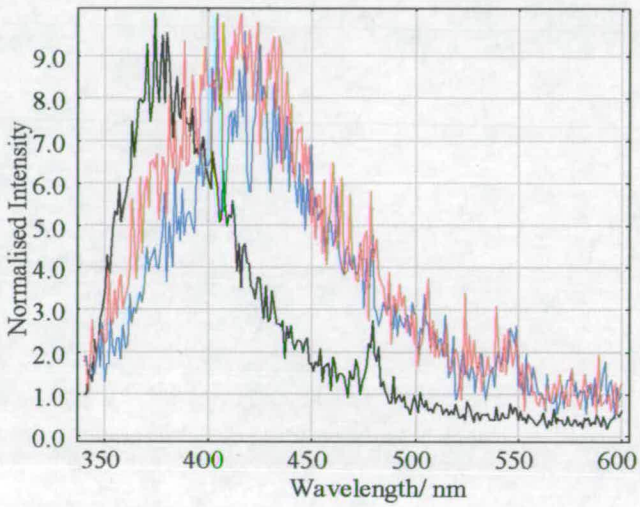

Figure 7.11- Emission spectra taken from single crystals of the ^{M}wt-AP$_{target}$ (black), ^{H}wt-AP$_{opp}$ (blue) and ^{H}wt-AP$_{adj}$ (red) ternary complexes. Excitation was with the Ti-sapphire laser at 320nm.

The steady-state emission spectrum, shown in Figure 7.11, for ^{M}wt-AP$_{target}$ is considerably blue shifted, relative to the spectra of the ^{H}wt-AP$_{opp}$, ^{H}wt-AP$_{adj}$ and even the ^{H}wt-GP$_{out}$ and ^{H}wt-TP$_{out}$ (Figure 6.7) complexes. This is entirely consistent with the observation, discussed in Chapter 6, that 2AP forms a ground state complex with adjacent bases in the DNA duplex, which in turn causes a red shift in its excitation and emission spectra. Here, the 2AP in the ^{M}wt-AP$_{target}$ complex is flipped out of the DNA duplex and into the protein active site. The emission from this sample closely resembles that of the free 2AP base in aqueous solution indicating that the

2AP does not form a π-stacked complex in the enzyme active site. Indeed, the crystal structure of the M.HhaI active site described by Klimasauskas *et al*[107] contains no aromatic amino acid residues, capable of coupling with the flipped 2AP in this manner.

7.3.1.2 Time-Resolved Studies on Single Crystals

Table 7.1 shows the results of the global analysis of the fluorescence response functions of all the crystalline ternary complexed systems investigated.

DNA Duplex	A-Factor				Lifetimes/ ns			
	A1	A2	A3	A4	τ1	τ2	τ3	τ4
AP_{target} (AdoMet)	-	0.36	0.27	0.40	-	0.26	1.75	7.47
GP_{out}	0.64	0.19	0.14	0.03	0.07	0.53	2.07	7.36
TP_{out}	0.61	0.20	0.15	0.04	0.09	0.67	2.26	7.31
AP_{adj}	0.55	0.32	0.10	0.04	0.19	0.91	3.54	10.13
AP_{opp}	0.50	0.30	0.15	0.05	0.15	0.94	3.41	9.39
T250G mutants								
AP_{target} (AdoHcy)	-	0.07	0.17	0.77	-	1.10	6.30	10.85
AP_{target} (AdoMet)	-	0.07	0.13	0.79	-	0.91	5.86	11.05

Table 7.1- Parameters derived from global fits of decay curves collected from single crystals of ternary DNA-HhaI-cofactor complex. Fits shown are for emission at 390nm.

7.3.1.2.1 The effect of base flipping on the 2AP fluorescence response

Table 7.1 shows that the four component decay curve of 2AP in DNA is reduced to a three component response in the crystal complexes where 2AP is flipped out of the helix. This multiexponential response indicates that the 2AP experiences some environmental heterogeneity within the active site of both the wild-type and mutant enzymes. The notable absence of a ~100ps lifetime in the ^{M}wt-AP_{target}, ^{M}m-AP_{target} and ^{H}m-AP_{target} complexes, where 2AP is flipped out of the DNA duplex, indicates that the efficient quenching of excited-state 2AP requires it to be in a stacked conformation within the duplex. This is convincing evidence that the short

~100ps lifetime of 2AP in DNA is the result of π-π interactions between 2AP and its flanking bases.

Consider the ^{M}wt-AP$_{target}$ complex in relation to the ^{H}wt-GP$_{out}$ complex. In the free duplex, both the AP$_{target}$ and GP$_{out}$ duplexes contain 2AP flanked by, and base paired to, guanine. The similarity of these duplexes allows a useful comparison to be made with regards to the photophysical behaviour of 2AP as a probe of base flipping. Results of the global analysis of the fluorescence decays collected for each of these crystals are shown in Table 7.2 and Table 7.3.

Global Lifetimes: τ2=0.26ns, τ3=1.75ns, τ4=7.47ns
Global χ^2=1.041

Emission Wavelength/ nm	A1	A2	A3	A4	Local χ^2
370	-	0.33	0.27	0.41	1.033
390	-	0.36	0.27	0.38	1.034
410	-	0.38	0.29	0.33	1.055

Table 7.2- Globally fitted parameters derived from the ^{M}wt-AP$_{target}$ crystal fluorescence response. A 2 component fit of this data gives a global χ^2 = 1.343.

Global Lifetimes: τ1=0.07ns, τ2=0.53ns, τ3=2.07ns, τ4=7.36ns
Global χ^2=1.052

Emission Wavelength/ nm	A1	A2	A3	A4	Local χ^2
370	0.62	0.21	0.14	0.03	1.038
390	0.64	0.19	0.14	0.03	1.073
410	0.66	0.16	0.15	0.03	1.045

Table 7.3- Globally fitted parameters derived from the ^{H}wt-GP$_{out}$ crystal fluorescence response. A 3 component fit of this data gives a global χ^2 = 1.503.

The fluorescence decays of the crystalline ^{H}wt-GPout and ^{M}wt-AP$_{target}$ complexes give a definitive description of the photophysical response of 2AP to base flipping, as shown in Figure 7.12.

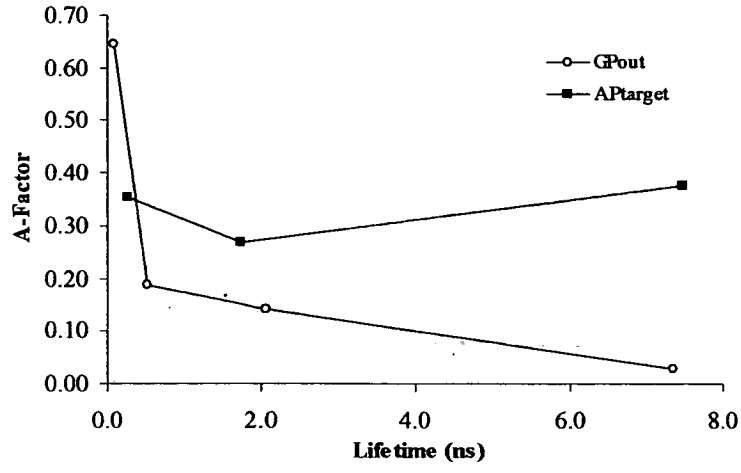

Figure 7.12- Plot showing A-factor (at an emission wavelength of 390nm) versus lifetime for the crystalline ternary complexes containing the GPout (circles) and APtarget (squares) duplexes. The different responses of these two systems show the characteristic effect of base flipping on the fluorescence response of 2AP.

The fluorescence responses of 2AP in the ^{M}wt-AP$_{target}$ complex and the ^{H}wt-GP$_{out}$ complex relate information about the fluorescence response of 2AP in the enzyme active site and in the DNA duplex, respectively. However, of the lifetimes fitted to the fluorescence responses of these complexes, the longest-lived component is observed in both systems. This long-lived excited-state species has a lifetime comparable to free 2AP base experiencing a polar, aqueous solution-like environment. It has been shown, in Chapter 6, that in the DNA duplex, this long-lived species can be thought of as 2AP that adopts an extrahelical orientation. It accounts for only 3% of the emitting species in the crystalline ^{H}wt-GP$_{out}$ complex. The A-factor for this long-lived 2AP species, increases by approximately an order of magnitude on base flipping by HhaI. It accounts for 40% of the emitting 2AP species in the ^{M}wt-AP$_{target}$ complex. Hence, disruption of the π-π stacking interactions, that 2AP experiences in the DNA duplex, through base flipping, leads to a significant increase in the A-factor for the long-lived 2AP species. This observation is in good agreement with the previously presented results for the pure crystalline 2AP, where the π-π overlap between adjacent molecules in the crystal is particularly good and no fluorescence with a lifetime approaching 7ns is noted.

The fluorescence response of the ^{M}wt-AP$_{target}$ complex crystal shows two further discrete lifetime components of 0.26ns and 1.75ns. These components of the fluorescence response represent a significant proportion of the emitting 2AP molecules within the system- 36% and 27% respectively. These components of the fluorescence response represent some heterogeneity of the orientation of the flipped 2AP within the crystal active site. Both of these components have short lifetimes, relative to the long-lived 2AP species. Hence, they represent 2AP molecules that interact closely with the HhaI enzyme, in comparison to the long-lived 2AP species.

7.3.1.2.2 The Effect of the T250G mutation on the base flipping response

Both the ^{M}m-AP$_{target}$ and ^{H}m-AP$_{target}$ complexes have similar fluorescence responses. Results of the global analysis from each of these crystals are shown in Table 7.4 and Table 7.5, respectively.

Global Lifetimes: τ2=0.91ns, τ3=5.86ns, τ4=11.05ns
Global χ^2=1.018

Emission Wavelength/ nm	A1	A2	A3	Local χ^2
370	0.11	0.21	0.68	1.024
390	0.07	0.13	0.79	1.015
410	0.06	0.08	0.87	1.016

Table 7.4- Globally fitted parameters derived from the ^{M}m-AP$_{target}$ crystal fluorescence response. A 2 component fit of this data gives a global χ^2 = 1.061.

Global Lifetimes: τ2=1.10ns, τ3=6.30ns, τ4=10.85ns
Global χ^2=1.023

Emission Wavelength/ nm	A1	A2	A3	Local χ^2
370	0.12	0.21	0.67	1.042
390	0.07	0.17	0.77	1.004
410	0.04	0.13	0.84	1.023

Table 7.5- Globally fitted parameters derived from the ^{H}m-AP$_{target}$ crystal fluorescence response. A 2 component fit of this data gives a global χ^2 = 1.084.

The global χ^2 values for two or three component fits of the data presented in Table 7.4 and Table 7.5 are quite similar and on the basis of their values alone, it is not justified to add a third component to the fit. However, there is some deviation in the fit at the peak of the decay curve with a two component fit. The use of a three component fit is supported by the global analysis of data collected for the ^{H}m-AP$_{target,}$ to 30000 counts in the peak channel, shown in Table 7.6 (data presented in Table 7.4 was collected to 10000 counts in the peak channel). Both sets of data were collected on the same day, using the same experimental conditions. Decays were typically collected to only 10000 counts in the peak channel. Comparisons of this data with decays collected to 30000 counts in the peak channel showed no significant variation in the results derived from these decays. Since only a limited amount of time was available on the shared instrumentation in the COSMIC facility where measurements were made collection of decays to 10000 counts allowed a good compromise between the data quality and the number of systems investigated.

A-Factor			Lifetimes/ ns			Global χ2
A1	A2	A3	τ1	τ2	τ3	
0.24	0.76	-	3.28	10.43	-	1.222
0.14	0.26	0.60	1.10	6.30	10.85	1.083

Table 7.6- Parameters derived from global analysis using two and three component fits for the ^{M}m-AP$_{target}$ crystal, where decays were recorded to 30000 counts in the peak channel.

The presence of the methyl group of AdoMet has little effect on the fluorescence response of 2AP in the ^{M}m-AP$_{target}$ and ^{H}m-AP$_{target}$ complexes. This is in good agreement with the crystal structure obtained for the ^{H}m-AP$_{target}$ complex, which shows the 2AP to be located some distance from the HhaI active site with the 2AP C8 atom some 9.54Å from the sulphur atom of the AdoHcy cofactor (Figure 7.13). Since the flipped base must lie in close proximity to the cofactor for the enzyme to perform the methylation reaction, it is clear that in this mutant complex the 2AP does not reside in the 'normal' active site for HhaI.

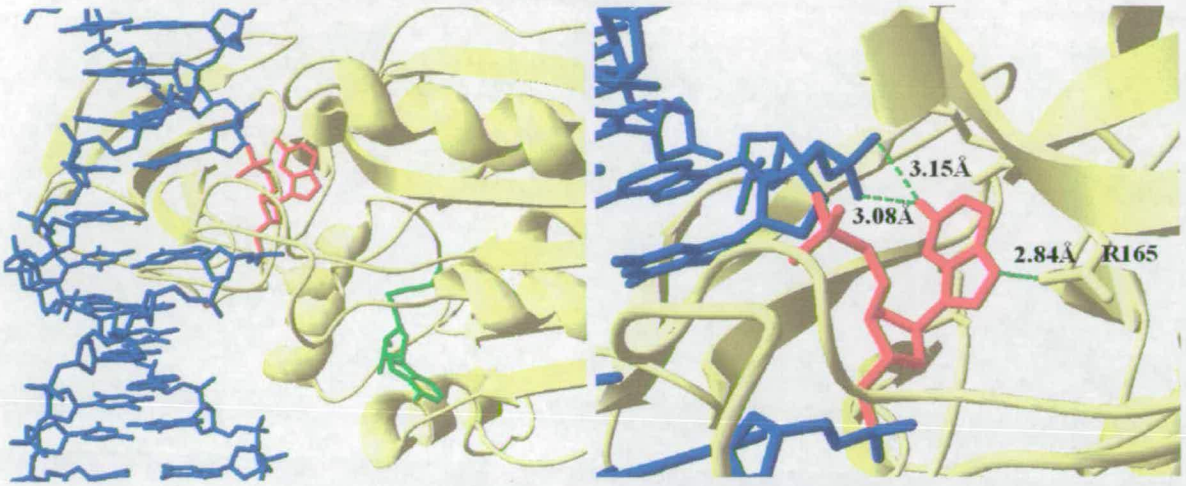

Figure 7.13- The crystal structure of the ^{H}m-AP$_{target}$ complex. The DNA duplex is shown in blue, with 2AP in red. The T250G mutant of HhaI is in yellow with the AdoHcy cofactor analogue in green. The image to the left shows the large separation between 2AP and the AdoHcy cofactor analogue. The image on the right shows the local environment and the hydrogen bonding interactions the flipped 2AP experiences. Distances shown are for donor-acceptor seperation in hydrogen bonding interactions.

The three lifetimes of the ^{H}m-AP$_{target}$ and ^{M}m-AP$_{target}$ duplexes are notably longer than those of the analogous wild-type complex. The decays of these complexes are dominated by the component of the long-lived 2AP species, whose A-factor is considerably greater in the mutant complexes, than in the wild-type complex. Hence, the fluorescence responses of the mutant and wild-type crystals indicate that the extrahelical environment of the 2AP is distinct in each.

Figure 7.8 shows that the T250G mutation creates a void in proximity to the DNA phosphate backbone, which is occupied by the flipped 2AP in the complex. In the wild-type complex, the 'normal' active site is indicated by the region that cytosine is flipped into in Figure 7.8. O'Gara *et al* have shown that adenine flipped into the wild-type HhaI enzyme adopts a similar orientation to that chosen by cytosine[114] and so it seems reasonable to expect that flipped 2AP will lie in a similar region of the enzyme active site. Figure 7.14 shows the local environment of adenine in this instance.

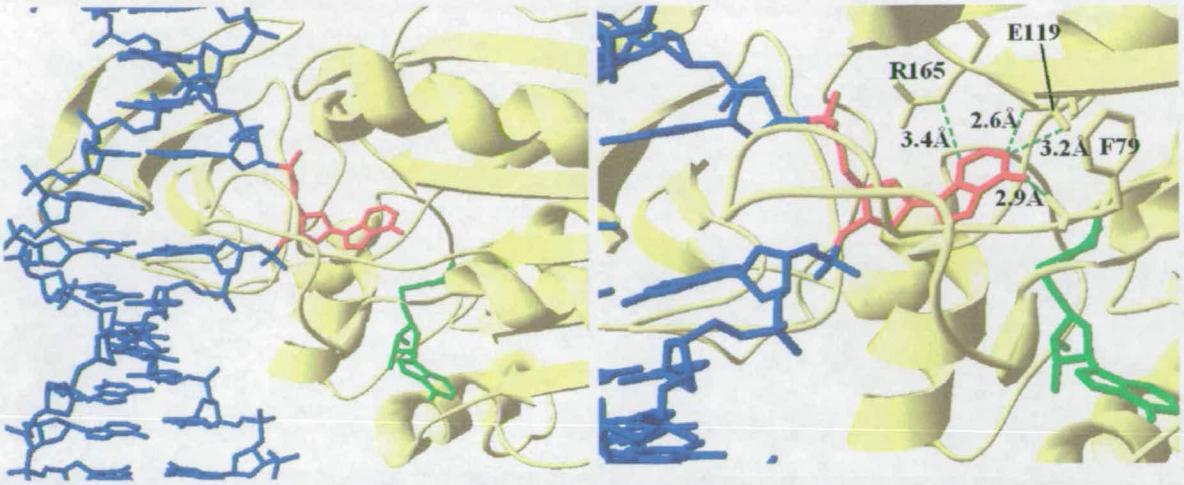

Figure 7.14- Crystal structure for adenine flipped into the active site of wild-type HhaI. The DNA duplex is shown in blue, with 2AP in red. Wild-type HhaI is in yellow with the AdoHcy cofactor analogue in green. The image to the left shows the adenine in the active site of HhaI, in close proximity to the AdoHcy cofactor analogue. The image on the right shows the local environment and the hydrogen bonding interactions the flipped 2AP experiences. Distances shown are for donor-acceptor seperation in hydrogen bonding interactions.

Figure 7.13 and Figure 7.14 show how the immediate environment of 2AP might (since Figure 7.14 is for a flipped adenine base) differ in the mutant and wild-type complexes. Comparison of the images shown on the left-hand-side of these Figures indicates that there is more 'free' volume available in the active site of wild-type HhaI, compared to that in the cavity occupied by 2AP in the T250G mutant. Acrylamide quenching experiments by Vilkaitis *et al* are in good agreement with this observation[119]. They show that the fluorescence of 2AP is 5-6 times more quenched in the wild-type enzyme than in the T250G mutant, indicating that the 2AP in the wild-type complex is far more accessible to solvent molecules than in the T250G mutant complex. The relatively small pocket that the 2AP finds itself within in the T250G mutant complex is likely to restrict the dynamics of the flipped base. This is consistent with the large A-factor for the long-lived 2AP species in the decay of these mutant complexes, which indicates that the flipped base is largely constrained to a single, narrow distribution of orientations. Contrast this to the ^{M}wt-AP$_{target}$ crystal complex, where each of the three components to the

decay have similar A-factors, indicating that there is little energetic or steric requirement for the flipped base to adopt any particular one of these three orientations within the enzyme active site.

The short lifetimes of the ^{M}wt-AP$_{target}$ complex, compared with those of the mutant crystal complexes suggest that the overall environment of the flipped 2AP is less polar in the wild-type than mutant crystals. Indeed, in the T250G mutant of HhaI the flipped 2AP lies in a highly polarised environment. Figure 7.13 shows that, at one end of the 2AP, the amine group is hydrogen bonded to the negatively charged phosphate group of the DNA, 5' of the flipped base. At the other end of the 2AP, the N7 lone pair of electrons is hydrogen bonded to the side chain of the positively charged arginine 165 residue.

Studies on the solution-phase free 2AP base, described earlier in this thesis, found that the fluorescence lifetime of the 7H tautomeric form of 2AP was 13.5ns, as compared to 11.0ns for the 9H tautomer. In a manner analogous to the formation of the 7H tautomer in the free 2AP base, Arg165 withdraws electron density from the N7 of 2AP in the ^{H}m-AP$_{target}$ complex. This seems a probable source of the long fluorescence lifetime, τ_4, of 2AP in the ^{H}m-AP$_{target}$ and ^{M}m-AP$_{target}$ complexes. Importantly, there is a water-filled region in the active site of the wild-type enzyme in the vicinity of N7 of adenine in the crystal structure. The absence of any lifetime greater than 7.5ns in the ^{H}wt-AP$_{target}$ complex illustrates the importance of N7 in determining the magnitude of the lifetime of the long-lived 2AP species.

In both ^{H}m-AP$_{target}$ and ^{M}m-AP$_{target}$ the lifetimes of τ_2 and τ_3 resemble those quoted for τ_3 and τ_4 in the pure 2AP crystal (1.18ns and 4.85ns respectively). In fact, the interactions experienced by 2AP in all three of these systems are remarkably similar. In all, hydrogen bonds are formed between the amine protons and oxygen atoms, and a proton hydrogen bonds to N7. It seems likely, then, that lifetimes for 2AP with magnitudes in this range are induced by intermolecular hydrogen bonding interactions of 2AP.

7.3.1.2.3 The effect of flipping the base adjacent to or opposite 2AP

Both the ^{H}wt-AP$_{opp}$ and ^{H}wt-AP$_{adj}$ complexes are described by similar fluorescence responses, the parameters derived from which are shown in Table 7.7 and Table 7.8, respectively.

Global Lifetimes: $\tau 1$=0.15ns $\tau 2$=0.94ns, $\tau 3$=3.41s, $\tau 4$=9.39ns
Global χ^2=1.084

Emission Wavelength/ nm	A1	A2	A3	A4	Local χ^2
370	0.58	0.27	0.11	0.04	1.145
390	0.50	0.30	0.15	0.05	1.045
410	0.44	0.31	0.17	0.08	1.062

Table 7.7- Globally fitted parameters derived from the ^{H}wt-AP$_{opp}$ crystal fluorescence response. A 3 component fit of this data gives a global χ^2 = 1.402.

Global Lifetimes: $\tau 1$=0.19ns $\tau 2$=0.91ns, $\tau 3$=3.54s, $\tau 4$=10.13ns
Global χ^2=1.085

Emission Wavelength/ nm	A1	A2	A3	A4	Local χ^2
370	0.61	0.30	0.07	0.02	1.117
390	0.55	0.32	0.10	0.04	1.052
410	0.49	0.32	0.14	0.05	1.087

Table 7.8- Globally fitted parameters derived from the ^{H}wt-AP$_{adj}$ crystal fluorescence response. A 3 component fit of this data gives a global χ^2 = 1.692.

The fluorescence responses of both of the crystalline ^{H}wt-AP$_{opp}$ and ^{H}wt-AP$_{adj}$ complexes are described by four discrete components and are dominated by a short-lived component with a lifetime less than 200ps, which represents approximately 55% of the emitting species. In this sense the decays of these two complexes are similar to that presented for the ^{H}wt-GP$_{out}$ complex, presented in Table 7.3. Hence, the fluorescence responses of the ^{H}wt-AP$_{opp}$ and ^{H}wt-AP$_{adj}$ complexes are characteristic of a 2AP population which is predominantly an intrahelical species.

It is perhaps surprising, given that base flipping affects the 2AP in each in a distinctly different manner, that both ^{H}wt-AP$_{opp}$ and ^{H}wt-AP$_{adj}$ complexes show similar fluorescence responses. The crystal structures confirm that the 2AP molecules in these complexes adopt predominantly intrahelical conformations. Crucially, the intrahelical nature of the 2AP is maintained by the enzyme through hydrogen bonding interactions, as shown in Figure 7.15a and Figure 7.16a.

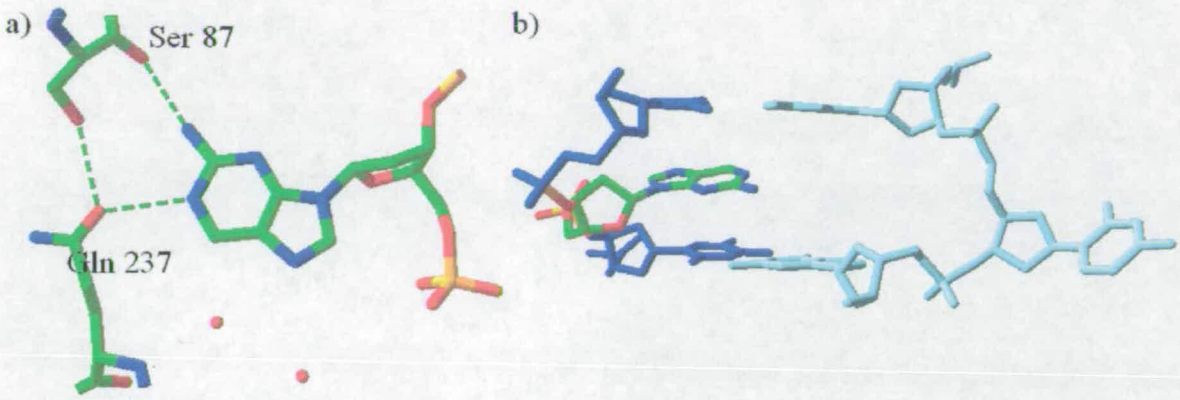

Figure 7.15- Images derived from the crystal structure of the ^{H}wt-AP$_{opp}$ complex. a) showing the hydrogen bonding interactions felt by 2AP (looking along the DNA helical axis) and; b) the DNA duplex in the immediate vicinity of the 2AP.

Figure 7.15 shows the 2AP in the 'orphaned' position, opposite the target site for base flipping. As in the normal HhaI recognition sequence, where the orphan base is a guanine (shown in Figure 7.6), the enzyme infiltrates the duplex via the glutamine 237 and serine 87 residues. 2AP is similar in structure to guanine but, importantly, lacks the carboxyl group of guanine at C6. Hence, the hydrogen bonding interactions formed in the crystal structure for the complexes where guanine is the orphan base are different from those where 2AP is at this position. Indeed, the crystal structures illustrated in Figure 7.6 and Figure 7.15 indicate that both binding of the orphan base and the bonding between serine 87 and glutamine 237 are weaker when 2AP, rather than guanine, is the orphan base. This significantly decreases the ability of the enzyme to bind the DNA duplex, where 2AP is the orphan base, as will become apparent in the investigation of the solution-phase complexes that follows.

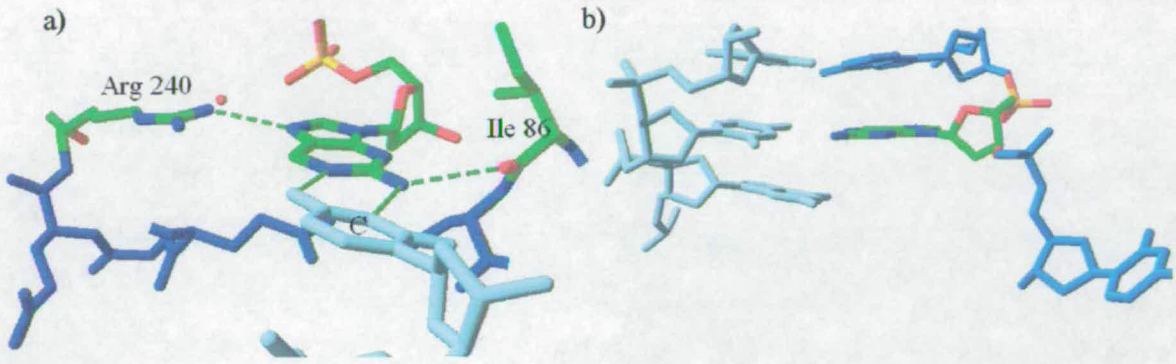

Figure 7.16- Images derived from the crystal structure of the ^{H}wt-AP$_{adj}$ complex. a) Showing the hydrogen bonding interactions felt by 2AP (looking across the C-2AP base pair) and; b) the DNA duplex in the immediate vicinity of the 2AP.

Figure 7.16a shows that, the 2AP adjacent to the target site for base flipping forms a relatively stable 'wobble' base pair with the cytosine opposite it. It is interesting to note that the enzyme carefully maintains the fidelity of this base pair during flipping, through interactions between arginine 240 and isoleucine 86 and the 2AP. This evolved mechanism of stabilising the duplex illustrates the importance of the bases either side of the flipped base in stabilising the duplex during flipping. The fact that the enzyme has evolved a mechanism for stabilising these bases, indicates that the base pairs are dynamic, and require stabilisation, on the timescale of base flipping. Figure 7.16b shows that the aromatic π-π stacking interactions experienced by the 2AP adjacent to the target site for base flipping are completely disrupted in the 3' direction. However, the possibility that some orbital interaction exists between the lone pair electrons of the oxygen and nitrogen atoms on the glutamine and serine residues and the adjacent 2AP remains.

It has been shown, from studies on the 2AP crystal and those results discussed previously in this chapter, that a fluorescence lifetime of ~100ps for 2AP is indicative of efficient non-radiative de-excitation of 2AP* via some mechanism (most probably electron transfer) that is sensitive to the π-π overlap between 2AP and its flanking bases. Table 7.1 shows that both the ^{H}wt-AP$_{opp}$ and ^{H}wt-AP$_{adj}$ complexes have fluorescence responses, where around 50% of the 2AP in the system has a lifetime of a similar magnitude to this. In both complexes, the magnitude of τ1 is greater than 100ps, indicating that the probability of electron transfer through π-π stacking interactions in these duplexes is less than that seen for the 2AP in the ^{H}wt-GP$_{out}$ and ^{H}wt-TP$_{out}$

complexes. This is certainly not surprising for the ^{H}wt-AP$_{adj}$ crystal, where the π-π interactions between 2AP and its flanking bases are substantially disrupted by base flipping. The occurrence of this component in the fluorescence response of the ^{H}wt-AP$_{adj}$ crystal shows that electron transfer requires the presence of only one adjacent π-stacking interaction in order to take place. Observations made by O'Neill and Barton, show electron transfer from guanine to 2AP occurs most efficiently in the 3'→5' direction[99]. Hence, the long, 190ps lifetime of the shortest-lived 2AP species in the ^{H}wt-AP$_{adj}$ crystal is in good agreement with the fact that the cytosine bridging base between 2AP and the nearest intrahelical guanine base, has been flipped from the duplex into the enzyme active site. The pathway for intrahelical electron transfer has been cut off, giving what is a relatively long lifetime for this shortest-lived 2AP species.

The magnitudes of three longest lifetimes in both the ^{H}wt-AP$_{opp}$ and ^{H}wt-AP$_{adj}$ complexes are large in comparison with the other 'intrahelical' 2AP complexes (^{H}wt-GP$_{out}$ and ^{H}wt-TP$_{out}$). This effect is most probably a result of the distortion of the DNA duplex by the enzyme in proximity to the 2AP in both the ^{H}wt-AP$_{opp}$ and ^{H}wt-AP$_{adj}$ complexes.

7.3.2 Solution Phase Systems

The time resolved fluorescence response of the series of five different 2AP labelled DNA duplexes has been monitored as a function of M.HhaI enzyme binding. The remainder of this chapter presents the results of studies of the these duplexes in four different solution phase complexes, where the DNA is complexed by the wild-type or T250G mutants of HhaI, each either with or without the appropriate cofactor. Many of the arguments that are presented with this work are developed alongside the results presented. Hence, full arguments are generally presented alongside the results of the studies on the solution phase ternary complexes, where direct comparison can be made to the studies on crystalline samples.

7.3.2.1.1 DNA Duplexes

For ease of reference, the results previously given for the time-resolved fluorescence studies of the DNA duplexes in Chapter 5 are presented in Table 7.9, with nomenclature that is relevant to the present discussion.

DNA Duplex	A-Factor				Lifetimes/ ns			
	A1	A2	A3	A4	τ1	τ2	τ3	τ4
AP_{target}	0.53	0.26	0.14	0.06	0.08	0.58	2.94	9.60
GP_{out}	0.70	0.13	0.10	0.08	0.04	0.50	2.95	11.01
TP_{out}	0.64	0.15	0.10	0.11	0.04	0.44	2.71	10.70
AP_{adj}	0.83	0.09	0.05	0.02	0.04	0.45	2.63	10.33
AP_{opp}	0.64	0.16	0.11	0.10	0.05	0.50	2.98	9.81

Table 7.9- Parameters derived from global fits of the fluorescence decays for free 2AP labelled DNA duplexes in buffered aqueous solution. Fits shown are for emission at 390nm.

7.3.2.1.2 The Wild-Type HhaI-DNA Binary Complex

The fluorescence response for the binary complex between each 2AP labelled deoxyoligonucleotide and the wild-type M.HhaI (wt.HhaI) enzyme was recorded. Experimental decays were recorded and fitted using the same procedure as for the free DNA duplexes. The parameters derived from the fitting are shown in Table 7.10.

DNA Duplex	A-Factor				Lifetimes/ ns			
	A1	A2	A3	A4	τ1	τ2	τ3	τ4
AP_{target}	0.29	0.22	0.21	0.28	0.14	0.97	4.34	9.65
GP_{out}	0.75	0.11	0.07	0.07	0.04	0.45	2.73	10.05
TP_{out}	0.45	0.20	0.16	0.19	0.06	0.55	3.04	9.79
AP_{adj}	0.82	0.10	0.05	0.02	0.04	0.41	2.51	9.69
AP_{opp}	0.75	0.12	0.07	0.06	0.05	0.51	2.77	9.60

Table 7.10- Data derived from global analysis of fluorescence decay curves for 2AP labelled DNA duplexes complexed with wt.HhaI. Reported A-factors are for 2AP emission at 390nm.

The changes in 2AP A-factor and lifetime created by protein binding to the free DNA duplexes, for the cases where the 2AP is not base flipped, are summarised in Figure 7.17 and Figure 7.18 respectively.

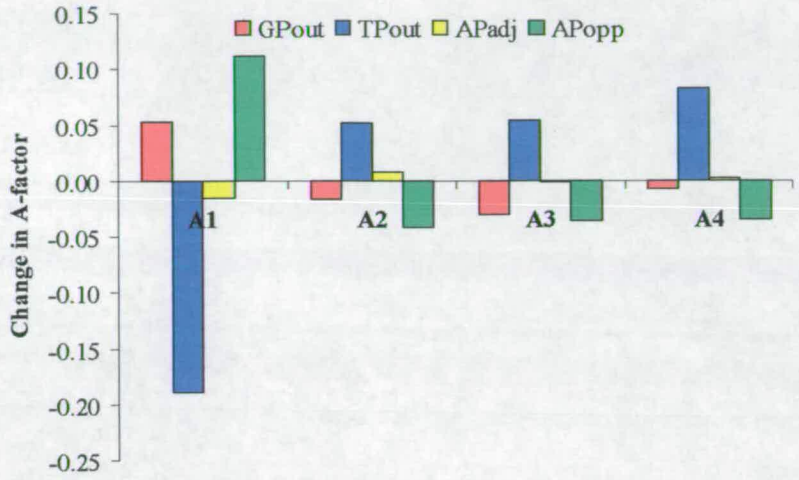

Figure 7.17- Bar chart showing the change in A-factors produced by wt.HhaI binding of the free DNA duplex for each of the four DNA duplexes tested, where the 2AP is 'intrahelical'. Changes are calculated for emission at 390nm.

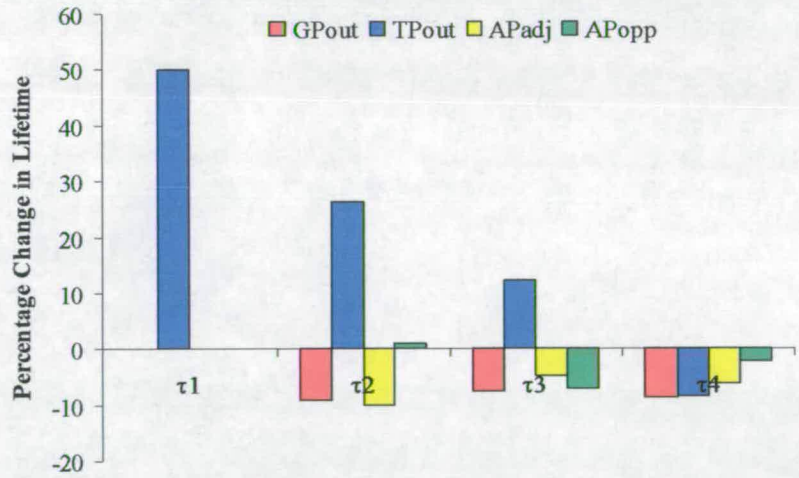

Figure 7.18- Bar chart showing the percentage change in fluorescence lifetimes produced by wt.HhaI binding of the free DNA duplex for each of the four DNA duplexes tested, where the 2AP is 'intrahelical'.

7.3.2.1.3 The GP_{out}/Wild Type HhaI Binary Complex

Table 7.11 describes the parameters derived from the global analysis of the wt-GP_{out} binary complex.

Global Lifetimes: τ1=0.04ns, τ2=0.45ns, τ3=2.73ns, τ4=10.05ns

Emission Wavelength/ nm	A1	A2	A3	A4
370	0.81	0.07	0.05	0.07
390	0.75	0.11	0.07	0.07
410	0.76	0.13	0.06	0.04

Table 7.11- Parameters derived from the globally fitted decays of the wt-GP_{out} complex.

This duplex was studied as a control sample, with the 2AP lying beyond the HhaI recognition sequence and not being contacted in any way by the enzyme. The bases in the immediate vicinity of the 2AP are identical to those surrounding 2AP in the AP_{target} duplex. No significant change in the A-factors or lifetimes of the GP_{out} duplex is observed upon protein binding.

7.3.2.1.4 The AP_{target}/Wild Type HhaI Binary Complex

The data derived from the global fits of the decays collected for the binary wt-AP_{target} complex is shown in Table 7.12.

Global Lifetimes: τ1=0.14ns, τ2=0.97ns, τ3=4.34ns, τ4=9.65ns

Emission Wavelength/ nm	A1	A2	A3	A4
370	0.25	0.19	0.23	0.32
390	0.29	0.22	0.21	0.28
410	0.36	0.23	0.18	0.23

Table 7.12- Parameters derived from the globally fitted decays of the wt-AP_{target} complex.

Figure 7.19 clearly indicates that a four component fit is required to globally fit the experimental data for this system.

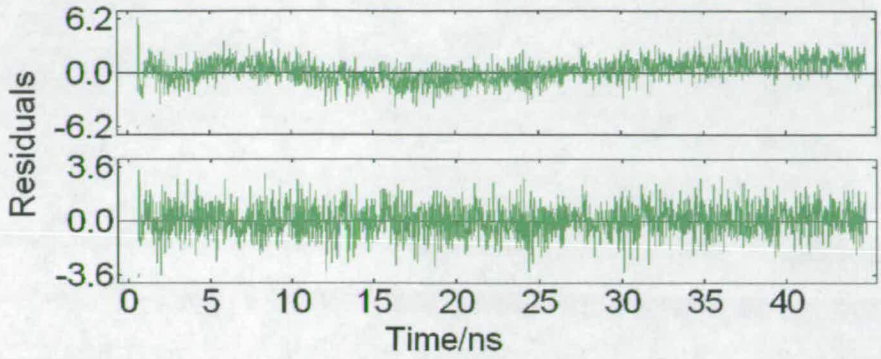

Figure 7.19- Residuals for the 3 component (top) and four component (bottom) fits of the data collected for the wt-AP_{target} system. Residuals are from fits where the parameters derived from the global analysis have been fixed and fitted to a single decay curve. The decay curve used was for emission at 390nm on the 50ns timescale. χ^2 was 1.711 for the 3 component fit and 1.067 for the four component fit.

There is a dramatic change in the fluorescence response of the AP_{target} duplex upon protein binding as indicated by Table 7.10. Figure 7.20 shows, through comparison of the decay parameters for the GP_{out} and Ap_{target} binary complexes, that base flipping of 2AP by wt.HhaI leads to a distinctive change in the decay parameters of the 2AP labelled duplexes.

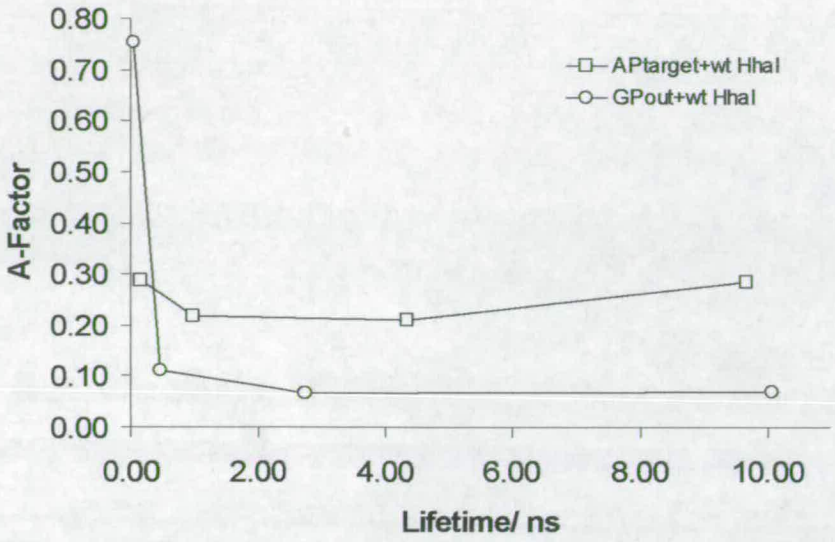

Figure 7.20- Plot of lifetime versus A-factor for the wt-AP_{target} binary complex (squares) and free AP_{target} duplex (circles). Reported A-factors are for emission at 390nm.

In the solution phase, base flipping of 2AP, in the binary DNA-enzyme complex, leads to a significant decrease in the A-factor of the shortest lifetime component, with an increase in the A-factors of all other components. This is in excellent agreement with the observations made on the crystalline ternary DNA-enzyme-cofactor complexes. Hence, the definitive signature of base flipping, seen for the crystalline 2AP labelled DNA duplexes, is also noted in binary complexes, in solution.

Figure 7.20 shows that almost all of the 2AP decay parameters change with base flipping, indicating a significant change in the local environment of the 2AP. Notably, however, the magnitude of τ_4, the lifetime of the long-lived 2AP species, for the free AP_{target} duplex is unchanged by protein binding (9.6ns for the free duplex compared to 9.7ns for the binary DNA-enzyme complex). This indicates that the environment of the flipped 2AP, in the enzyme binding pocket is similar to that experienced by the 'extrahelical' 2AP in the free DNA duplex. The proportion of these similar 2AP species increases from only 6% in the free DNA to 28% upon protein binding, clearly indicating that the enzyme facilitates the adoption of this extrahelical orientation by 2AP.

There is good evidence, from the ^{19}F studies carried out by Klimasauskas *et al* that although enzyme binding of the DNA may be complete, an equilibrium between the flipped and unflipped conformations of the target base exists[115]. Hence, in the DNA-HhaI complex, some 2AP stacked within the DNA duplex exists. This unflipped 2AP must have a similarly short lifetime to that in the free DNA duplex and, hence, τ_1 is assigned to this efficiently quenched form of the probe. The feasibility of this assertion is enforced by the change in A-factor for this species on protein binding. The magnitude of A1 decreases by the same amount as that of A4, which represents the extrahelical 2AP, increases. The increase in the magnitude of τ_1 upon protein binding could be due to the conformational constraints enforced on the DNA duplex by enzyme binding, which lower the probability of non-radiative decay through electron transfer. A similar effect to this was seen in the crystalline ^{H}wt-AP$_{opp}$ and ^{H}wt-AP$_{adj}$ complexes, where the lifetime of stacked 2AP (τ_1) is longer than anticipated around the target site for base flipping, where the enzyme binds and distorts the duplex.

The increase in magnitude of both τ_2 and τ_3 upon enzyme binding shows that the environment of these molecules is sensitive to protein binding, and indeed, may be completely changed by base flipping. It is becoming increasingly apparent that 2AP with lifetimes between 0.5 and 7ns are ubiquitous in the systems investigated, regardless of whether the 2AP molecules are intra or extrahelical. Furthermore, these species constitute a significant part of the 2AP population. It seems likely that these lifetimes represent 2AP molecules in stable, hydrogen bonded, conformations, where relatively few solvent molecules have access to their immediate environment. The propensity for hydrogen bonding by 2AP implies that these species can exists both within the DNA duplex and within the protein active site, where the 2AP in both instances undergoes similar intermolecular interactions.

Further discussion of the arguments presented for this binary complex is given for the ternary complexes in the remainder of this chapter, where important comparisons with the studies of the crystalline ternary complexes can be unambiguously made.

7.3.2.1.5 The TP_{out}/Wild Type HhaI Binary Complex

The parameters derived from the global analysis of the wt-TP_{out} system are shown in Table 7.13.

Global Lifetimes: τ1=0.06ns, τ2=055ns, τ3=3.04ns, τ4=9.79ns

Emission Wavelength/ nm	A1	A2	A3	A4
370	0.53	0.15	0.14	0.17
390	0.45	0.20	0.16	0.19
410	0.46	0.23	0.16	0.15

Table 7.13- Parameters derived from the globally fitted decays of the wt-TP_{out} complex.

Figure 7.17 and Figure 7.18 show that changes in both the fluorescence lifetime and the A-factor of the stacked 2AP molecules (A1, τ_1) in the TP_{out} duplex are brought about by enzyme binding. This result appears somewhat surprising, since there is no contact between the enzyme and the 2AP, or even the bases in the immediate vicinity of the 2AP. Furthermore, in the GP_{out} duplex, where the 2AP is in the same position, relative to the protein active site, no change in the fluorescence response of this species is observed upon protein binding. The TP_{out} duplex shows a decrease in the proportion of stacked 2AP, accompanied by an increase in its lifetime. This suggests that the stacking interactions are perturbed by enzyme binding. As will be shown in the following discussion, the fluorescence response of this duplex is affected in a similar way by enzyme binding in all of the systems studied.

Evidence for a distortion of the DNA duplex is seen in the fluorescence response of the wt-TP_{out} complex and not the wt-GP_{out} complex. This is almost certainly due to the relatively stable Watson-Crick interaction formed between 2AP and T compared with the mismatched 2AP-G base-base interaction. Hence, the 2AP-G base pair, 2AP experiences a similar environment in both the free duplex and protein bound duplex, whereas the 2AP in the 2AP-T base pair is disrupted by protein binding and so the fluorescence response of the bound and free TP_{out} duplexes are distinctly different. This point is discussed in greater detail in relation to the ternary complexes, where the crystal structures obtained for the TP_{out} and GP_{out} duplexes can be used to clarify the reasons for this behaviour.

7.3.2.1.6 The AP_{adj} and AP_{opp} /Wild Type HhaI Binary Complexes

Figure 7.17 and Figure 7.18 show that the fluorescence response of neither of these two duplexes is significantly changed by enzyme binding and subsequent base flipping of the adjacent (AP_{adj}) or opposite (AP_{opp}) cytosine base. Table 7.14 and Table 7.15 show the parameters fitted to the decays of the wt-AP_{adj} and wt-AP_{opp} binary complexes, respectively.

Global Lifetimes: τ1=0.04ns, τ2=0.41ns, τ3=2.51ns, τ4=9.69ns

Emission Wavelength/ nm	A1	A2	A3	A4
370	0.86	0.08	0.04	0.02
390	0.82	0.11	0.05	0.02
410	0.78	0.13	0.06	0.02

Table 7.14- Parameters derived from the globally fitted decays of the wt-AP_{adj} complex.

Global Lifetimes: τ1=0.05ns, τ2=0.51ns, τ3=2.77ns, τ4=9.60ns

Emission Wavelength/ nm	A1	A2	A3	A4
370	0.78	0.10	0.06	0.06
390	0.75	0.12	0.07	0.06
410	0.75	0.14	0.07	0.05

Table 7.15- Parameters derived from the globally fitted decays of the wt-AP_{opp} complex.

In the case of the wt-AP_{adj} complex, binding of the DNA by the duplex is relatively weak and it is possible that, in this binary duplex, not all of the DNA is bound by HhaI. Poor binding of this duplex by HhaI was previously observed by Holz *et al*[24].

Binding of the AP_{opp} duplex by HhaI is expected to be complete at the concentrations used here[124]. There is some change in the fluorescence response of this duplex upon enzyme binding to indicate that this is the case. Most notable is an increase of approximately 0.1 in the A-factor for τ1 upon protein binding. This, however, is a relatively small effect. The effect of enzyme

binding on the fluorescence response of these duplexes is discussed in detail for the ternary complex systems, where enzyme binding is known to be complete[24].

7.3.2.2 The DNA/Wild-Type HhaI/Cofactor Ternary Complex

The fluorescence response of ternary DNA-HhaI-cofactor complexes were recorded, where the cofactor used is AdoMet for the AP_{target} duplex and AdoHcy for all other complexes. Fluorescence decay curves were collected on 20 and 50ns timescales and at three emission wavelengths (370nm, 390nm and 410nm) with excitation at 320nm. Global analysis was performed as with data for the free duplexes and binary complexes. Table 7.16, Figure 7.21 and Figure 7.22 summarise the data derived from the studies of these ternary complexes, with A-factors shown for 2AP emission at 390nm.

DNA	A-Factor				Lifetimes/ ns			
Duplex	A1	A2	A3	A4	$\tau 1$	$\tau 2$	$\tau 3$	$\tau 4$
AP_{target}	0.22	0.26	0.23	0.29	0.12	0.95	4.23	10.49
GP_{out}	0.70	0.12	0.08	0.10	0.03	0.47	2.82	10.25
TP_{out}	0.60	0.15	0.12	0.13	0.06	0.64	3.07	10.09
AP_{adj}	0.79	0.15	0.04	0.02	0.08	0.32	2.35	9.91
AP_{opp}	0.65	0.18	0.09	0.08	0.06	0.44	2.68	9.37

Table 7.16- Parameters derived from average of global fits, on the 20ns and 50ns timescales, of the fluorescence responses collected from the ternary DNA-wt-HhaI-cofactor complexes taken at an emission wavelength of 390nm.

Note that the data shown in Figure 7.21 and Figure 7.22 is derived from the differences between lifetimes and A-factors for the binary complexes and the ternary complexes.

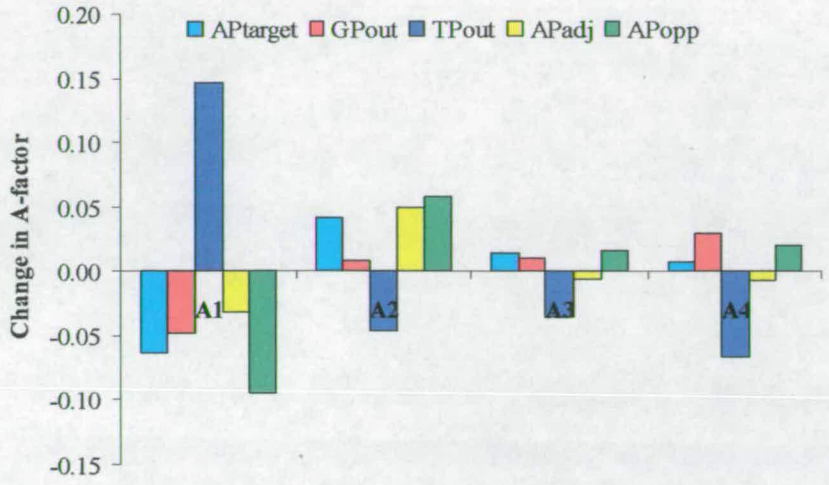

Figure 7.21- Bar chart showing the change in A-factors produced, at an emission wavelength of 390nm, by cofactor binding for each of the five DNA-wild-type HhaI binary complexes.

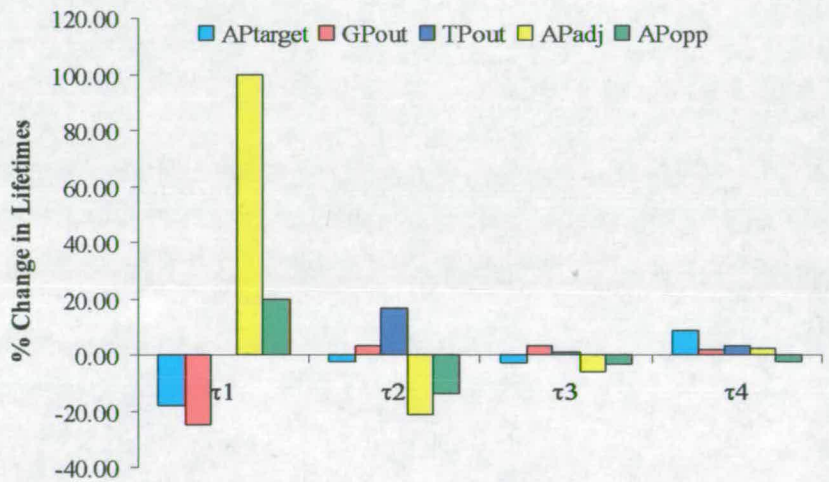

Figure 7.22- Bar chart showing the percentage change in lifetimes produced, at an emission wavelength of 390nm, by cofactor binding for each of the five DNA-wild-type HhaI binary complexes.

7.3.2.2.1 The GP_{out}/Wild-Type HhaI/AdoHcy Ternary Complex

This duplex behaves admirably as a control system. Table 7.17 shows the parameters derived from the global fits of the decay curves collected for the ^{H}wt-GP_{out} complex.

Global Lifetimes: τ1=0.03ns, τ2=0.47ns, τ3=2.82ns, τ4=10.25ns

Emission Wavelength/ nm	A1	A2	A3	A4
370	0.80	0.07	0.06	0.07
390	0.70	0.12	0.08	0.10
410	0.70	0.14	0.08	0.08

Table 7.17- Parameters derived from the globally fitted decays of the ^{H}wt-GP_{out} complex.

Figure 7.21 and Figure 7.22 show that the fluorescence response for the ternary ^{M}wt-GP_{out} complex is essentially identical to that obtained for the free GP_{out} DNA duplex. This result is as expected for this duplex, where the duplex in the vicinity of the 2AP is not expected to be perturbed by enzyme binding. However, as noted previously for the TP_{out} binary complex (and, indeed, as will be shown for the TP_{out} ternary complex), this region of the duplex is perturbed by enzyme binding and the subsequent base flipping. Thus, the results presented for this GP_{out} duplex in Figure 7.21 and Figure 7.22 illustrate how the conformation and dynamics of 2AP, at this point in the duplex, are determined by the interactions the 2AP feels from the base opposite it. Since there is little or no hydrogen bonding interaction between the opposite 2AP and guanine bases in this duplex the π-π stacking interaction is critical in determining the conformation of the 2AP, relatively to the bases in its immediate vicinity. Such is the significance of this interaction that the crystal structure for this complex, discussed in Chapter 6, shows that 2AP adopts an anti-conformation in order to achieve good π-overlap with the guanine base 3' of it. This is in stark contrast to the analogous TP_{out} ternary complex (discussed below), which shows relatively large changes in its fluorescence response upon enzyme binding.

7.3.2.2.2 The AP_{target}/Wild-Type HhaI/AdoMet Ternary Complex

Table 7.18 shows the parameters derived from the globally fitted decay curves for the ^{M}wt-AP_{target} complex.

Global Lifetimes: τ1=0.12ns, τ2=0.95ns, τ3=4.23ns, τ4=10.49ns

Emission Wavelength/ nm	A1	A2	A3	A4
370	0.28	0.26	0.21	0.25
390	0.22	0.26	0.23	0.29
410	0.21	0.23	0.24	0.32

Table 7.18- Parameters derived from the globally fitted decays of the ^{M}wt-AP_{target} complex.

Figure 7.23 shows the residuals derived from the global fits of this data with a three and four component fit. The value of χ^2 is marginally better for the four, as compared to the three, component fit. The residuals clearly show that there is some deviation of the three component fit from the experimental data on short timescales.

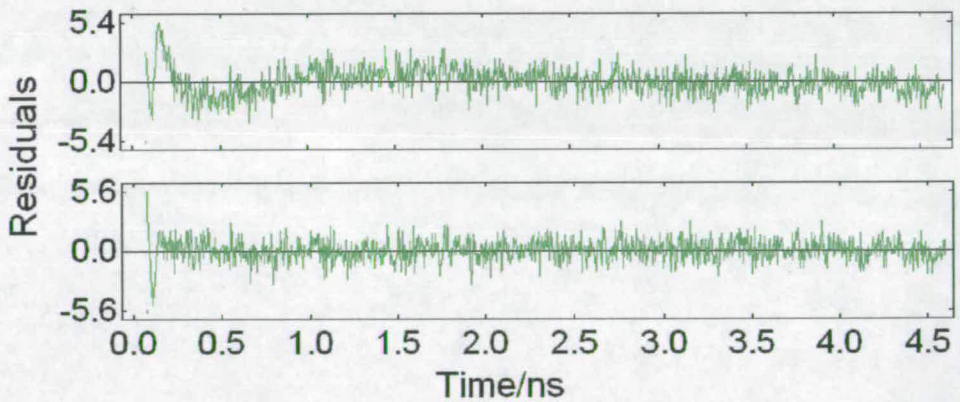

Figure 7.23- Residuals for the 3 component (top) and four component (bottom) fits of the data collected for the ^{m}wt-AP_{target} system. Residuals are from fits where the parameters derived from the global analysis have been fixed and fitted to a single decay curve. The decay curve used was for emission at 390nm on the 20ns timescale. χ^2 was 1.165 for the 3 component fit and 1.067 for the four component fit.

Figure 7.21 and Figure 7.22 show that the fluorescence response of the ternary ^{M}wt-AP$_{target}$ complex is remarkably similar to that of the binary complex. Hence, the enzyme binding of this duplex is not significantly improved by the addition of cofactor and the arguments that applied to the binary complex can also be applied here. This behaviour is in good agreement with studies by Holz *et al*[24], who also note strong DNA binding by HhaI, where 2AP is at the target site for base flipping.

The base flipping of 2AP by HhaI has a distinctive fluorescence signature. A decrease in the A-factor of the ~100ps lifetime of the AP$_{target}$ duplex is accompanied by an increase of a similar magnitude in the A-factor for the AP-aq species. An increase in the lifetimes of all of the 2AP species is also observed.

Approximately one quarter of the 2AP molecules in the ^{M}m-AP$_{target}$ complex have a short lifetime of ~100ps. It is pobbisle that this short lifetime could represent a highly quenched population of 2AP molecules within the enzyme active site. However, it would be consistent with observations made by Klimasauskas *et al*[115] to argue that this lifetime represents a distribution of 2AP molecules that are stacked within the DNA duplex. The study by Klimasauskas *et al*[115], made using ^{19}F-NMR, led to the proposal of the three-state (bound and stacked, bound and flipped, bound flipped and locked) mechanism for base flipping shown in Figure 7.24.

It is important to note that, in the ternary complex, Klimasauskas *et al* estimate that almost all of the target cytosine base will be flipped and locked within the HhaI active site. Binding equilibria appear somewhat different in the case of a 2AP target base, where strong binding of the DNA duplex by HhaI is noted in both the presence and absence of AdoHcy[24]. It seems reasonable to assume that, although the duplex is strongly bound by HhaI, the flipped 2AP can not be locked into the enzyme active site as the enzyme has evolved to bind cystosine, which is structurally dissimilar to 2AP. Hence, the dynamics of DNA binding and base flipping for the AP$_{target}$ duplex by HhaI are as described in Figure 7.24.

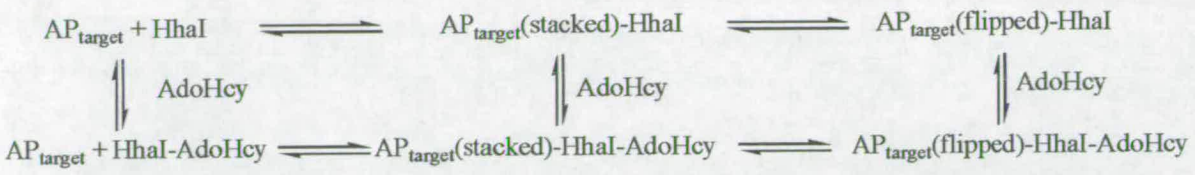

Figure 7.24- Scheme for binding of AP_{target} duplex by HhaI and AdoHcy.

Note that, although AdoHcy association with HhaI is shown as reversible in Figure 7.24, the dissociation constant for AdoHcy from the AdoHcy-HhaI complex is of the order of nanomoles[109]. Concentrations of cofactor of over 30 times in excess of enzyme concentration were used throughout these studies to ensure that the equilibrium lies well toward ternary, rather than binary, complex formation.

Some comparison can be made between the fluorescence responses of the crystalline and solution phase ^{M}wt-AP_{target} complexes, shown in Table 7.1 and Table 7.16, respectively. The large amplitude vibrations and motions of the enzyme and duplex, present in solution, are restricted in the crystal phase. Hence, this comparison potentially illustrates the striking effect of the dynamic behaviour of the DNA-enzyme complex on its fluorescence response and will be examined further, following the presentation of the results for the solution phase T250G mutant complexes, in the discussion that follows.

7.3.2.2.3 The TP_{out}/Wild-Type HhaI/AdoHcy Ternary Complex

The parameters derived from global fit of the fluorescence responses of the ^{H}wt-TP_{out} complex are described in Table 7.19.

Global Lifetimes: τ1=0.06ns, τ2=0.64ns, τ3=3.07ns, τ4=10.09ns

Emission Wavelength/ nm	A1	A2	A3	A4
370	0.59	0.15	0.12	0.13
390	0.60	0.15	0.12	0.13
410	0.60	0.18	0.12	0.10

Table 7.19- Parameters derived from the globally fitted decays of the ^{H}wt-TP_{out} complex.

Figure 7.21 and Figure 7.22 show that the A-factors and lifetimes of the ^{H}wt-TP$_{out}$ complex are remarkably similar to those that describe the fluorescence response of the binary wt-TP$_{out}$ complex.

In comparison to the fluorescence response of the free DNA duplex, ternary complex formation leads to an increase in the lifetimes of the two shortest-lived 2AP species. The magnitude of τ_1 increases by approximately 20ps, as was observed for the formation of the binary complex. This increase is relatively small but is certainly significant and suggests some change in the π-π stacking interactions of the 2AP. The increase in the magnitude of τ_2 is far more significant. The lifetime of this species increases by 200ps clearly on ternary complex formation, indicating a change in the environment of the 2AP brought about by the enzyme and cofactor binding. In a similar manner to the changes observed on enzyme binding these changes in lifetime reflect the conformational changes conferred on the DNA duplex by HhaI and AdoHcy binding. This effect is 'felt' by the 2AP at some distance from the HhaI recognition sequence as it forms a stable hydrogen bond to the thymine opposite it and, hence, the magnitudes of the lifetimes of the 2AP population are sensitive to the interstrand interactions in the duplex. These results imply that the interstrand interactions along an extended section of the DNA duplex are disrupted by the base flipping mechanism.

7.3.2.2.4 The AP$_{adj}$/Wild-Type HhaI/AdoHcy Ternary Complex

The parameters derived from global fits of the fluorescence response of the ^{H}wt-AP$_{adj}$ complex are recorded in Table 7.20.

Global Lifetimes: τ1=0.08ns, τ2=0.32ns, τ3=2.35ns, τ4=9.91ns

Emission Wavelength/ nm	A1	A2	A3	A4
370	0.83	0.12	0.03	0.02
390	0.79	0.15	0.04	0.02
410	0.74	0.18	0.06	0.02

Table 7.20- Parameters derived from the globally fitted decays of the ^{H}wt-AP$_{adj}$ complex.

The addition of AdoHcy to the HhaI-DNA complex greatly improves the binding of the AP_{adj} DNA duplex by HhaI[24] and binding is expected to be complete for this duplex, under our experimental conditions. As a result of this, the fluorescence response of the ^{H}wt-AP_{adj} complex is distinct from that for either the binary complex or the free AP_{adj} duplex. The magnitude of τ_1 in this complex is double that of τ_1 in the free AP_{adj} duplex. This increase illustrates the importance of the role played by π-π interactions in mediating the efficient de-excitation of 2AP. Crucially, however, this species is still present illustrating that 2AP need only experience a π-π interaction on one of its faces in order to achieve efficient quenching through electron transfer. τ_2 decreases significantly on ternary complex formation and minor changes in the magnitudes of τ_3 and τ_4 are observed. These changes in lifetime reflect the change in the environment of the 2AP probe molecule caused by base flipping and the resulting disruption of the π-stacking interactions 3' of the 2AP.

The A-factors of the 2AP in the ^{H}wt-AP_{adj} complex are essentially unchanged by base flipping, showing that the excision of the base 3' to 2AP does not significantly affect the conformational populations of the 2AP base within the duplex. The disruption of the π-stacking of 2AP on one side of the base only does not appear to increase the extrahelical nature of the 2AP population within this sample, illustrating the extraordinary specificity of HhaI for the target base of its recognition sequence.

7.3.2.2.5 The AP_{opp} Wild-Type HhaI/AdoHcy Ternary Complex

The parameters derived from global fits of the fluorescence response of the ^{H}wt-AP_{opp} complex are recorded in Table 7.21.

Global Lifetimes: τ1=0.06ns, τ2=0.44ns, τ3=2.68ns, τ4=9.37ns

Emission Wavelength/ nm	A1	A2	A3	A4
370	0.69	0.16	0.07	0.08
390	0.65	0.18	0.09	0.08
410	0.65	0.19	0.09	0.07

Table 7.21- Parameters derived from the globally fitted decays of the ^{H}wt-AP$_{opp}$ complex.

The fluorescence responses resulting from this system underline the precise nature of base flipping by HhaI and give some indication of just how good is the beautifully evolved mechanism for stabilising the DNA duplex. The fluorescence response of the AP$_{opp}$duplex does not change when the base opposite 2AP is flipped out of the DNA duplex. Hence, despite the supreme sensitivity of the 2AP fluorescence response to its immediate environment it is not noticeably affected when the cytosine base is whipped from its proximity and replaced with the HhaI glutamine 237 residue.

7.3.2.3 The DNA/T250G Mutant HhaI Binary Complex

Solution phase measurements were made on systems analogous to those discussed for the wild-type HhaI enzyme, but using the 'T250G' mutant of the enzyme, where the thymine at residue 250 of the amino acid chain is mutated to a glycine residue. The crystal structure obtained for the mutated enzyme, Figure 7.13, shows that flipped 2AP in this complex occupies a region of the enzyme that is not accessible to the flipped base in the wild-type enzyme. In the crystalline phase, this results in an increase in the A-factor of the longest-lived 2AP species and a general increase in the magnitudes of the lifetimes of 2AP relative to the wild-type enzyme complex. The solution phase results for the binary DNA-(T250G)HhaI complexes are summarised in Table 7.22.

DNA Duplex	A-Factor				Lifetimes/ ns			
	A1	A2	A3	A4	τ1	τ2	τ3	τ4
AP$_{target}$	0.19	0.17	0.19	0.46	0.14	1.01	5.26	12.58
GP$_{out}$	0.67	0.16	0.09	0.08	0.05	0.49	2.78	10.32
TP$_{out}$	0.47	0.19	0.17	0.18	0.08	0.70	3.61	10.62
AP$_{adj}$	0.80	0.11	0.06	0.03	0.05	0.44	2.61	9.94
AP$_{opp}$	0.66	0.15	0.10	0.09	0.05	0.51	2.98	9.78

Table 7.22- Parameters derived from global fits of the fluorescence decays for binary (T250G)HhaI-DNA complexes in buffered aqueous solution. A-factors shown are for emission at 390nm.

The changes in A-factors and lifetimes that result from the T250G mutant enzyme binding of the DNA duplexes, where the 2AP is not flipped from the duplex by protein binding, are summarised in Figure 7.25 and Figure 7.26, respectively.

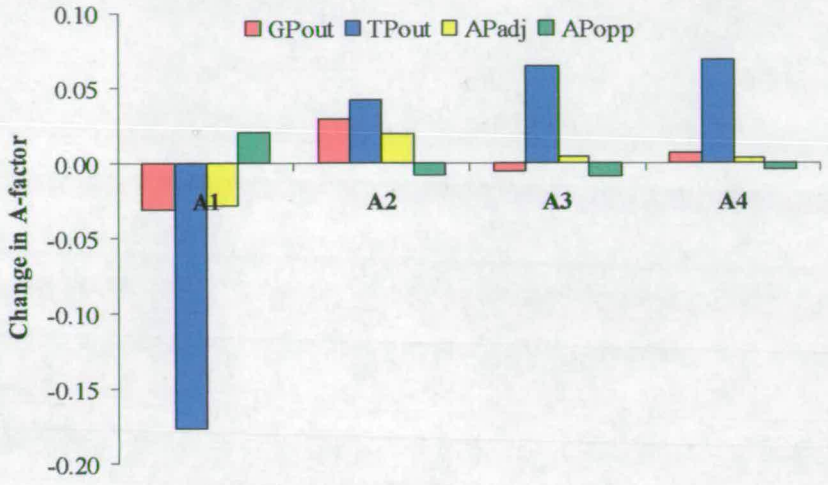

Figure 7.25- Bar chart showing the change in A-factors produced by (T250G)HhaI binding for each of the four DNA duplexes where the 2AP is not flipped from the duplex by protein binding.

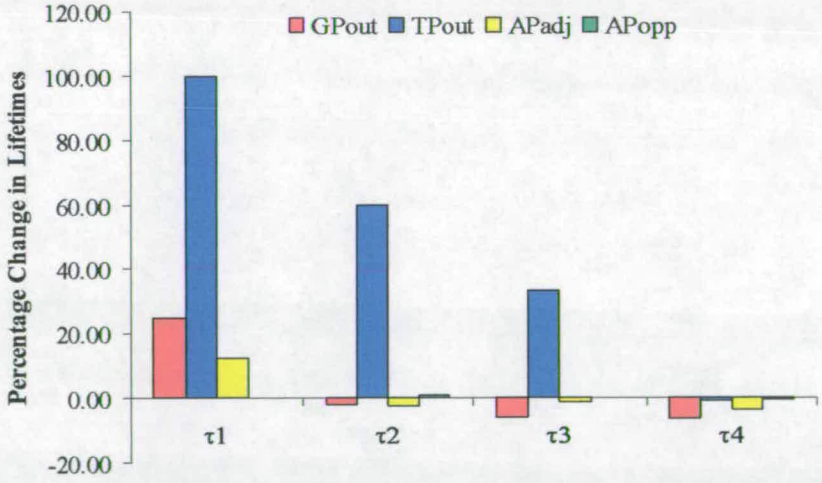

Figure 7.26- Bar chart showing the percentage change in lifetimes produced by (T250G)HhaI binding for each of the four DNA duplexes where the 2AP is not flipped from the duplex by protein binding.

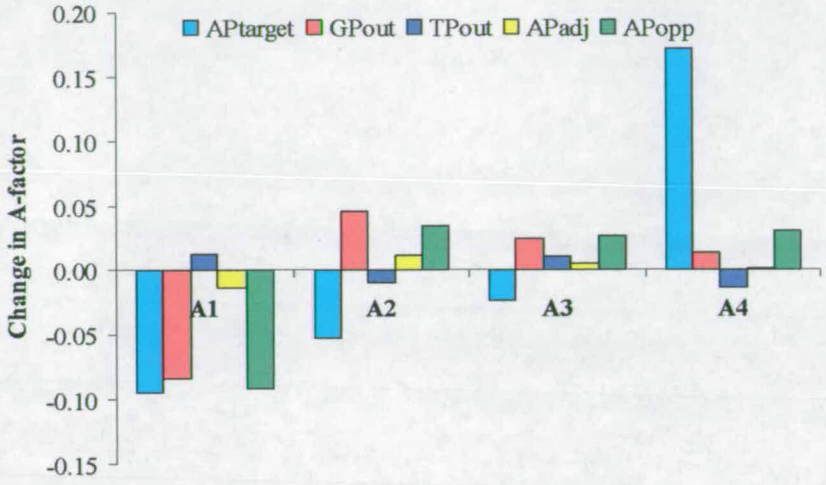

Figure 7.27- Bar chart showing the change in A-factor, for the binary enzyme-DNA complex, arising from the T250G mutation of the wild-type HhaI enzyme

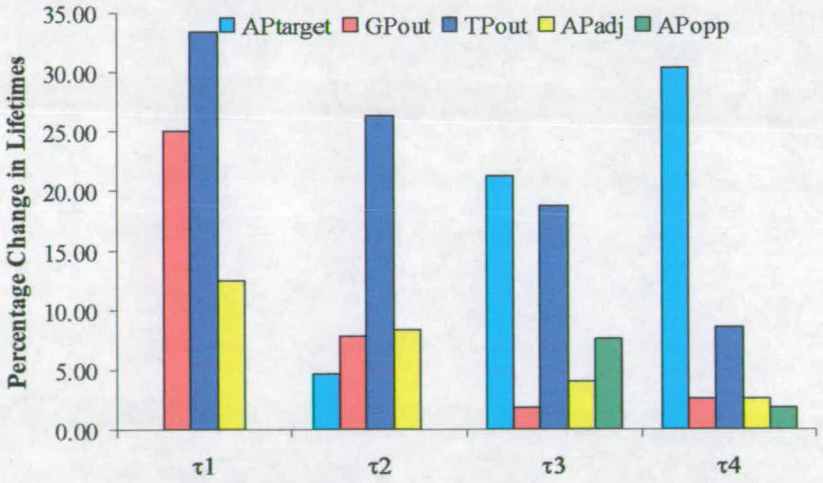

Figure 7.28- Bar chart showing the percentage change in lifetimes, for the binary enzyme-DNA complex, arising from the T250G mutation of the wild-type HhaI enzyme.

In general, this system behaves in a very similar fashion to the binary wt-HhaI-DNA complex, where significant changes in the lifetimes and amplitudes of only the AP_{target} and TP_{out} duplex fluorescence responses are observed. By comparing the fluorescence responses for the wild-type and T250G mutant complexes, some assessment can be made of how this very specific structural change is described by the fluorescence response of 2AP. Figure 7.27 and Figure 7.28 summarise the changes in lifetimes and A-factors of the 2AP brought about by the T250G mutation of wild-type HhaI.

7.3.2.3.1 The GP_{out}/T250G Mutant HhaI Binary Complex

The globally fitted parameters for the m-GP_{out} binary complex are shown in Table 7.23.

Global Lifetimes: τ1=0.05ns, τ2=0.49ns, τ3=2.78ns, τ4=10.32ns

Emission Wavelength/ nm	A1	A2	A3	A4
370	0.75	0.09	0.07	0.08
390	0.67	0.16	0.09	0.08
410	0.66	0.19	0.09	0.06

Table 7.23 Parameters derived from the globally fitted decays of the m-GP_{out} complex.

There is little change in the fluorescence response of this system on duplex binding by the T250G HhaI mutant. Figure 7.25 and Figure 7.26 illustrate this for the A-factors and lifetimes of the binary m-GP_{out} complex, respectively. The fitted parameters are also similar to those seen for the wild-type enzyme binding, as shown by Figure 7.27 and Figure 7.28. Given the magnitude of τ_1, it is not plausible to argue that the longer lifetime of the short-lived 2AP, in the mutant relative to the wild-type enzyme, noted in Figure 7.28, is real. This is certainly consistent with the relatively large separation between the 2AP in the GP_{out} duplex and the site of the T250G mutation.

7.3.2.3.2 The AP_{target}/T250G Mutant HhaI Binary Complex

The globally fitted data for each decay curve collected from the m-AP_{target} system are shown in Table 7.24.

Global Lifetimes: τ1=0.14ns, τ2=1.01ns, τ3=5.26ns, τ4=12.58ns

Emission Wavelength/ nm	A1	A2	A3	A4
370	0.19	0.14	0.22	0.45
390	0.19	0.17	0.19	0.46
410	0.26	0.20	0.16	0.39

Table 7.24- Parameters derived from the globally fitted decays of the m-AP_{target} complex.

Figure 7.29 illustrates the improvement in the fitted function when a four component, as opposed to a three component, fit is used. The three component fit clearly does not model the experimental well on short timescales.

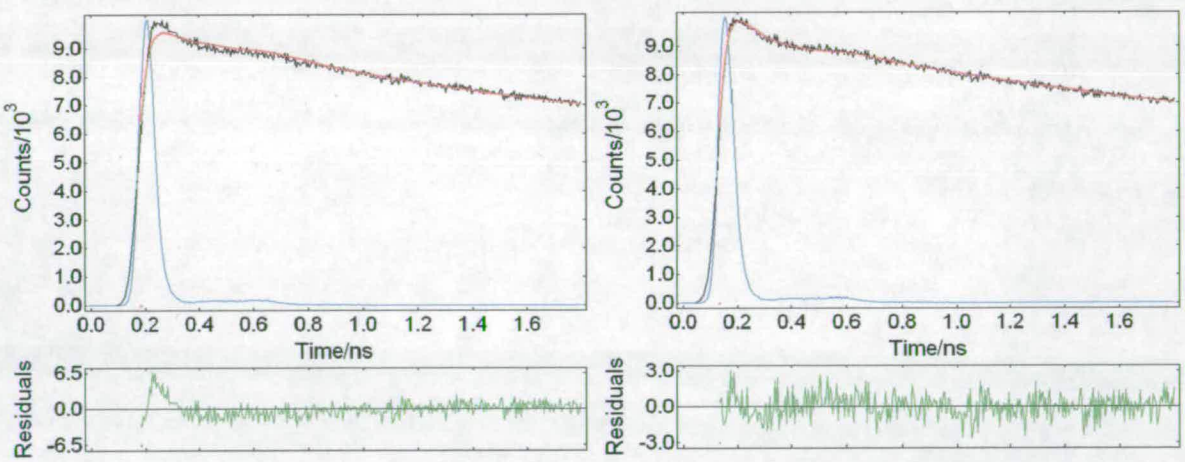

Figure 7.29- Comparison of the fluorescence decays of the m-AP_{target} system, fitted using a three (left) and four (right) component fit. The figure shows IRF (blue), experimental data (black), fitted function (red) and the residuals (green). Fits were made using the parameters derived from the global analysis, which have been fixed and fitted to a single

decay curve. The decay curve used was for emission at 370nm on the 20ns timescale. χ^2 was 1.174 for the 3 component fit and 1.033 for the four component fit.

Binding of the T250G mutant HhaI to the AP_{target} duplex results in a change in the fluorescence response of 2AP that is now a definitive signal for base flipping in this system. Figure 7.30 shows that a large decrease in the population of the short-lived 2AP, with a lifetime of ~100ps, is accompanied by an increase in the long-lived 2AP population of a similar magnitude. The fluorescence lifetimes of all of the 2AP species are seen to increase significantly upon enzyme binding.

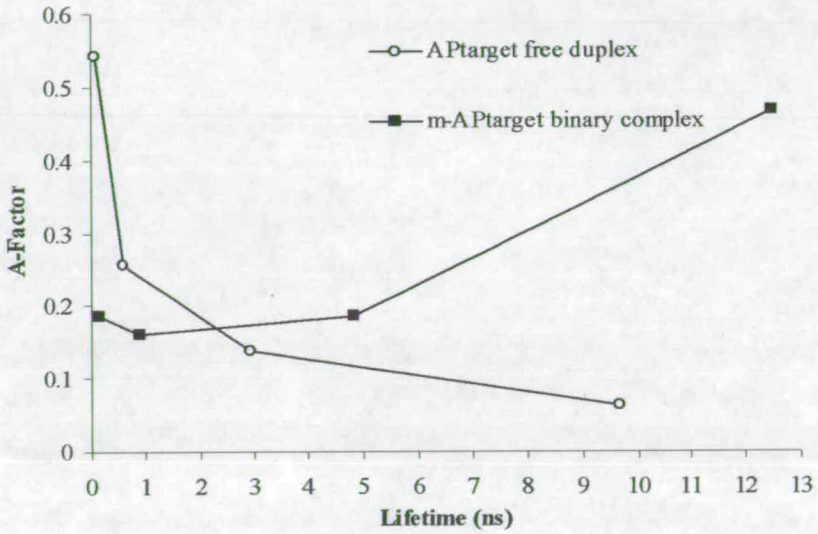

Figure 7.30- Plot showing A-factor (at an emission wavelength of 390nm) versus lifetime for the free AP_{target} duplex (circles) and the m-AP_{target} binary complex (squares) duplexes.

Figure 7.27 shows that, in the T250G complex there is a decrease in the A-factor of the short-lived 2AP species (A1) of approximately 0.1 and an increase of a similar magnitude in A4, relative to the wt-AP_{target} complex. This suggests that the proportion of extrahelical 2AP is greater in the m-AP_{target} complex, compared with the wt-AP_{target} complex. Under the experimental conditions used where all of the DNA is bound by enzyme this observation indicates that, in the equilibrium shown in Figure 7.24, a greater proportion of the DNA is 'bound and flipped' by the mutant enzyme than the wild-type enzyme.

Figure 7.28 shows that there is a significant increase in the magnitudes of τ_3 and τ_4 for 2AP in the m-AP_{target} complex as compared with the wt-AP_{target} complex. Neither τ_1 nor τ_2 are significantly altered by the T250G mutation of the bound HhaI. This is strong evidence that, for this duplex, both τ_3 and τ_4 represent 2AP molecules that are within the active site of HhaI, whose environment is grossly affected by the mutation of the T250 residue. Of course, this also implies that τ_1 and τ_2 represent populations of stacked 2AP molecules. This evidence for the existence of both intra- and extrahelical 2AP species in the DNA-enzyme complex is in excellent agreement with the previous study by Klimasauskas et al[115], which lead to the proposal of the scheme shown in Figure 7.24.

7.3.2.3.3 The TP_{out}/T250G Mutant HhaI Binary Complex

The fluorescence response of 2AP within the TP_{out} duplex is unmistakeably sensitive to duplex binding by HhaI. The globally fitted parameters for the m-TP_{out} binary complex are shown in Table 7.25.

Global Lifetimes: τ1=0.08ns, τ2=0.70ns, τ3=3.61ns, τ4=10.62ns

Emission Wavelength/ nm	A1	A2	A3	A4
370	0.48	0.16	0.17	0.19
390	0.47	0.19	0.17	0.18
410	0.46	0.24	0.16	0.14

Table 7.25- Parameters derived from the globally fitted decays of the m-TP_{out} complex.

In a similar fashion to the wt-TPout binary complex, the fluorescence response of the m-TPout complex suggests that the 2AP becomes somewhat more unstacked upon enzyme binding. This is shown in Figure 7.25 as a decrease in the magnitude of A1, with small but notable increases in the magnitudes of A3 and A4. Furthermore, Figure 7.26 shows that the magnitudes τ1, τ2 and τ3 are all considerably greater in the m-TPout complex than in the free DNA. Indeed, the increases in these lifetimes are far greater than those observed upon wild-type HhaI binding of the TPout duplex, as shown by Figure 7.28. Hence, mutation of the enzyme apparently leads to some

change in DNA binding or its bound conformation that is significant enough to be felt outside the HhaI recognition sequence. Despite this, crystallographic comparisons of the wild-type and T250G mutant ternary complexes show that, structurally, there is little difference between the two complexes[119]. The T250 residue contacts the DNA phosphate backbone at the phosphate group 5' of the flipped base. Removing the relatively bulky threonine residue and replacing it with a glycine residue creates a void in proximity to this region of the DNA backbone but water molecules, which facilitate hydrogen bonding between the enzyme and DNA backbone, fill this void. Although there is no doubt that the T250G mutation has little effect on the structure of the DNA duplex, it is hard to believe that this does not impact on its dynamics. The fluorescence results point to a duplex in which π-π stacking interaction are weakened by the binding of the mutant enzyme relative to the wild-type HhaI.

7.3.2.3.4 The AP_{adj} and AP_{opp}/T250G Mutant HhaI Binary Complexes

These duplexes show a striking lack of any change in their fluorescence response when they are bound by the T250G HhaI mutant. Table 7.26 describes the globally fitted data for the m-AP_{adj} complex, whereas Table 7.27 shows similarly fitted data for the m-AP_{opp} complex.

Global Lifetimes: τ1=0.05ns, τ2=0.44ns, τ3=2.61ns, τ4=9.94ns

Emission Wavelength/ nm	A1	A2	A3	A4
370	0.86	0.07	0.04	0.02
390	0.80	0.11	0.06	0.03
410	0.74	0.16	0.08	0.03

Table 7.26- Parameters derived from the globally fitted decays of the m-AP_{adj} complex.

Global Lifetimes: τ1=0.05ns, τ2=0.51ns, τ3=2.98ns, τ4=9.78ns				
Emission Wavelength/ nm	A1	A2	A3	A4
370	0.71	0.12	0.08	0.09
390	0.66	0.15	0.10	0.09
410	0.61	0.20	0.11	0.08

Table 7.27- Parameters derived from the globally fitted decays of the m-AP_{opp} complex.

There is so little change in the fluorescence responses of either of these duplexes upon addition of the T250G mutant enzyme to the system that it is difficult to believe that any significant binding of the DNA has taken place. It is perhaps the case with these duplexes that the combined effects of removing the threonine 250 residue and changing a base in the recognition sequence prevents the enzyme from achieving any specific binding of the DNA duplexes.

7.3.2.4 The DNA/T250G Mutant HhaI/Cofactor Ternary Complex

Improved binding of the DNA duplex by HhaI is afforded by the addition of either the AdoMet or AdoHcy cofactors to the binary systems; K_D for the binary complex is 3.6nm, whereas for the ternary complex, this figure is only 4.2pM. The fluorescence responses resulting from the ternary DNA-(T250G)HhaI-cofactor systems are summarised in Table 7.28.

DNA Duplex	A-Factor				Lifetimes/ ns			
	A1	A2	A3	A4	τ1	τ2	τ3	τ4
AP_{target}	0.16	0.14	0.20	0.50	0.17	1.14	6.01	12.63
GP_{out}	0.66	0.16	0.10	0.08	0.04	0.49	2.73	10.73
TP_{out}	0.46	0.20	0.16	0.19	0.07	0.63	3.35	10.47
AP_{adj}	0.81	0.12	0.04	0.02	0.09	0.40	2.48	10.01
AP_{opp}	0.60	0.20	0.10	0.10	0.07	0.47	2.91	9.60

Table 7.28- Parameters derived from global fits of the fluorescence decays for ternary DNA/(T250G)HhaI/cofactor complexes in buffered aqueous solution. Fits shown are for emission at 390nm.

The changes produced in the A-factors and lifetimes of the fluorescence responses of the binary complexes by cofactor binding are summarised in Figure 7.31 and Figure 7.32, respectively.

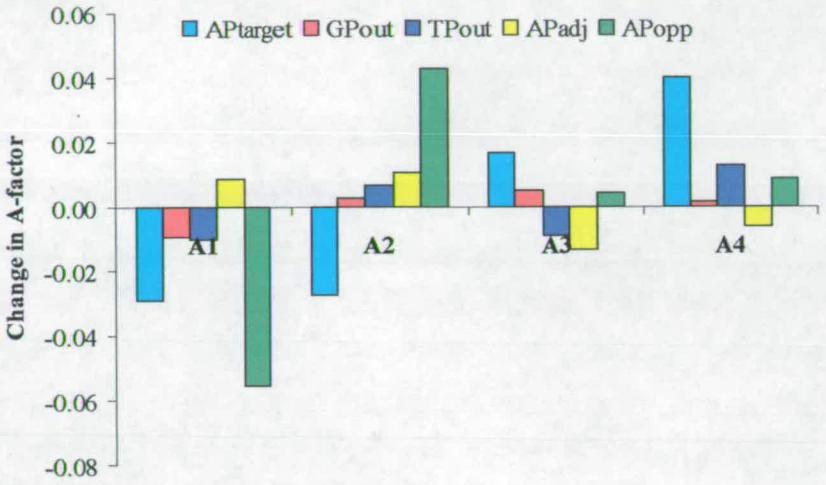

Figure 7.31- Bar chart showing the change in A-factors produced by cofactor binding for each of the five binary complexes tested.

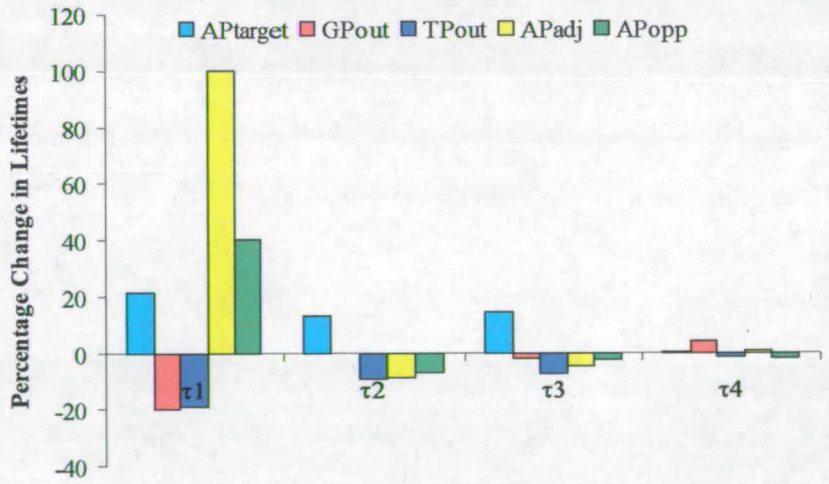

Figure 7.32- Bar chart showing the percentage change in lifetimes produced by cofactor binding for each of the five binary complexes tested.

7.3.2.4.1 The GP_{out}/T250G Mutant HhaI/AdoHcy Ternary Complex

Table 7.29 describes the parameters for the globally fitted fluorescence responses of the ^{H}m-GP_{out} complex.

Global Lifetimes: τ1=0.04ns, τ2=0.49ns, τ3=2.73ns, τ4=10.73ns

Emission Wavelength/ nm	A1	A2	A3	A4
370	0.75	0.10	0.07	0.08
390	0.66	0.16	0.10	0.08
410	0.61	0.21	0.12	0.06

Table 7.29- Parameters derived from global fits of ^{H}m-GP_{out} complex on the 50ns timescale.

Figure 7.31 and Figure 7.32 show that there is no discernable change in the A-factors of the fluorescence response of the binary m-GP_{out} complex on addition of cofactor. There is a decrease in the lifetime of the shortest lifetime component to the decay curve but it is not possible to reliably argue that a decrease in lifetime from 50ps to 40ps is real. None of the other lifetimes are affected by the cofactor addition.

The lack of any notable change in the fluorescence response of the GP_{out} duplex has been consistently observed for all the systems investigated. This is a clear indication that the fluorescence response of 2AP in this duplex is ignorant of the DNA duplex beyond its local environment. The changes imposed on DNA conformational dynamics by enzyme binding, for example, do not affect the fluorescence response of 2AP in the GP_{out} duplex.

7.3.2.4.2 The AP_{target}/T250G Mutant HhaI/AdoMet Ternary Complex

The signature of base flipping is clearly evident in the fluorescence response of 2AP in the ^{M}m-AP_{target} ternary complex. The parameters fitted to the fluorescence decays of this system are shown in Table 7.30.

Global Lifetimes: τ1=0.17ns, τ2=1.14ns, τ3=6.01ns, τ4=12.63ns

Emission Wavelength/ nm	A1	A2	A3	A4
370	0.16	0.12	0.25	0.47
390	0.16	0.14	0.20	0.50
410	0.24	0.17	0.16	0.43

Table 7.30- Parameters derived from the globally fitted decays of the ^{M}m-AP$_{target}$ complex.

Figure 7.33 shows the residuals derived from the global fits of this data with a three and four component fit. The value of χ^2 is improved for the four (χ^2=1.011), as compared to the three (χ^2=1.308), component fit. The residuals clearly show that the fit is significantly improved upon the addition of a fourth term.

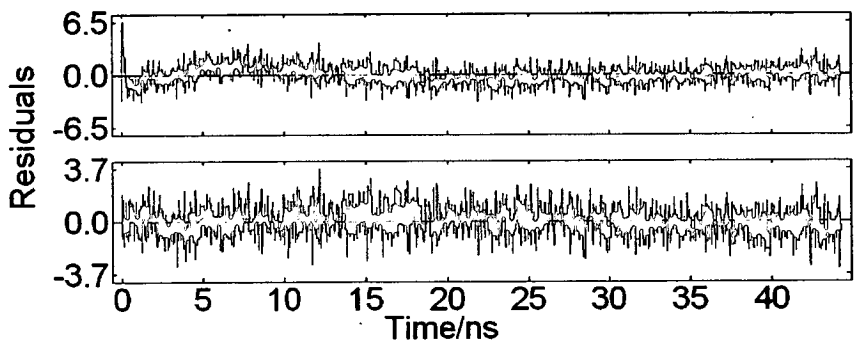

Figure 7.33- Residuals for the 3 component (top) and four component (bottom) fits of the data collected for the ^{M}m-AP$_{target}$ system. Residuals are from fits where the parameters derived from the global analysis have been fixed and fitted to a single decay curve. The decay curve used was for emission at 370nm on the 50ns timescale. χ^2 was 1.308 for the 3 component fit and 1.011 for the four component fit.

Figure 7.31 shows that the all of the A-factors fitted to the m-AP$_{target}$ fluorescence response change by less than 0.04 upon addition of the AdoMet cofactor. These changes are between 8 and 17% of the value of the A-factors presented for the binary complex, and so are quite significant relative to the expected standard deviation for these experiments (<5% relative standard deviation). The addition of the cofactor decreases the dissociation constant of the

complex by three orders of magnitude[116] and so the binding between the DNA and enzyme is clearly changed by the addition of the cofactor. The decrease in the proportion of the two shortest-lived 2AP species with cofactor addition is consistent with the observations made for the binary m-AP_{target} complex, that these two components of the decay represent populations of 2AP that are intrahelical and distinct from the two long lifetime (extrahelical) components.

Figure 7.32 shows that the addition of cofactor to the binary complex results in an increase in the lifetimes of the three shortest-lived emitting species. Interestingly, the lifetime of the long-lived 2AP species is unaffected by the addition of the cofactor. This is good evidence that this population of 2AP species does not reside in the 'normal' active site of the HhaI enzyme. As indicated by the crystal structure, shown in Figure 7.13, the 2AP flipped into the T250G mutant active site is quite remote from the cofactor binding site.

There is a significant increase in the magnitude of all four of the 2AP lifetimes on AP_{target} binding by the HhaI-AdoMet complex. This is in line with the observations made for base flipping by the ^{M}wt-AP_{target} complex, though in the mutant enzyme the increase in all lifetimes is greater. The magnitudes of τ_2, τ_3 and τ_4 compare favourably with the three lifetimes used to fit the fluorescence response of the crystalline ^{M}m-AP_{target} complex (Table 7.1). The similarity of the fluorescence responses from the solution and crystal phase measurements goes some way towards validating the structure determined from the crystal as being truly representative of the solution-phase complex conformation.

The fluorescence response of the crystalline ^{M}m-AP_{target} complex shows no evidence of a short component from π-stacked 2AP. In contrast, approximately 15% of the 2AP population have a lifetime of 170ps in the analogous solution phase complex. The presence of this decay component in the solution phase complex is indicative of the dynamic nature of base flipping by HhaI in the solution phase. The relatively long lifetime of the stacked 2AP in this complex, compared to that for the free DNA duplex, indicates that the stacking is disrupted, relative to the free duplex. Such long lifetimes for this component have been noted for the other solution phase, enzyme bound AP_{target} duplexes and for the crystalline ^{H}wt-AP_{adj} and ^{H}wt-AP_{opp} complexes, where the stacking interactions of the "AP have been significantly disrupted.

2AP that has a lifetime of approximately 1ns is common to AP_{target} DNA in complexes with both the wild-type and mutant HhaI (Sections 7.3.2.3 and 7.3.2.5). Since 2AP with a lifetime similar to this is not observed in any other system, this must be a result of some specific interaction between the AP_{target} duplex and HhaI.

The two species with the longest lifetime in this system are 2AP molecules that are not only extrahelical but are also within the HhaI active site. This must be the case since the lifetimes of both of these species are significantly greater in the ^{M}m-AP_{target} complex than in the ^{M}wt-AP_{target} complex. Indeed, these lifetimes are the only ones in the entire data set that are significantly affected by the T250G mutation. The increase in these lifetimes is brought about by the more polar and less solvent accessible cavity that 2AP experiences in the T250G mutant HhaI, relative to the wild-type HhaI active site. The crystal structure shows that interactions between HhaI and the amine group and N7 of 2AP could play a role in defining these lifetimes.

7.3.2.4.3 The TP_{out}/T250G Mutant HhaI/AdoHcy Ternary Complex

The remarkable sensitivity of the 2AP within the TP_{out} duplex to enzyme binding is in stark contrast to the behaviour of the GP_{out} duplex. Table 7.31 shows the parameters derived from the global fitting of the decay curves collected for this ternary complex.

Global Lifetimes: τ1=0.07ns, τ2=0.63ns, τ3=3.35ns, τ4=10.47ns

Emission Wavelength/ nm	A1	A2	A3	A4
370	0.51	0.15	0.15	0.19
390	0.46	0.20	0.16	0.19
410	0.46	0.25	0.15	0.14

Table 7.31- Parameters derived from the globally fitted decays of the ^{H}m-TP_{out} complex.

Figure 7.31 and Figure 7.32 show that formation of the ternary complex results in no significant changes in the fluorescence responses as compared to the binary complex. Hence, tighter binding (in the sense that the dissociation constant has decreased by three orders of magnitude) of the DNA duplex by the HhaI-AdoHcy complex does not significantly affect the environment

of the 2AP in the TP_{out} duplex. Largely, this is consistent with the measurements made using the wild-type HhaI, where cofactor addition was shown to have no effect on the lifetimes of the 2AP.

The contrasting behaviour of the TP_{out} and GP_{out} duplexes is initially somewhat surprising given the identical nature of the positions and sequence contexts (at least in a single strand) of these duplexes. In physical terms, the important difference between these two duplexes is how the 2AP interacts with its local environment. In the TP_{out} duplex, the dominant intermolecular interaction for the 2AP is the stable Watson-Crick hydrogen bond that it forms with thymine. This makes the fluorescence response of the 2AP in the TP_{out} duplex sensitive to changes in the interstrand dynamics of the duplex. In the GP_{out} duplex, this Watson-Crick interaction does not exist. The dominant intermolecular interactions felt by the 2AP here are the π-π interactions with adjacent bases. Hence, the fluorescence response of the 2AP in the GP_{out} duplex is more sensitive to changes in the intrastrand, π-π stacking interactions. Thus, the fluorescence response of 2AP within these two similar duplexes relates information on very different interactions within the DNA helix.

7.3.2.4.4 The AP_{adj}/T250G Mutant HhaI/AdoHcy Ternary Complex

The AP_{adj} duplex illustrates the effect of disruption of the π-π interactions within the DNA duplex on the fluorescence response of 2AP. The parameters derived from fitting the decay curves of this system are shown in Table 7.32.

Global Lifetimes: τ1=0.09ns, τ2=0.40ns, τ3=2.48ns, τ4=10.01ns

Emission Wavelength/ nm	A1	A2	A3	A4
370	0.86	0.09	0.03	0.02
390	0.81	0.12	0.04	0.02
410	0.75	0.16	0.07	0.02

Table 7.32- Parameters derived from the globally fitted decays of the ^{H}m-AP_{adj} complex.

In general, the A-factors of the free AP_{adj} duplex are not perceptibly affected by the ternary complex formation. Indeed, the only parameter fitted that appears to be sensitive to the enzyme and cofactor binding and subsequent base flipping is $\tau 1$. The lifetime of this species increases from 40 to 90ps when the cytosine adjacent to the 2AP is flipped from the DNA duplex and replaced by glutamine 237. The fact that this parameter is the only one significantly affected by base flipping is further confirmation that $\tau 1$ represents an intrahelical, stacked 2AP population.

7.3.2.4.5 The AP_{opp}/T250G Mutant HhaI/AdoHcy Ternary Complex

There is little notable change in the fluorescence response of the AP_{opp} duplex as it is bound by the (T250G)HhaI-AdoHcy complex. The results of global fits for the $^{H}m\text{-}AP_{opp}$ complex are shown in Table 7.33.

Global Lifetimes: $\tau 1$=0.07ns, $\tau 2$=0.47ns, $\tau 3$=2.91ns, $\tau 4$=9.60ns

Emission Wavelength/ nm	A1	A2	A3	A4
370	0.67	0.16	0.08	0.10
390	0.60	0.20	0.10	0.10
410	0.57	0.23	0.12	0.09

Table 7.33- Parameters derived from the globally fitted decays of the $^{H}m\text{-}AP_{opp}$ complex.

Figure 7.31 and Figure 7.32 show that the parameters derived from the fluorescence response of 2AP are relatively unperturbed by the binding of the T250G mutant HhaI and AdoHcy cofactor to the AP_{opp} duplex. The magnitude of $\tau 1$ increases from 50 to 70ps perhaps indicating some slight disruption of the π-π stacking in the strand opposite 2AP.

The stabilisation of the DNA duplex by HhaI during base flipping is critical in order for the enzyme to successfully methylate the DNA molecule, without causing irreversible damage to it. Consider the situation where the base opposite the target for flipping is free to move and capable of adopting some extrahelical conformation whilst the base opposite it is flipped out of the duplex. If both bases are simultaneously in extrahelical conformations, then the DNA duplex is

liable to collapse, trapping both of these bases in a 'flipped' conformation. In order to avoid this disastrous collapse of the DNA, HhaI has evolved to stabilise the duplex during flipping, using predominantly the Glu 237 and Ser87 residues. The lack of any significant change in the fluorescence response of the free AP_{opp} duplex upon ternary complex formation confirms that it performs this task with amazing aptitude. The structural similarity of 2AP to guanine, which is naturally the base opposite the flipping site, means that the fluorescence response of the AP_{opp} duplex is a good measure of the ability of HhaI to mimic the flipped cytosine base.

7.4 Conclusions

A definitive fluorescence signature for base flipping has been identified from the combined crystal and solution phase results. With 2AP at the target site for base flipping, it has been shown that enzyme binding and the subsequent base flipping of 2AP leads to a significant decrease in the A-factor for the stacked 2AP species (τ~100ps) with a corresponding increase in the A-factor of the unquenched 2AP (τ~10ns).

2AP has been shown to be a sensitive probe of its immediate environment and, through correlation of the crystal structures and fluorescence data, it has been possible to characterise some of the features of the fluorescence response for 2AP. The magnitude of the lifetime of stacked 2AP has been shown to increase as a result of weakening the π-stacking interactions felt by the probe. For the long-lived 2AP, the formation of an electron withdrawing interaction at N7 has been shown to lead to a significant increase its lifetime. It remains unclear as to whether or not the intermediate lifetime species represent mainly intra- or extrahelical 2AP molecules. These two lifetimes vary considerably in the various systems examined and are likely to simply represent a distribution of 2AP molecules which are not favourably oriented for quenching via electron transfer nor are flipped completely out of the DNA helix. A distribution of 2AP molecules with similarly intermediate lifetimes are also present in the enzyme active site.

The conformations adopted by the flipped 2AP in the wild-type and T250G mutant HhaI are quite different. The crystal structure for the mutant enzyme shows that 2AP occupies a highly

polar environment, which leads to a significant increase in the fluorescence lifetimes of the flipped 2AP population compared to the flipped 2AP in wild-type HhaI.

The base flipping mechanism in the solution phase has been shown to be dynamic; both the short- and long-lived 2AP species are present in the solution phase ^{M}wt-AP$_{target}$ complex, despite carefully selected experimental conditions to ensure complete binding of the DNA by HhaI. Longer lifetimes for the unquenched 2AP in T250G mutant as compared to the wild-type show that, as in the crystal phase, the 2AP in the solution phase complex occupies distinctly different regions of the enzyme active site. This change in conformation leads to changes in only the τ_3 and τ_4 parameters, suggesting that only these two lifetimes are due entirely to 2AP molecules within the enzyme active site.

When 2AP is placed adjacent to or opposite the target site for base flipping its fluorescence response has been shown to vary little between the free DNA and enzyme bound duplexes. Some changes in the magnitude of the stacked 2AP lifetime indicate changes in the stacking interactions within the duplex upon enzyme binding. However, the lack of any substantial change in the other fitted parameters shows that HhaI is superbly evolved to stabilise the DNA duplex during base flipping.

Some indication of the sensitivity of 2AP to its environment has been noted for the experiments where 2AP has been placed beyond the recognition sequence of HhaI. In the case where 2AP is paired with guanine, the π-stacking interactions about 2AP determine its behaviour and enzyme binding is shown not to disrupt these interactions. However, for the 2AP-to-thymine Watson-Crick-type base pair, the interstrand interactions have been shown to influence the dynamic behaviour of 2AP. This interaction, and hence the fluorescence response of 2AP is perturbed upon enzyme binding. Thus base flipping appears to change the interstrand interactions several base pairs along the duplex from its recognition sequence.

Chapter 8

2-Aminopurine as a probe of DNA-Protein Interactions; the TaqI methyltransferase enzyme

8.1 Introduction

This Chapter is intended as a brief epilogue to the extensive work that has been carried out on the M.HhaI system. It details the results of recent studies on base flipping by the M.TaqI enzyme using two different 2AP labelled DNA duplexes.

The M.TaqI enzyme is part of the R-M system of *Thermus aquaticus* and is an N6-adenine DNA methyltransferase. TaqI methylates the exocyclic amine group of adenine at the 3' of end its four-base recognition sequence, 5'-TCGA-3'[125]. The crystal structure of TaqI in a ternary complex with a 10-base DNA duplex and a nonreactive cofactor, (5'-[2-(amino)ethylthio]-5'-deoxyadenosine (AETA) (an analogue of AdoMet), was published by Goedecke *et al*[71]. The structure shows that TaqI uses a similar base flipping mechanism to HhaI in order to orient the adenine base such that it is in close proximity to the AETA cofactor. Figure 8.1 shows the structure of the ternary complex.

Figure 8.1 shows that the DNA duplex is bound within a cleft of the C-shaped TaqI enzyme and is extensively distorted by the enzyme. The base flipping mechanism extricates the target adenine from the helix and, to some extent, its neighbouring, 3' cytosine. Furthermore, the 'orphan base', i.e. the thymine opposite the flipped adenine, shifts across the helix, occupying a position part way into the vacancy opposite it that results from base flipping. Thus, in the upper part of Figure 8.1, the DNA duplex appears to be somewhat squashed on the side opposite the flipped adenine base.

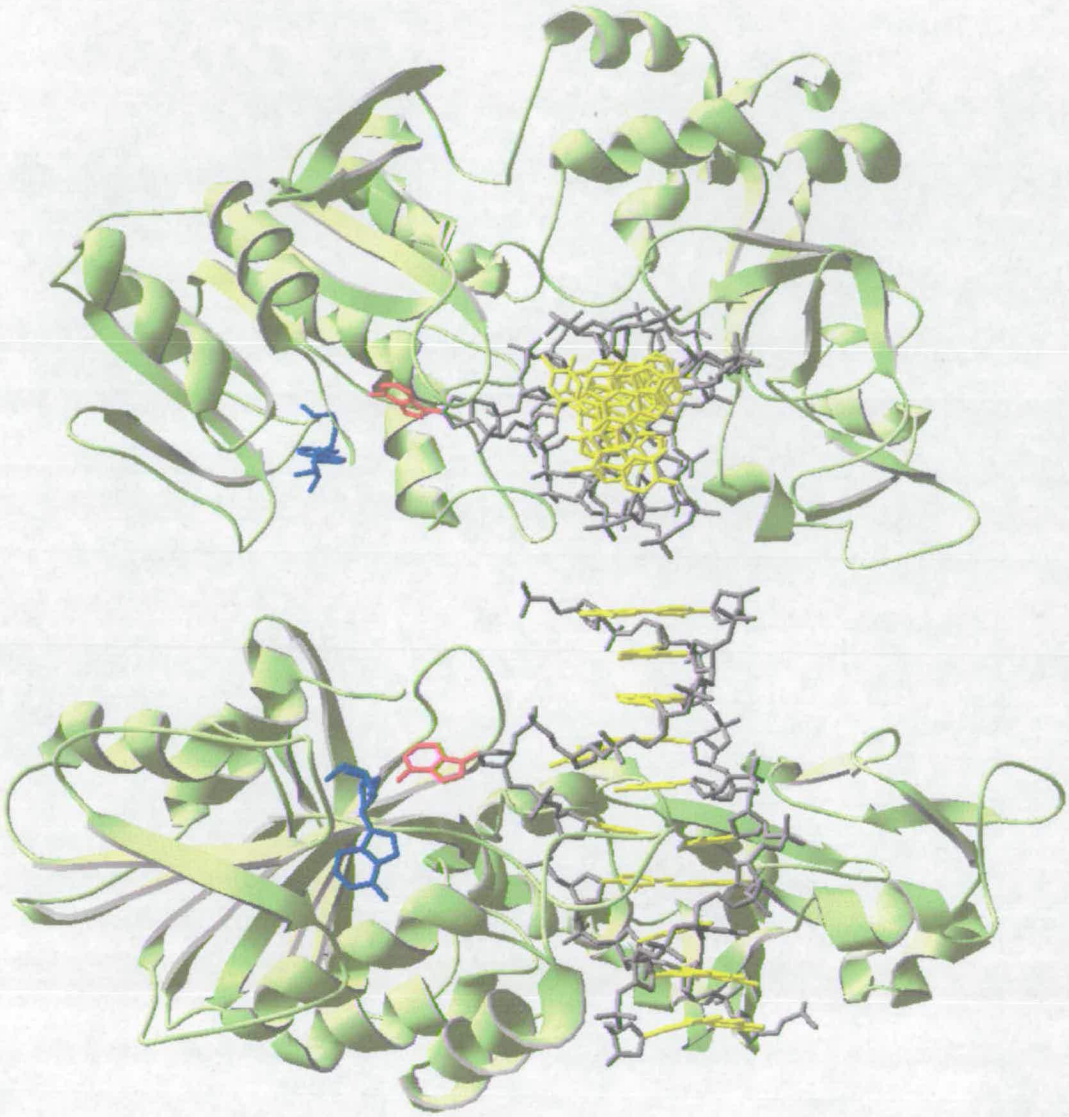

Figure 8.1- Images from the crystal structure of the ternary DNA-TaqI-AETA complex published by Goedecke *et al*[71]. TaqI is shown in green, ribbon form with the AETA cofactor in blue. The DNA backbone is grey with the bases in yellow. The flipped adenine base is shown in red. Upper and lower images show view along and perpendicular to the helical axis of the DNA respectively.

The positioning of the orphan thymine base plays a crucial role in the stabilisation of the DNA duplex during base flipping. Figure 8.2 shows the conformation adopted by the DNA duplex during base flipping by TaqI.

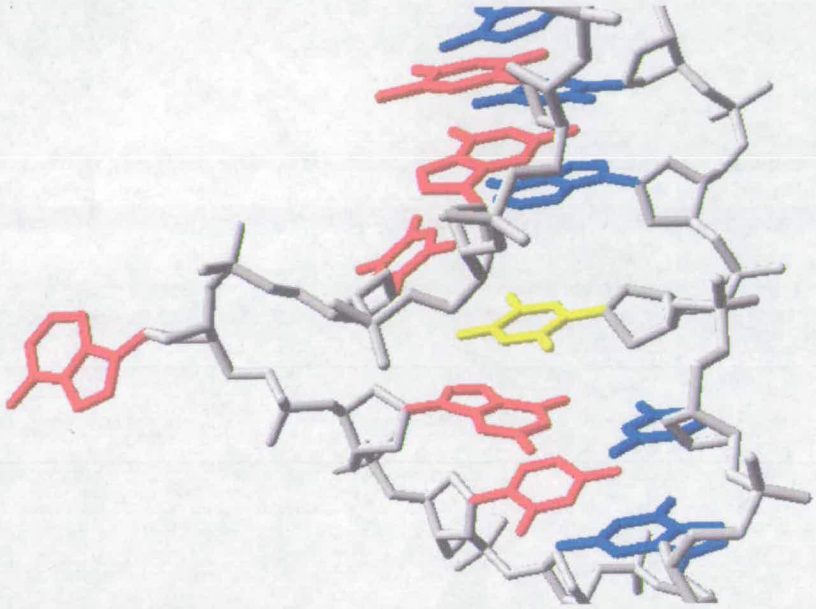

Figure 8.2- The distorted DNA duplex resulting from base flipping by TaqI. DNA bases are shown in red and blue for each strand of the duplex. The backbone is grey with the orphan thymine base shown in yellow.

During base flipping the orphan thymine base moves across the helix and forms an interstrand π-π stacking interaction with the guanine base 5' of the flipped adenine. This motion plays a role analogous to the insertion of Gln 237 by HhaI, in ensuring the DNA duplex does not collapse during base flipping.

In the native DNA recognition sequence for TaqI, the flipped adenine base is stabilised within the active site of the protein by several intermolecular interactions. Figure 8.3 shows the structure of the enzyme in the immediate vicinity of the flipped adenine base.

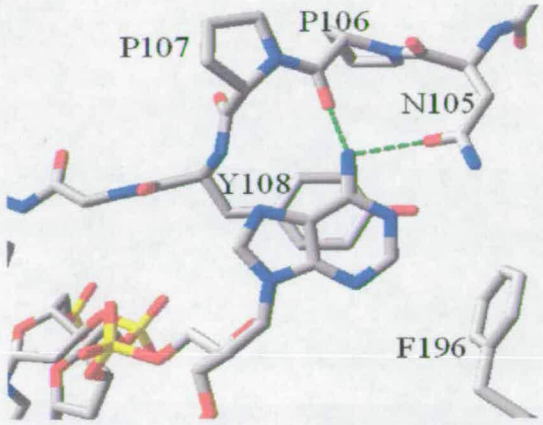

Figure 8.3- Adenine flipped out of the DNA duplex and into the active site of TaqI. The DNA backbone is shown at the bottom left of the image. Hydrogen bonding interactions between adenine and TaqI are shown in green.

The flipped adenine base forms hydrogen bonds through its excocyclic amine group to the carbonyl group of proline 106 and that of asparagine 105. A π-π interaction with tryptophan 108 further stabilises the flipped adenine, with the tryptophan lying, at the point of closest contact, 3.3Å below the adenine base.

In the following work, the fluorescence responses for two DNA duplexes were recorded. The DNA sequence used is shown in Figure 8.4.

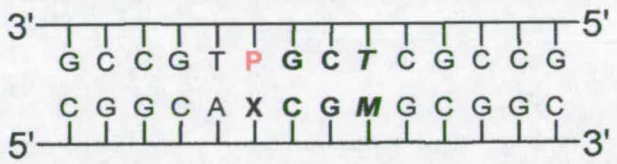

Figure 8.4- The DNA duplex used for studies with the TaqI enzyme. The recognition sequence for TaqI is emboldened. 2AP is denoted by P and is at the target site for base flipping. X represents either T (for the 'AP-T' duplex) or an abasic site (the 'AP-D' duplex)

These duplexes were chosen so that time-resolved fluorescence could be used to investigate the mechanism of base excision by M.TaqI. By using a duplex with an abasic site opposite the 2AP,

which is simply the deoxyribose sugar with no base attached to N1', a potentially important feature of the mechanism for base flipping is removed from the duplex. Figure 8.2 shows that the thymine opposite the flipped adenine is shifted across the duplex during flipping. The question that this experiment was designed to investigate was whether or not this reorientation of the thymine is a cause or consequence of base flipping. In other words, does M.TaqI use the thymine to push the adenine from the duplex, or is it moved after flipping to stabilise the DNA duplex?

8.2 Experimental

Solutions of approximately 100μL were examined in a quartz cuvette with a 1cm path length. The solutions contained 1μM DNA in buffer composed of 20 mM Tris/AcOH, 10 mM Mg(AcO)2, 50 mM KAcO, 1 mM DTT and 0.01% Triton X-100. M.TaqI was added to give a final enzyme concentration of 4μM. The effect of a cofactor on enzyme binding was not investigated. The dissociation constant for the 2AP labelled DNA-M.TaqI complex is 120nM[24].

8.3 Results and Discussion

8.3.1 Free DNA duplexes

Global Lifetimes: τ1=0.03ns, τ2=0.57ns, τ3=2.38ns, τ4=7.82ns
Global χ^2=1.082

Emission Wavelength/ nm	A1	A2	A3	A4	Local χ^2
370	0.90	0.03	0.06	0.02	1.141
390	0.81	0.06	0.09	0.04	1.038
410	0.89	0.05	0.03	0.03	1.07

Table 8.1-Parameters derived from the global fitting of the decays from the free AP-T duplex

Table 8.1 and Table 8.2 describe the globally fitted parameters for the fluorescence decays of the AP-T and AP-D duplexes respectively.

Global Lifetimes: τ1=0.03ns, τ2=0.29ns, τ3=4.70ns, τ4=9.35ns
Global χ^2=1.048

Emission Wavelength/ nm	A1	A2	A3	A4	Local χ^2
370	0.74	0.02	0.07	0.17	1.044
390	0.59	0.06	0.11	0.24	1.031
410	0.47	0.13	0.13	0.27	1.07

Table 8.2- Parameters derived from the global fitting of the decays from the free AP-D duplex

Both the decay curves show similar fluorescence responses to those previously observed for free DNA duplexes in this study and both are dominated by the highly quenched fluorescence emission (τ1=30ps) that is the result of a π-π interaction between 2AP and the bases adjacent to it.

For the AP-T duplex, Table 8.1 shows that the π-stacked 2AP accounts for at least 80% of the population of 2AP molecules in the sample. The other components to this decay are in good agreement with those previously measured for DNA duplexes where 2AP is base-paired to thymine, though the lifetime of τ4 is the shortest seen for such a sample.

The emission from the AP-D duplex is also predominantly from 2AP that forms a π-stacked complex with its neighbouring molecules. Table 8.2 shows, however, that the A-factor for π-stacked 2AP decreases dramatically with increasing emission wavelength, over the range of wavelengths examined. Hence, the excitation and emission spectra of π-stacked 2AP in the AP-D duplex peak at significantly shorter wavelengths than those spectra for similar 2AP in the AP-T duplex. The magnitude of τ3 in the AP-D duplex is significantly greater than that of any of the other DNA duplexes in this study. Hence, it appears that the absence of a base opposite the 2AP leads to a significant increase in the magnitude of τ3. Work in the previous Chapter shows that this is an environment where hydrogen bonding interactions are predominant and that the lifetime of 2AP is determined by these interactions and the polarity of its immediate environment.

The long-lived 2AP species in the AP-D duplex accounts for around a quarter of the population of 2AP molecules. As a result of the abasic site opposite 2AP, it is clearly relatively free to move within the duplex. The absence of a base pair reduces the energetic barrier to the 2AP adopting an extrahelical conformation. Hence, in this duplex, the long-lived 2AP species clearly accounts for a higher proportion of the 2AP population than that observed for any of the other DNA duplexes in this study.

8.3.2 DNA-TaqI Binary Complexes

Table 8.3 and Table 8.4 describe the parameters fitted to the fluorescence responses of the AP-T and AP-D duplexes bound by TaqI.

Global Lifetimes: τ1=0.41ns, τ2=1.89ns, τ3=7.33ns, τ4=13.51ns
Global χ^2=1.086

Emission Wavelength/ nm	A1	A2	A3	A4	Local χ^2
370	0.23	0.58	0.19	0.00	1.111
390	0.21	0.66	0.13	0.00	1.05
410	0.20	0.57	0.20	0.03	1.032

Table 8.3- Parameters derived from the global fitting of the decays from the M.TaqI bound AP-T duplex

Global Lifetimes: τ2=0.35ns, τ3=4.40ns, τ4=10.36ns
Global χ^2=1.015

Emission Wavelength/ nm	A1	A2	A3	A4	Local χ^2
370	-	0.14	0.14	0.73	1.024
390	-	0.09	0.11	0.79	0.998
410	-	0.10	0.10	0.80	1.021

Table 8.4- Parameters derived from the global fitting of the decays from the M.TaqI bound AP-D duplex

Figure 8.5 shows examples of the fits for the AP-T and AP-D duplexes, complexed by M.TaqI. In the case of the AP-T/M.TaqI complex, the fit to three components is clearly poor and the use of four components in the results presented in Table 8.3 is justified. For the AP-D/M.TaqI duplex the use of a three component fit cannot be justified on the basis of the χ^2(global) value alone, as this is less than 1.1 for the two component fit. Notably, however, there is a deviation in the fit around the peak of the decay curve for the two component model shown in Figure 8.5. This deviation is well fitted when an extra component is added to the modelled decay curve. Since this component has a short lifetime (350ps), its presence or absence in the fit has little bearing on the value of χ^2 on the 50ns timescale and so this is not regarded as a good indicator of the quality of the fit in this instance.

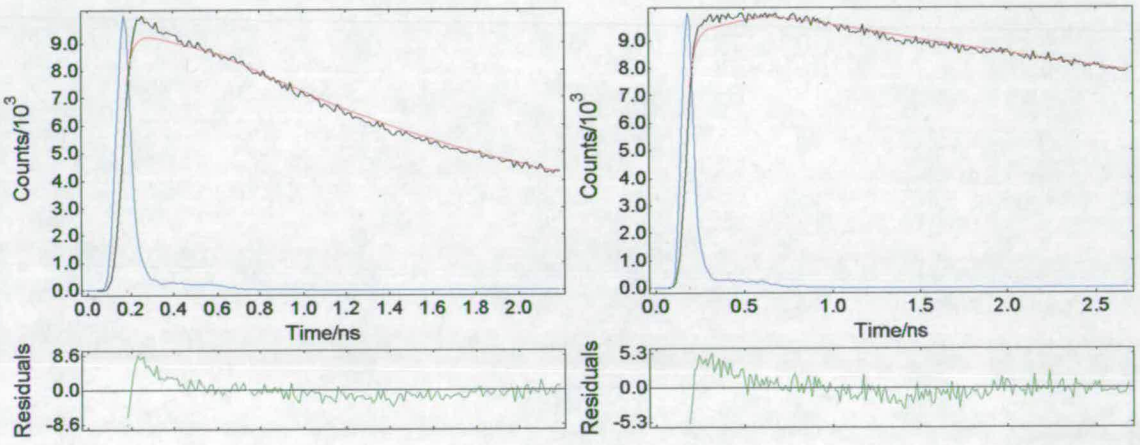

Figure 8.5- Peaks of decay curves for fits made using one less component than those presented in Table 8.3 and Table 8.4. Figures show IRF (blue), recorded decay (for emission at 370nm) (black), fitted decay (red) and residuals (green). Left: Example of the fit from the global analysis of the AP-T/ M.TaqI complex with 3 components giving χ^2(global)= 1.226. Right: Example of the fit from the global analysis of the AP-D/ M.taqI complex with two components giving χ^2(global)= 1.072.

Table 8.3 shows that the fluorescence response of the TaqI bound AP-T duplex is described by four components. The predominant component has a lifetime, τ_2, of 1.89ns, and represents around 60% of the 2AP population. There is an extremely small proportion of 2AP with a

lifetime of 13.5ns in this system. Although the amount of emission from this species is negligible at wavelengths of 370nm and 390nm, this component is required for a satisfactory global fit of the data.

Perhaps the most significant result from this system is the complete lack of a lifetime that suggests the presence of 2AP that is π-stacked in the DNA duplex. This is entirely consistent with the proposed base flipping of 2AP by TaqI and the previous results from the HhaI-based system, which show that 2AP behaves similarly on flipping by HhaI. The population of the π-stacked 2AP complex is indicative of the extent of the flipping by each enzyme. Hence, the absence of π-stacked 2AP suggests that base flipping by TaqI is more complete than flipping by HhaI, where 20% of the 2AP population in the ternary DNA-enzyme-cofactor complex appears to remain π-stacked within the DNA duplex.

The AP-T DNA bound by TaqI is a similarly heterogeneous system to that observed for the solution phase the HhaI system. The process of base flipping by TaqI is dynamic, and the 2AP that is the target for base flipping can adopt several different conformations once the enzyme is bound to the DNA. The magnitudes of τ_2-τ_4 are significantly greater than these lifetimes in any other system in this investigation. In the DNA-TaqI complex, the lifetimes named τ_1-τ_3 are similar to, but consistently shorter than, τ_2-τ_4 for the free DNA. This similarity between the two fluorescence responses is indicative of either the similarity of the protein active site to the DNA duplex or that the 2AP is not entirely flipped from the duplex and adopts similar unstacked conformations to those accessible to it in the free duplex. Given the complete absence of a ~100ps lifetime it is certain that the π-stacking interactions of 2AP with the duplex have been disrupted. Figure 8.2 clearly shows that for the 'native' DNA duplex, with adenine as the target for methylation, that the target base is flipped from the duplex and into the enzyme's active site. Given the structural similarity of 2AP to adenine, it seems likely that this will also be the case for the M.TaqI bound AP-T duplex. The similarity of the fluorescence response of the enzyme-bound AP-T duplex therefore appears to be indicative of the similarity of the enzyme active site to the DNA duplex. Indeed, Figure 8.3 shows that, with a π-stacking interaction on one side of the flipped base and hydrogen bonds formed to the adenine amine group, the TaqI active site is structurally quite similar to the DNA duplex.

Steady-state measurements by Holz *et al*[24] show that the increase in fluorescence intensity on base flipping of 2AP by TaqI is lower than that observed for the analogous HhaI system (13-fold increase for TaqI compared to a 54-fold increase in fluorescence intensity for HhaI). Holz *et al* postulate that this difference in photophysical behaviour is the result of either the different environments of the HhaI and TaqI active sites, or is due to a lower propensity for base flipping in the TaqI complex than in the HhaI system. The latter of these arguments is in contrast to the fluorescence lifetime measurements presented in Table 8.3, which show that base flipping of 2AP by TaqI is complete and leaves no 2AP π-stacked within the DNA duplex. Hence, the different fluorescence enhancements given by base flipping must be the result of the different environments of the active sites of the respective enzymes.

The work by Holz *et al* argues that the active site of HhaI is more hydrophilic than that of TaqI. Since the emission intensity of 2AP increases in increasingly polar solvents, this argument is in good agreement with the authors observations. However, the results of the time-resolved fluorescence measurements presented here show that the lifetimes of 2AP in the TaqI active site are generally greater in magnitude than those observed for 2AP in the (wild-type) HhaI active site. This indicates that, in fact, the 2AP interacts with more polar amino acid residues in the TaqI active site than in the HhaI active site. The important aspect of the fluorescence response, with respect to the steady-state emission of 2AP, is that approximately 60% of the 2AP molecules extruded from the DNA duplex by TaqI adopt an orientation where their lifetime is only 1.9ns. This compares to the flipped 2AP in the HhaI active site, where the most prolific 2AP species (~30% of the population) has a lifetime of 10.5ns. Hence, in the steady-state measurements, the fluorescence enhancement given for base flipping of 2AP by HhaI is much greater than that for base flipping by TaqI. These results emphasise the fact that the mechanism used for stabilising the extrahelical 2AP in each enzyme is quite different. Even in systems where there is no detectable change in 2AP emission intensity, time-resolved fluorescence measurements should reveal a change in the 2AP fluorescence response on base flipping.

The comparison of the time-resolved with steady-state fluorescence measurements illustrates a result of fundamental importance to the interpretation of the 2AP steady-state response with regards to base flipping. These systems, and the corresponding fluorescence response of 2AP, cannot be understood or interpreted through the application of a simple, generalised theory, of

the type that is assumed from steady-state fluorescence measurements. This is clearly illustrated by the failure of the assumption made by Holz *et al* in interpreting the relative fluorescence enhancements given by TaqI and HhaI on base flipping, which states that the more hydrophilic active site will give more intense fluorescence[24]. This argument is certainly correct and, based in the evidence available to the authors, is consistent with their experimental data. However, the time-resolved fluorescence response of 2AP shows that this, as discussed previously, is not the reason for the difference in the behaviour of 2AP in these two systems. Furthermore, the steady-state fluorescence intensity of 2AP is not necessarily a good indicator of base flipping, as was shown by Gowher *et al* for the EcoRV enzyme[126]. This enzyme shows base flipping activity but no increase in the emission intensity of 2AP, when it is the target for base flipping and the enzyme is bound to the duplex. This, presumably, is indicative of a mechanism, used by EcoRV for the stabilisation of the flipped 2AP, which efficiently quenches its fluorescence.

The results presented from both the HhaI and TaqI systems, however, show that the time-resolved fluorescence response of 2AP can be used as an indicator of base flipping. In both systems a fluorescence lifetime for 2AP of ~100ps is characteristic of π-stacked 2AP within the DNA duplex. A dramatic decrease in the A-factor of this species clearly shows that HhaI and TaqI operate via a base flipping mechanism.

Table 8.4 illustrates the effect of the absence of a base opposite 2AP, on the fluorescence response of the flipped 2AP. By removing the orphan thymine base, the mechanism used by TaqI to stabilise the DNA duplex during flipping is likely to be severely disrupted, as suggested by Figure 8.2. In terms of the molecular biology of the system, this experiment was designed to address the driving force of base flipping by TaqI. The fluorescence response of the 2AP for the AP-D-TaqI complex is dominated by a component with a lifetime of 10.4ns. This long-lived 2AP species is clearly extrahelical and it accounts for approximately 80% of the 2AP population. There is no short-lived (τ<100ps), stacked 2AP evident in this system. This evidence points to the fact that the 2AP is flipped out of the DNA duplex, even in the absence of the thymine base opposite it. Hence, the thymine base is not required to drive the base flipping by M.TaqI. This then, implies that its movement to an 'interstrand' position, by M.TaqI, as shown in Figure 8.2, is a step used by the enzyme to stabilise the DNA duplex during flipping.

8.4 Conclusions

The distinctive fluorescence response exhibited by 2AP when it is base flipped by the M.HhaI enzyme has been observed when for base flipping by the M.TaqI enzyme. The environment in the enzyme active site, into which 2AP is flipped, has been shown to be crucial in defining the fluorescence response of the 2AP-labelled DNA-enzyme complex. Hence, the use of time-resolved fluorescence measurements, as opposed to steady-state measurements, to investigate the behaviour of these systems is vital.

This investigation clearly demonstrates that the base opposite the target base for base flipping is not used by M.TaqI to initiate the flipping. Rather, this base is used by the enzyme in order to stabilise the DNA duplex during base flipping.

Chapter 9

Conclusions

The aim of this thesis was to employ steady-state and time-resolved fluorescence techniques to validate and employ 2AP as a probe of structural distortions of the DNA duplex.

It has been established, using both steady-state fluorescence and fluorescence lifetime measurements that 2AP exists as both the 9H and the 7H tautomer in four different solvents at room temperature. In the polar, protic solvents, there is a substantial proportion of the 7H isomer in the emitting population: about 40% in water and about 20% in ethanol. In aprotic solvents only 3-5% of the emitting population is in the 7H tautomeric form. The two tautomers have closely overlapping fluorescence spectra but can be distinguished by their fluorescence lifetimes.

For the first time the crystal structure of 2AP has been determined. The structure shows that 2AP experiences a π-stacked, highly hydrogen-bonded environment in the crystal. These interactions are analogous to those experienced by 2AP in duplex DNA. Fluorescence studies on 2AP in the crystal phase have been used to show that its photophysical properties are largely defined by the π-stacking interactions that the molecule experiences. The interactions between neighbouring 2AP molecules in the π-stacks results in fluorescence excitation and emission spectra that are substantially red-shifted relative to those of locally excited, or solution phase 2AP. The crystal also contains 2AP molecules at defect sites, which are essentially unperturbed by intermolecular interactions. These 2AP molecules have excitation and emission spectra similar to those recorded for 2AP in aqueous solution, which are characteristic of locally excited 2AP. It was argued that this relatively short-wavelength 2AP emission may be associated with the presence of a small fraction of the 7H tautomer in the crystal lattice.

The time-resolved fluorescence response of the crystalline 2AP is dominated by a short-lived species with a lifetime of ~40ps. The fluorescence responses of both the isolated and stacked 2AP species are multiexponential. In the case of the isolated 2AP, this multiexponential decay

reflects the heterogeneous structure of defect sites in the crystal. The short-wavelength fluorescence typical of 2AP-labelled DNA resembles that of isolated 2AP in the crystal.

Red-shifted emission from a stacked conformational state of 2AP in DNA has been observed. The electronic structure of 2AP in this conformational state is significantly perturbed by interaction with its neighbouring bases. Such red-shifted fluorescence from 2AP may be a widespread phenomenon and may well be observed wherever 2AP forms close π-stacking interactions with other aromatic species.

The conformation of the DNA duplex is critical in defining the fluorescence lifetime of 2AP. In the duplex, the fluorescence response of 2AP is characterised by four discrete lifetimes, which represent at least three distinct populations of emitting species. These populations are defined by the conformation of the DNA duplex and relate some information on the orientation of the 2AP in relation to the helix. A short lifetime component of ~100ps is characteristic of 2AP stacked within the DNA duplex, in an orientation favourable for hole-transfer to guanine. Extrahelical 2AP molecules have lifetimes of greater than 7ns. The two intermediate lifetime components of the 2AP fluorescence response represent 2AP that is intrahelical and is in an orientation that is unfavourable for non-radiative decay through hole-transfer to guanine.

Fluorescence decays were recorded for both crystalline and solution phase DNA duplexes. The responses of both systems were similar. The crystal structures of the 2AP-labelled DNA confirm the stacked orientation of the 2AP base in the DNA duplexes investigated. This stacked orientation for 2AP persists, even in the case where 2AP is mismatched with a guanine base. Here, the crystal structure shows that the 2AP adopts the *syn-* isomeric form, as opposed to the normal *anti-* form. The result of this isomerisation is to increase the stacking interactions between the 2AP and its 5'-guanine. This results in a reduction in the lifetime of the three shortest components of the 2AP fluorescence response and is good evidence to suggest that these components represent predominantly intrahelical 2AP species.

The 'stacked' and 'intermediate' components of the fluorescence response exhibit distinct fluorescence emission spectra. Presently, it is unclear as to whether or not the 2AP can move between these orientations on the timescale of the excited-state lifetime. However, it is clear that some small amplitude motions must occur on this timescale. In the case of the stacked

component of the 2AP decay the reorientation of the 2AP plays an important role in allowing hole-transfer to guanine and, hence, in precisely defining the lifetime of this species.

The lifetime of stacked 2AP in the DNA duplex is largely described by the rate of non-radiative decay through electron transfer from guanine. Some correlation between the proximity of the nearest guanine base to 2AP and the lifetime of the stacked component of the 2AP fluorescence response has been demonstrated.

The time-resolved fluorescence response of 2AP has been shown to be an indicator of base flipping by the M.HhaI and M.TaqI enzymes. For M.HhaI, combined crystal and solution phase time-resolved fluorescence measurements demonstrate that a clear change in the fluorescence response of 2AP results from base flipping. This fluorescence signature for base flipping is in the form of a significant decrease in the A-factor for the stacked 2AP species (τ~100ps) with a corresponding increase in the A-factor of the long-lived 2AP (τ~10ns).

The magnitude of the lifetime of the stacked 2AP species has been shown to increase as a result of weakening the π-stacking interactions felt by the probe. For the long-lived 2AP species, the formation of an electron withdrawing interaction at N7 has been shown to lead to a significant increase in its lifetime. When 2AP is in the DNA duplex, intermediate lifetime species represent intrahelical (but imperfectly stacked) 2AP populations.

The conformations adopted by the flipped 2AP in the wild-type and T250G mutant M.HhaI are quite different. The crystal structure for the mutant enzyme shows that 2AP occupies a highly polar environment, which leads to a significant increase in the fluorescence lifetimes of the flipped 2AP population compared to the flipped 2AP in wild-type HhaI. Hence, comparative studies on the wild-type and T250G mutant M.HhaI enzymes suggest that when 2AP is flipped into the enzyme active site, the two longest-lived decay components represent extrahelical species, whereas the two shortest-lived components are the result of mainly intrahelical 2AP populations.

Both the intrahelical and the long-lived 2AP species are present in the solution phase ^{M}wt-AP$_{target}$ complex. Hence, the base flipping mechanism in the solution phase is dynamic. Longer lifetimes

for the long-lived 2AP in T250G mutant as compared to the wild-type show that, as in the crystal phase, the 2AP in the solution phase occupies distinctly different regions of the enzyme active site.

Given the sensitivity of 2AP to its environment, it is remarkable that when is placed adjacent to or opposite the target site for base flipping its fluorescence response varies little between the free DNA and enzyme-bound duplexes. Slight changes in the magnitude of the short-lived 2AP lifetime indicate some changes in the stacking interactions within the duplex upon enzyme binding. The notable absence of any substantial change in the other fitted parameters demonstrates that HhaI is superbly evolved to stabilise the DNA duplex during base flipping.

The interstrand interactions of the DNA duplex have been shown to be affected by the enzyme binding at a point where the enzyme forms no direct contacts with the bases of the duplex. The 2AP to thymine Watson-Crick-type base pair is disturbed by enzyme binding despite being outside the enzyme recognition sequence. Where this base pair was a 2AP-G mismatch, no change in the fluorescence response upon enzyme binding was observed.

For the M.TaqI enzyme, 2AP has been used to demonstrate that the enzyme does not use the base opposite the target for base flipping to push the target base out of the DNA duplex. Instead, the base that is orphaned by base flipping is used by M.TaqI to stabilise the DNA duplex during flipping.

2AP has the potential to offer a unique insight into the fascinating and beautifully evolved mechanisms by which enzymes interact with the DNA duplex. This work has demonstrated how the intricacies of the complex time-resolved fluorescence response of 2AP can begin to be unpicked and related to well-defined structural or conformation features of the DNA-enzyme interaction.

References

(1) Watson, J. D.; Crick, F. H. C. *Cold Spring Harbor Symposia on Quantitative Biology* **1953**, *18*, 123-131.

(2) Lycksell, P. O.; Graslund, A.; Claesens, F.; McLaughlin, L. W.; Larsson, U.; Rigler, R. *Nucl.Acids.Res.* **1987**, *15*, 9011-9025.

(3) Stryer, L. *Biochemistry*; W.H. Freeman and Co.: 1981.

(4) Hollas, J. M. *Modern Spectroscopy*; John Wiley and Sons: 1996.

(5) Simons, J. P. *Photochemistry and Spectroscopy*; John Wiley and Sons: 1971.

(6) Murrell, J. N. *The theory of Electronic Spectra of Organic Molecules*; Methuen and Co. Ltd: 1962.

(7) Barltrop, J. A.; Coyle, J. D. *Excited States in Organic Chemistry*; John Wiley and Sons: 1975.

(8) Lakowicz, J. R. *Principles of Fluorescence Spectroscopy*; Kluwer Academic/ Plenum Publishers: 1999.

(9) Wright, J. D. *Molecular Crystals*; Cambridge University Press: Cambridge, 1995.

(10) O'Connor, D. V.; Phillips, D. *Time-correlated Single Photon Counting*; Academic Press: 1984.

(11) Berg, J. M.; Tymoczko, J. L.; Stryer, L. *Biochemistry*; W.H. Freeman and Co.: 2001.

(12) Wilkins, M. H. F.; Hooper, C. W.; Seeds, W. E.; Stokes, A. R.; Wilson, H. R. *Transactions of the Faraday Society* **1954**, *50*, 299.

(13) Franklin, R. E.; Gosling, R. G. *Transactions of the Faraday Society* **1954**, *50*, 298-299.

(14) Calladine, C. R.; Drew, H. R. *Understanding DNA; The Molecule and How it Works*; Academic Press: 1999.

(15) Schultz, T.; Samoylova, E.; Radloff, W.; Hertel, I. V.; Sobolewski, A. L.; Domcke, W. *Science* **2004**, *306*, 1765-1768.

(16) Malak, R. A.; Gao, Z. N.; Wishart, J. F.; Isied, S. S. *J.Am.Chem.Soc.* **2004**, *126*, 13888-13889.

(17) Cramer, T.; Volta, A.; Blumen, A.; Koslowski, T. *J.Phys.Chem.B* **2004**, *108*, 16586-16592.

(18) Cramer, T.; Krapf, S.; Koslowski, T. *J.Phys.Chem.B* **2004**, *108*, 11812-11819.

(19) Chang, C. M.; Neto, A. H. C.; Bishop, A. R. *Chem Phys* **2004**, *303*, 189-196.

(20) Kelley, S. O.; Barton, J. K. *Science* **1999**, *283*, 375-381.

(21) Treadway, C. R.; Hill, M. G.; Barton, J. K. *Chem Phys* **1999**, *281*, 409-428.

(22) Cheng, X.; Blumenthal, R. M. *S-Adenosylmethionine-Dependent Methyltransferases: Structure and Functions*; World Scientific: Singapore, 1999.

(23) Wilson, G. G.; Murray, N. E. *Annual Review of Genetics* **1991**, *25*, 585-627.

(24) Holz, B.; Klimasauskas, S.; Serva, S.; Weinhold, E. *Nucl.Acids.Res.* **1998**, *26*, 1076-1083.

(25) Stryer, L.; Ward, D. C.; Reich, E. *J.Bio.Chem.* **1969**, *244*, 1228-1237.

(26) Evans, K.; Xu, D.; Kim, Y.; Nordlund, T. M. *J.Fluoresc* **1992**, *2*, 209-216.

(27) Rachofsky, E. L.; Osman, R.; Ross, J. B. A. *Biochemistry* **2001**, *40*, 946-956.

(28) Rachofsky, E. L.; Ross, J. B. A.; Krauss, M.; Osman, R. *J.Phys Chem.A* **2001**, *105*, 190-197.

(29) Eastman, J. W. *Ber.Bunsenges.Phys.Chem.* **1969**, *73*, 407-412.

(30) Dreyfus, M.; Dodin, G.; Bensuade, O.; Dubois, J. E. *J.Am.Chem.Soc.* **1975**, *97*, 2369.

(31) Cohen, B.; Hare, P. M.; Kohler, B. *J.Am.Chem.Soc.* **2003**, *125*, 13594-13601.

(32) Brown, R.; Godfrey, P.; McNaughton, D.; Pierlot, P. *Chem Phys Letters* **1989**, *156*, 61-63.

(33) Plutzer, C.; Kleinermanns, K. *Phys.Chem.Chem.Phys.* **2002**, *4*, 4877-4882.

(34) Salter, L. M.; Chaban, G. M. *J.Phys Chem.A* **2002**, *106*, 4251-4256.

(35) Gu, J. D.; Leszczynski, J. *J.Phys Chem.A* **1999**, *103*, 2744-2750.

(36) Majobe, M.; Millie, Ph.; Chinsky, L.; Turpin, P. Y.; Vergoten, G. *J Mol Struct* **1995**, *355*, 147-158.

(37) Schumacher, M.; Gunther, H. *J.Am.Chem.Soc.* **1982**, *104*, 4167-4173.

(38) Gonella, N. C.; Roberts, J. D. *J.Am.Chem.Soc.* **1982**, *104*, 3162-3164.

(39) Chenon, M.-T.; Pugmire, R. J.; Grant, D. M.; Panzica, R. P.; Townsend, L. B. *J.Am.Chem.Soc.* **1975**, *97*, 4636-4642.

(40) Broo, A.; Holmen, A. *Chem Phys* **1996**, *211*, 147-161.

(41) Holmen, A.; Norden, B.; Albinsson, B. *J.Am.Chem.Soc.* **1997**, *119*, 3114-3121.

(42) Santhosh, C.; Mishra, C. P. *Spectrochim.Acta A* **1991**, *47*, 1685-1693.

(43) Larsen, O. F. A.; van Stokkum, I. H. M.; Groot, M. L.; Kennis, J. T. M.; van Grondelle, R.; van Amerongen, H. *Chem Phys Letters* **2003**, *371*, 157-163.

(44) Rachofsky, E. L.; Sowers, L.; Hawkins, M. L.; Balis, F. M.; Laws, W. R.; Ross, J. B. A. *Proc.SPIE* **1998**, *3256*, 68-75.

(45) Broo, A. *J.Phys Chem.A* **1998**, *102*, 526-531.

(46) Nordlund, T. M.; Andersson, S.; Nilsson, L.; Rigler, R. *Biochemistry* **1989**, *28*, 9095-9103.

(47) Rachofsky, E. L.; Seibert, E.; Stivers, J. T.; Osman, R.; Ross, J. B. A. *Biochemistry* **2001**, *40*, 957-967.

(48) Hochstrasser, R. A.; Carver, T. E.; Sowers, L. C.; Millar, D. P. *Biochemistry* **1994**, *33*, 11971-11979.

(49) Guest, C. R.; Hochstrasser, R. A.; Sowers, L. C.; Millar, D. P. *Biochemistry* **1991**, *30*, 3271-3279.

(50) O'Neill, M. A.; Dohno, C.; Barton, J. K. *J.Am.Chem.Soc.* **2004**, *126*, 1316-1317.

(51) Hall, K. B.; Williams, J. *RNA* **2004**, *10*, 34-47.

(52) Lynch, D. E.; McClenaghan, I. *Acta Crystallographica Section C-Crystal Structure Communications* **2003**, *59*, O53-O56.

(53) Harnden, M. R.; Jarvest, R. L.; Slawin, A. M. Z.; Williams, D. J. *Nucleosdies Nucleotides* **1992**, *9*, 499.

(54) Mennucci, B.; Toniolo, A.; Tomasi, J. *J.Phys Chem.A* **2001**, *105*, 4749-4757.

(55) Jean, J. M.; Hall, K. B. *J.Phys Chem.A* **2000**, *104*, 1930-1937.

(56) Broomhead, J. M. *Acta Crystallogr.* **1948**, *1*, 324.

(57) Chen, H. H.; Clark, L. B. *Journal of Chemical Physics* **1973**, *58*, 2593-2603.

(58) Rist, M.; Wagenknecht, H. A.; Fiebig, T. *Chemphyschem* **2002**, *3*, 704.

(59) Johnson, N. P.; Baase, W. A.; von Hippel, P. H. *Proc.Natl.Acad.Sci.USA* **2004**, *101*, 3426-3431.

(60) Jean, J. M.; Hall, K. B. *Proc.Natl.Acad.Sci.USA* **2001**, *98*, 37-41.

(61) Jean, J. M.; Showalter, S. A.; Hall, K. B. *Biophys.J.* **2002**, *82*, 1729.

(62) Sheldrick, G. M. *SADABS, version 2004/1* **2004**, University of Gottingen, Germany.

(63) Altomare, A.; Cascarano, G.; Giacovazzo, G.; Guagliardi, A.; Burla, M. C.; Polidori, G.; Camalli, M. *J.Appl.Cryst.* **2004**, *27*, 435.

(64) Betteridge, P. W.; Carruthers, J. R.; Cooper, R. I.; Prout, K.; Watkin, D. J. *J.Appl.Cryst.* **2003**, *36*, 1487.

(65) Neely, R. K.; Magennis, S. W.; Dryden, D. T. F.; Jones, A. C. *J.Phys.Chem.B* **2004**, *108*, 17606-17610.

(66) Drew, H. R.; Dickerson, R. E. *J.Mol Biol* **1981**, *151*, 535-556.

(67) ElHassan, M. A.; Calladine, C. R. *Phil.Trans.Royal Soc.London, A* **1997**, *355*, 43-100.

(68) Frisch, M. J.; Trucks, G. W.; Schlegel, H. B.; Scuseria, G. E.; Robb, M. A.; Cheeseman, J. R.; Zakrzewski, V. G.; Montgomery, J. A.; Stratmann, R. E.; Burant, J. C.; Dapprich, S.; Millam, J. M.; Daniels, A. D.; Kudin, K. N.; Strain, M. C.; Farkas, O.; Tomasi, J.; Barone, V.; Cossi, M.; Cammi, R.; Mennucci, B.; Pomelli, C.; Adamo, C.; Clifford, S.; Ochterski, J.; Petersson, G. A.; Ayala, P. Y.; Cui, Q.; Morokuma, K.; Malick, D. K.; Rabuck, A. D.; Raghavachari, K.; Foresman, J. B.; Cioslowski, J.; Ortiz, J. V.; Baboul, A. G.; Stefanov, B. B.; Liu, G.; Liashenko, A.; Piskorz, P.; Komaromi, I.; Gomperts, R.; Martin, R. L.; Fox, D. J.; Keith, T.; Al-Laham, M. A.; Peng, C. Y.; Nanayakkara, A.; Gonzalez, C.; Challacombe, M.; Gill, P. M. W.; Johnson, B.; Chen, W.; Wong, M. W.; Andres, J. L.; Gonzalez, C.; Head-Gordon, M.; Replogle, E. S.; Pople.J.A. *Gaussian 98, Revision A.7* **1998**, Gaussian Inc, Pittsburgh PA 1998.

(69) Jean, J. M.; Hall, K. B. *Biochemistry* **2002**, *41*, 13152-13161.

(70) Su, T. J.; Connolly, B. A.; Darlington, C.; Mallin, R.; Dryden, D. T. F. *Nucl.Acids.Res.* **2004**, *32*, 2223-2230.

(71) Goedecke, K.; Pignot, M.; Goody, R. S.; Scheidig, A. J.; Weinhold, E. *Nature Struct Biol* **2001**, *8*, 121-125.

(72) Bloom, L. B.; Otto, M. R.; Beechem, J. M.; Goodman, M. F. *Biochemistry* **1993**, *32*, 11247-11258.

(73) Raney, K. D.; Sowers, L. C.; Millar, D. P.; Benkovic, S. J. *Proc.Natl.Acad.Sci.USA* **1994**, *91*, 6644-6648.

(74) McCullough, A. K.; Dodson, M. L.; Scharer, O. D.; Lloyd, R. S. *J.Biol.Chem.* **1997**, *272*, 27210-27217.

(75) Stivers, J. T. *Nucl.Acids.Res.* **1998**, *26*, 3837-3844.

(76) Stivers, J. T.; Pankiewicz, K. W.; Watanabe, K. A. *Biochemistry* **1999**, *38*, 952-963.

(77) Allan, B. W.; Reich, N. O. *Biochemistry* **1998**, *38*, 5308-5314.

(78) Allan, B. W.; Reich, N. O. *Biochemistry* **1996**, *35*, 14757-14762.

(79) Allan, B. W.; Beechem, J. M.; Lindstrom, W. M.; Reich, N. O. *J.Biol.Chem.* **1998**, *273*, 2368-2373.

(80) Eritja, R.; Kaplan, B. E.; Mhaskar, D.; Sowers, L. C.; Petruska, J.; Goodman, M. F. *Nucl.Acids.Res.* **1986**, *14*, 5869-5884.

(81) McLaughlin, L. W.; Leong T; Benseler F; Piel N *Nucl.Acids.Res.* **1988**, *16*, 5631-5644.

(82) Law, S. M.; Eritja, R.; Goodman, M. F.; Breslauer, K. J. *Biochemistry* **1996**, *35*, 12329-12337.

(83) Sowers, L. C.; Fazakerley, G. V.; Eritja, R.; Kaplan, B. E.; Goodman, M. F. *Proc.Natl.Acad.Sci.USA* **1986**, *83*, 5434-5438.

(84) Sowers, L. C.; Boulard, Y.; Fazakerley, G. V. *Biochemistry* **2000**, *39*, 7613-7620.

(85) Jean, J. M.; Hall, K. B. *Biophys.J.* **2001**, *80*, 35.

(86) Purohit, V.; Grindley, N. D. F.; Joyce, C. M. *Biochemistry* **2003**, *42*, 10200-10211.

(87) Ramreddy, T.; Sen, S.; Rao, B. J.; Krishnamoorthy, G. *Biochemistry* **2003**, *42*, 12085-12094.

(88) Seibert, E.; Ross, J. B. A.; Osman, R. *Biochemistry* **2002**, *41*, 10976-10984.

(89) Tashiro, R.; Sugiyama, H. *Angew Chem Int Ed* **2003**, *42*, 6018-6020.

(90) Nordlund, T. M.; Xu, D.; Evans, K. O. *Biochemistry* **1993**, *32*, 12090-12095.

(91) Xu, D. G.; Nordlund, T. M. *Biophys.J.* **2000**, *78*, 1042-1058.

(92) Rai, P.; Cole, T. D.; Thompson, E.; Millar, D. P.; Linn, S. *Nucl.Acids.Res.* **2003**, *31*, 2323-2332.

(93) Steenken, S.; Jovanovic, S. V. *J.Am.Chem.Soc.* **1997**, *119*, 617-618.

(94) Wan, C.; Fiebig, T.; Schiemann, O.; Barton, J. K.; Zewail, A. H. *Proc.Natl.Acad.Sci.USA* **2000**, *97*, 14052-14055.

(95) Larsen, O. F. A.; van Stokkum, I. H. M.; Gobets, B.; van Grondelle, R.; van Amerongen, H. *Biophys.J.* **2001**, *81*, 1115-1126.

(96) Wan, C.; Fiebig, T.; Kelley, S. O.; Treadway, C. R.; Barton, J. K.; Zewail, A. H. *Proc.Natl.Acad.Sci.USA* **1999**, *96*, 6014-6019.

(97) Jean, J. M.; Hall, K. B. *Biochemistry* **2004**, *43*, 10277-10284.

(98) O'Neill, M. A.; Barton, J. K. *J.Am.Chem.Soc.* **2002**, *124*, 13053-13066.

(99) O'Neill, M. A.; Barton, J. K. *Proc.Natl.Acad.Sci.USA* **2002**, *99*, 16543-16550.

(100) O'Neill, M. A.; Becker, H. C.; Wan, C. Z.; Barton, J. K.; Zewail, A. H. *Angew Chem Int Ed* **2003**, *42*, 5896-5900.

(101) Aishima, J.; Gitti, R. K.; Noah, J. E.; Gan, H. H.; Schlick, T.; Wolberger, C. *Nucl.Acids.Res.* **2002**, *30*, 5244-5252.

(102) Bouvier, B.; Dognon, J. P.; Lavery, R.; Markovitsi, D.; Millie, P.; Onidas, D.; Zakrzewska, K. *J.Phys.Chem.B* **2003**, *107*, 13512-13522.

(103) O'Neill, M. A.; Barton, J. K. *J.Am.Chem.Soc.* **2004**, *126*, 13234-13235.

(104) O'Neill, M. A.; Barton, J. K. *J.Am.Chem.Soc.* **2004**, *126*, 11471-11483.

(105) Kumar, S.; Cheng, X. D.; Pflugrath, J. W.; Roberts, R. J. *Biochemistry* **1992**, *31*, 8648-8653.

(106) Cheng, X. D.; Kumar, S.; Posfai, J.; Pflugrath, J. W.; Roberts, R. J. *Cell* **1993**, *74*, 299-307.

(107) Klimasauskas, S.; Kumar, S.; Roberts, R. J.; Cheng, X. D. *Cell* **1994**, *76*, 357-369.

(108) Reinisch, K. M.; Chen, L.; Verdine, G. L.; Lipscomb, W. N. *Cell* **1995**, *82*, 143-153.

(109) Wu, J. C.; Santi, D. V. *J.Biol.Chem.* **1987**, *262*, 4778-4786.

(110) Dryden, D. T. F. Bacterial DNA methyltransferases; In *S-Adenosylmethionine-dependent methyltransferases: Structure and functions*; Cheng, X., Blumenthal, R. M., eds. World Scientific: 1998; pp 283-340.

(111) Erlanson, D. A.; Chen, L.; Verdine, G. L. *J.Am.Chem.Soc.* **1993**, *115*, 12583-12584.

(112) Ogara, M.; Klimasauskas, S.; Roberts, R. J.; Cheng, X. D. *J.Mol Biol* **1996**, *261*, 634-645.

(113) Klimasauskas, S.; Roberts, R. J. *Gene* **1995**, *157*, 163-164.

(114) O'Gara, M.; Horton, J. R.; Roberts, R. J.; Cheng, X. D. *Nature Struct Biol* **1998**, *5*, 872-877.

(115) Klimasauskas, S.; Szyperski, T.; Serva, S.; Wuthrich, K. *EMBO J.* **1998**, *17*, 317-324.

(116) Vilkaitis, G.; Merkiene, E.; Serva, S.; Weinhold, E.; Klimasauskas, S. *J.Biol.Chem.* **2001**, *276*, 20924-20934.

(117) Daujotyte, D.; Serva, S.; Vilkaitis, G.; Merkiene, E.; Venclovas, D.; Klimasauskas, S. *Structure* **2004**, *12*, 1047-1055.

(118) Klimasauskas, S.; Roberts, R. J. *Nucl.Acids.Res.* **1995**, *23*, 1388-1395.

(119) Vilkaitis, G.; Dong, A.; Weinhold, E.; Cheng, X.; Klimasauskas, S. *J.Biol.Chem.* **2000**, *275*, 38722-38730.

(120) Klimasauskas, S. *Personal Communication* **2005**.

(121) Beechem, J. M.; Otto, M. R.; Bloom, L. B.; Eritja, R.; Reha-Krantz, L. J.; Goodman, M. F. *Biochemistry* **1998**, *37*, 10144-10155.

(122) Gowher, H.; Jeltsch, A. *J.Mol Biol* **2000**, *303*, 93-110.

(123) Reddy, Y. V. R.; Rao, D. N. *J.Mol Biol* **2000**, *298*, 597-610.

(124) Daujotyte, D. *Personal Communication* **2003**.

(125) Blumenthal, R. M.; Cheng, X. D. *Nature Struct Biol* **2001**, *8*, 101-103.

(126) Gowher, H.; Jeltsch, A. *J.Mol Biol* **2000**, *303*, 93-110.

Appendix

DNA Duplexes

Tables A.1 to A18 show the parameters derived from the global fitting of the fluorescence data collected on the 20ns and 50ns timescales for the DNA duplexes used is this study.

Global Lifetimes: τ1=0.12ns, τ2=0.40ns, τ3=2.69ns, τ4=10.83ns
Global χ2=1.043

Emission Wavelength/ nm	A1	A2	A3	A4	Local χ^2
370	0.89	0.07	0.02	0.02	1.072
390	0.86	0.09	0.03	0.02	1.029
410	0.87	0.08	0.02	0.02	1.027

Figure A.1- Parameters derived from the global analysis of the experimental data from the PT(AC)2 duplex on the 20ns timescale.

Global Lifetimes: τ1=0.12ns, τ2=0.37ns, τ3=2.73ns, τ4=10.78ns
Global χ2=1.114

Emission Wavelength/ nm	A1	A2	A3	A4	Local χ^2
370	0.88	0.08	0.02	0.02	1.111
390	0.83	0.12	0.03	0.02	1.099
410	0.75	0.16	0.06	0.03	1.131

Figure A.2- Parameters derived from the global analysis of the experimental data from the PT(AC)2 duplex on the 50ns timescale.

Global Lifetimes: τ1=0.05ns, τ2=0.37ns, τ3=2.52ns, τ4=8.45ns
Global χ2=1.072

Emission Wavelength/ nm	A1	A2	A3	A4	Local χ^2
370	0.81	0.10	0.05	0.04	1.078
390	0.78	0.12	0.06	0.04	1.077
410	0.74	0.14	0.07	0.05	1.060

Figure A.3- Parameters derived from the global analysis of the experimental data from the PT(CC)1 duplex on the 20ns timescale.

Global Lifetimes: τ1=0.05ns, τ2=0.38ns, τ3=2.66ns, τ4=8.56ns
Global χ2=1.186

Emission Wavelength/ nm	A1	A2	A3	A4	Local χ^2
370	0.69	0.17	0.08	0.06	1.195
390	0.73	0.14	0.07	0.05	1.139
410	0.63	0.21	0.09	0.06	1.224

Figure A.4- Parameters derived from the global analysis of the experimental data from the PT(CC)1 duplex on the 50ns timescale.

Global Lifetimes: τ1=0.03ns, τ2=0.45ns, τ3=2.62ns, τ4=10.78ns
Global χ2=1.114

Emission Wavelength/ nm	A1	A2	A3	A4	Local χ^2
370	0.96	0.01	0.01	0.01	1.107
390	0.93	0.03	0.02	0.02	1.069
410	0.88	0.06	0.04	0.02	1.166

Figure A.5- Parameters derived from the global analysis of the experimental data from the PT(CC)2 duplex on the 20ns timescale.

Global Lifetimes: τ1=0.03ns, τ2=0.44ns, τ3=2.61ns, τ4=10.77ns
Global χ2=1.133

Emission Wavelength/ nm	A1	A2	A3	A4	Local χ^2
370	0.95	0.02	0.01	0.02	1.133
390	0.90	0.04	0.03	0.02	1.094
410	0.82	0.09	0.06	0.03	1.172

Figure A.6- Parameters derived from the global analysis of the experimental data from the PT(CC)2 duplex on the 50ns timescale.

Global Lifetimes: τ1=0.12ns, τ2=0.58ns, τ3=2.53ns, τ4=8.27ns
Global χ2=1.072

Emission Wavelength/ nm	A1	A2	A3	A4	Local χ^2
370	0.49	0.35	0.11	0.05	1.075
390	0.46	0.36	0.12	0.06	1.038
410	0.44	0.36	0.14	0.06	1.102

Figure A.7- Parameters derived from the global analysis of the experimental data from the PT(TA) duplex on the 20ns timescale.

Global Lifetimes: τ1=0.12ns, τ2=0.57ns, τ3=2.35ns, τ4=8.01ns
Global χ2=1.125

Emission Wavelength/ nm	A1	A2	A3	A4	Local χ^2
370	0.48	0.34	0.12	0.06	1.092
390	0.45	0.35	0.13	0.07	1.127
410	0.39	0.39	0.14	0.08	1.156

Figure A.8- Parameters derived from the global analysis of the experimental data from the PT(TA) duplex on the 50ns timescale.

Global Lifetimes: τ1=0.04ns, τ2=0.43ns, τ3=2.68ns, τ4=10.71ns
Global χ2=1.107

Emission Wavelength/ nm	A1	A2	A3	A4	Local χ^2
370	0.75	0.09	0.07	0.09	1.153
390	0.69	0.13	0.09	0.10	1.034
410	0.65	0.18	0.10	0.07	1.135

Figure A.9- Parameters derived from the global analysis of the experimental data from the PT(GG)/ TP_{out} duplex on the 20ns timescale.

Global Lifetimes: τ1=0.04ns, τ2=0.44ns, τ3=2.73ns, τ4=10.68ns
Global χ2=1.066

Emission Wavelength/ nm	A1	A2	A3	A4	Local χ^2
370	0.69	0.11	0.09	0.11	1.055
390	0.60	0.17	0.11	0.12	1.099
410	0.60	0.20	0.12	0.08	1.043

Figure A.10- Parameters derived from the global analysis of the experimental data from the PT(GG)/ TP_{out} duplex on the 50ns timescale.

Global Lifetimes: τ1=0.04ns, τ2=0.45ns, τ3=2.62ns, τ4=10.34ns
Global χ2=1.125

Emission Wavelength/ nm	A1	A2	A3	A4	Local χ^2
370	0.90	0.05	0.03	0.02	1.108
390	0.85	0.08	0.05	0.02	1.157
410	0.79	0.13	0.06	0.02	1.109

Figure A.11- Parameters derived from the global analysis of the experimental data from the PC(GC)/ AP_{adj} duplex on the 20ns timescale.

Global Lifetimes: τ1=0.04ns, τ2=0.45ns, τ3=2.64ns, τ4=10.31ns
Global χ2=1. 130

Emission Wavelength/ nm	A1	A2	A3	A4	Local χ^2
370	0.88	0.06	0.03	0.02	1.097
390	0.82	0.11	0.05	0.02	1.085
410	0.75	0.15	0.08	0.03	1.209

Figure A.12- Parameters derived from the global analysis of the experimental data from the PC(GC)/ AP_{adj} duplex on the 50ns timescale.

Global Lifetimes: τ1=0.05ns, τ2=0.48ns, τ3=2.89ns, τ4=9.82ns
Global χ2=1.079

Emission Wavelength/ nm	A1	A2	A3	A4	Local χ^2
370	0.72	0.11	0.08	0.09	1.093
390	0.66	0.15	0.10	0.09	1.051
410	0.60	0.21	0.11	0.09	1.093

Figure A.13- Parameters derived from the global analysis of the experimental data from the PC(MC)/ AP_{opp} duplex on the 20ns timescale.

Global Lifetimes: τ1=0.05ns, τ2=0.52ns, τ3=3.07ns, τ4=9.80ns
Global χ2=1.099

Emission Wavelength/ nm	A1	A2	A3	A4	Local χ^2
370	0.67	0.13	0.09	0.11	1.107
390	0.61	0.17	0.11	0.10	1.121
410	0.57	0.22	0.12	0.09	1.07

Figure A.14- Parameters derived from the global analysis of the experimental data from the PC(MC)/ AP_{opp} duplex on the 50ns timescale.

Global Lifetimes: τ1=0.08ns, τ2=0.58ns, τ3=2.9ns, τ4=9.7ns
Global χ2=1.137

Emission Wavelength/ nm	A1	A2	A3	A4	Local χ^2
370	0.61	0.17	0.13	0.09	1.174
390	0.54	0.26	0.14	0.06	1.086
410	0.53	0.30	0.13	0.04	1.153

Figure A.15- Parameters derived from the global analysis of the experimental data from the PG(GG)1/ AP_{target} duplex on the 20ns timescale.

Global Lifetimes: τ1=0.08ns, τ2=0.58ns, τ3=3.0ns, τ4=9.6ns
Global χ2=1. 136

Emission Wavelength/ nm	A1	A2	A3	A4	Local χ^2
370	0.58	0.20	0.14	0.09	1.166
390	0.52	0.27	0.14	0.06	1.097
410	0.50	0.31	0.14	0.05	1.144

Figure A. 16- Parameters derived from the global analysis of the experimental data from the PG(GG)1/ AP_{target} duplex on the 50ns timescale.

Global Lifetimes: τ1=0.04ns, τ2=0.48ns, τ3=2.9ns, τ4=11.0ns
Global χ2=1.129

Emission Wavelength/ nm	A1	A2	A3	A4	Local χ^2
370	0.79	0.07	0.08	0.06	1.151
390	0.72	0.12	0.09	0.07	1.089
410	0.66	0.18	0.10	0.06	1.146

Figure A.17- Parameters derived from the global analysis of the experimental data from the PG(GG)2/ GP_{out} duplex on the 20ns timescale.

Global Lifetimes: τ1=0.04ns, τ2=0.51ns, τ3=3.0ns, τ4=11.0ns
Global χ2=1.112

Emission Wavelength/ nm	A1	A2	A3	A4	Local χ^2
370	0.76	0.08	0.09	0.07	1.113
390	0.68	0.14	0.10	0.08	1.008
410	0.63	0.20	0.11	0.07	1.216

Figure A.18- Parameters derived from the global analysis of the experimental data from the PG(GG)2/ GP_{out} duplex on the 50ns timescale.

DNA-Wild Type HhaI complexes

Tables A.19 to A28 show the parameters derived from the global fitting of the fluorescence data collected on the 20ns and 50ns timescales for the DNA/wild-type HhaI complexes used is this study.

Global Lifetimes: τ1=0.04ns, τ2=0.42ns, τ3=2.66ns, τ4=10.05ns
Global χ2=1.137

Emission Wavelength/ nm	A1	A2	A3	A4	Local χ^2
370	0.82	0.07	0.05	0.06	1.137
390	0.75	0.12	0.07	0.07	1.166
410	0.77	0.13	0.06	0.04	1.108

Figure A.19- Parameters derived from the global analysis of the experimental data from the wt-GP_{out} complex on the 20ns timescale.

Global Lifetimes: τ1=0.04ns, τ2=0.48ns, τ3=2.80ns, τ4=10.05ns
Global χ2=1.151

Emission Wavelength/ nm	A1	A2	A3	A4	Local χ^2
370	0.80	0.08	0.05	0.07	1.186
390	0.76	0.10	0.07	0.07	1.172
410	0.76	0.13	0.06	0.05	1.094

Figure A.20- Parameters derived from the global analysis of the experimental data from the wt-GP_{out} complex on the 50ns timescale.

Global Lifetimes: τ1=0.14ns, τ2=0.89ns, τ3=4.16ns, τ4=9.61ns
Global χ2=1.007

Emission Wavelength/ nm	A1	A2	A3	A4	Local χ^2
370	0.25	0.21	0.23	0.31	1.008
390	0.28	0.23	0.22	0.27	1.006

Figure A.21- Parameters derived from the global analysis of the experimental data from the wt-AP_{target} complex on the 20ns timescale. Time constraints meant that no data was collected at 410nm for this sample.

Global Lifetimes: τ1=0.14ns, τ2=1.04ns, τ3=4.52ns, τ4=9.69ns
Global χ2=1. 065

Emission Wavelength/ nm	A1	A2	A3	A4	Local χ^2
370	0.26	0.18	0.22	0.34	1.056
390	0.29	0.21	0.20	0.30	1.06
410	0.36	0.23	0.18	0.23	1.065

Figure A. 22- Parameters derived from the global analysis of the experimental data from the wt-AP_{target} complex on the 50ns timescale.

Global Lifetimes: τ1=0.06ns, τ2=0.54ns, τ3=2.83ns, τ4=9.79ns
Global χ2=1.034

Emission Wavelength/ nm	A1	A2	A3	A4	Local χ^2
370	0.61	0.12	0.12	0.14	1.073
390	0.47	0.19	0.15	0.19	1.033
410	0.49	0.21	0.15	0.15	0.995

Figure A.23- Parameters derived from the global analysis of the experimental data from the wt-TP_{out} complex on the 20ns timescale.

Global Lifetimes: τ1=0.06ns, τ2=0.56ns, τ3=3.25ns, τ4=9.78ns
Global χ2=1.088

Emission Wavelength/ nm	A1	A2	A3	A4	Local χ^2
370	0.46	0.18	0.16	0.20	1.124
390	0.44	0.21	0.16	0.19	1.08
410	0.43	0.25	0.17	0.15	1.06

Figure A.24- Parameters derived from the global analysis of the experimental data from the wt-TP_{out} complex on the 50ns timescale.

Global Lifetimes: τ1=0.04ns, τ2=0.40ns, τ3=2.49ns, τ4=9.67ns
Global χ2=1.136

Emission Wavelength/ nm	A1	A2	A3	A4	Local χ^2
370	0.88	0.07	0.03	0.02	1.175
390	0.83	0.10	0.04	0.02	1.119
410	0.79	0.13	0.06	0.02	1.114

Figure A.25- Parameters derived from the global analysis of the experimental data from the wt-AP_{adj} complex on the 20ns timescale.

Global Lifetimes: τ1=0.04ns, τ2=0.41ns, τ3=2.52ns, τ4=9.71ns
Global χ2=1. 186

Emission Wavelength/ nm	A1	A2	A3	A4	Local χ^2
370	0.85	0.08	0.04	0.03	1.257
390	0.80	0.11	0.06	0.03	1.139
410	0.77	0.14	0.07	0.03	1.162

Figure A. 26- Parameters derived from the global analysis of the experimental data from the wt-AP_{adj} complex on the 50ns timescale.

Global Lifetimes: τ1=0.05ns, τ2=0.47ns, τ3=2.69ns, τ4=9.58ns
Global χ2=1.126

Emission Wavelength/ nm	A1	A2	A3	A4	Local χ^2
370	0.78	0.09	0.06	0.06	1.115
390	0.75	0.12	0.07	0.06	1.146
410	0.76	0.14	0.06	0.05	1.118

Figure A.27- Parameters derived from the global analysis of the experimental data from the wt-AP_{opp} complex on the 20ns timescale.

Global Lifetimes: τ1=0.05ns, τ2=0.54ns, τ3=2.85ns, τ4=9.62ns
Global χ2=1.154

Emission Wavelength/ nm	A1	A2	A3	A4	Local χ^2
370	0.78	0.10	0.06	0.06	1.144
390	0.74	0.12	0.07	0.07	1.197
410	0.74	0.13	0.08	0.05	1.121

Figure A.28- Parameters derived from the global analysis of the experimental data from the wt-AP_{opp} complex on the 50ns timescale.

DNA/Wild-Type HhaI/Cofactor Complexes

Tables A.29 to A38 show the parameters derived from the global fitting of the fluorescence data collected on the 20ns and 50ns timescales for the DNA/wild-type HhaI/ cofactor complexes used is this study.

Global Lifetimes: τ1=0.03ns, τ2=0.39ns, τ3=2.4ns, τ4=10.2ns
Global χ2=1.096

Emission Wavelength/ nm	A1	A2	A3	A4	Local χ^2
370	0.86	0.05	0.04	0.04	1.108
390	0.83	0.08	0.05	0.05	1.097
410	0.84	0.09	0.05	0.03	1.084

Figure A.29- Parameters derived from the global analysis of the experimental data from the ^{H}wt-GP_{out} complex on the 20ns timescale.

Global Lifetimes: τ1=0.03ns, τ2=0.54ns, τ3=3.2ns, τ4=10.3ns
Global χ2=1.246

Emission Wavelength/ nm	A1	A2	A3	A4	Local χ^2
370	0.74	0.08	0.08	0.09	1.285
390	0.58	0.16	0.11	0.15	1.145
410	0.57	0.20	0.11	0.12	1.307

Figure A.30- Parameters derived from the global analysis of the experimental data from the ^{H}wt-GP$_{out}$ complex on the 50ns timescale.

Global Lifetimes: τ1=0.10ns, τ2=0.92ns, τ3=4.16ns, τ4=10.49ns
Global χ2=1.003

Emission Wavelength/ nm	A1	A2	A3	A4	Local χ^2
370	0.24	0.24	0.22	0.30	0.988
390	0.20	0.26	0.23	0.31	1.009
410	0.19	0.22	0.25	0.33	1.013

Figure A.31- Parameters derived from the global analysis of the experimental data from the ^{M}wt-AP$_{target}$ complex on the 20ns timescale.

Global Lifetimes: τ1=0.13ns, τ2=0.97ns, τ3=4.30ns, τ4=10.49ns
Global χ2=1. 060

Emission Wavelength/ nm	A1	A2	A3	A4	Local χ^2
370	0.32	0.28	0.20	0.21	1.103
390	0.25	0.26	0.22	0.27	0.997
410	0.22	0.24	0.24	0.30	1.082

Figure A.32- Parameters derived from the global analysis of the experimental data from the ^{M}wt-AP$_{target}$ complex on the 50ns timescale.

Global Lifetimes: τ1=0.06ns, τ2=0.63ns, τ3=3.04ns, τ4=10.09ns
Global χ2=1.056

Emission Wavelength/ nm	A1	A2	A3	A4	Local χ^2
370	0.60	0.15	0.13	0.13	1.081
390	0.62	0.14	0.12	0.12	1.007
410	0.61	0.18	0.12	0.10	1.081

Figure A.33- Parameters derived from the global analysis of the experimental data from the ^{H}wt-TP$_{out}$ complex on the 20ns timescale.

Global Lifetimes: τ1=0.06ns, τ2=0.65ns, τ3=3.10ns, τ4=10.09ns
Global χ2=1.092

Emission Wavelength/ nm	A1	A2	A3	A4	Local χ^2
370	0.57	0.16	0.12	0.14	1.108
390	0.58	0.17	0.12	0.13	1.069
410	0.59	0.19	0.12	0.10	1.099

Figure A.34- Parameters derived from the global analysis of the experimental data from the ^{H}wt-TP$_{out}$ complex on the 50ns timescale.

Global Lifetimes: τ1=0.08ns, τ2=0.33ns, τ3=2.37ns, τ4=9.94ns
Global χ2=1.146

Emission Wavelength/ nm	A1	A2	A3	A4	Local χ^2
370	0.84	0.11	0.03	0.02	1.156
390	0.80	0.14	0.04	0.02	1.116
410	0.75	0.17	0.06	0.02	1.165

Figure A.35- Parameters derived from the global analysis of the experimental data from the ^{H}wt-AP$_{adj}$ complex on the 20ns timescale.

Global Lifetimes: τ1=0.08ns, τ2=0.31ns, τ3=2.33ns, τ4=9.87ns
Global χ2=1.120

Emission Wavelength/ nm	A1	A2	A3	A4	Local χ^2
370	0.82	0.13	0.03	0.02	1.147
390	0.77	0.16	0.04	0.02	1.075
410	0.73	0.19	0.07	0.02	1.138

Figure A.36- Parameters derived from the global analysis of the experimental data from the ^{H}wt-AP$_{adj}$ complex on the 50ns timescale.

Global Lifetimes: τ1=0.06ns, τ2=0.42ns, τ3=2.62ns, τ4=9.36ns
Global χ2=1.119

Emission Wavelength/ nm	A1	A2	A3	A4	Local χ^2
370	0.69	0.16	0.07	0.08	1.109
390	0.66	0.17	0.08	0.08	1.13
410	0.66	0.19	0.08	0.07	1.117

Figure A.37- Parameters derived from the global analysis of the experimental data from the ^{H}wt-AP$_{opp}$ complex on the 20ns timescale.

Global Lifetimes: τ1=0.06ns, τ2=0.45ns, τ3=2.73ns, τ4=9.38ns
Global χ2=1.146

Emission Wavelength/ nm	A1	A2	A3	A4	Local χ^2
370	0.68	0.16	0.08	0.08	1.189
390	0.65	0.18	0.09	0.09	1.144
410	0.64	0.20	0.09	0.07	1.104

Figure A.38- Parameters derived from the global analysis of the experimental data from the ^{H}wt-AP$_{opp}$ complex on the 50ns timescale.

DNA/T250G Mutant HhaI Complexes

Tables A.39 to A48 show the parameters derived from the global fitting of the fluorescence data collected on the 20ns and 50ns timescales for the DNA/T250G mutant HhaI complexes used is this study.

Global Lifetimes: τ1=0.05ns, τ2=0.47ns, τ3=2.76ns, τ4=10.31ns
Global χ2=1.116

Emission Wavelength/ nm	A1	A2	A3	A4	Local χ^2
370	0.77	0.09	0.07	0.07	1.103
390	0.68	0.15	0.09	0.08	1.078
410	0.66	0.18	0.10	0.06	1.168

Figure A. 39- Parameters derived from the global analysis of the experimental data from the m-GP_{out} complex on the 20ns timescale.

Global Lifetimes: τ1=0.05ns, τ2=0.50ns, τ3=2.80ns, τ4=10.32ns
Global χ2=1. 095

Emission Wavelength/ nm	A1	A2	A3	A4	Local χ^2
370	0.74	0.10	0.08	0.08	1.101
390	0.65	0.17	0.10	0.08	1.087
410	0.66	0.20	0.07	0.07	1.097

Figure A. 40- Parameters derived from the global analysis of the experimental data from the m-GP_{out} complex on the 50ns timescale.

Global Lifetimes: τ1=0.14ns, τ2=0.90ns, τ3=4.82ns, τ4=12.48ns
Global χ2=1.013

Emission Wavelength/ nm	A1	A2	A3	A4	Local χ^2
370	0.19	0.13	0.21	0.47	1.032
390	0.19	0.16	0.19	0.47	0.97
410	0.26	0.19	0.15	0.40	1.036

Figure A. 41- Parameters derived from the global analysis of the experimental data from the m-AP_{target} complex on the 20ns timescale.

Global Lifetimes: τ1=0.14ns, τ2=1.12ns, τ3=5.70ns, τ4=12.67ns
Global χ2=1. 077

Emission Wavelength/ nm	A1	A2	A3	A4	Local χ^2
370	0.19	0.14	0.23	0.44	1.098
390	0.20	0.17	0.19	0.45	1.045
410	0.26	0.20	0.16	0.38	1.088

Figure A. 42- Parameters derived from the global analysis of the experimental data from the m-AP_{target} complex on the 50ns timescale.

Global Lifetimes: τ1=0.09ns, τ2=0.68ns, τ3=3.55ns, τ4=10.62ns
Global χ2=1.024

Emission Wavelength/ nm	A1	A2	A3	A4	Local χ^2
370	0.46	0.16	0.18	0.20	1.038
390	0.45	0.18	0.17	0.20	1.01
410	0.45	0.25	0.16	0.14	1.024

Figure A. 43- Parameters derived from the global analysis of the experimental data from the m-TP_{out} complex on the 20ns timescale.

Global Lifetimes: τ1=0.07ns, τ2=0.71ns, τ3=3.67ns, τ4=10.62ns
Global χ2=1.109

Emission Wavelength/ nm	A1	A2	A3	A4	Local χ^2
370	0.49	0.16	0.16	0.19	1.121
390	0.48	0.20	0.16	0.16	1.08
410	0.48	0.22	0.15	0.15	1.125

Figure A. 44- Parameters derived from the global analysis of the experimental data from the m-TP_{out} complex on the 50ns timescale.

Global Lifetimes: τ1=0.04ns, τ2=0.44ns, τ3=2.59ns, τ4=9.94ns
Global χ2=1.128

Emission Wavelength/ nm	A1	A2	A3	A4	Local χ^2
370	0.87	0.07	0.04	0.02	1.114
390	0.82	0.11	0.05	0.02	1.118
410	0.75	0.15	0.07	0.02	1.152

Figure A. 45- Parameters derived from the global analysis of the experimental data from the m-AP_{adj} complex on the 20ns timescale.

Global Lifetimes: τ1=0.05ns, τ2=0.44ns, τ3=2.62ns, τ4=9.94ns
Global χ2=1. 118

Emission Wavelength/ nm	A1	A2	A3	A4	Local χ^2
370	0.86	0.08	0.04	0.03	1.058
390	0.79	0.12	0.06	0.03	1.09
410	0.73	0.17	0.08	0.03	1.205

Figure A. 46- Parameters derived from the global analysis of the experimental data from the m-AP_{adj} complex on the 50ns timescale.

Global Lifetimes: τ1=0.05ns, τ2=0.49ns, τ3=2.96ns, τ4=9.77ns
Global χ2=1.074

Emission Wavelength/ nm	A1	A2	A3	A4	Local χ^2
370	0.75	0.11	0.07	0.07	1.103
390	0.69	0.14	0.08	0.08	1.08
410	0.64	0.18	0.10	0.07	1.039

Figure A. 47- Parameters derived from the global analysis of the experimental data from the m-AP_{opp} complex on the 20ns timescale.

Global Lifetimes: τ1=0.05ns, τ2=0.52ns, τ3=3.00ns, τ4=9.78ns
Global χ2=1. 106

Emission Wavelength/ nm	A1	A2	A3	A4	Local χ^2
370	0.67	0.13	0.09	0.11	1.12
390	0.62	0.16	0.11	0.11	1.125
410	0.58	0.21	0.12	0.09	1.074

Figure A. 48- Parameters derived from the global analysis of the experimental data from the m-AP_{opp} complex on the 50ns timescale.

DNA/T250G Mutant HhaI/Cofactor Complexes

Tables A.49 to A58 show the parameters derived from the global fitting of the fluorescence data collected on the 20ns and 50ns timescales for the DNA/T250G/cofactor mutant HhaI complexes used is this study.

Global Lifetimes: τ1=0.04ns, τ2=0.46ns, τ3=2.65ns, τ4=10.72ns
Global χ2=1.157

Emission Wavelength/ nm	A1	A2	A3	A4	Local χ^2
370	0.76	0.09	0.07	0.08	1.16
390	0.67	0.16	0.09	0.08	1.133
410	0.62	0.21	0.11	0.06	1.177

Figure A.49- Parameters derived from the global analysis of the experimental data from the ^{H}m-GP_{out} complex on the 20ns timescale.

Global Lifetimes: τ1=0.04ns, τ2=0.51ns, τ3=2.80ns, τ4=10.74ns
Global χ2=1.159

Emission Wavelength/ nm	A1	A2	A3	A4	Local χ^2
370	0.73	0.10	0.07	0.09	1.178
390	0.65	0.16	0.10	0.09	1.102
410	0.60	0.21	0.12	0.07	1.197

Figure A.50- Parameters derived from the global analysis of the experimental data from the ^{H}m-GP_{out} complex on the 50ns timescale.

Global Lifetimes: τ1=0.17ns, τ2=1.05ns, τ3=5.4ns, τ4=12.6ns
Global χ2=1.038

Emission Wavelength/ nm	A1	A2	A3	A4	Local χ^2
370	0.15	0.11	0.24	0.49	1.027
390	0.17	0.13	0.20	0.51	1.049
410	0.24	0.16	0.16	0.43	1.037

Figure A. 51- Parameters derived from the global analysis of the experimental data from the ^{M}m-AP$_{target}$ complex on the 20ns timescale.

Global Lifetimes: τ1=0.17ns, τ2=1.23ns, τ3=6.6ns, τ4=12.7ns
Global χ2=0.970

Emission Wavelength/ nm	A1	A2	A3	A4	Local χ^2
370	0.16	0.13	0.26	0.45	0.957
390	0.16	0.15	0.21	0.48	0.943
410	0.24	0.18	0.16	0.42	1.011

Figure A. 52- Parameters derived from the global analysis of the experimental data from the ^{M}m-AP$_{target}$ complex on the 50ns timescale.

Global Lifetimes: τ1=0.07ns, τ2=0.63ns, τ3=3.33ns, τ4=10.47ns
Global χ2=1.048

Emission Wavelength/ nm	A1	A2	A3	A4	Local χ^2
370	0.52	0.14	0.14	0.19	1.063
390	0.46	0.19	0.16	0.19	1.079
410	0.46	0.24	0.15	0.14	1.003

Figure A. 53- Parameters derived from the global analysis of the experimental data from the ^{H}m-TP$_{out}$ complex on the 20ns timescale.

Global Lifetimes: τ1=0.06ns, τ2=0.63ns, τ3=3.36ns, τ4=10.47ns
Global χ2=1.141

Emission Wavelength/ nm	A1	A2	A3	A4	Local χ^2
370	0.51	0.16	0.15	0.19	1.096
390	0.45	0.20	0.16	0.19	1.168
410	0.46	0.25	0.15	0.14	1.159

Figure A. 54- Parameters derived from the global analysis of the experimental data from the ^{H}m-TP$_{out}$ complex on the 50ns timescale.

Global Lifetimes: τ1=0.09ns, τ2=0.41ns, τ3=2.50ns, τ4=10.06ns
Global χ2=1.102

Emission Wavelength/ nm	A1	A2	A3	A4	Local χ^2
370	0.87	0.08	0.03	0.02	1.13
390	0.83	0.11	0.04	0.02	1.088
410	0.76	0.15	0.07	0.02	1.088

Figure A. 55- Parameters derived from the global analysis of the experimental data from the ^{H}m-AP$_{adj}$ complex on the 20ns timescale.

Global Lifetimes: τ1=0.09ns, τ2=0.39ns, τ3=2.45ns, τ4=9.96ns
Global χ2=1.111

Emission Wavelength/ nm	A1	A2	A3	A4	Local χ^2
370	0.85	0.10	0.03	0.02	1.081
390	0.80	0.13	0.05	0.02	1.173
410	0.73	0.17	0.07	0.02	1.080

Figure A. 56- Parameters derived from the global analysis of the experimental data from the ^{H}m-AP$_{adj}$ complex on the 50ns timescale.

Global Lifetimes: τ1=0.07ns, τ2=0.47ns, τ3=2.87ns, τ4=9.62ns
Global χ2=1.088

Emission Wavelength/ nm	A1	A2	A3	A4	Local χ^2
370	0.68	0.15	0.08	0.10	1.083
390	0.61	0.19	0.10	0.10	1.099
410	0.58	0.22	0.11	0.08	1.081

Figure A. 57- Parameters derived from the global analysis of the experimental data from the ^{H}m-AP$_{opp}$ complex on the 20ns timescale.

Global Lifetimes: τ1=0.07ns, τ2=0.47ns, τ3=2.94ns, τ4=9.57ns
Global χ2=1.103

Emission Wavelength/ nm	A1	A2	A3	A4	Local χ^2
370	0.66	0.16	0.08	0.10	1.076
390	0.59	0.20	0.10	0.11	1.072
410	0.56	0.23	0.12	0.09	1.160

Figure A. 58- Parameters derived from the global analysis of the experimental data from the ^{H}m-AP$_{opp}$ complex on the 50ns timescale.

Lectures and Conferences

Postgraduate Lectures and Courses

Laser Physics (18 Lectures)
Introduction to HTML
More HTML
Physical Chemistry Section Seminars
COSMIC Seminars
GRAD Schools Management Training Course

Conferences and Meetings

8th Conference on Methods and Applications of Fluorescence: Spectroscopy, Imaging and Probes, *Prague*, August 2003.

Biophysical Chemistry 2004: Ligand-Protein Interactions, *The University of Edinburgh*, September 2004.

RSC Photochemistry Group, Young Researchers' Meeting, *Rutherford-Appleton Laboratory*, December 2004

Physical Chemistry Section Meetings, Firbush Point

Reprints of Publications

Evidence of tautomerism in 2-aminopurine from fluorescence lifetime measurements, R.K Neely, S.W. Magennis. D.T.F. Dryden and A.C. Jones, J.Phys Chem B., **108**, 17606-17610

Evidence of Tautomerism in 2-Aminopurine from Fluorescence Lifetime Measurements

Robert K. Neely,[†,‡] Steven W. Magennis,[‡] David T. F. Dryden,[†,‡] and Anita C. Jones*[,†,‡]

School of Chemistry and Collaborative Optical Spectroscopy, Micromanipulation and Imaging Centre (COSMIC), The University of Edinburgh, West Mains Road, Edinburgh EH9 3JZ, United Kingdom

Received: March 1, 2004; In Final Form: August 18, 2004

The fluorescence decay characteristics of 2-aminopurine (2AP) and 2-aminopurine riboside (2APr) have been investigated as a function of excitation and emission wavelength in aqueous and ethanolic solutions. Global analysis of the decay data shows that 2AP exists as two emitting species, whereas 2APr exists as a single species. This is attributed to 9H/7H tautomerism of 2AP. The proportion of 7H tautomer is estimated to be 20% in ethanol and 40% in water.

Introduction

Fluorescence spectroscopy is finding increasing application for probing interactions of DNA with ligands and monitoring changes in DNA conformation by introducing fluorescent probes into specific locations within the DNA chain. The natural bases of DNA are not useful as fluorescent probes because of their extremely low quantum yields, and thus the use of extrinsic probes is necessary. 2-Aminopurine (2AP), a fluorescent analogue of adenine, is one such probe which, because of its structural similarity to adenine (6-aminopurine), can be introduced into DNA with minimal perturbation to the system.[1] The structures of 2AP and adenine are shown in Figure 1. The fluorescence properties of 2AP and a number of its derivatives were first reported by Ward et al.[2] It has a quantum yield of about 0.6 in aqueous solution, compared with $\sim 10^{-3}$ for adenine, and an emission maximum at ~370 nm. Its excitation maximum is at ~303 nm, to the red of the naturally occurring DNA bases, allowing it to be excited selectively in DNA.

The aminopurines, adenine and 2AP, can, in principle, exist in several tautomeric forms. For both molecules, the 9H tautomer is the most stable. Adenine is known to tautomerise by proton transfer between N7 and N9 (Figure 1).

This process has been studied in solution phase by UV absorption and steady-state fluorescence spectroscopy (the 7H tautomer is fluorescent)[3] and temperature jump measurements in conjunction with UV absorption[4] and most recently by ultrafast transient absorption spectroscopy;[5] in the gas phase by microwave spectroscopy,[6] infrared and high-resolution electronic spectroscopy;[7] and in computational studies.[8,9] The 9H tautomer of adenine is predominant in the gas phase, but the two tautomers coexist in polar solution at room temperature, because of the greater dipole moment of the 7H tautomer. The fraction of the 7H isomer in solution has been reported as 6% in butanol[3] and 20% in aqueous solution.[4,5] For the parent molecule, purine, the 7H and 9H tautomers have been found to exist in approximately equal proportions in aqueous solution at room temperature.[10−13]

For 2AP, ab initio computational studies[14] have shown that, like adenine, only the 9H and 7H tautomers have low enough energy to be observed at room temperature. As for adenine, the 7H tautomer was predicted to have a significantly greater dipole moment than the 9H tautomer, 4.46 D compared with 3.41 D. Thus, the tautomeric equilibrium is expected to shift toward the 7H form in polar solution. In aqueous solution (using a bulk solvation model) the population of 7H tautomers was predicted to be 3%.[14] There is very little experimental evidence for tautomerism in 2AP. In a study of transition moments, Holmen et al.[15] found that the linear dichroism (LD) spectrum of 2AP in stretched PVA films differed from that of related 9-substituted molecules (which cannot tautomerise). They attributed this to the presence of a small amount of the 7H tautomer. In an early time-resolved fluorescence study, using flash lamp excitation, Santhosh and Mishra[16] found the fluorescence response function of 2AP in water to consist of a rise time of 2.1 ns and a decay time of 24.6 ns. They assigned the two lifetime components to the 9H and 7H tautomers. However, the validity of this work is questionable, since subsequent measurements with superior time resolution (vide infra), including the present work, have found no evidence of a rise in the 2AP fluorescence response, nor a decay time as long as 25 ns. Recently, an ultrafast transient absorption study of 2AP in aqueous solution reported the observation of a multiexponential decay, implying heterogeneity of the chromopohore in the excited state.[17] In addition to a picosecond solvent relaxation time, two nanosecond decay components were observed with lifetimes of ~3.5 and ~14 ns (these values have low precision because of the short (5 ns) time window of the experiments). However, assignment of the two lifetimes to the 7H and 9H tautomers was ruled out because similar behavior was observed for 9-substituted 2AP in which tautomerism is prevented. Instead, the 3.5-ns component was ascribed to a fluorescent state of the 9H tautomer and the 14-ns component to a dark state of the same tautomer. This interpretation is inconsistent with results of time-resolved fluorescence measurements which find the fluorescence lifetime of 2AP in water to be ~12 ns, as discussed below.

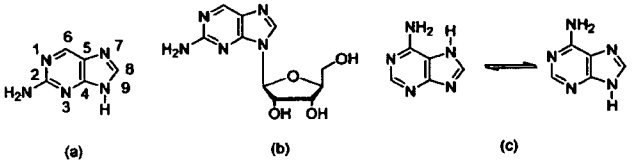

Figure 1. The structures of (a) 2AP (9-H tautomer), (b) 2AP riboside, and (c) the 7H and 9H tautomers of adenine.

* Corresponding author. Phone: 0131-650-6449. Fax: 0131-650-4743. E-mail: a.c.jones@ed.ac.uk.

† School of Chemistry.

‡ Collaborative Optical Spectroscopy, Micromanipulation and Imaging Centre (COSMIC).

10.1021/jp0490857 CCC: $27.50
Published on Web 10/15/2004

The fluorescence decay of 2AP in water is widely accepted to be monoexponential, with lifetime values of 11 to 12 ns reported in the literature.[15,18-20] But, in previous studies, the fluorescence lifetime has generally been measured at only a single excitation wavelength and a single emission wavelength. To obtain a more complete picture of the photophysics of 2AP, and to explore the possibility of 9H−7H tautomerism, we have investigated the fluorescence decay as a function of both excitation and emission wavelengths in aqueous and ethanolic solution, and made comparative measurements on 2AP riboside, in which the 7H tautomer is precluded.

Materials and Methods

2-Aminopurine (>99%) was purchased from Aldrich and 2-aminopurine riboside (2APr) from Sigma; both were used as received. Water was freshly distilled and ethanol was of spectroscopic grade (Aldrich). Both solvents were checked for background fluorescence prior to use. 2AP and 2APr were dissolved to concentrations of 10^{-5} M in both solvents.

Fluorescence lifetimes were determined with use of the time-correlated single photon counting method. Fluorescence decay curves were recorded for sample solutions in fused silica cells of 1 cm path length, using an Edinburgh Instruments spectrometer equipped with TCC900 photon counting electronics. The excitation source was a tuneable, mode-locked Ti−Sapphire laser system (Coherent Mira Ti−Sapphire laser pumped by Coherent 10W Verdi), producing ~200-fs pulses at a repetition rate of 76 MHz. The pulse repetition rate was reduced to 4.75 MHz by using a pulse picker (Coherent 9200) and the light was frequency tripled with a Coherent 5-050 harmonic generator. Fluorescence emission was detected orthogonal to the excitation beam through a polarizer set at the magic angle with respect to the vertically polarized excitation. A band-pass of 10 nm was used in the emission monochromator and photons were detected by using a cooled microchannel plate detector (Hammamatsu R3809 series). The instrument response function, measured by scattering the excitation beam from a dilute suspension of colloidal silica (Ludox), was 50 ps fwhm.

Fluorescence decay curves were recorded on a time scale of 50 ns, resolved into 4096 channels, to a total of 20 000 counts in the peak channel. Decay curves were analyzed by using a standard iterative reconvolution method in the F900 (Edinburgh Instruments Ltd), Level 2 (Edinburgh Instruments Ltd) and FAST (Alango Ltd) software packages. A multiexponential decay function (eq 1) was assumed

$$I(t) = \sum_{i=1}^{n} A_i \exp\left(\frac{-t}{\tau_i}\right) \qquad (1)$$

where A_i is the fractional amplitude and τ_i is the fluorescence lifetime of the ith decay component.

The quality of fit was judged on the basis of the reduced chi-square statistic, χ^2, and the randomness of residuals. Typically, we find that a χ^2 value <1.2 indicates an acceptable fit. In global analysis, a family of decay curves was fitted simultaneously, with lifetimes, τ_i, as common parameters.

Results

2AP in Water. The fluorescence excitation and emission spectra of 2AP in water are shown in Figure 2.

The fluorescence decay of 2AP in aqueous solution was measured at emission wavelengths of 370, 390, and 420 (or 410) nm, and at three excitation wavelengths, 280, 300, and 320 nm. Each decay curve could be well fitted by a single-exponential function and the lifetimes obtained are shown in Table 1.

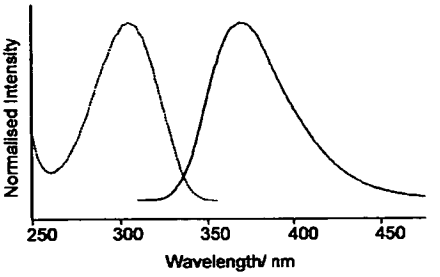

Figure 2. Fluorescence excitation (dotted line) and emission (solid line) spectra of 2AP in aqueous solution.

TABLE 1: Fluorescence Lifetimes and Reduced χ^2 Values for 2AP Fluorescence Decays Measured in Water, as a Function of Excitation Wavelength and Emission Wavelength

excitation wavelength/nm	emission wavelength/nm	τ/ns	χ^2
280	370	11.8	1.11
	390	12.0	1.12
	420	12.1	1.06
300	370	11.9	1.09
	390	12.1	1.05
	420	12.1	1.15
320	370	12.2	1.20
	390	12.3	1.12
	410	12.3	1.13

TABLE 2: For 2AP in Water, Results of Global Fitting of All Decay Curves to a Monoexponential Function with Common Lifetime: Global Fluorescence Lifetime, Global χ^2, and Individual χ^2 Values for Each Decay

τ(global) = 12.1 ns		χ^2(global) = 1.39
excitation wavelength/nm	emission wavelength/nm	χ^2
280	370	2.34
	390	1.52
	420	1.20
300	370	1.23
	390	1.05
	420	1.08
320	370	1.20
	390	1.48
	410	1.62

It can be seen that there is a significant variation in the lifetime with emission and excitation wavelength, ranging from 11.8 ns (excitation at 280 nm, emission at 370 nm) to 12.3 ns (excitation at 320 nm, emission at 390/410 nm). On the basis of measurements of a standard fluorophore with a known single exponential decay, we would expect a statistical variation of <1% in the fluorescence lifetime. This wavelength dependence suggests that there may be more than one emitting species present. Global analysis of the nine decays confirmed that they cannot be adequately described by a single fluorescence lifetime, as shown by the χ^2 values in Table 2. However, global analysis in terms of two common lifetimes yielded excellent fits, as shown in Table 3. Thus, there are two emitting species, with lifetimes of 11.0 and 13.5 ns, contributing to the fluorescence of 2AP in aqueous solution.

2AP in Ethanol. The presence of two emitting species is also clearly apparent in ethanol. As for aqueous solutions, fluorescence decays were measured at three emission wavelengths and three excitation wavelengths. Individual fitting of

TABLE 3: For 2AP in Water, Results of Global Fitting of All Decay Curves to a Biexponential Function with Common Lifetimes: Global Fluorescence Lifetimes and Global χ^2, Followed by the A Factors and χ^2 Values for Each Decay

excitation wavelength/ nm	emission wavelength/ nm	τ_1(global) = 11.0 ns A_1	τ_2(global) = 13.5 ns A_2	χ^2(global) = 1.06 χ^2
280	370	0.70	0.30	1.03
	390	0.65	0.35	1.04
	420	0.53	0.47	1.06
300	370	0.65	0.35	1.05
	390	0.59	0.41	1.02
	420	0.57	0.43	1.06
320	370	0.52	0.48	1.07
	390	0.50	0.50	1.04
	410	0.49	0.51	1.04

TABLE 4: For 2AP in Ethanol, Results of Global Fitting of All Decay Curves to a Monoexponential Function with Common Lifetime: Global Fluorescence Lifetime, Global χ^2 and Individual χ^2 Values for Each Decay

τ(global) = 6.4 ns		
excitation wavelength/nm	emission wavelength/nm	χ^2(global) = 1.47 χ^2
280	370	1.84
	390	1.56
	420	1.36
300	370	1.56
	390	1.25
	420	1.24
320	370	1.20
	390	1.67
	410	1.52

TABLE 5: For 2AP in Ethanol, Results of Global Fitting of All Decay Curves to a Biexponential Function with Common Lifetimes: Global Fluorescence Lifetimes and Global χ^2, Followed by the A Factors and χ^2 Values for Each Decay

excitation wavelength/ nm	emission wavelength/ nm	τ_1(global) = 5.8 ns A_1	τ_2(global) = 7.5 ns A_2	χ^2(global) = 1.09 χ^2
280	370	0.87	0.13	1.08
	390	0.83	0.17	1.09
	420	0.80	0.20	1.04
300	370	0.84	0.16	1.09
	390	0.79	0.21	1.07
	420	0.79	0.21	1.08
320	370	0.72	0.28	1.02
	390	0.66	0.34	1.01
	410	0.65	0.35	1.07

each decay curve to a single-exponential function yielded poor χ^2 values of about 1.5, and significant variation in lifetime with excitation and emission wavelength, ranging from 6.1 ns (at 280-nm excitation, 370-nm emission) to 6.5 ns (at 320-nm excitation, 410-nm emission). As shown in Tables 4 and 5, global analysis confirmed that the decays could not be described by a single lifetime, but are well fitted by a biexponential decay with common lifetimes. The two emitting species have lifetimes of 5.8 and 7.5 ns.

2AP Riboside. To determine whether the two emitting species could be identified with the two tautomeric forms of 2AP, comparative measurements were made on 2AP riboside. As shown in Figure 1, the presence of the ribose substituent at N9 in 2APr prevents formation of the 7H tautomer.

The fluorescence decays of 2APr were measured in aqueous and ethanolic solutions at emission wavelengths of 370, 390, and 410 nm and excitation wavelengths of 300 and 320 nm. In each solvent, global analysis showed that the fluorescence decays of 2APr across the entire excitation/emission space could

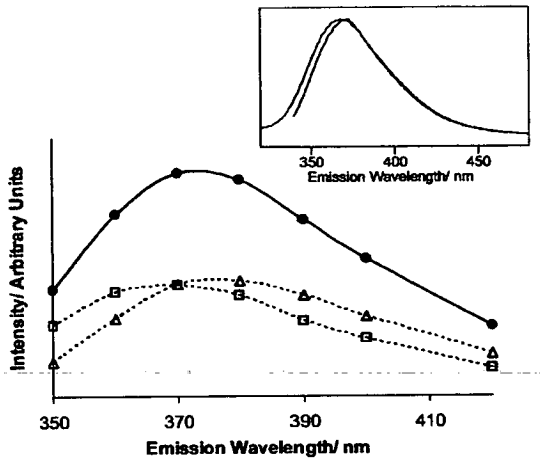

Figure 3. The emission spectra (at an excitation wavelength of 320 nm) of the 9H tautomer (squares) and the 7H tautomer (triangles) of 2-AP in aqueous solution, derived from time-resolved fluorescence data. The total emission spectrum is shown by the solid line. The inset shows the red shift in the total emission spectrum when the excitation wavelength is shifted from 280 (dotted line) to 330 nm (solid line).

be fitted by a single common fluorescence lifetime, with all χ^2 values <1.2, indicating the presence of a single emitting species. The fluorescence lifetime of 2APr was found to be 10.6 ns in water and 5.8 ns in ethanol.

Discussion

Current understanding of the photophysics of 2AP in aqueous solution holds that its fluorescence decay is single exponential with a lifetime of around 11.5 ns.[15,18-20] Our results show that, for an individual decay curve measured at a particular excitation and emission wavelength, this is indeed the case. However, measurement over a range of excitation and emission wavelengths reveals biexponential decay kinetics in both aqueous and ethanolic solutions of 2AP, indicating the presence of two emitting species. Comparison with 2APr, which demonstrably behaves as a single emitting species in both solvents, leads to the conclusion that the two species observed for 2AP are the 9H and 7H tautomers. In water, the 2APr lifetime of 10.6 ns is very similar to the 11 ns decay component of 2AP; therefore, we assign the latter to the 9H tautomer and the 13.5-ns lifetime to the 7H tautomer. Similarly, in ethanol, the 5.8-ns lifetime is assigned to the 9H tautomer (cf. 5.8 ns 2APr lifetime) and the 7.4-ns lifetime to the 7H tautomer. The marked decrease in the fluorescence lifetimes in ethanol is consistent with the previously reported lifetime of 6 ns for 2AP in ethanol and the observation of a decreasing trend in lifetime with decreasing solvent polarity.[12] Our observation of a biexponential decay for 2AP and a monoexponential decay for 2APr is analogous to the excited-state decay behavior of adenine and 9-methyladenine reported in a recent transient absorption study,[5] which was also interpreted in terms of 9H/7H tautomerism.

The fractional contribution of the ith lifetime component to the total integrated (steady state) emission intensity, at a particular excitation and emission wavelength, is given by $A_i\tau_i/\sum_i A_i\tau_i$. Thus, measurement of the fluorescence decay of 2AP in water at a series of wavelengths across the emission envelope allowed the emission spectra of the two tautomers to be constructed, as shown in Figure 3.

The spectra overlap closely; the maxima are separated by about 7 nm (~500 cm^{-1}), with the spectrum of the 7H tautomer lying at longer wavelength. The excitation wavelength depen-

dence of the A factors in Tables 3 and 5 also suggests that the excitation spectrum of the 7H tautomer is red-shifted relative to the 9H tautomer. These observations are in agreement with the results of ab initio calculations by Broo[21] that predict both tautomers to be fluorescent (having lowest excited states of $\pi\pi^*$ character) and the emission maximum (for a vertical transition from the relaxed excited state) of the 7H tautomer to be about 1000 cm^{-1} below that of the 9H tautomer. The existence of the two tautomers should be apparent in the steady state emission of 2AP and, indeed, it was found that excitation on the red edge of the excitation spectrum gave an emission spectrum significantly red-shifted from that obtained with blue-edge excitation, as shown in the inset to Figure 3. For 2APr, the emission spectrum is independent of excitation wavelength.

If the radiative lifetimes of the two tautomers can be assumed to be similar, then the A factors indicate the fraction of the emitting population constituted by each tautomer. This appears to be a reasonable assumption, since the fluorescence lifetimes of the two tautomers are similar and their oscillator strengths are predicted to be similar,[21] 0.37 for 9H and 0.25 for 7H. Examination of the A factors in Tables 3 and 5 indicates that the proportion of the 7H tautomer in both solvents is substantial, about 40% in water and about 20% in ethanol. These values are somewhat greater than those reported for adenine, 20% in water[4,5] and 6% in butanol,[3] although the 40% value in water is similar to the observation of equal proportions of 7H and 9H tautomers for purine[11-13] in aqueous solution. The observation of a greater fraction of the 7H tautomer in water than in ethanol is consistent with the prediction of a larger dipole moment for this tautomer.[14] However, the magnitude of the 7H tautomer population is much greater than the 3% predicted for 2AP in water[14] in the same ab intio study. The calculations may significantly underestimate the effect of polar solvation in shifting the equilibrium toward the 7H tautomer, since they neglect specific solvent−solute interactions.

It is important to recognize that in these experiments we are observing the excited-state tautomer population and to consider how this relates to the ground-state population. Ab initio calculations by Broo[21] predict the 7H tautomer to be much closer in energy to the 9H tautomer in the excited state than in the ground state, for both 2AP and adenine in the gas phase. If the solvent effect on the relative excited state energies of the two tautomers were of the same magnitude as that in the ground state, this would result in the two tautomers lying very close in energy, giving comparable proportions in the equilibrated excited state population. This might account for our observation of a relatively high proportion of 7H tautomer. However, we see no sign, in the fluorescence response functions, of any rise components (negative A factors) that would indicate a shift in the tautomer equilibrium following excitation. If the reequilibration on excitation occurs faster than the time resolution of our measurements, i.e., on the picosecond time scale or less, we may be observing the fluorescence decay of the fully equilibrated excited-state tautomer population. However, we see a definite dependence of the A factors (proportions of 7H and 9H tautomers in the emitting population) on excitation wavelength, indicating that memory of the ground-state population is retained in the emitting population. It seems more likely, therefore, that the response of the tautomer equilibrium to excitation is slow compared with the lifetime of the excited state, and the excited-state population that we observe reflects the composition of the ground-state population.

We have found further evidence of tautomerism in 2AP from X-ray crystallography. The X-ray structure of 2AP crystals grown from ethanol solution shows the presence of both 9H and 7H tautomers in the crystal lattice, with the occupancy of the 7H form being about 15%.[22] This is in good agreement with the tautomer population in ethanol solution estimated from the fluorescence data. Further support for our derivation of ground state 2AP tautomer populations from the fluorescence decay amplitudes comes from the recent analogous study of adenine excited-state decay by ultrafast transient absorption spectroscopy.[5] In the latter work, the fractional population of the 9H and 7H adenine tautomers was calculated from the decay amplitudes, giving a value of 22% for the 7H tautomer, in good agreement with previous measurements.[4,13]

Conclusion

Fluorescence lifetime measurements have shown that 2AP exists as both the 9H and the 7H tautomer in aqueous and ethanolic solution at room temperature. There is a substantial proportion of the 7H isomer in the emitting population: about 40% in water and about 20% in ethanol. The two tautomers have closely overlapping fluorescence spectra but can be distinguished by their fluorescence lifetimes. The tautomeric composition of the emitting population depends on excitation wavelength and we see no evidence of a change in the tautomeric equilibrium in response to excitation. We conclude, therefore, that the observed excited state tautomer population arises directly from that in the ground state.

The observation of tautomerism in 2AP is further evidence of the similarity of this molecule to adenine and affirms its suitability as a fluorescent analogue of the nucleic base. It also offers the opportunity of applying sensitive fluorescence methods to the study of the tautomerization process.

Acknowledgment. We gratefully acknowledge the Scottish Higher Education Funding Council for funding the COSMIC and the EPSRC for the award of a research grant to D.T.F.D. (GR/N19748) and a studentship to R.K.N.

References and Notes

(1) Eritja, R.; Kaplan, B. E.; Mhaskar, D.; Sowers, L. C.; Petruska, J.; Goodman, M. F. *Nucleic Acids Res.* **1986**, *14*, 5869−5884.
(2) Stryer, L.; Ward, D. C.; Reich, E. *J. Biol. Chem.* **1969**, *244*, 1228−1237.
(3) Eastman, J. W. *Ber. Bunsen-Ges. Phys. Chem.* **1969**, *73*, 407−412.
(4) Dreyfus, M.; Dodin, G.; Bensuade, O.; Dubois, J. E. *J. Am. Chem. Soc.* **1975**, *97*, 2369.
(5) Cohen, B.; Hare, P. M.; Kohler, B. *J. Am. Chem. Soc.* **2003**, *125*, 13594−13601.
(6) Brown, R.; Godfrey, P.; McNaughton, D.; Pierlot, P. *Chem. Phys. Lett.* **1989**, *156*, 61−63.
(7) Plutzer, C.; Kleinermanns, K. *Phys. Chem. Chem. Phys.* **2002**, *4*, 4877−4882.
(8) Salter, L. M.; Chaban, G. M. *J. Phys Chem. A* **2002**, *106*, 4251−4256.
(9) Gu, J. D.; Leszczynski, J. *J. Phys Chem. A* **1999**, *103*, 2744−2750.
(10) Majobe, M.; Millie, Ph.; Chinsky, L.; Turpin, P. Y.; Vergoten, G. *J Mol. Struct.* **1995**, *355*, 147−158.
(11) Schumacher, M.; Gunther, H. *J. Am. Chem. Soc.* **1982**, *104*, 4167−4173.
(12) Gonella, N. C.; Roberts, J. D. *J. Am. Chem. Soc.* **1982**, *104*, 3162−3164.
(13) Chenon, M.-T.; Pugmire, R. J.; Grant, D. M.; Panzica, R. P.; Townsend, L. B. *J. Am. Chem. Soc.* **1975**, *97*, 4636−4642.
(14) Broo, A.; Holmen, A. *Chem. Phys.* **1996**, *211*, 147−161.
(15) Holmen, A.; Norden, B.; Albinsson, B. *J. Am. Chem. Soc.* **1997**, *119*, 3114−3121.
(16) Santhosh, C.; Mishra, C. P. *Spectrochim. Acta A* **1991**, *47*, 1685−1693.
(17) Larsen, O. F. A.; van Stokkum, I. H. M.; Groot, M. L.; Kennis, J. T. M.; van Grondelle, R.; van Amerongen, H. *Chem. Phys. Lett.* **2003**, *371*, 157−163.

(18) Rachofsky, E. L.; Osman, R.; Ross, J. B. A. *Biochemistry* **2001**, *40*, 946−956.
(19) Rachofsky, E. L.; Sowers, L.; Hawkins, M. L.; Balis, F. M.; Laws, W. R.; Ross, J. B. A. *Proc. SPIE* **1998**, *3256*, 68−75.
(20) Lakowicz, J. R. *Principles of Fluorescence Spectroscopy*, 2nd ed.; Kluwer Academic/Plenum Publishers: New York, 1999.
(21) Broo, A. *J. Phys Chem. A* **1998**, *102*, 526−531.
(22) Neely, R. K.; Parsons, S.; Jones, A. C. In preparation.